Local Design Methodologies for a Hierarchic Control Architecture

Jonathan P. How
Steven R. Hall
Edward F. Crawley

Final Report for AFOSR Contract
#F49620-88-C-0015
April 12, 1990

SSL

MASSACHUSETTS INSTITUTE OF TECHNOLOGY

SPACE SYSTEMS LABORATORY
DEPT. OF AERONAUTICS AND ASTRONAUTICS
MASSACHUSETTS INSTITUTE OF TECHNOLOGY
CAMBRIDGE, MA 02139

(a)

Local Design Methodologies for a Hierarchic Control Architecture

Jonathan P. How
Steven R. Hall
Edward F. Crawley

Final Report for AFOSR Contract
#F49620-88-C-0015
April 12, 1990

Unclassified

SECURITY CLASSIFICATION OF THIS PAGE

REPORT DOCUMENTATION PAGE

1a. REPORT SECURITY CLASSIFICATION: Unclassified	1b. RESTRICTIVE MARKINGS: ----------
2a. SECURITY CLASSIFICATION AUTHORITY: ----------	3. DISTRIBUTION/AVAILABILITY OF REPORT: approved for public release/distribution unlimited
2b. DECLASSIFICATION/DOWNGRADING SCHEDULE: ----------	
4. PERFORMING ORGANIZATION REPORT NUMBER(S): MIT - SSL #14-89	5. MONITORING ORGANIZATION REPORT NUMBER(S): ~~AFOSR-TR-90-0524~~
6a. NAME OF PERFORMING ORGANIZATION: Space Systems Laboratory, MIT, Dept. Aero & Astro	6b. OFFICE SYMBOL (If applicable): --------
7a. NAME OF MONITORING ORGANIZATION: AFOSR	
6c. ADDRESS (City, State and ZIP Code): 37-361 MIT, Cambridge, MA 02139	7b. ADDRESS (City, State and ZIP Code): Bolling Air Force Base AFOSR/NA Bldg 410, Washington, DC 20332-6448
8a. NAME OF FUNDING/SPONSORING ORGANIZATION: AFOSR	8b. OFFICE SYMBOL (If applicable): AFOSR/NA
9. PROCUREMENT INSTRUMENT IDENTIFICATION NUMBER: contract #F49620-88-C-0015	
8c. ADDRESS (City, State and ZIP Code): Bolling Air Force Base, Washington, DC 20332-6448 AFOSR/ Bldg 410	10. SOURCE OF FUNDING NOS. PROGRAM: 61102F; PROJECT: 2305; TASK: B1; WORK UNIT NO.:
11. TITLE (Include Security Classification): "LOCAL CONTROL DESIGN METHODOLOGIES FOR A HIERARCHIC CONTROL ARCHITECTURE"	
12. PERSONAL AUTHOR(S): How, Jonathan P.; Hall, Steven R.; Crawley, Edward F.	
13a. TYPE OF REPORT: final	13b. TIME COVERED: FROM 9/1/88 TO 30/6/89
14. DATE OF REPORT (Yr., Mo., Day): 12 April 1990	15. PAGE COUNT: 217
16. SUPPLEMENTARY NOTATION: Form 10	
17. COSATI CODES: FIELD / GROUP / SUB. GR.	18. SUBJECT TERMS (Continue on reverse if necessary and identify by block number): Active Control, Distributed, Hierarchic Control; Local Control Designs

19. ABSTRACT (Continue on reverse if necessary and identify by block number)

The problems associated with the control of large intelligent space structures with many sensors and actuators has previously led to the development of a hierarchic control architecture. This control arrangement consists of a two level combination of a centralized global controller and a set of local controllers which are distributed to complement the dynamic behavior of the structure. Four decentralized control methodologies which are suitable for implementation at the lower level of the hierarchic architecture are developed and analyzed in this thesis. The first design only allows colocated feedback. The second design allows feedback from within a region of the structure. The third allows communication between adjacent local controllers so that information from neighboring regions can be used for the feedback. The last employs a distributed implementation of the full state feedback. The simulation results for the control of a long beam in bending show that employing the more complicated decentralized designs at the lower level of the hierarchic architecture will slightly improve the overall performance. However, the implementation

20. DISTRIBUTION/AVAILABILITY OF ABSTRACT: UNCLASSIFIED/UNLIMITED ☒ SAME AS RPT. ☐ DTIC USERS ☐	21. ABSTRACT SECURITY CLASSIFICATION: unclassified
22a. NAME OF RESPONSIBLE INDIVIDUAL: Dr Spencer T Wu	22b. TELEPHONE NUMBER (Include Area Code): (202) 767-6962
	22c. OFFICE SYMBOL: AFOSR/NA

DD FORM 1473, 83 APR EDITION OF 1 JAN 73 IS OBSOLETE.

unclassified

SECURITY CLASSIFICATION OF THIS PAGE

19. Continued, abstract

costs for these more sophisticated designs are shown to increase dramatically. The most efficient hierarchic design for this beam example is one which combines a good flobal design with a simple colocated feedback. This conclusion may change for structures which require more performance at the local level. Keywords — to field 8

Executive Summary of "Local Design Methodologies for a Hierarchic Control Architecture"

This final report documents the work performed at MIT during the period of September, 1987 to June, 1989. The original AFOSR contract (#F49620-88-C-0015) was written for one year. There was an option for the two following years, but this was not exercised by the Air Force. Consequently, this research was partially funded by Professor Crawley's Presidential Young Investigators Award NSF Grant #8451627-MSM. The objective of the proposed research was to investigate the theoretical advantages of embedding a highly distributed sensor/processor network in a composite "intelligent" structure. This work specifically dealt with the design of an efficient control architecture for a structure with many sensors, actuators, and distributed microprocessors. The aims of the first year of the project were to finalize the hierarchic control architecture, develop suitable local controllers, and to compare the control architecture with other designs for accuracy and computational efficiency.

Status:

The work associated with each of these objectives has been completed, and the results are included in this final report. The procedure for designing a hierarchic controller has been formalized and a four step algorithm is given in Chapter 2. The decoupling between the two levels of control is explicitly included in the architecture, as seen in Figure 2.4. The analysis of the architecture showed that, for structures with hundreds of sensors and actuators, the hierarchic controller is capable of achieving near optimal performance in a computationally efficient manner. Several types of local control designs were analyzed for the example of the control of a long beam in bending. These were compared in terms of both the performance improvements available and the implementation costs. This provided the framework for a performance/implementation cost trade-off analysis of the different local designs.

Publications:

Two papers have been developed from this work. The first (essentially Chapter 2 of this report) has been accepted for publication. The second will be submitted to the same Journal.

Hall, S., Crawley, E., How, J., and Ward, B., "A Hierarchic Control Architecture for Intelligent Structures," to be published in the *AIAA Journal Guidance, Control,*

and Dynamics, (Space Systems Laboratory Report #19-88), November, 1988

How, J., and Hall, S., "Local Control Design Methodologies for a Hierarchic Control Architecture," to be submitted to the *AIAA Journal Guidance, Control, and Dynamics*, April, 1990.

Personnel:

Three professors and two graduate level students were funded by this contract.

Professor Edward F. Crawley (resume at the back)
Professor Steven R. Hall (resume at the back)
Professor Stephen D. Senturia (resume at the back)
Jonathan P. How (Master's Student)
David Warkentin (Master's Student)

One S.M. Degree was awarded to Jonathan P. How in November, 1989 for the work covered in this final report; thesis title: "Local Control Design Methodologies for a Hierarchic Control Architecture."

Presentations:

This work has been presented at the following seminars:

Hall, S., Crawley, E., How, J., and Ward, B., "A Hierarchic Control Architecture for Intelligent Structures," To be presented at the AIAA Guidance, Navigation and Control Conference, Portland, OR, August 20-22, 1990.

Hall, S., Crawley, E., and How, J., "A Hierarchic Control Architecture for Intelligent Structures," First Annual Symposium of the MIT Space Engineering Research Center, Jet Propulsion Laboratory, Pasadena, CA, August 31, 1989.

Hall, S., Crawley, E., and How, J., "A Hierarchic Control Architecture for Intelligent Structures," Sixth Annual Air Force Symposium on Space Structures, Atlanta, GA, April 7-8, 1988.

Contents

1 Introduction **16**

1.1 Background 16

1.2 Control Approaches 18

1.3 Overview 24

2 Hierarchic Control **26**

2.1 Introduction 26

2.2 Architecture 27

2.3 Mass Condensation 32

2.4 Defining the Global and Residual Coordinates 35

2.5 Decoupling the Control/Structural Model 38

2.6 Alternative Choices for the Element Interpolation. 46

2.7 Hierarchic Control Synthesis 52

3 Local Control Design **54**

3.1 Introduction 54

3.2 Colocated Feedback 56

3.3 Block Diagonal Feedback 59

3.3.1 Introduction 59
3.3.2 The Calculation of the Gains 59
3.3.3 Transformations for Spatially Symmetric Systems 64
3.3.4 An Overview of Multivariate Function Minimization 75
3.3.5 Numerical Approximation of the Gradient and Hessian 80
3.3.6 The Solution Algorithm 83
3.3.7 Discussion of the Results 84
3.4 Block Tri-Diagonal Feedback 88
3.4.1 Introduction 88
3.4.2 Calculation of the Gains 92
3.4.3 Conclusions 101
3.5 A Decentralized Implementation of Full State Feedback 101
3.5.1 Introduction 101
3.5.2 Calculation of the Gains 103
3.6 Conclusions 108

4 Examples **112**

4.1 Introduction 112
4.2 Discussion of the Model 114
4.3 The Global Control Design 127
4.4 A Comparison of the Local Control Designs 133
4.4.1 Introduction 133
4.4.2 Colocated Feedback 135
4.4.3 Block Diagonal Feedback 137
4.4.4 Block Tri-Diagonal Feedback 138

4.4.5 Conclusions 143
4.5 An Analysis of the Full Hierarchic Control Designs 143
4.6 Conclusions 150

5 Implementation Issues **152**

5.1 Introduction 152
5.2 Operations Count 153
5.2.1 Introduction 153
5.2.2 Task Analysis for the Controllers 154
5.2.3 Incorporating Different Controller Frequencies 160
5.2.4 Operations Count with only the Lower Modes Retained . . . 161
5.2.5 Operation Counts for the Local Controllers 164
5.2.6 Communication Requirements 167
5.2.7 Typical Examples 168
5.3 Closed Loop Stability 173
5.3.1 Introduction 173
5.3.2 Lyapunov Test 176
5.3.3 Connective Stability 177
5.4 Controller Robustness 180
5.5 Selecting the Appropriate Processor Location 181

6 Conclusions and Recommendations **185**

6.1 Summary 185
6.2 Conclusions and Contributions 186
6.3 Recommendations 189

References 190

Appendices 197

A The Necessary Conditions for a Constrained Optimal Regulator 197

List of Figures

1.1 A typical HAC/LAC design. 22

2.1 A two-level echelon feedback architecture for the implementation of hierarchic control. 28

2.2 A representation of a finite-dimensional model by a coarse or global finite element model. 30

2.3 The division of control functions in a two-level hierarchic controller. 31

2.4 The hierarchic control architecture. 44

2.5 A comparison of the control architectures for the HAC/LAC and hierarchic control designs. 45

2.6 The hierarchic control architecture for the case where only the n_l lower frequency modes of the global model are retained. 49

3.1 The architecture for a local controller based on colocated feedback. 57

3.2 The architecture for a local controller based on block diagonal feedback. 60

3.3 An example of a circulant system. 66

3.4 The displacement weighted displacement gain matrix for a nine node bay. 86

3.5 The displacement weighted velocity gain matrix for a nine node bay. 86

3.6 The displacement weighted displacement gain matrix for a nine node bay, plotted across the rows. 87

3.7 The displacement weighted velocity gain matrix for a nine node bay, plotted across the rows. 87

3.8 The architecture for a local controller based on block tri-diagonal feedback. 90

3.9 Two types of gain matrices for the block tri-diagonal feedback approach. 91

3.10 A model of an infinite dimensional symmetric beam. 93

3.11 The form of the FEM mass and stiffness matrices for the infinite beam example. 94

3.12 The displacement weighted gains in the frequency domain. 97

3.13 The displacement weighted gains in the spatial domain. 97

3.14 The energy weighted gains in the frequency domain. 98

3.15 The energy weighted gains in the spatial domain. 98

3.16 The velocity weighted gains in the frequency domain. 99

3.17 The velocity weighted gains in the spatial domain. 99

3.18 The optimal displacement weighted regulator gains for an actuator in the middle of a long beam. 100

3.19 A schematic of the decentralized implementation of full state feedback. 102

3.20 A w-frequency domain comparison of the optimal and approximate gains. 105

3.21 A spatial domain comparison of the optimal and approximate gains. 105

3.22 A more detailed representation of the control architecture for the decentralized implementation. 107

3.23 The full local control architecture. 109

4.1 A 30 node beam model. 115

4.2 A comparison of the modal frequencies for various approximations of the mass matrix in the FEM. 119

4.3 A 30 node beam condensed mass matrix. 120

4.4 The four Hermite polynomials. 122

4.5 The form of the interpolation function matrix T_g. 123

4.6 The aggregation matrix with a block tri-diagonal approximation of the condensed mass matrix. 125

4.7 The closed loop pole locations from the global controller. 130

4.8 The closed loop pole locations from the lower global mode controller. 131

4.9 A comparison of two approximations of the mass matrix used in the control and observation filtering. 132

4.10 The closed loop poles from the colocated controller. 136

4.11 The closed loop poles from the full block diagonal controller. 139

4.12 The closed loop poles from the two bay block diagonal controller. . . 140

4.13 The closed loop poles from the full block tri-diagonal controller. . . . 141

4.14 The closed loop poles from the banded block tri-diagonal controller. 142

4.15 The closed loop poles for a full hierarchic controller with a local control based on colocated natural feedback. 145

4.16 The closed loop poles for a full hierarchic controller with a local control based on block diagonal feedback. 146

4.17 Performance evaluation using a graph of state cost versus control effort. 148

4.18 Performance evaluation: an emphasis on the local control designs. . 149

4.19 The hierarchic control applied to the evaluation model. 151

5.1 The layout for the global and structural nodes. 154

5.2 The computational requirements for various global controllers. . . . 170

5.3 A comparison of the computational requirements for various local controllers: $n_{gn} = 6$. 171

5.4 A comparison of the computational requirements for various local controllers: $n_{gn} = 20$. 172

5.5 Two methods of locating the processors. 182

List of Tables

2.1 A comparison of two methods of implementing the hierarchic control architecture. 50

4.1 A comparison of the flexible mode frequencies with various approximations of the mass matrix. 118

4.2 The flexible mode frequencies from the global model. 126

5.1 A comparison of the operations count for two system sizes. 169

Nomenclature

A_g, A_r = coefficient matrices

BD(...) = block diagonal matrix with the listed blocks along the main diagonal

e = vector of residuals

$F_e, F_{\dot{e}}$ = residual feedback gain matrices

$F_g, F_{\dot{g}}$ = global feedback gain matrices

$F_{gg}, F_{rr}, F_{gr}, F_{rg}, F_{g\dot{g}}, F_{r\dot{r}}, F_{g\dot{r}}, F_{r\dot{g}}$

= elements of transformed system feedback matrices

h_g = number of structural nodes per finite control element

I_n = $n \times n$ identity matrix

j = $\sqrt{-1}$

J = quadratic cost

K = finite element model stiffness matrix

$K_{gg}, K_{rr}, K_{gr}, K_{rg}$ = elements of transformed system stiffness matrix

L = augmented cost function

M = finite element model mass matrix

$M_{gg}, M_{rr}, M_{gr}, M_{rg}$ = elements of transformed system mass matrix

n = number of dof's in finite element model of system

n_e = number of finite control elements

n_g = number of global degrees of freedom

n_{gn} = number of global nodes

$n_{g_{dof}}$ = number of degrees of freedom per global node

n_l = number of modes of the global model retained in alternative interpolation method 1

n_r = number of residual degrees of freedom

ω_N = N^{th} complex root of 1

Q = generalized forces in the finite element model

Q_e = generalized forces in the finite element model due to residual feedback

Q_g = generalized forces in the global model

q = vector of finite element model degrees of freedom

q_g = vector of global degrees of freedom

q_r = vector of residual degrees of freedom

q_{rm} = vector of residual dof's in alternative interpolation method 1

R_{xx}, R_{uu} = LQR state and control weighting matrices

R^g_{xx}, R^g_{uu} = LQR state and control weighting matrices for the global model

S_e = residual force distribution matrix

S_g = global force distribution matrix

T_g = interpolation matrix for global degrees of freedom

T_{gl} = interpolation matrix for global degrees of freedom in alternative interpolation method 1

T_{g0} = interpolation matrix for global degrees of freedom in alternative interpolation method 2

T_r = interpolation matrix for residual degrees of freedom

u = vector of control inputs

u_e = vector of control inputs due to residual feedback

u_g = vector of control inputs due to global feedback

u_r = vector of control inputs due to residual feedback, after spatial filtering

W = positive definite weighting matrix

x = finite element model state vector

x_g = global model state vector

y = vector of measurements

$Z(\cdot)$ = z-transform of $(\cdot)$

α, β = scalar feedback gains

ϕ_g = mode shapes of the global model in the global coordinate system

ϕ_0 = mode shapes of the finite element model

Φ = matrix of system eigenvalues

Φ_n = transformation matrix for a circulant system based on I_n

Ψ = finite element model control influence matrix

ξ_g = modal degrees of freedom of the global model

ξ_0 = modal degrees of freedom of the finite element model

superscripts:

$(\cdot)^l$ = lower in frequency set of $(\cdot)$

$(\cdot)^u$ = upper in frequency set of $(\cdot)$

$(\cdot)^{-L}$ = left pseudoinverse of $(\cdot)$

$(\cdot)^{-R}$ = right pseudoinverse of $(\cdot)$

$(\cdot)^{-1}$ = inverse of $(\cdot)$

$\overline{(\cdot)}$ = circulant transformed representation of $(\cdot)$

$(\cdot)^T$ = transpose of $(\cdot)$

$(\cdot)^H$ = hermitian of $(\cdot)$

$(\cdot)^*$ = complex conjugate of $(\cdot)$

subscripts:

$(\cdot)_c$ = causal part of $(\cdot)$

$(\cdot)_{ac}$ = anti-causal part of $(\cdot)$

$(\cdot)_{cond}$ = condensed version of $(\cdot)$

Chapter 1

Introduction

1.1 Background

Within the last decade, there has been a great deal of interest in the control of Large Flexible Space Structures (*LFSS*) [6,13,61,65,70]. The objective of eliminating the unwanted vibratory motion of a structure is recognized as being a particularly difficult in part because of the physical characteristics of the plant. For instance, a typical structure will tend to be large in size, lightly damped, and modally rich. Also, with the missions envisioned for future spacecraft, such as a space based inferometer, the performance requirements are becoming more stringent as well. This will tend to push the control bandwidth higher, so that some of the flexible modes will have a significant influence on the performance objective. The launch weight/cost tradeoff for these devices naturally leads to plants which have low structural rigidity, and this will accentuate the problem of densely packed modes in the structure. This phenomena of very high modal densities can also be seen in Earth based telescopes [4]. As mentioned, these LFSS tend to possess very low inherent damping. Values for the material damping of about 0.1 percent and for the entire structure of about 1.0 percent are typical for most materials envisioned for use on

LFSS [20]. There will be no aerodynamic damping present either. Another problem that must be faced is that the structures are really of infinite order. Since math models are typically finite, there will obviously be errors due to truncation, but there will also be uncertainties in the parameters of the modes which have been modelled. The designer must therefore ensure that the controller is robust to these uncertainties. Standard control design techniques such as the Linear Quadratic Gaussian (LQG) assume that the plant is both well modelled and finite [35], so the LFSS pose a serious challenge to these design techniques.

Due to the size of the plant, it is clear that some form of reduction of the order of the controller must be carried out for the design to be considered practical. Several techniques for this have been developed. Some perform open loop reduction on the plant [26,63] and then develop the controller for this design model, while others perform a control design on a larger model and then eliminate those states of the closed loop system which are deemed to be the least important in some weighted sense [72]. Other approaches are based on the Optimal Projection approach of Bernstein and Hyland [11,30].

This reduction in size allows the design step to become computationally feasible, but when a reduced order controller is implementated on the evaluation model or on the structure itself, *spillover* between the modelled and unmodelled modes will occur [6]. Spillover is apparent in several forms. Observation spillover is the measurement of dynamics which are not associated with the controlled set of modes. Similarly, control spillover accounts for the action of the control commands on this set of neglected modes. If the both of these forms are present (as will usually be the case for a truncated model controller acting on the evaluation model), then the resulting coupling may destabilize the closed loop system [6]. If only one form of the spillover is present, then destabilization may not occur, but there most likely will be a degradation in the performance due to the coupling of the dynamics through the measurement or control action. These problems have led to a class of control de-

signs which incorporate some degree of spillover alleviation in the design procedure [7,17,59]. For this reason, it is important to actively or passively supplement the damping of the higher frequency modes of the structure so that they have some degree of stability margin. This will enable them to withstand the adverse influences of the spillover. The complexity of typical structures has lead to several approaches to the control design.

1.2 Control Approaches

Coupled with the difficulties presented by the plant are numerous problems with the implementation of the controller. The most commonly employed control designs employ a central computer to perform the compensation. Typical approaches include the use of optimal or suboptimal output feedback gains directly on the measurements [34,38], or the use of a full or reduced order estimators driven by the measurements in conjunction with full state feedback [11,38,63]. Each of these techniques require that the central computer receive all measurements and compute each control command. These techniques were originally designed with a focus on the case where the number of sensors and actuators is small in relation to the plant dimension. The major difficulties with any centralized control design are the communication problems and the possibly prohibitive computational demands on the central computer. For LFSS, it may also be necessary to transfer information over large distances. The minimum computation for a centralized output feedback controller is of the order of the number of sensors times the number of actuators. For the case of a dynamic compensator, more computations will be required as the state estimate must be updated at each time step and then a gain multiplication of the order of the number of actuators times the number of states must be performed. If the controller's bandwidth is a multiple of the highest frequency to be controlled, which varies linearly or as the square of the number of modes in the

structural model, then taking n as the number of sensor and/or actuator pairs or the modelled modes, the computational requirements of these centralized schemes increase at a rate between n^3 and n^4, which is clearly quite prohibitive for any large scale system. The solution to this problem appears to be incorporating some form of distribution of the control effort among several processors, *i.e.*, making the approach more parallel in nature.

One approach is to employ a decentralized controller which consists of several regional (in the sense of knowledge and influence) controllers which are distributed throughout the structure [9,39,54,56,65,68]. Many decentralized control techniques are also discussed in the survey paper by Sandell *et al.* [57]. The difficulty with this approach is that there typically is very little global control authority to handle the longer wavelength motions since each regional controller can only measure and influence the adjacent portions of the structure, and it is unaware of the gross motions of the entire body. Most of these approaches are more particularly suited to the design of controllers for structures which can easily be written in terms of lightly coupled subsystems. In this case, the interactions are small enough that they can be ignored during the design phase and the resulting coupling in the structure will have only a small influence on the closed loop subsystems and an argument about the overall stability can then be made [60]. This would be effective for a space structure if it can easily be partitioned into the weakly linked subsystems or appendages, an approach which is employed in reference [56]. However, these designs are not particularly suited to systems which are strongly coupled, so the designer is not free to arbitraily break up the plant into subsections and expect the decentralized control design to remain stable. Some techniques have been employed which try to account for this coupling [54], but the resulting design tends to expend a large amount of control effort just trying to decouple the systems. Some emphasis has also been placed on the design of decentralized controllers to supplement the damping of the structure [3,33,39,54,61]. Young [71] introduces a very interesting

decentralized control technique called *controlled component synthesis*. It is based on the familiar component mode synthesis (CMS) method of modelling structures. The idea is essentially to develop *controlled components* of the structure which can then be assembled into the full model using the standard CMS techniques.

Another approach is to incorporate two levels of controllers. This type is commonly referred to as *hierarchic control architectures*. Examples exist which employ these controllers for large scale systems like traffic patterns or power stations [15,43,62]. These designs typically have two levels of controllers, though many levels could be used. The control tasks are split so that the lower level performs the "daily" tasks, while the higher level performs the job of "coordinating" the activities of the lower controllers with a more global picture of the performance in mind [15]. Reference [23] proposes a two level approach for the control of LFSS. The resulting control design is essentially a decentralized control architecture which employs a second level to eliminate some of the spillover effects. The resulting lower control design procedure is a succesive loop closure, and the function of the central computer is to employ residual mode filters which counteract the effects of the observation spillover.

References [18] and [64] develop a structural model reduction technique which is interesting in terms of this work since the reduction is also done in a manner which complements the structure of the plant. Krylov vectors are introduced as a type of static mode, and these are used in a parameter matching algorithm to develop a good reduced order model of the lower frequency modes of the system. It is shown how these vectors can be generated to eliminate the control and observation spillover from the residual system, so that the resulting closed loop system is a combination of the smaller closed loop systems coupled only through their dynamics. A similar approach based on aggregation using the sensor and actuator influence functions as the transformations is developed by Yam [69]. Using these functions, it is shown that the control and observation spillover can be eliminated between the aggregated and

residual systems. The control design is then done for the reduced order aggregated system, and then applied to full system. The influence of the control through the dynamic coupling of the two systems is investigated using a perturbation analysis.

One other important technique, which also employs a division in the control effort, is the High Authority/Low Authority [HAC/LAC] control design [3,27]. The degree of authority is a measure of the influence of the controller on the structure. The typical influences of the two control levels are shown in Figure 1.2. The objective of the LAC is to supplement the natural damping of the structure by providing some active damping at colocated sensors and actuators, thereby reducing the possibility of destabilization due to control and observation spillover (it increases the damping ratio for the region of uncertainty above zero). In this way, the LAC loop enhances the stability characteristics of the structure, see reference [6]. Research by Bernstein [10] on the control of uncertain systems has shown that the optimal control design approaches that of rate feedback for the higher frequency modes. Consequently, including the LAC offsets some of the uncertainties in the plant model. The HAC loop is designed to meet the performance specifications for the plant. Any design technique can be employed at this level. Reference [27] employs a frequency shaped cost functional approach, but the designer could just as easily employ a modal space controller [45]. An important characteristic of this architecture is that there is no coordination between the control effort of the two levels. The input/output requirements of this approach are the same as those for a single central controller as the HAC loop generally will require all of the measurements to determine the control forces.

The control approach to be discussed in this thesis is also hierarchic in nature [29]. It is specifically developed for *intelligent* structures which have many densely packed actuators and sensors. The feasibilty of such structures is made possible by the development of small piezo-electric actuators and other forms of sensors that are suitable to be directly imbedded in a composite structure reference [21,22]. In

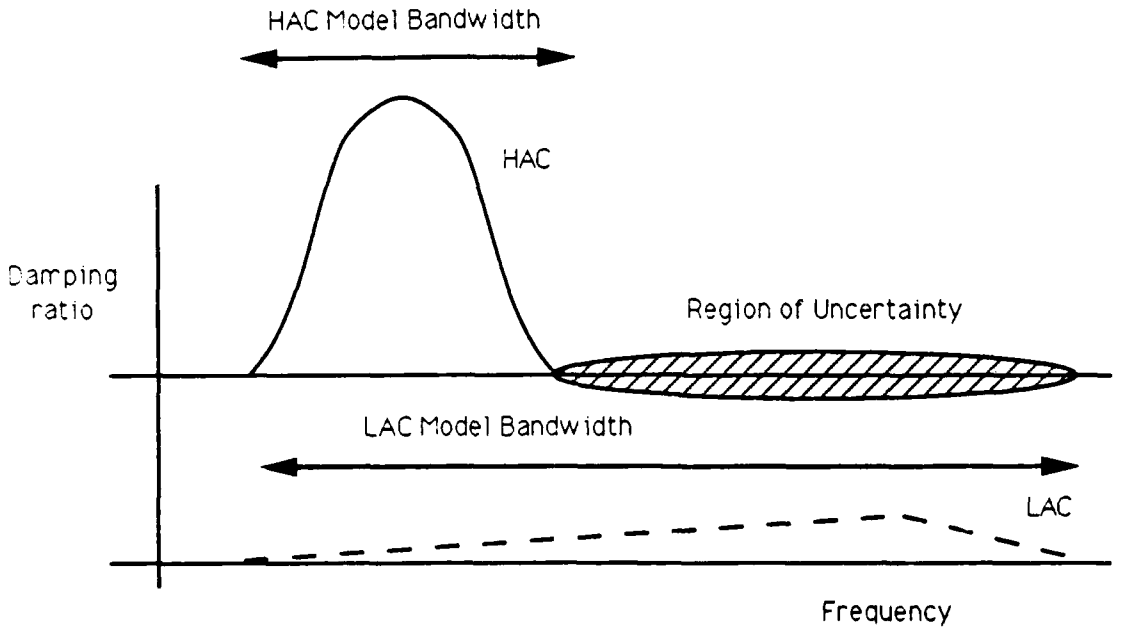

Figure 1.1: A typical HAC/LAC design.

fact, it is explicitly assumed in this analysis that there are enough actuators on the structure that a model condensed to this size would still accurately reflect the dynamics of the structure, at least for the lower frequency modes. A typical example of the applicability of this control architecture would be the shape control of a mirror surface whose back surface is covered with these piezo-electric actuators. In contrast to some of the other techniques already discussed which are aimed at controlling structural vibrations with only a few actuators and sensors, in this research it is assumed that there are hundreds or thousands of these devices on the structure. In this case, efficiently handling the amount of information available to the controller becomes an important issue.

The aim of this hierarchic architecture is to take advantage of the number of actuators and sensors and to distribute the control function between two types of controllers. This will reduce both the computational burden and the input/output requirements of any one processor. This is done in a way which complements the dynamic behavior of the plant, so that the processing is distributed to reflect the

physical distribution of the information flow in the structure.

As mentioned, the hierarchic architecture considered here consists of two levels, though reference [48] discusses the possibility of extending this to several more levels. As will be discussed in detail in Chapter 2, the first level consists of many regional processors which interface with the actuators/sensors in separate regions of the structure. The control at this level is regionally banded so that the processors are, in some sense, independent. This will be discussed in far more detail in Chapters 2 and 3. The second level consists of a global processor whose task is to coordinate the lower level controllers and perform the "global" control functions. In this implementation, the emphasis is more on the performing of the global control functions, as little local coordination will be required. In this way, some of the benefits (parallel in nature) but not the all of the disadvantages (retains a lot of global control authority) of both the centralized and decentralized schemes have been incorporated into one architecture.

The hierarchic control architecture that is discussed in this report is an improvement over other technique because it allows the designer to perform independent control development at the global and local levels, not just successive loop closure. It also allows for a far more sophisticated inner loop, a point that is the major theme of Chapter 3. The key benefit, though, is in the way that the measurements are processed. The information is independently aggregated by the local controllers at the lower level and then a reduced subset is passed to the central processor. This procedure will be discussed in far more detail in Chapter 2. Finally, this method provides virtually equivalent performance to the Linear Quadratic Regulator (LQR), but it is implemented in a much more computationally efficient manner.

Most of the ground work for this control architecture is detailed in references [48] and [67]. These cover the initial investigation of the computer structure and the ability of this control architecture to meet the specified performance objectives. The aim of this research was to expand the original control design and relax some of

the restrictions placed on the structure and the approach. The main emphasis has been on developing a set of local controllers which meet various conditions on the amount of information that is available. The final goal of the research effort is to be able to make a decision about which form of the local controller to employ based on a cost analysis which incorporates both the implementation and control issues. With this in mind, the various forms of the local controller are analyzed in terms of both their performance and communication requirements.

1.3 Overview

Chapter 2 presents an outline of the hierarchic control architecture. The decoupling of the structure into two subsystems is presented, as are the equations for implementating the two controllers. Various methods for reducing this coupling are also discussed. The final architecture is shown in Figure 2.4. The chapter then concludes with an outline of the design algorithm.

The purpose of Chapter 3 is to investigate several designs for the local controller. The four cases introduced are distinguished by the restrictions placed on the amount of information available for the calculation of the commands. The most basic design only allows colocated feedback at the local level. The next level of sophistication allows sensor to actuator feedback within a restricted neighborhood of the plant. The two remaining designs then relax this restriction even more so that adjacent processors can communicate directly. Several numerical examples are given for these local controllers.

Chapter 4 presents an example to show the high level of performance that can be obtained with this hierarchic architecture. The model used in this chapter is a long uniform beam. Several implementation issues are also addressed. Also, the performances of several local controllers are compared.

Chapter 5 discusses several other issues concerning the implementation of this

controller, the most important of which is the operations count for each type of local controller. Finally, Chapter 6 discusses the contributions of this research and suggests several possible extensions.

Chapter 2

Hierarchic Control

2.1 Introduction

The purpose of this chapter is to provide an overview of the development of a two-level echelon hierarchic control methodology for implementation on Flexible Large Scale "Intelligent" Structures. An intelligent structure is defined here as being one which has a high density of sensors and actuators, and even possibly microcomputers. This discussion will concentrate on the development of the control architecture and the assumptions about the structure. The rest of the chapter is organized in the following manner. The division of control authority between the two levels is outlined in Section 2.4 after a brief discussion of the overall architecture in Section 2.2. The purpose of Section 2.3 is to analyze the technique of mass condensation which is employed to eliminate the un-actuated states from the structural model. Sections 2.5 and 2.6 discuss ways to reduce the coupling between the two design models, the final section presents the algorithm for the control synthesis.

As a basic overview of the architecture, a schematic is shown in Figure 2.1. At level one, the local controllers sense and actuate on the structure directly, communicate the reduced information set to the global controller, and perform the local

control. At the second level, the global controller exchanges information directly with the local controllers, and it performs the global control tasks. There is also the possibility that the local controllers are linked at level one and that some form of communication is feasible.

Most of this work was originally presented by Hall *et al.* in reference [29] and it follows from the original work by Ward in reference [67]. The goal of this chapter is to show that this control architecture provides a feasible way to meet the required performance specifications and that it offers several benefits over other methods of controlling the vibratory motion of large structures, especially as the number of sensors and actuators becomes very large. These advantages will be discussed as the architecture is developed.

2.2 Architecture

The fundamental idea behind the hierarchic control formulation presented here is to develop a parallelism between the element/global hierarchy of a structural model and the regional/global hierarchy of the active control. In structural dynamic analysis it is not uncommon to model elements or components of the structure in detail, and then, by techniques such as component mode analysis or condensation, extract from the detailed local models that information which governs the overall or global motion. In a parallel manner, local controllers should be able to regulate the detailed behavior within a component or region, while the coordinated effort of a global controller regulates the gross or overall motion. From a physical perspective, just as short wavelength disturbances are propagated in a structure locally, the short wavelength control is performed by the local controllers. As it is possible for long wavelength disturbances to develop into modes, there is a global controller for control of the overall motion.

The point of departure of the structural modeling is assumed to be a condensed

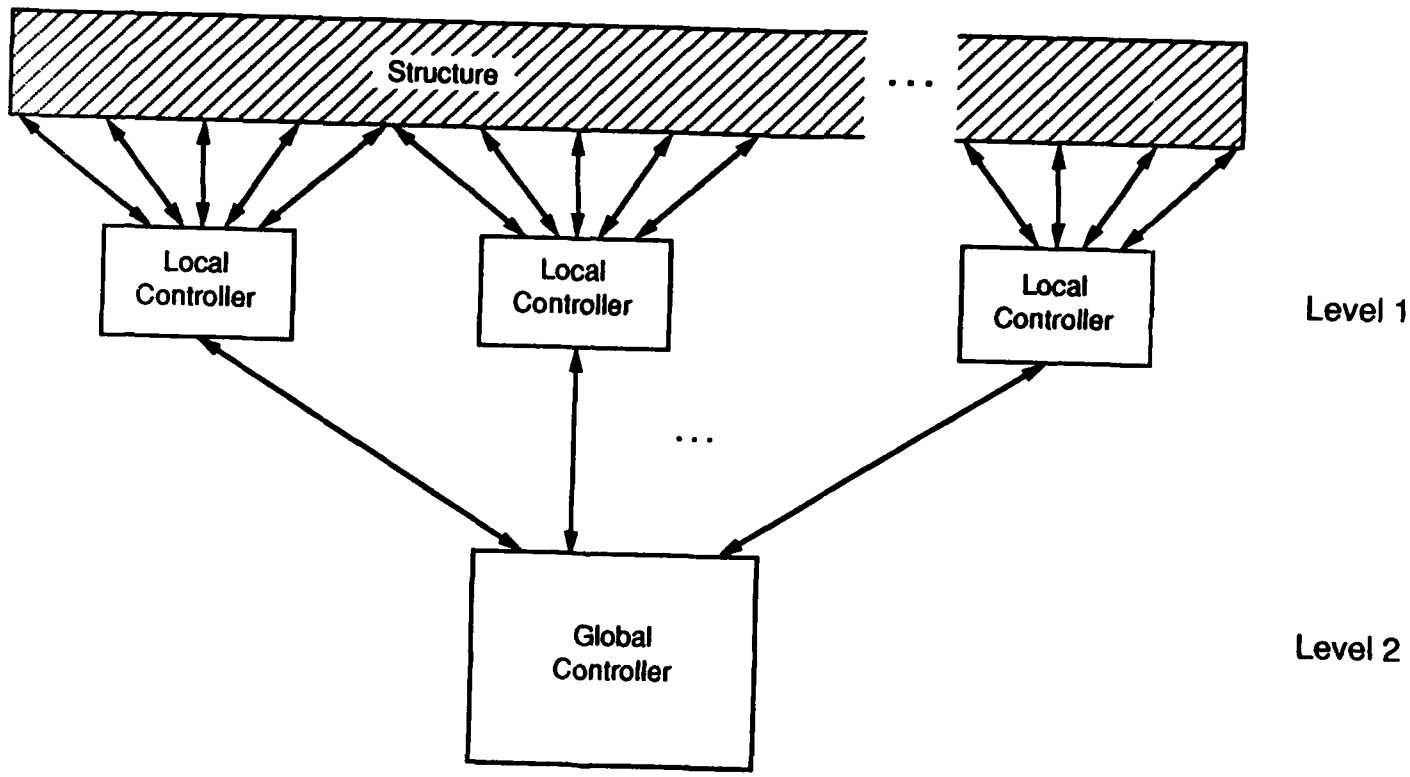

Figure 2.1: A two-level echelon feedback architecture for the implementation of hierarchic control.

finite dimensional model of the structure and its associated degrees of freedom q, see Figure 2.2. This condensation procedure will be outlined in the following section. The purpose of this step is to produce an fairly accurate model of the structure which has an actuator and sensor at each structural node. In this way, both the measurement and control influence matrices to be introduced in Section 2.3 are of full rank.

The coarser or global model represents the structural motion by the displacements q_g at discrete node points located at the boundaries of the finite control elements. The global displacements are related to the degrees of freedom of the original finite dimensional model by the element interpolation functions (*e.g.*, T_{g2}^1), in a manner discussed below. Likewise, there are forces Q in the original model associated with the degrees of freedom q, and global forces Q_g which can be thought of as acting at the global node points.

The corresponding division of control functions in a two-level hierarchic controller is outlined in Figure 2.3. The global controller is responsible for implementing control functions based on the global states $x_g^T = [q_g^T \; \dot{q}_g^T]$. The objective of the global controller is to control the overall behavior of the structure. The three basic tasks which are involved in implementing the global control are shown in Figure 2.3: the measurement aggregation, which reduces the measurements y into measurements of the states in the global model x_g; the computation by the global controller of the global control commands Q_g based on the global states; and the distribution of the global control which calculates the physical control forces u_g to be applied to the structure. Note that both the measurement aggregation and the control distribution require communication with the structure through the local controllers, so that these functions are performed cooperatively between the global and regional processors.

There are a number of regional controllers, each associated with a finite control element. Each operates on the residual e, the difference of the actual local mea-

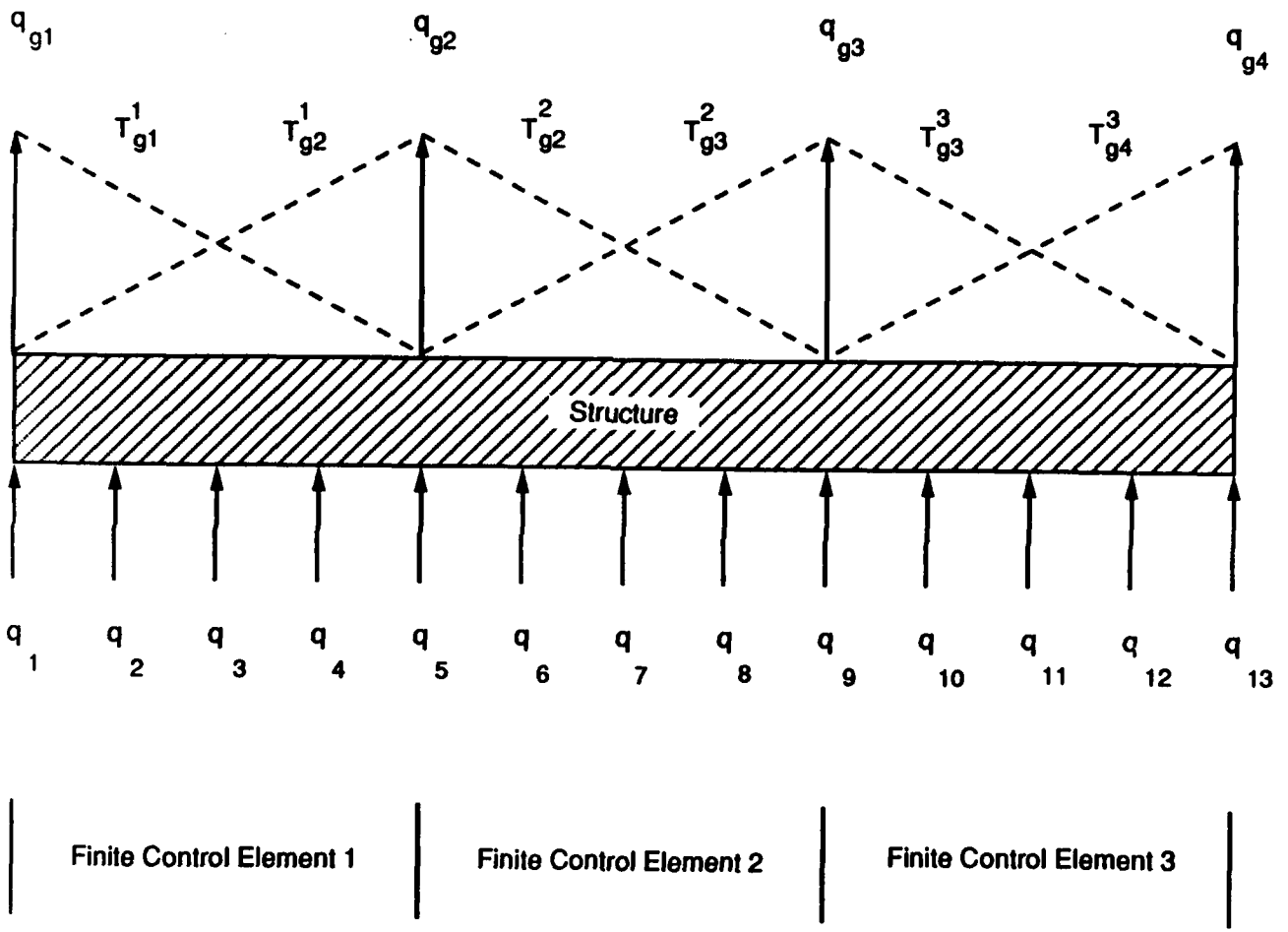

Figure 2.2: A representation of a finite-dimensional model by a coarse or global finite element model denoted by $(\cdot)_g$. The shape functions $T^i_{g_j}$ relate the structural nodes in element (i) to global node (j).

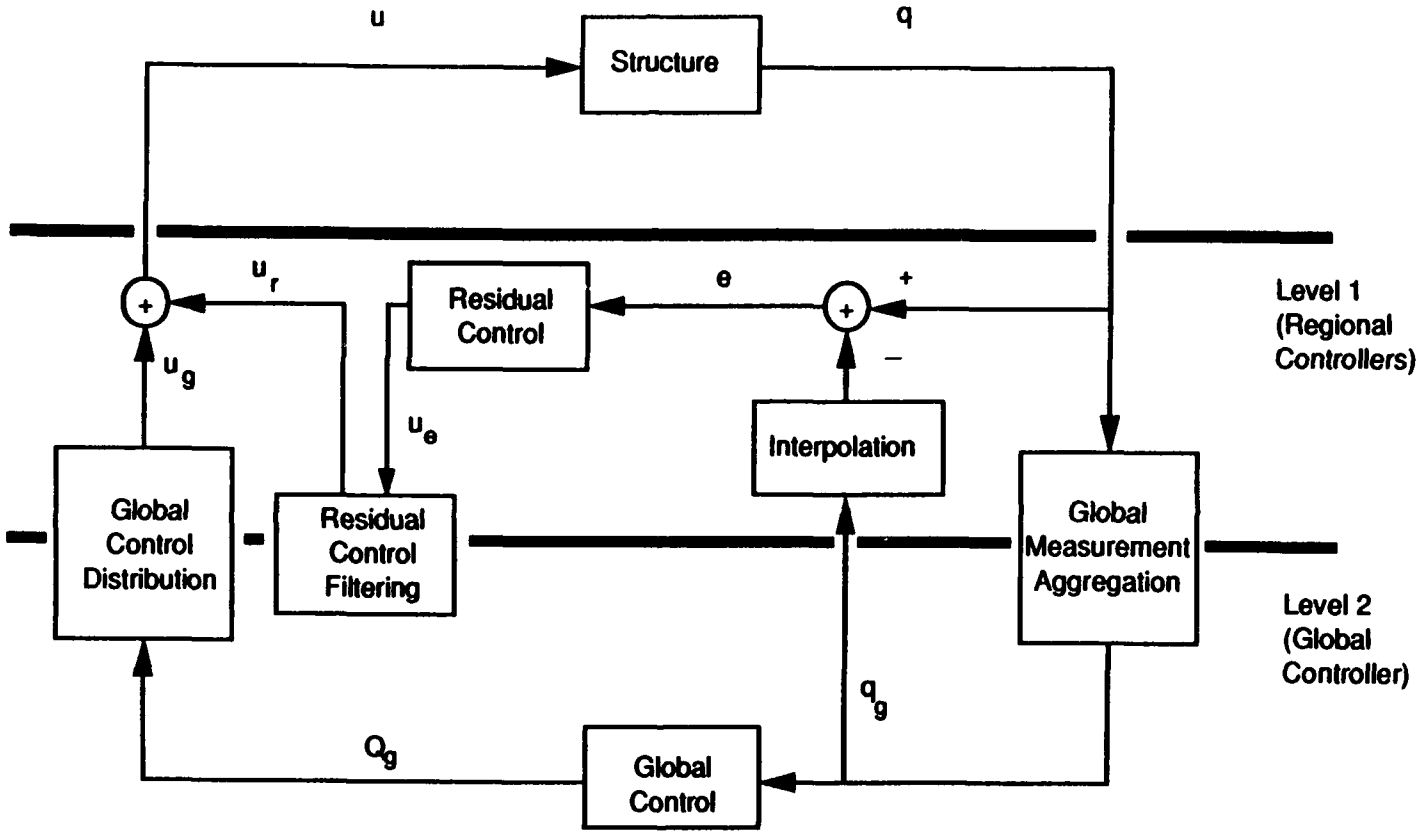

Figure 2.3: The division of control functions in a two-level hierarchic controller. The measurement aggregation, the control distribution, and the residual filtering tasks are shared between the two levels.

surements y and the interpolation of the local estimates from the global states x_g. The specific objective of the regional controller is to perform inner loop compensation within each region on this residual in order to force the structure to track the behavior expected by the global model. The residual controller calculates control forces u_e, which are then spatially filtered to ensure that the global modes are not excited by the residual control. It will be seen that this spatial filtering is more easily accomplished by a cooperative effort between the global and regional processors than by the regional processors alone. The resulting control command, u_r, is added to the global control u_g to form the total control command u to the structure.

2.3 Mass Condensation

As was mentioned in the previous section, a condensation procedure is employed to eliminate the unactuated states from the evaluation model. This section will introduce two condensation techniques. It will be shown that the appropriate one to employ depends on the form of the mass matrix.

For large scale examples, it has been common practice [2,44] to use the approximate lumped form of the mass matrix for the finite element method (FEM) of modelling structures. The assumption here is that the structure can be represented as a collection of point masses with no moments of inertia. The mass matrix then takes the form of having the lumped masses as the diagonal elements for the translational degrees of freedom and zeroes for the rotational ones. Zero entries along the diagonal of the mass matrix correspond to displacements which are not critical to the problem and can be eliminated. This technique is particularly useful for the reduction of the size of an eigenvalue problem. It is noted that this procedure, called *static condensation*, is as accurate as the assumption that the lumped mass matrix is a good approximation of the consistent mass matrix, as no extra assumptions are made beyond that point. How accurate a model this approximation can provide

will be discussed in Chapter 4.

There is also a similar approach when the inertia forces of a subset of the states can be considered to be far more important than those for the rest of the states. This distinction between master (the former set) and slave (the latter) coordinates was first proposed by Irons in reference [31]. This procedure is also commonly known as both *mass condensation* [44] and *Guyan reduction* [28].

As detailed in reference [31], slave displacements should be selected as those states which are associated with areas of high stiffness and low mass. In particular, the rotational degrees of freedom of a beam or a plate are given as good examples of slave degrees of freedom.

The basic argument is to ignore the inertial forces on the slave degrees of freedom and to assume that they are in static equilibrium. This is equivalent to assuming that the potential energy of the system has a minimum with respect to the slave displacements. Since the elements of the mass matrix for the slave degrees of freedom are small but not zero, this assumption is only approximately valid, so an error is introduced at this point.

Reordering the states of the original model and grouping them as master and slave yields

$$q = \begin{bmatrix} q_m \\ q_s \end{bmatrix} \tag{2.1}$$

and the potential and kinetic energies can be written as

$$V = \frac{1}{2} q^T K q \tag{2.2}$$

$$T = \frac{1}{2} \dot{q}^T M \dot{q} \tag{2.3}$$

where the system mass and stiffness matrices can now be partitioned in the following symmetric forms

$$K = \begin{bmatrix} K_{mm} & K_{ms} \\ K_{sm} & K_{ss} \end{bmatrix} \tag{2.4}$$

$$M = \begin{bmatrix} M_{mm} & M_{ms} \\ M_{sm} & M_{ss} \end{bmatrix} \tag{2.5}$$

where $(\cdot)_{sm} = (\cdot)_{ms}^T$. Then, assuming equilibrium, and taking the first derivative of the potential energy of the system with respect to the slave coordinates yields the following constraint

$$\frac{\partial V}{\partial q_s} = K_{sm} q_m + K_{ss} q_s = 0 \tag{2.6}$$

This constraint equation allows the full set of states in Equation 2.1 to be expressed in terms of only the master degrees of freedom using the transformation

$$C = \begin{bmatrix} I \\ -K_{ss}^{-1} K_{sm} \end{bmatrix} \tag{2.7}$$

where the inverse of K_{ss} is assumed to exist. This would be expected to be the case since the master degrees of freedom are assumed to contain sufficient information to model the rigid body modes of the plant. The resulting condensed mass and stiffness matrices can then be obtained in the following way:

$$K_{cond} = C^T K C = K_{mm} - K_{ms} K_{ss}^{-1} K_{sm} \tag{2.8}$$

$$\begin{aligned} M_{cond} = C^T M C &= M_{mm} - K_{ms} K_{ss}^{-1} M_{sm} - M_{ms} K_{ss}^{-1} K_{sm} \\ &\quad + K_{ms} K_{ss}^{-1} M_{ss} K_{ss}^{-1} K_{sm} \end{aligned} \tag{2.9}$$

As is discussed in [44], this is an approximation, and it can be shown to be equivalent to ignoring the terms in the expansion of the eigenvalue problem $Ku = \lambda Mu$ which are of order λ^2 and higher. This approximation is valid for low frequencies only if the coefficients of these terms are small compared to the condensed mass and stiffness matrices. This is true if the slave degrees of freedom are associated with states that have low mass and high stiffness. Although it was not shown here, the form of the stiffness matrix is the same for the mass and static condensations, which indicates that no information has been lost in the stiffness terms. However,

it can be seen from Equation 2.9 that the condensed mass matrix now includes information from the stiffness matrix so the eigenvalue problem has been changed slightly. In reference [28] it is reported that the resulting eigenproblem is closely but not exactly preserved. Archer [2], does a comparative analysis of the accuracy that can be achieved by condensing out certain degrees of freedom of the structure. In particular, the rotational degrees of freedom of a free-free beam are condensed out. The results of the tests seem to indicate that the agreement between the condensed and consistent models are very good for the lower frequency modes. These results will be discussed in more detail in Chapter 4.

2.4 Defining the Global and Residual Coordinates

In view of the architectural objectives, it is necessary to derive a partitioning of the structural dynamic model which achieves the greatest possible dynamic decoupling of the global and residual models. The first step is the suitable definition of the global and residual coordinates. The dynamics of the structure are first represented in the form of an evaluation model which contains all of the degrees of freedom of the system. Following the format of the previous section, the state vector q is then partitioned into two subsets, namely the master and slave coordinates, so the state equation becomes

$$\begin{bmatrix} M_{mm} & M_{ms} \\ M_{sm} & M_{ss} \end{bmatrix} \begin{bmatrix} \ddot{q}_m \\ \ddot{q}_s \end{bmatrix} + \begin{bmatrix} K_{mm} & K_{ms} \\ K_{sm} & K_{ss} \end{bmatrix} \begin{bmatrix} q_m \\ q_s \end{bmatrix} = \begin{bmatrix} \Psi \\ 0 \end{bmatrix} u \tag{2.10}$$

where it is assumed that only the master states are actuated upon directly.

Employing the technique of mass condensation and noting that

$$C^T \begin{bmatrix} \Psi \\ 0 \end{bmatrix} = \Psi \tag{2.11}$$

the condensed dynamics of the structure can then be represented by an undamped

finite dimensional model of the form

$$M_{cond}\ddot{q} + K_{cond}q = \Psi u = \Psi(u_g + u_r) \tag{2.12}$$

where $q \in R^n$ is the vector of the generalized coordinates, $u \in R^m$ is the vector of control inputs, $M \in R^{n\times n}$ is a symmetric, positive definite mass matrix, $K \in R^{n\times n}$ is a symmetric, positive semidefinite stiffness matrix, and $\Psi \in R^{n\times m}$ is the control influence matrix. Note that, because of the form of the design model discussed in the previous section (*i.e.*, a condensed model), complete measurements of all states (q and $\dot{q}$) are available, and the system has as many non-redundant actuators as generalized coordinates (*i.e.*, Ψ is square and full rank). The subscript $(\cdot)_{cond}$ will now be dropped for notational convenience.

The coarser or global model is assumed to have n_g degrees of freedom, and associated interpolation functions, represented by the matrix $T_g \in R^{n\times n_g}$. Then the actual displacements are a sum of the interpolated displacements of the global model and a vector of n residuals

$$q = T_g q_g + e \tag{2.13}$$

where $q_g \in R^{n_g}$, and $e \in R^n$. For any set of actual displacements q and assumed interpolation functions T_g, q_g can be defined so as to minimize a weighted quadratic of the residual error

$$J = e^T W e \tag{2.14}$$

where W is an appropriately selected positive definite weighting matrix. Although there are n entries in e, there are only $n_r = n - n_g$ independent degrees of freedom designated q_r, so that e may be expressed as

$$e = T_r q_r \tag{2.15}$$

where $T_r \in R^{n\times n_r}$ is yet to be determined. The actual displacements can then be expressed in terms of the global displacements and the residual coordinates as

$$q = T_g q_g + T_r q_r = \begin{bmatrix} T_g & T_r \end{bmatrix} \begin{bmatrix} q_g \\ q_r \end{bmatrix} \tag{2.16}$$

The condition that q_g is defined so as to minimize Equation 2.14 establishes that the global degrees of freedom are related to the original degrees of freedom q by

$$q_g = \left(T_g^T W T_g\right)^{-1} T_g^T W q = T_g^{-L} q \tag{2.17}$$

where the superscript $(\cdot)^{-L}$ denotes the left pseudoinverse of $(\cdot)$. The global degrees of freedom determined by Equation 2.17 will produce the best weighted least squares fit to the actual displacements. By substituting Equation 2.16 into Equation 2.17, or equivalently, using the optimal projection theorem [32], one obtains

$$T_g^T W T_r = 0 \tag{2.18}$$

indicating that the two subspaces spanned by the columns of the matrices T_g and T_r are orthogonal with respect to the weighting matrix W. The substitution of Equation 2.17 into Equation 2.13 yields this expression for the residuals e in terms of the displacements q

$$e = (I - T_g T_g^{-L}) q \tag{2.19}$$

Similarly, the expression for the residual degrees of freedom q_r in terms of q is given by

$$q_r = T_r^{-L} q \tag{2.20}$$

T_r may be determined by a number of methods, e.g., by performing a Gram-Schmidt orthogonalization on any set of n_r columns that, when combined with the columns of T_g, form a linearly independent set. Note, however, that the columns of T_r are not unique; the only requirement is that they span the subspace that is orthogonal (with respect to the weighting matrix W) to the column space of T_g. Furthermore, it will be seen that in many cases it is not necessary to calculate T_r in order to develop the hierarchic controller.

2.5 Decoupling the Control/Structural Model

Having established the relationships among the various representations of the degrees of freedom q, q_r, q_g, and e, these relationships can be used to analyze the extent to which the dynamics of the global and residual degrees of freedom's can be decoupled. To examine the subspace coupling, Equation 2.16 is substituted into Equation 2.12 and pre-multiplied by $[T_g\, T_r]^T$ to give

$$\begin{bmatrix} T_g & T_r \end{bmatrix}^T M \begin{bmatrix} T_g & T_r \end{bmatrix} \begin{bmatrix} \ddot{q}_g \\ \ddot{q}_r \end{bmatrix} + \begin{bmatrix} T_g & T_r \end{bmatrix}^T K \begin{bmatrix} T_g & T_r \end{bmatrix} \begin{bmatrix} q_g \\ q_r \end{bmatrix} = \begin{bmatrix} T_g & T_r \end{bmatrix}^T \Psi(u_g + u_r) \tag{2.21}$$

The degree of coupling in each of the three terms of Equation 2.21 can now be examined. The first step is to expand the control influence terms on the right hand side. The inputs u_g are the physical forces based on the n_g commanded global forces Q_g, each associated with a global displacement q_g. The global forces Q_g are distributed into the physical inputs u_g according to a relation of the form

$$u_g = S_g Q_g \tag{2.22}$$

where S_g is the global force distribution matrix. Assuming that a global state feedback law will be derived by an appropriate method, the global forces are given by

$$Q_g = -F_g q_g - F_{\dot{g}} \dot{q}_g \tag{2.23}$$

The residual control forces will similarly be commanded (within a finite control element) by the residual controller. The physical forces will be distributed as

$$u_r = S_e Q_e \tag{2.24}$$

where Q_e is the vector of the n commanded forces associated with the residuals e, which are of course related to the residual degrees of freedom q_r through Equation 2.15. Assuming a state feedback law for the residuals given by

$$Q_e = -F_e e - F_{\dot{e}} \dot{e} \tag{2.25}$$

completes the description of the control inputs.

The nature of the coupling of the global and residual degrees of freedom's can be evaluated by substituting Equations 2.15, 2.22, 2.23, 2.24 and 2.25 into Equation 2.21 giving

$$\begin{bmatrix} T_g^T M T_g & T_g^T M T_r \\ T_r^T M T_g & T_r^T M T_r \end{bmatrix} \begin{bmatrix} \ddot{q}_g \\ \ddot{q}_r \end{bmatrix} + \begin{bmatrix} T_g^T K T_g & T_g^T K T_r \\ T_r^T K T_g & T_r^T K T_r \end{bmatrix} \begin{bmatrix} q_g \\ q_r \end{bmatrix} =$$

$$- \begin{bmatrix} T_g^T \Psi S_g F_g & T_g^T \Psi S_e F_e T_r \\ T_r^T \Psi S_g F_g & T_r^T \Psi S_e F_e T_r \end{bmatrix} \begin{bmatrix} q_g \\ q_r \end{bmatrix} - \begin{bmatrix} T_g^T \Psi S_g F_{\dot{g}} & T_g^T \Psi S_e F_{\dot{e}} T_r \\ T_r^T \Psi S_g F_{\dot{g}} & T_r^T \Psi S_e F_{\dot{e}} T_r \end{bmatrix} \begin{bmatrix} \dot{q}_g \\ \dot{q}_r \end{bmatrix} \quad (2.26)$$

or, equivalently

$$\begin{bmatrix} M_{gg} & M_{gr} \\ M_{rg} & M_{rr} \end{bmatrix} \begin{bmatrix} \ddot{q}_g \\ \ddot{q}_r \end{bmatrix} + \begin{bmatrix} K_{gg} & K_{gr} \\ K_{rg} & K_{rr} \end{bmatrix} \begin{bmatrix} q_g \\ q_r \end{bmatrix} =$$

$$- \begin{bmatrix} F_{gg} & F_{gr} \\ F_{rg} & F_{rr} \end{bmatrix} \begin{bmatrix} q_g \\ q_r \end{bmatrix} - \begin{bmatrix} F_{g\dot{g}} & F_{g\dot{r}} \\ F_{r\dot{g}} & F_{r\dot{r}} \end{bmatrix} \begin{bmatrix} \dot{q}_g \\ \dot{q}_r \end{bmatrix} \quad (2.27)$$

Equation 2.27 should now be examined in light of the stated objective of minimizing the coupling between the global and residual systems. There are four matrices in Equation 2.27 which must be decoupled, although the two control influence matrices on the right hand side are of very similar form.

By comparing the off-diagonal blocks of the transformed mass and stiffness matrices with Equation 2.18, it is clear that the appropriate choice of W in the definition of q_g can cause either the off-diagonal terms of the mass or the stiffness matrices to be driven to zero. Choosing W to be M would inertially decouple the residuals, whereas choosing W to be K would elastically decouple them. In that M is positive definite it is the preferred choice. Furthermore, the selection of W equal to M would cause Equation 2.18 to resemble the primary orthogonality relation of the dynamic system.

The choice of the defining weighting matrix W to be M identically sets M_{gr} and M_{rg} equal to zero, thereby block diagonalizing the transformed mass matrix of Equation 2.27. However, to some extent, it also diagonalizes the stiffness matrix. In the ideal case, the n_g modes of the original system can be exactly represented by q_g coordinates and their associated shape functions T_g, such that all of the modes can be given by

$$\Phi = \begin{bmatrix} T_g & T_r \end{bmatrix} \begin{bmatrix} A_g & 0 \\ 0 & A_r \end{bmatrix} \tag{2.28}$$

where Φ is a $n \times n$ matrix of eigenvectors of M and K, A_g is an $n_g \times n_g$ matrix of coefficients and A_r is an $n_r \times n_r$ matrix of coefficients. In such a case, T_g contains the exact shapes of n_g modes, and

$$T_g^T K T_r = K_{gr} = 0 \tag{2.29}$$

In the less ideal case when T_g closely approximates a subset of n_g modes of the original system, the off-diagonal terms of the stiffness matrix K_{gr} are small compared to K_{gg} and K_{rr}. Clearly, this is a desirable property to have in the shape functions.

The matrices on the right hand side of Equation 2.26 can be block diagonalized by proper choice of constitutive matrices. Examining the lower left hand term F_{rg} (or equivalently $F_{r\dot{g}}$), which expresses the spillover of the global control into the residual model, we have that

$$F_{rg} = T_r^T \Psi S_g F_g \tag{2.30}$$

T_r has been established by the initial choice of shape functions and Equation 2.18, and Ψ by the location and type of the actuators. One would prefer not to place restrictions on F_g or $F_{\dot{g}}$ which would complicate the subsequent control design synthesis. Therefore, only the form of the global force distribution matrix S_g can be specified so as to drive this term to zero. In the case of Ψ invertible, a sufficient choice is

$$S_g = \Psi^{-1} M T_g \tag{2.31}$$

which has the units of mass. A rationally normalized sufficient choice is

$$S_g = \Psi^{-1} M T_g \left(T_g^T M T_g \right)^{-1} = \Psi^{-1} T_g^{-LT} \tag{2.32}$$

where the superscript $(\cdot)^{-LT}$ denotes the transpose of the left pseudoinverse. Substituting Equation 2.32 into Equation 2.22 gives

$$\Psi u_g = T_g^{-LT} Q_g \tag{2.33}$$

The implication of this equation is that the n_g global control forces are distributed to the n actuators using the same shape functions and weighting matrices as are used in aggregating the information of the n sensors to form the n_g global displacements in Equation 2.17. This symmetry of global state aggregation and global control distribution results from the requirements that the global and residual degrees of freedom be uncoupled, both in the inertial term in the dynamics equation, and in the feedback term.

The upper right hand entry F_{gr}, which expresses the spillover of the residual control into the global modes, is

$$F_{gr} = T_g^T \Psi S_e F_e T_r \tag{2.34}$$

Again, T_g, T_r and Ψ have already been prescribed, so a proper choice of S_e coupled with a form of F_e must be made to drive this term to zero. One sufficient choice is

$$S_e = \Psi^{-1} M T_r T_r^T \tag{2.35}$$

which parallels Equation 2.31. Similarly, a normalized version of this is

$$S_e = \Psi^{-1} M T_r (T_r^T M T_r)^{-1} T_r^T = \Psi^{-1} T_r^{-LT} T_r^T \tag{2.36}$$

At this point, all of the coupling terms of Equation 2.26 have been examined. The choice of W to be M in Equation 2.14 plus the expressions in Equations 2.32

and 2.36 reduce Equation 2.26 to

$$\begin{bmatrix} M_{gg} & 0 \\ 0 & M_{rr} \end{bmatrix} \begin{bmatrix} \ddot{q}_g \\ \ddot{q}_r \end{bmatrix} + \begin{bmatrix} K_{gg} & K_{gr} \\ K_{rg} & K_{rr} \end{bmatrix} \begin{bmatrix} q_g \\ q_r \end{bmatrix} =$$
$$- \begin{bmatrix} F_g & 0 \\ 0 & T_r^T F_e T_r \end{bmatrix} \begin{bmatrix} q_g \\ q_r \end{bmatrix} - \begin{bmatrix} F_{\dot{g}} & 0 \\ 0 & T_r^T F_{\dot{e}} T_r \end{bmatrix} \begin{bmatrix} \dot{q}_g \\ \dot{q}_r \end{bmatrix} \tag{2.37}$$

where the mass and control influence matrices are completely uncoupled, and the stiffness matrix is uncoupled to the extent that T_g models n_g of the modes of the original finite dimensional system.

The effect of the global and residual control on the original finite dimensional model can also be determined by substituting Equations 2.17, 2.20, 2.22, 2.23, 2.24, 2.25, 2.32, and 2.36 into Equation 2.12 to obtain

$$\begin{aligned} M\ddot{q} + Kq = & - \left\{ T_g^{-LT} F_g T_g^{-L} + T_r^{-LT} T_r^T F_e T_r T_r^{-L} \right\} q \\ & - \left\{ T_g^{-LT} F_{\dot{g}} T_g^{-L} + T_r^{-LT} T_r^T F_{\dot{e}} T_r T_r^{-L} \right\} \dot{q} \end{aligned} \tag{2.38}$$

The physics of the control decoupling can be seen by examining the first of the two terms on the right hand side of Equation 2.38. Examining the terms in detail, the role of T_g^{-L} is to aggregate or average the elements of q to determine the global coordinates q_g. Multiplying by the matrix F_g produces the global forces Q_g (due to displacement feedback), which are then distributed by T_g^{-LT}. The roles of T_r, T_r^{-L}, and F_e are similar in the residual subspace. T_r^{-L} aggregates the measurements to form the residual coordinates q_r, and then T_r redistributes them to form the vector of the residuals e. F_e then multiplies e to produce the residual forces Q_e. Finally, $T_r^{-LT} T_r^T$ acts as a spatial filter, which produces forces which affect only the residual degrees of freedom q_r. This may be seen by use of the identity

$$T_r T_r^{-L} = I - T_g T_g^{-L} \tag{2.39}$$

That is, $T_r^{-LT} T_r^T$ is a projection matrix which, when multiplying Q_e, eliminates those components of force which affect the q_g subspace.

An alternative way to write the first term on the right hand side of Equation 2.38 is to use the relation 2.39 above to give

$$\Psi u_q = -\left\{T_g^{-LT} F_g T_g^{-L} + (I - T_g^{-LT} T_g^T) F_e (I - T_g T_g^{-L})\right\} q \qquad (2.40)$$

which suggests the architecture in Figure 2.4. (u_q is that part of the control u due to feedback of q.) Loop "o" is the process by which the global motion is filtered from the overall motion to form the residual (observation filtering). Loop "c" is the process by which the global component is filtered out of the residual commands (control filtering). Also shown in the figure is the distribution of the computing resources between global and residual controllers. Note that in this architecture, there is never a need to explicitly calculate T_r, or to determine q_r. Also, note that the processing is performed in such a way that the residual processors carry out most of the calculations in parallel at the local level, with the global processor performing control only on the global states q_g, as well as communicating this information to the residual controllers. It is interesting to note that Equations 2.38 and 2.40 show that the combination of the two sets of gains and the control architecture generate full gain matrices which have a specified internal structure.

At this point, this control architecture can be compared to the HAC/LAC design discussed in Chapter 1. A comparison of the control architectures for the two designs is shown in Figure 2.5. The first point to consider is one of the key issues of this control design. The assumption that the structure is "intelligent" implies that there are many sensors and actuators for the controller to govern. The advantage of this hierarchic control architecture is that the work load is separated between the two levels. The measurements are aggregated before any communication with the global processor is performed. This step can be implemented efficiently because the local controllers are distributed in such a manner as to complement the dynamic behaviour of the structure. The work at level one is also done in parallel which is the most efficient way to organize the effort. This aggregation procedure is split between the two levels so that each controller is only required to act on the information that

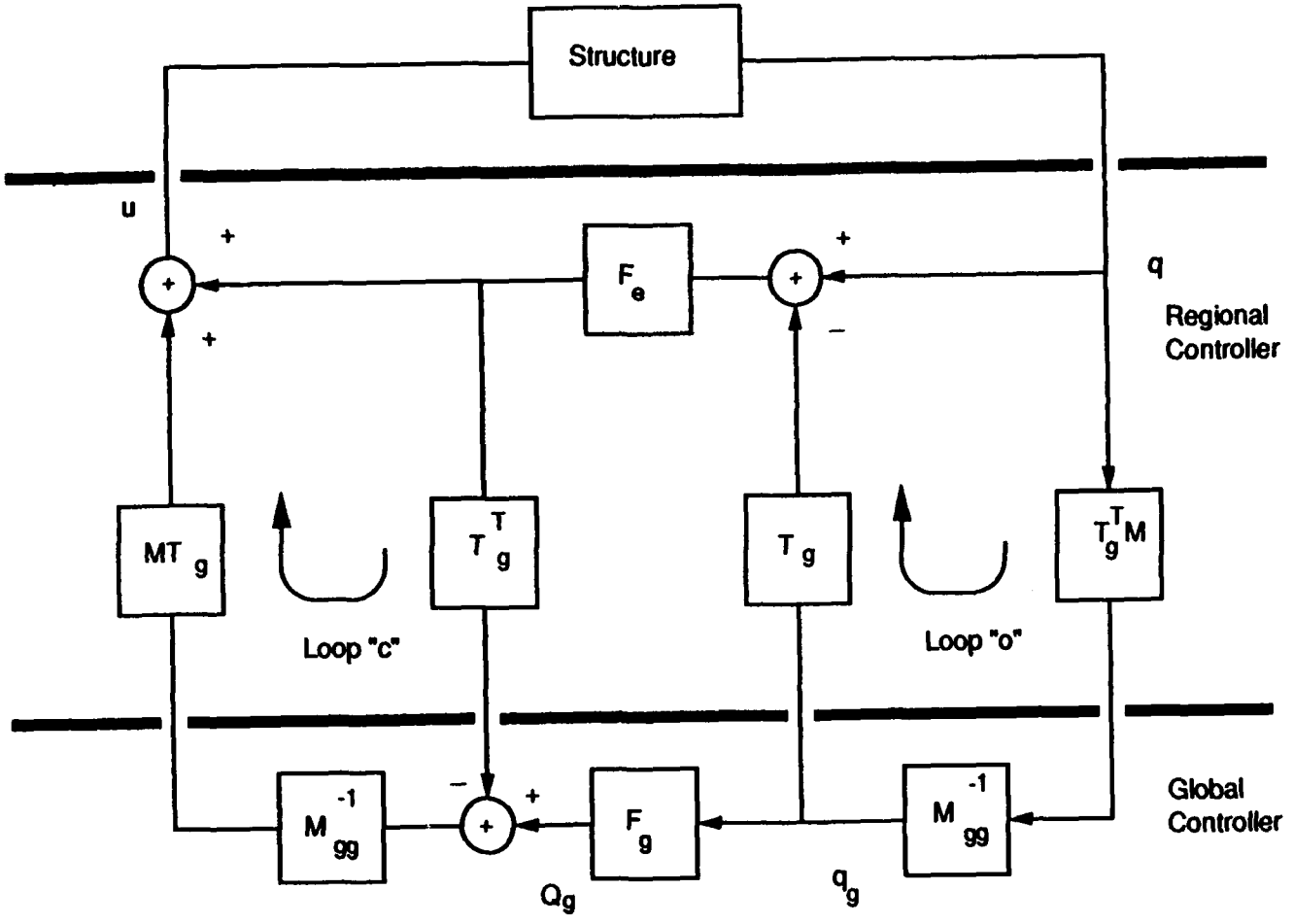

Figure 2.4: The hierarchic control architecture. This figure clearly shows the division of control effort between the two levels. Loop "o" is the observation filtering step which removes the global motion from the overall motion. Loop "c" is the control filtering step which eliminates the global component from the residual control commands.

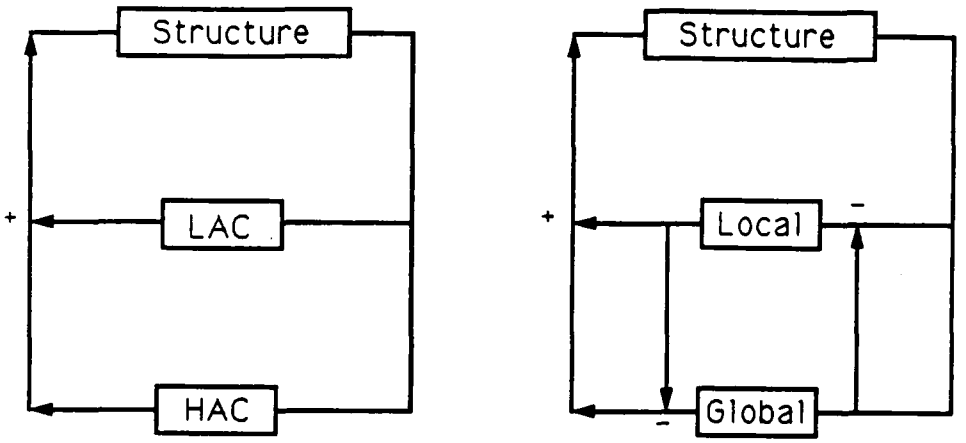

Figure 2.5: A comparison of the control architectures for the HAC/LAC (a) and hierarchic control designs (b).

is has directly available, a point which will be addressed in Chapter 4 when some of the implementation issues are discussed. In contrast, the HAC/LAC design will typically require all of the measurements to be transfered directly to the central computer to allow the commands to be calculated.

Another important issue involves spillover. Through the assumptions made about the plant, the observation and control spillover can be eliminated in the hierarchic design by adding the extra filtering arms in the loops. It is these two extra paths which differentiate the architectures in Figure 2.5. Since the global and residual subsystems are not completely decoupled, dynamic spillover will still exist. However, it is possible to modify the design to reduce the influence of this affect, see Section 2.6. The resulting architecture allows for independent control design at each of the two levels. In contrast, Figure 1.2 in Chapter 1 shows that typical HAC and LAC control designs overlap. This means that direct control spillover can occur.

Another point which is apparent from Figure 2.4 is that it would be beneficial

if the two control loops could be operated at different frequencies, since they are primarily targeted at different frequency modes of the vibratoion. However, it can be seen that the loops are not entirely independent, as the observation and control filtering loops should also operate at the higher rate. However, it is possible to implement them at the slower rate and accept a degradation in performance. This will be discussed in more detail in Chapter 5.

The transformed and untransformed state representations (Equations 2.37 and 2.38 respectively), which include the coupled residual and global control, have now been developed. The two remaining key questions are: (1) how to choose the shape function T_g so as to minimize the the stiffness matrix coupling; (2) how to synthesize the global and residual control to be regional in form.

2.6 Alternative Choices for the Element Interpolation.

A key issue that must be recognized at this point is that the number of global degrees of freedom and the shape functions must be selected to provide a good model of the important modes of both the open and closed loop systems. For the vibration control work performed here, this will typically be the set of lower frequency modes. Though it will depend on the performance requirements of the closed loop system, in general, it is not enough to choose the number of global degrees of freedom purely on the basis of providing a good model for the open loop modes. The number of degrees of freedom must also be selected so that the global controller has sufficient authority to place the "important" closed loop poles at the desired frequencies and damping ratios. The importance of a particular mode to the global cost function can be analyzed using the modal cost analysis by Skelton [63]. If the global model is made too small and does not acurrately reflect all of the important modes, then

the closed loop performance will be poor.

In forming Equation 2.16, several alternatives for the choice of T_g have been developed with the aim of minimizing the K_{gr} stiffness coupling term between the two subsystems.

Alternative 1. The first alternative to be considered is the option of keeping fewer modes in the global model than there are global degrees of freedom. This follows directly from common experience with finite element models in that, at best, the designer can have confidence in only the lower half of the modelled modes, and in general, the number is usually significantly less than this. In the model of the structure which includes only shapes which can be built up from T_g, some of the modes of the original finite dimensional system will be well modelled, but some (generally the upper frequency modes) will be modelled more poorly. Since, in general, the degree to which K_{gr} approaches zero depends on the ability of T_g to represent a subset of the modes of the original finite-dimensional model, it may be desirable to reduce the number of modes retained in the global model (n_l) to a value less than n_g, while keeping the number of global degrees of freedom at n_g. As in the discussion above, note that retaining only the lower frequency set of the global modes effectively reduces the bandwidth of the central controller and reduces the control authority. There may be a performance penalty associated with this step if the bandwidth is made too small.

The displacements of the original finite dimensional model were expressed in terms of the global displacements q_g and the residuals e as

$$q = T_g q_g + e \tag{2.13}$$

In this first alternative, let q_g be expanded by the modes of the global model

$$q_g = \begin{bmatrix} \phi_g^l & \phi_g^u \end{bmatrix} \begin{bmatrix} \xi_g^l \\ \xi_g^u \end{bmatrix} \tag{2.41}$$

where $(\cdot)^l$ refers to the lower (in frequency) set, and $(\cdot)^u$ to the upper set. Substituting Equation 2.41 into Equation 2.13,

$$q = T_g \begin{bmatrix} \phi_g^l & \phi_g^u \end{bmatrix} \begin{bmatrix} \xi_g^l \\ \xi_g^u \end{bmatrix} + e \tag{2.42}$$

If only the lower modes are to be maintained in the global model, then the upper modes can be considered to form a part of the residual, so that

$$q = T_g \phi_g^l \xi_g^l + e_m = T_{gl} \xi_g^l + T_{rl} q_{rm} \tag{2.43}$$

where Equation 2.43 now parallels Equation 2.13. Minimizing the quadratic of the new residual e_m weighted by the mass matrix yields the appropriate definition of the lower global coordinates

$$\begin{aligned} \xi_g^l &= \left(T_{gl}^T M T_{gl}\right)^{-1} T_{gl}^T M q \\ &= \left(\left(\phi_g^l\right)^T T_g^T M T_g \left(\phi_g^l\right)\right)^{-1} \left(\phi_g^l\right)^T T_g^T M q \end{aligned} \tag{2.44}$$

All of the previously derived results can now be used in this variation, with the expression for the modified interpolation functions

$$T_{gl} \equiv T_g \phi_g^l \tag{2.45}$$

substituted for T_g.

A way to implement this alternative is shown in Figure 2.6. This can be compared with the original setup in Figure 2.4. The implementation of these two alternatives are compared in Table 2.1. These results show the difference in the size of the matrices used in the aggregation and control distribution steps. An analysis of the difference in the computational requirements for these two methods is performed in Chapter 5.

Alternative 2. Recall that we are trying to select interpolation functions T_g in such a way that the coupling through the stiffness term K_{gr} is reduced. A direct

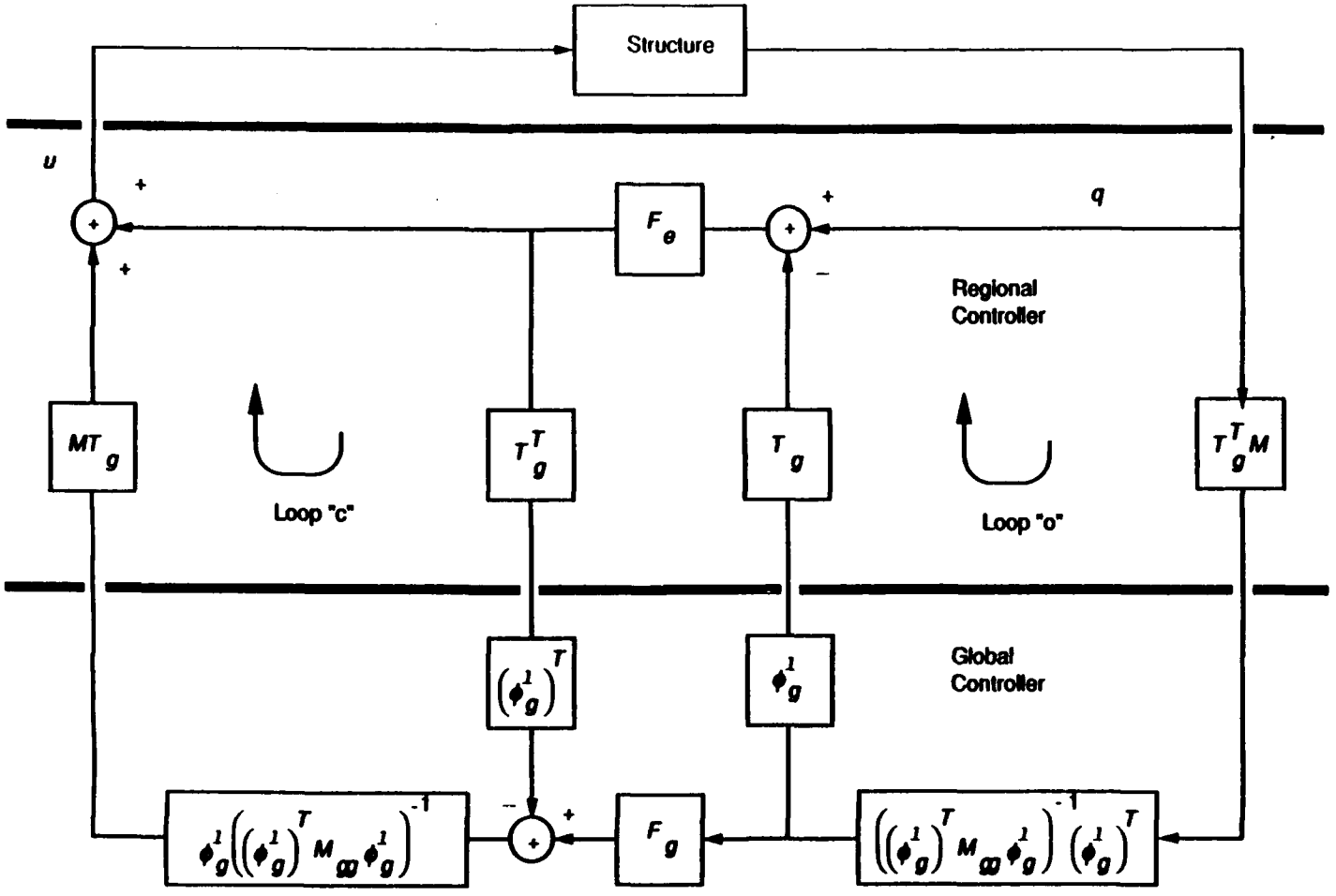

Figure 2.6: The hierarchic control architecture for the case where only the n_l lower frequency modes of the global model are retained. This can be compared to the case in Figure 2.4 where all of the global modes are retained. The matrix ϕ_g^l represents the set of global modes that were retained in the model.

Table 2.1: A comparison of two methods of implementing the hierarchic control architecture. The first method retains all of the modes in the global model. The second method retains only the n_l lower modes.

Box Number	All Global Modes	Dimension	n_l Lower Modes Retained	Dimension
1	$T_g^T M$	$[n_g \times n]$	$T_g^T M$	$[n_g \times n]$
2	M_{gg}^{-1}	$[n_g \times n_g]$	$\left(\left(\phi_g^l\right)^T M_{gg} \phi_g^l\right)^{-1} \left(\phi_g^l\right)^T$	$[n_l \times n_g]$
2a			ϕ_g^l	$[n_g \times n_l]$
3	T_g	$[n \times n_g]$	T_g	$[n \times n_g]$
4	Local control		Local control	
5	Global control	$[n_g \times 2n_g]$	Lower control	$[n_l \times 2n_l]$
6	T_g^T	$[n_g \times n]$	T_g^T	$[n_g \times n]$
6a			$\left(\phi_g^l\right)^T$	$[n_l \times n_g]$
7	M_{gg}^{-1}	$[n_g \times n_g]$	$\phi_g^l \left(\left(\phi_g^l\right)^T M_{gg} \phi_g^l\right)^{-1}$	$[n_g \times n_l]$
8	MT_g	$[n \times n_g]$	MT_g	$[n \times n_g]$

way to do this is to simply choose the interpolation functions to be the first n_g modes of the system. This will result in the complete decoupling of the global and residual systems. That is, the original degrees of freedom may be expressed as

$$q = \phi_0 \xi_0 \tag{2.46}$$

where ϕ_0 is the matrix whose columns are the modes of the system, and ξ_0 is the vector of modal amplitudes. Assuming that n_g of these will be used to represent the global model, we have that

$$q = \phi_0^l \xi_0^l + \phi_0^u \xi_0^u = \phi_0^l \xi_0^l + e_0 \tag{2.47}$$

where in this case the superscript $(\cdot)^l$ denotes the lower (in frequency) set of modes. So the lower modes now constitute the modified interpolation functions

$$T_{g0} = \phi_0^l \tag{2.48}$$

Minimizing the quadratic error of e_0 weighted by the mass matrix M yields the following new definition of the global coordinates

$$\xi_g^l = \left(\left(\phi_0^l\right)^T M \left(\phi_0^l\right) \right)^{-1} \left(\phi_0^l\right)^T M q \tag{2.49}$$

where the term within the inverse is diagonal if the actual normal modes are used. In this case, the global and residual subspaces are completely uncoupled since the off-diagonal terms of the stiffness matrix, K_{gr}, are now zero. All of the previous results are now valid, with $T_{g0} = \phi_0^l$ substituted for T_g.

The difference in this second alternative is not primarily in derivation or form, but in the computational implementation, or, equivalently, in how much information must be passed from each local processor to the global processor. In this variant, n_g pieces of information must in general be passed by each element processor to the global processor. In the case when there are fewer than n_g sensors per element, all of the measurements must be passed up to the global processor.

Alternative 3. The final alternative in the definition of the element interpolation function is to use component modes. The derivation of this alternative is identical to the previous alternative, except that the ϕ_0^l matrix now contains component modes and is block diagonal. The number of pieces of information which must be passed to the global processor corresponds to the number of modes retained in the description of each element.

Each of these last two methods resort to the use of modes for the interpolation functions which results in the loss of one of the implementation advantages of this technique. These modes are in general non-zero over the entire structure, whereas the standard interpolation functions of beam or rod finite element models are non-zero only over a few elements. Consequently, the use of modes would mean that each element controller would have to calculate the contribution of the local measurements to each mode of the system, and then all of these would have to be communicated to the central computer were they would be combined to form the modal coordinates. This represents significantly more work than having each controller only calculate the contribution to the shape functions which are non-zero within its region. The introduction of modes as in a component mode synthesis offers the advantage of being able to incorporate constraint or attachment modes (see reference [19]) into the model, but there is a trade-off in terms of the degree of decoupling that is required between the two systems and the increased cost of the control calculation.

2.7 Hierarchic Control Synthesis

Having derived the options for partial or total subspace decoupling, the subspace controllers must now be synthesized. The following algorithm is an outline of the steps to be followed in designing a hierarchic control system.

1. The choice of the element interpolation functions.

   As discussed in the previous section, the number of global degrees of freedom and the interpolation functions must be selected to provide a good model of the lower frequency modes and a central controller which has sufficient control authority to perform the global tasks. In the selection of the shape functions, T_g, the minimization of the coupling between the global and residual models should be emphasized, and it can be checked by looking at the relative norms of the off-diagonal blocks on the left hand side of Equation 2.26.

2. Global control design.

   Assume the stiffness coupling is zero ($K_{gr} = 0$), and design the global control for the global design model

$$M_{gg}\ddot{q}_g + K_{gg}q_g = Q_g = -F_g q_g - F_{\dot{g}}\dot{q}_g \tag{2.50}$$

   by any appropriate means. This is a simple control design because, by definition, all of the states are available to be fed back, so any full state feedback approach can be implemented. An approach using a Linear Quadratic Regulator will be developed in Chapter 4.

3. Local control design.

   Design the local controller for the residual design model so that it provides good shape control as per the stated objectives of the local controller.

4. Performance evaluation.

   The performance can then be evaluated by using Equation 2.37 to measure the influence of the dynamic spillover and the degree of suboptimal behavior that is introduced by this coupling between the subsystems. If the coupling is found to be too high, then some of the alternatives provided in Section 2.6 can be employed to reduce the interaction.

Chapter 3

Local Control Design

3.1 Introduction

The architecture of the hierarchic controller was developed in the previous chapter, and the resulting algorithm for the control design was given in Section 2.7. One step of this procedure which remains to be discussed in detail is the selection of the form of the local controller. The development in Chapter 2 alluded to the fact that the local controllers should be independent in some sense. The purpose of this chapter is to discuss this point and investigate several forms of local control which are distinguished by the constraints imposed on the amount of information available to calculate the command. The aim of this study will be to evaluate the trade-offs between the improved performance as the sophistication and/or complexity of the local controllers is increased and the implementation costs in terms of the number of computations that are required and the amount of information which must be transfered both internal and external to the element. This chapter will develop the controllers. Chapter 4 will discuss their performance, and Chapter 5 will investigate the computational aspects of their implementation.

Figure 2.4 gives the main architecture of the hierarchic controller. It can be

seen from this diagram that the lower level controller, which acts on the residuals e, can be viewed in a slightly different manner. By eliminating the outer loop of the global controller, then the local controllers can be visualized as acting on q alone. This simplifies the design procedure since the local control can be designed for the states, q, and then applied directly to the residuals, e. Since the local controllers are assumed to possess only information within a limited region, the control at this level can be considered to be essentially a decentralized feedback on the structure.

As was discussed in Chapter 2, the main function of the local controllers is to maintain the shape, within their region, that the interpolation of the global coordinates produces. With this criterion in mind, the local controllers will mainly be designed as shape controllers. However, it is also possible to incorporate other tasks into the design, such as maintaining a certain level of damping in the higher frequency modes. Since these controllers act only on a "short" length of the structure, in the sense that they do not act on the entire device, they are aimed primarily at the short wavelength/high frequency vibrations. In fact, as was discussed in Section 2.5, the control at this level will be filtered of its low frequency component to eliminate any control spillover with the global model.

Provided that the assumptions of an "intelligent" structure are met, then this architecture is valid for any structure. However, for the sake of clarity, an example of a long beam will be used where appropriate. The four local controllers that will be examined are colocated feedback, block diagonal feedback, block tri-diagonal feedback, and an novel implementation of the full state centralized feedback. These were selected since they cover a large range of possible decentralized control techniques. The first pair allow for an increase in the sophistication of the isolated controllers. The second pair include two degrees of allowable communication directly between the local controllers. The following sections will discuss these types of controllers and develop the methodologies necessary to derive the appropriate gain matrices.

3.2 Colocated Feedback

This type of controller was selected as the first to be considered since it is by far the easiest to implement because it requires no communication of measurements between any of the sensors or actutators, except for the colocated pair. In fact, it would be very feasible to implement this form of the local control using only analog circuits, something which becomes much harder for some of the later designs. Analog circuitry is less flexible, but far simpler to implement and embed in the structure. The goal of this type of controller is primarily to actively augment the natural damping of the structure.

There are actually two forms that could be considered. The first is pure rate feedback

$$u = -\alpha m \dot{q} \tag{3.1}$$

and the second is a combination of rate and displacement feedback commonly known as *natural control* [61]

$$u = -\beta^2 m q - 2\beta m \dot{q} \tag{3.2}$$

where m is a measure of the local mass of the structure, so that the applied force is directly related to the mass of the structure. The additional displacement feedback term in this second form of the feedback has the effect of increasing the stiffness of the structure in such a manner that, in the ideal case of continuous control actuation, the closed loop poles move into the left-half s-plane with the same frequency (complex part) as the parameter β is increased. A root locus would show the poles moving leftward at the same complex value. The term natural control is applied to this form of feedback as the mode shapes are not changed by the implementation of the control [61]. In the ideal case, every closed loop pole would shift so that the real part is at $-\beta$. This type of feedback is also known as *uniform damping.*

The form of the local controller is given in Figure 3.1. The processors are shown to be associated with each sensor and actuator pair, but this could also be

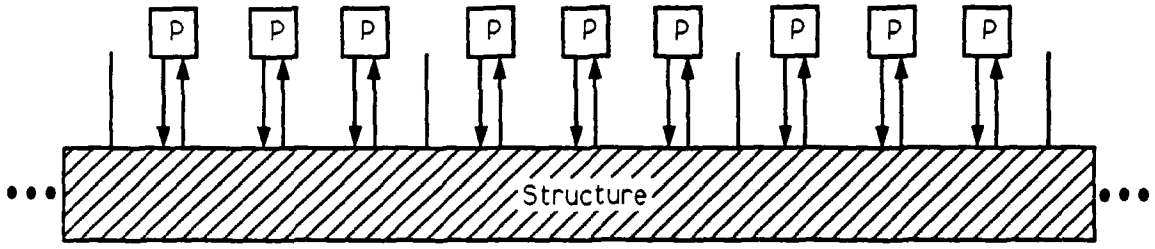

Figure 3.1: The architecture for a local controller based on colocated feedback.

implemented using one processor per finite control element. The resulting gain matrices will be diagonal with elements which correspond to the local mass of the structure weighted by α and β as in Equations 3.1 and 3.2.

The procedure for evaluating the gains essentially is a process of just picking the desired decay rate. As stated, ideally each pole would move to this value of β, but with discrete controllers the same does not hold as some modes are more controllable than others. The result is a non-uniform distribution about the desired decay rate, a result which can be seen from the examples in reference [61]. For colocated rate feedback with dual actuators and sensors, the poles and zeroes alternate up the $j\omega$ axis. Dual feedback refers to like-sensor to like-actuator feedback (*i.e.*, velocity fed back to a force actuator), [49]. As the gain is increased, the poles will move along the root loci into the left-half s-plane, but as the gain is increased further, they will eventually reverse direction and return to the zeroes on the $j\omega$ axis. So the gain must be selected with this reversal in mind. However, typically the performance

requirement will demand only about 1 to 10 percent damping in the higher frequency modes [20], which can be achieved with fairly small gain values. Of course, the upper limit of the achievable performance is bounded by the actuator capabilites.

If α and β are selected to be greater than zero (as they should be), then the gain matrices are positive definite. Using a Lyapunov test function, which will be discussed in Chapter 5, of the system's energy, it can then be concluded that the resulting system is guaranteed to be stable for feedback under these gains. Several studies have been done [1,33] to investigate the stability and robustness of these forms of colocated feedback. In reference [33], it is shown that both types of feedback provide asymptotic stability, if the actuators and sensors are perfect, in a manner which is robust to the number of modes and the variation of the modal parameters. It is also shown that if the actuators and sensors can be modelled as high bandwidth first order systems, then a stable uniform damping controller can be designed as well. It was shown by Linder *et al.* [39], by an example on a typical section problem, that rate feedback is a positive real controller, but a uniform damping controller can only guarantee stability for frequencies above $\frac{\beta}{2}$. In essence, some robustness at low frequencies has been sacrificed for a higher level of performance. This is not a major concern in this case however, as these local controllers are primarily aimed at the higher frequency motions.

So, in conclusion, it would appear that this approach should be relatively easy to implement, but the shape control ability of the control design needs to be investigated, and this will be done in Chapter 4.

3.3 Block Diagonal Feedback

3.3.1 Introduction

This form of the local controller is important because, although it is an isolated controller, it allows for some sophistication since each control command within an element can be calculated using all of the measured information within that region of the structure. This type of controller allows for communication within an element but no external communication to other elements. This can pose a problem for the control design since points which are ϵ (*i.e.*, both are close) on either side of a node are equally important to the control calculation at that location, but if one measurement is outside of the element, then it is unavailable to be used in the calculation of the control command. Two forms of the control structure will be analyzed. The first is a full gain matrix the size of the element. The second is a gain matrix which itself is composed of block diagonal matrices *i.e.*, the controller gains have been developed for a "bay" which is smaller than the element. This would allow for a restriction on the communication within an element.

The architecture of this type of local controller is given in Figure 3.2. The resulting form of the gains for this case and a methodology for calculating them will be developed in the following sections.

3.3.2 The Calculation of the Gains

Specifying the components of the state vector which can be used for the feedback is similar to performing output feedback since the structure of the gain matrix is being specified before the optimization is performed. The problem to be looked at here is essentially a constrained feedback problem.

The aim is to develop a controller that can only feed back the states within an element. If the structure is broken up into N elements, the resulting control

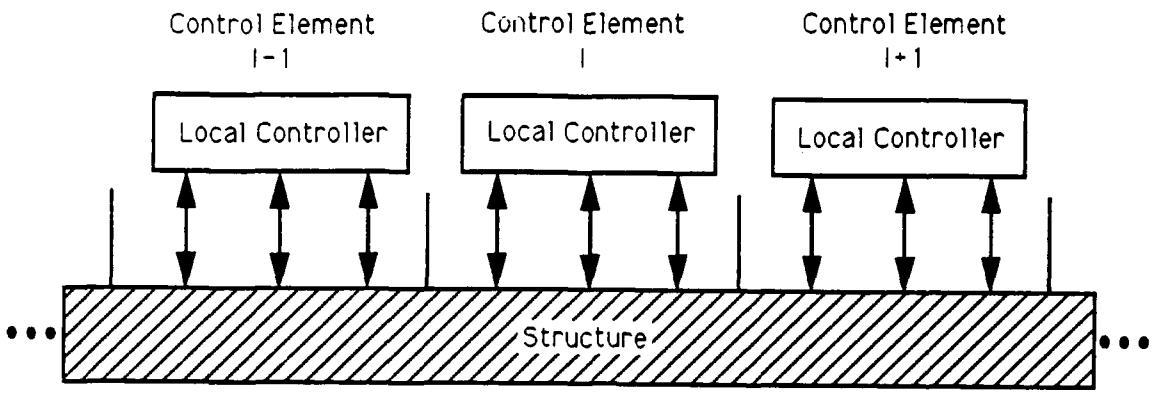

Figure 3.2: The architecture for a local controller based on block diagonal feedback.

equation is

$$\begin{bmatrix} u_1 \\ u_2 \\ \vdots \\ u_N \end{bmatrix} = - \begin{bmatrix} F_{q_1} & 0 & \cdots & 0 \\ 0 & F_{q_2} & & 0 \\ \vdots & & \ddots & \\ 0 & 0 & & F_{q_N} \end{bmatrix} \begin{bmatrix} q_1 \\ q_2 \\ \vdots \\ q_N \end{bmatrix} - \begin{bmatrix} F_{\dot{q}_1} & 0 & \cdots & 0 \\ 0 & F_{\dot{q}_2} & & 0 \\ \vdots & & \ddots & \\ 0 & 0 & & F_{\dot{q}_N} \end{bmatrix} \begin{bmatrix} \dot{q}_1 \\ \dot{q}_2 \\ \vdots \\ \dot{q}_N \end{bmatrix} \tag{3.3}$$

where q_i and u_i represent vectors of the states and control for each element, and the F_{q_i} are block matrices. Equivalently, this can be written as

$$u = -F_q q - F_{\dot{q}} \dot{q} \tag{3.4}$$

where

$$u = \left[u_1^T, u_2^T, \ldots, u_N^T\right]^T \tag{3.5}$$

$$q = \left[q_1^T, q_2^T, \ldots, q_N^T\right]^T \tag{3.6}$$

$$F_q = \mathrm{BD}\left(F_{q_1}, F_{q_2}, \ldots, F_{q_N}\right) \tag{3.7}$$

$$F_{\dot{q}} = \mathrm{BD}\left(F_{\dot{q}_1}, F_{\dot{q}_2}, \ldots, F_{\dot{q}_N}\right) \tag{3.8}$$

where BD(...) means that the matrix consists of the listed matrices as the elements of the main diagonal (*i.e.*, it is block diagonal) and it is assumed that F_{q_i} are block matrices which are the appropriate size for the elements chosen for the hierarchic architecture. This is the specified form of the gain matrix, and it corresponds to an extra constraint on the optimization procedure.

Due to the similarity between this work and the output feedback problem, the equations for this simpler case will be discussed first. The results for most of what will follow are derived in Appendix A. The standard output feedback problem assumes that only certain states can be measured and fed back by the controller. The system dynamics are represented as

$$\dot{x} = Ax + Bu \tag{3.9}$$

$$y = Cx \tag{3.10}$$

where $x \in R^n$, $y \in R^p$, and $u \in R^m$, and A, B, and C are appropriately sized matrices for the plant. The control is taken to be of the form

$$u = -Fy = -FCx \tag{3.11}$$

and the performance metric is taken to be the minimization of the cost J defined as

$$J = \frac{1}{2}\int_0^\infty \left(x^T R_{xx} x + u^T R_{uu} u\right) dt \tag{3.12}$$

with the standard restrictions that $R_{uu} = R_{uu}^T > 0$ and $R_{xx} = R_{xx}^T \geq 0$, and the triple $\left(A, B, R_{xx}^{\frac{1}{2}}\right)$ is both stabilizable and detectable. Then, as derived in reference [38] and in Appendix A by a slightly different method, the necessary condition is

$$R_{uu} FCQC^T - B^T PQC^T = 0 \tag{3.13}$$

where the symmetric postitive definite matrices P and Q solve the Lyapunov equations

$$PA_{cl} + A_{cl}^T P + R_{xx} - C^T F^T R_{uu} FC = 0 \tag{3.14}$$

$$QA_{cl}^T + A_{cl} Q + \Sigma = 0 \tag{3.15}$$

where

$$A_{cl} = A - BFC \tag{3.16}$$

is the closed loop dynamics and Σ represents the covariance of the states at the inital condition. Note that an augmented cost L is introduced in the appendix and it is essentialy equal to the cost J adjoined with the Lyapunov Equation 3.15 by the Lagrange multiplier matrix P which solves Equation 3.14. There are a couple of points to note about these equations. First, they are strongly coupled, in the sense that each equation contains at least two of F, P, and Q. The main difference between these necessary conditions and the more familiar ones for full state feedback is the addition of the C matrix in Equation 3.13. Note that if C^{-1} exists, then this equation reduces to

$$R_{uu}FC - B^T P = 0 \tag{3.17}$$

Then the solution, Q, of Equation 3.15 is no longer necessary for the solution of Equation 3.13, and Equation 3.14 reduces to the standard Riccati equation.

In Appendix A, the necessary conditions for the case where some of the blocks of the gain matrix are specified *à priori* to be zero are also developed. In this case, the set of necessary conditions becomes Equations 3.14 and 3.15 and a third equation which is

$$\frac{\partial L}{\partial F_k} = 0 \tag{3.18}$$

where F_k represents a non-zero sub-block of the gain matrix. What distinguishes the two cases is that only those components of the gradient which correspond to free parameters of the gain can be set to zero, and the rest are undetermined. So, in this case, the augmented cost now only has a zero gradient with respect to the non-zero blocks of F.

In reference [38] it was noted by Levine and Athans that these equations are particularly difficult to solve for several reasons. As was discussed previously, they are coupled matrix equations which are of the same order as the plant. There is also

the possibility that non-optimal solutions to these necessary conditions may exist, when a local minimum (as opposed to the global minimum) is found. From several examples for different element sizes that have been tried for a beam, it has also been found that the successive iteration technique outlined in reference [38] possesses poor convergence properties as the singular values of the second derivative were found to be much larger than one, and there was no contraction mapping.

The solution of this output feedback problem has been analyzed in many papers. One of the most important of these contributions was by Kosut in reference [34]. This paper introduces suboptimal approximations of the optimal output feedback gains based on projections of the optimal full state feedback (LQR) gains. These projections are based on a weighted pseudo-inverse of the measurement matrix of the system. This paper is important because it arises from a recognition of the difficulty of solving the optimal output feedback problem. The major difficulty with this approach is that the results are sub-optimal and can produce very poor closed loop performance. However, example problems based on small scale models have indicated that, if the "correct" information is available to be fed back, then the suboptimal closed loop performance is a very good approximation of the optimal results. The difficulty arises in determining and measuring the "correct" information for a given structure and performance specification. The simplest example is that, to be able to perform active damping, the "correct" information to be measured and fed back is the velocity.

Many other papers have addressed the issue of a numerical solution to the necessary conditions. These include discussions on topics such as the different gradient search techniques that can be employed (see reference [14]) and how to develop good initial guesses which are so critical in the solution procedure [53]. However, any numerical approach to solve these optimal necessary conditions still faces the problems associated with the dimension of the plant which governs the order of the matrix equations to be solved. For any system which is large enough to be

of interest, these equations will be of such a high order that they will be virtually impossible to solve.

With this difficulty in mind, a technique will be presented here which takes advantage of the symmetry and large extent of the structure to reduce the plant dimension (and consequently the order of the matrix equations) to a more manageable level. Since the end effects for a long structure tend to be negligible in the middle, it can be assumed that the structure's length is effectively infinite. This will have little influence on the results, but will help to simplify the analysis in the following sections.

The technique employs a spatial discrete transform on the structure to decompose it into many reduced order problems which are indexed by a transform variable. This idea was developed by Chu [16] and expanded by Wall [66] to include analysis of the control and estimation of large scale systems which possess spatial symmetry. More recently, this decomposition technique has been employed in the continuous sense in references [24,47]. The continuous approach applies a fourier decomposition directly to the differential equation for the structure, provided that these can be written down. The method that will be employed here actually applies a discrete transform to a finite element approximation of the structure to create a smaller FEM for each value of the index variable. The following sections will discuss how this transformation can be applied to the symmetric plant, and the associated benefits for the control design will also be discussed.

3.3.3 Transformations for Spatially Symmetric Systems

The following discussion will first of all describe the transformation which is appropriate for finite systems with circular symmetry which are called *circulant systems*. The aim will be to rederive the necessary conditions of the control problem in the transformed domain. This will be followed by an extension to systems of infinite

dimension which are known as *toeplitz systems*. To begin the discussion, define a block circulant matrix [66] of order N as one that can be partitioned in the form

$$A = \begin{bmatrix} A_0 & A_{N-1} & A_{N-2} & \dots & A_1 \\ A_1 & A_0 & A_{N-1} & & A_2 \\ A_2 & A_1 & A_0 & & A_3 \\ \vdots & & & \ddots & \\ A_{N-1} & A_{N-2} & A_{N-3} & & A_0 \end{bmatrix} \tag{3.19}$$

where the $A_i \in R^{n \times s}$. The dynamics of a N^{th} order circulant system are then defined to be of the form

$$\dot{x} = Ax + Bu \tag{3.20}$$

$$y = Cx \tag{3.21}$$

where now $A \in R^{Nn \times Nn}$, $B \in R^{Nn \times Nm}$, and $C \in R^{Np \times Nn}$ are appropriately sized block circulant matrices. For now, assume that this model can be derived using a finite element method and has the right circulant form. Another method for developing the transformed model directly will be presented in Section 3.4.2. Typically, the number of subsystems, N, is much larger than the dimension of each subsystem, n.

An example of a block circulant system is shown in Figure 3.3. This corresponds to four equal subsystems connected in a circle such that the complete system is symmetric. There are four nodes which represent the boundaries between the subsystems. In the example shown, the A_i correspond to the dynamic influences of the degrees of freedom in subsystem i on those in subsystem 0. The important properties of a circulant system are that each subsystem has the same internal dynamics, A_0, and the influence of any one subsystem on another is a function only of the relative separation between the two. As presented in reference [66] and to some extent in [16], the following discussion will show the spatial transform (actually a discrete fourier transform) that can be used to decouple the dynamics of the system.

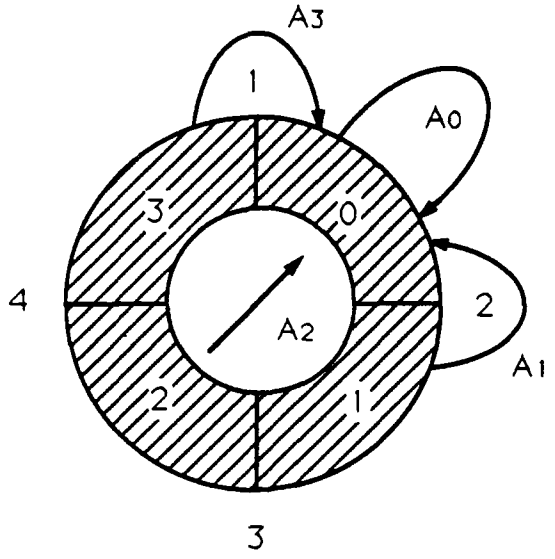

Figure 3.3: An example of a circulant system. The arrows represent the influence of that subsystem on subsystem 0.

Another definition is required to complete the process. The transformation matrix Φ_i is defined to be

$$\Phi_i = \begin{bmatrix} I_i & I_i & I_i & \dots & I_i \\ I_i & I_i\omega_N & I_i\omega_N^2 & & I_i\omega_N^{N-1} \\ I_i & I_i\omega_N^2 & I_i\omega_N^4 & & I_i\omega_N^{(N-1)2} \\ \vdots & & & \ddots & \\ I_i & I_i\omega_N^{N-1} & I_i\omega_N^{2(N-1)} & & I_i\omega_N^{(N-1)(N-1)} \end{bmatrix} \tag{3.22}$$

where it is assumed that there are N circulant blocks in the system, I_i is the $(i \times i)$ identity matrix, and $\omega_N = e^{\frac{2\pi j}{N}}$, *i.e.*, the N^{th} complex root of 1. The transformation matrix can be expressed in a more compact notation as

$$(\Phi_i)_{kl} = I_i\omega_N^{(k-1)(l-1)} \tag{3.23}$$

Note an interesting property of the inverse of Φ_i that

$$\left(\Phi_i^{-1}\right)_{kl} = \frac{1}{N} I_i \left(\omega_N^*\right)^{(k-1)(l-1)} = \frac{1}{N} I_i \omega_N^{-(k-1)(l-1)} \tag{3.24}$$

where $(\cdot)^\star$ denotes the complex conjugate of the expression. This equation has employed the fact that $\omega_N^\star = \omega_N^{-1}$, which follows directly from the definition of ω_N given above. So, the inverse transformation matrix is very easy to calculate directly.

It is this Φ_n matrix which forms the basis of the spatial transformation. It can be shown that if A is taken to have the form expressed in Equation 3.19, then

$$\overline{A} = \Phi_n^{-1} A \Phi_s = \begin{bmatrix} \overline{A}_0 & 0 & \dots & 0 \\ 0 & \overline{A}_1 & & 0 \\ \vdots & & \ddots & \\ 0 & 0 & & \overline{A}_{N-1} \end{bmatrix} \tag{3.25}$$

where

$$\overline{A}_k = \sum_{i=0}^{N-1} A_i \, \omega_N^{-ki} \tag{3.26}$$

$$A_k = \frac{1}{N} \sum_{i=0}^{N-1} \overline{A}_i \, \omega_N^{ki} \tag{3.27}$$

for $k = 0, 1, \dots,$ N-1.

So, the transformed block circulant matrix is block diagonal with blocks which are the discrete fourier transform of the top row of the circulant matrix. There are several very important and time saving properties concerning the symmetry of the transformed block matrices of this system which are discussed and proved by Wall in reference [66]. Considering an A matrix of the form of Equation 3.19, then, for instance, it is shown that

$$\mathrm{Re}\left\{\overline{A}_k\right\} = \mathrm{Re}\left\{\overline{A}_{N-k}\right\} \tag{3.28}$$

$$\mathrm{Im}\left\{\overline{A}_k\right\} = -\mathrm{Im}\left\{\overline{A}_{N-k}\right\} \tag{3.29}$$

If the matrix A is symmetric, then $A_k = A_{N-k}^T$ and the following identities hold

$$\mathrm{Re}\left\{\overline{A}_k\right\} = \mathrm{Re}\left\{\overline{A^T}_k\right\} \tag{3.30}$$

$$\mathrm{Im}\left\{\overline{A}_k\right\} = -\mathrm{Im}\left\{\overline{A^T}_k\right\} = \mathrm{Im}\left\{\overline{A}_{N-k}^H\right\} \tag{3.31}$$

where the $(\cdot)^H$ denotes the hermitian which is the complex conjugate transpose of the matrix.

Having shown how the transformation can be applied to a circulant matrix to produce a block diagonal matrix, the next step is to apply the transformation to the circulant system defined above. Defining

$$\overline{x} = \Phi_n^{-1} x \quad \overline{u} = \Phi_m^{-1} u \quad \overline{y} = \Phi_p^{-1} y \tag{3.32}$$

then transforming Equations 3.20 and 3.21 yields

$$\frac{d}{dt}\overline{x} = \overline{A}\,\overline{x} + \overline{B}\overline{u} \tag{3.33}$$

$$\overline{y} = \overline{C}\,\overline{x} \tag{3.34}$$

where each of the transformed matrices denoted as $\overline{(\cdot)}$ is block diagonal. Since this means that each of the subsystems is not influenced by the others in terms of either observation, control, or dynamic spillover, then it can be said that the transformed systems are decoupled in this new representation in the spatial frequency domain. These equations can also be rewritten to reflect this decoupling by expressing the dynamics of the k^{th} subsystem as

$$\frac{d}{dt}\overline{x}_k = \overline{A}_k\,\overline{x}_k + \overline{B}_k\overline{u}_k \tag{3.35}$$

$$\overline{y}_k = \overline{C}_k\,\overline{x}_k \quad \forall\, k \in [0,1,\ldots,\text{N-1}] \tag{3.36}$$

This decoupling technique can be applied to more complex equations as well. For example, for the steady state time invariant Lyapunov equation of the form of Equation 3.15

$$AQ + QA^T + \Sigma = 0 \tag{3.37}$$

where A, Q, and Σ are all block circulant matrices of order N, and Q is symmetric, then applying the transformation yields

$$\Phi_n^{-1} A \Phi_n \Phi_n^{-1} Q \Phi_n + \Phi_n^{-1} Q \Phi_n \Phi_n^{-1} A^T \Phi_n + \Phi_n^{-1} \Sigma \Phi_n = 0 \tag{3.38}$$

So the transformed equation is

$$\overline{A}\,\overline{Q} + \overline{Q}\,\overline{A^T} + \overline{\Sigma} = 0 \tag{3.39}$$

Note that $\overline{A^T} = \overline{A}^H$. Since each of the transformed matrices in Equation 3.39 are block diagonal, then this equation can be written in the equivalent decoupled form

$$\overline{A}_i\,\overline{Q}_i + \overline{Q}_i\,\overline{A}_i^H + \overline{\Sigma}_i = 0 \quad \forall\, i \in [0, 1, \ldots, \text{N-1}] \tag{3.40}$$

where $(\cdot)_i$ denotes the i^{th} diagonal sub-block of the matrix. This representation means that the $(Nn)^{th}$ order problem has been reduced to N, n^{th} order problems. Since the solution of a the Lyapunov equation is an n^3 operation, then it can be seen that this step has considerably reduced the amount of computation required, which is especially important considering the role of this equation in the numerical solution procedure which will be discussed at the end of the next section. Of course, there is some overhead involved in forming the transformed systems, but this can be implemented efficiently as a FFT, which is an $n^2 \log_2 n$ operation [37] but need only be performed once.

The same decoupling transformation can be shown to hold for the Riccati equation if all the matrices are block circulant. It should also be noted that $\overline{R^{-1}} = \overline{R}^{-1}$. The resulting transformed equation is

$$\overline{A}^H\,\overline{P} + \overline{P}\,\overline{A} + \overline{R}_{zz} - \overline{P}\,\overline{B}^H\,\overline{R}_{uu}^{-1}\,\overline{B}\,\overline{P} = 0 \tag{3.41}$$

which again is equivalent to N decoupled equations. This shows how the two Lyapunov equations of Section 3.3.2 can be transformed into the spatial frequency domain and represented in a decoupled manner. In Appendix A, it is also shown how the third necessary condition can be transformed as well. For the case where no blocks of the gain matrix F are constrained to be zero, the necessary condition can be written as

$$\frac{\partial L}{\partial \overline{F}_i} = 0 \quad \forall\, i \in [0, 1, \ldots, \text{N-1}] \tag{3.42}$$

which is shown in Appendix A to be equivalent to the results in Section 3.3.2. The constrained gain case for a circulant system is also investigated in Appendix A. Denoting the indices of the non-zero gain blocks by the set α, then it is shown in the Appendix A and by Wall in reference [66] that the resulting necessary condition is

$$\sum_{i=0}^{N-1} \left(\overline{C}_i \overline{Q}_i \overline{C}_i^H \overline{F}_i^H \overline{R}_{uu_i} - \overline{C}_i \overline{Q}_i \overline{P}_i \overline{B}_i \right) \omega_N^{-ik} = 0 \qquad \forall k \in \alpha \tag{3.43}$$

Then Equations 3.40, 3.41 and 3.43 represent the transformed necessary conditions of the control problem given in Section 3.3.2 when the gain structure of Equation 3.3 is imposed and the system is block circulant. Note that constraining some of the gain blocks to be zero recouples the necessary conditions in the transformed domain.

The extension of this work to infinite dimensional systems toeplitz systems follows from the analysis done by Chu in reference [16]. Since the system matrices are now assumed to be infinite dimensional, the equations are best represented in terms of summations. For a model of an infinite string of identical subsystems, the system dynamics for the k^{th} subsystem are given by

$$\dot{x}_k = \sum_{i=-\infty}^{\infty} (A_{k-i} x_i + B_{k-i} u_i) \tag{3.44}$$

$$y_k = \sum_{i=-\infty}^{\infty} C_{k-i} x_i \tag{3.45}$$

for $-\infty < k < \infty$. These equations indicate quite clearly that it is only the separation distance $k - i$ which determines the influence of one subsystem on another.

As with the circulant system, it is necessary at this point to introduce the transformation which will decouple the equations. The format of the transformation will be shown to be very similar to the one introduced for circulant systems, but an important distinction will be noted once the transformed equations have been developed. The decoupling can be achieved by employing the two-sided z-transform, which has many applications in both digital signal processing [51] and digital control [25]. This can be compared with the transformation for the circulant system which

was the discrete fourier transform. The z-transform of a sequence $h_l, -\infty < l < \infty$, is given as [25]

$$H(z) = Z\left[h_l\right] \equiv \sum_{l=-\infty}^{\infty} h_l z^{-l} \tag{3.46}$$

The inverse transform is more complicated in this case as it requires integration around a closed contour (typically the unit circle $\|z\|_2 = 1$) in the complex plane

$$h_l = Z^{-1}\left[H\left(z\right)\right] = \frac{1}{2\pi j} \oint H(z)\, z^{l-1} dz \tag{3.47}$$

where the contour is taken in the region of convergence of $H(z)$. The region of convergence is defined to be the region of the z-plane for which the summation of Equation 3.46 is absolutely convergent.

To apply this transformation to the system of Equations 3.44 and 3.45, it is then necessary to define the transform of the state vector as

$$X(z) = \sum_{l=-\infty}^{\infty} x_l z^{-l} \tag{3.48}$$

Then

$$\begin{aligned} \dot{X}(z) &= \sum_{l=-\infty}^{\infty} \dot{x}_l z^{-l} \\ &= \sum_{l=-\infty}^{\infty} \left[\sum_{i=-\infty}^{\infty} \left(A_{l-i} x_i + B_{l-i} u_i\right) \right] z^{-l} \end{aligned} \tag{3.49}$$

To proceed further, the convolution property of the z-transform must be introduced [25]

$$Z\left[\sum_{i=-\infty}^{\infty} f_1(i) f_2(l-i)\right] = F_1(z) F_2(z) \tag{3.50}$$

Applying this to Equation 3.49 and the measurement equation yields

$$\dot{X}(z) = A(z)X(z) + B(z)U(z) \tag{3.51}$$

$$Y(z) = C(z)X(z) \tag{3.52}$$

where it has been implicitly assumed that these transformations exist. This will be the case as long as the summation of Equation 3.46 is absolutely convergent which is true if and only if [25]

$$\sum_{l=-\infty}^{\infty} |h_l| < \infty \tag{3.53}$$

The extension to the matrix case is simply that this condition must hold for every element in the matrix.

These equations represent decoupled systems which are a function of a continuous complex index z. This is the major difference between the circulant and toeplitz transformed systems, since the index for the first case is only evaluated at a finite number of points around the unit complex circle. Consequently, the two systems will be virtually identical when the continuous index variable for the toeplitz system is approximated at a finite number of points on the unit circle.

As with the circulant system, it is possible to set up the control problem for a toeplitz system. The transformation can then be applied to this problem, and it is possible to express the necessary conditions in the transformed domain. Using the definition

$$< A(z) >_0 = \frac{1}{2\pi j} \oint A(z) z^{-1} dz \tag{3.54}$$

which is the zeroeth element of the inverse transformation, then, from Wall and Appendix A, the transformed necessary conditions are

$$< C(z)Q(z)C(z)^H F(z)^H R_{uu}(z) >_0 - < C(z)Q(z)P(z)B(z) >_0 = 0 \tag{3.55}$$

where $P(z)$ and $Q(z)$ solve

$$P(z)\,[A(z) - B(z)F(z)C(z)] + [A(z) - B(z)F(z)C(z)]^H P(z) +$$

$$+ R_{zz}(z) + C(z)^H F(z)^H R_{uu}(z) F(z) C(z) = 0 \tag{3.56}$$

$$[A(z) - B(z)F(z)C(z)]\,Q(z) + Q(z)\,[A(z) - B(z)F(z)C(z)]^H + \Sigma(z) = 0 \tag{3.57}$$

where it is recognized that since z will be evaluated on the unit circle, $z^{-1} = z^*$ and then $A(z^{-1})^T = A^H$.

These are very similar to the circulant equations, the major difference being that the summation has been replaced by an integration, but this is in keeping with the observation that one has a discrete index, and the other has a continuous one. This integral would be approximated numerically as a summation at a discrete number of points.

Since in general ω_N is a complex number, the transformed equations will be complex. This is a problem, as it requires the solution of complex coupled matrix equations. If the matrix A is complex so that it can be written as

$$A = \mathrm{Re}\{A\} + j\,\mathrm{Im}\{A\} \tag{3.58}$$

where $A \in C^{n\times n}$ and $X, Y \in R^{n\times n}$, then another way to represent it in terms of its real elements is

$$\tilde{A} = \begin{bmatrix} \mathrm{Re}\{A\} & \mathrm{Im}\{A\} \\ -\mathrm{Im}\{A\} & \mathrm{Re}\{A\} \end{bmatrix} \tag{3.59}$$

That these two representations are equivalent in the sense that they yield the same eigenvalues and eigenvectors can be seen by noting that, if a Unitary transformation matrix T_1 is defined as

$$T_1 = \frac{1}{\sqrt{2}} \begin{bmatrix} I_n & I_n \\ jI_n & -jI_n \end{bmatrix} \tag{3.60}$$

where $T_1^H = T_1^{-1}$, then

$$\begin{bmatrix} A & 0 \\ 0 & A^* \end{bmatrix} = T_1^H \tilde{A} T_1 = T_1^H \begin{bmatrix} \mathrm{Re}\{A\} & \mathrm{Im}\{A\} \\ -\mathrm{Im}\{A\} & \mathrm{Re}\{A\} \end{bmatrix} T_1 \tag{3.61}$$

From the properties of Unitary transformations, it is then known that the two representations of the matrix A will yield the same set of eigenvalues and eigenvectors [50].

This approach can also be applied to the Lyapunov equation which results in a real representation of a complex matrix equation. Taking the standard Lyapunov equation 3.40 with complex $\overline{A}_k$, $\overline{Q}_k$, and $\overline{\Sigma}_k$ matrices expressed in the alternative form given above, then the equation can be rewritten as

$$\begin{bmatrix} \mathrm{Re}\{\overline{A}_k\} & \mathrm{Im}\{\overline{A}_k\} \\ -\mathrm{Im}\{\overline{A}_k\} & \mathrm{Re}\{\overline{A}_k\} \end{bmatrix} \begin{bmatrix} \mathrm{Re}\{\overline{Q}_k\} & \mathrm{Im}\{\overline{Q}_k\} \\ -\mathrm{Im}\{\overline{Q}_k\} & \mathrm{Re}\{\overline{Q}_k\} \end{bmatrix} +$$

$$\begin{bmatrix} \mathrm{Re}\{\overline{Q}_k\} & \mathrm{Im}\{\overline{Q}_k\} \\ -\mathrm{Im}\{\overline{Q}_k\} & \mathrm{Re}\{\overline{Q}_k\} \end{bmatrix} \begin{bmatrix} \mathrm{Re}\{\overline{A}_k\} & -\mathrm{Im}\{\overline{A}_k\} \\ \mathrm{Im}\{\overline{A}_k\} & \mathrm{Re}\{\overline{A}_k\} \end{bmatrix}^T + \begin{bmatrix} \mathrm{Re}\{\overline{\Sigma}_k\} & \mathrm{Im}\{\overline{\Sigma}_k\} \\ -\mathrm{Im}\{\overline{\Sigma}_k\} & \mathrm{Re}\{\overline{\Sigma}_k\} \end{bmatrix} = 0 \tag{3.62}$$

where for example, through Equations 3.30 and 3.31, the symmetry of Q requires that

$$\begin{aligned} \mathrm{Re}\{\overline{Q}_k\} &= \mathrm{Re}\{\overline{Q^T}_k\} \\ \mathrm{Im}\{\overline{Q}_k\} &= -\mathrm{Im}\{\overline{Q^T}_k\} \end{aligned}$$

so that Equation 3.62 can be rewritten as

$$\begin{bmatrix} \mathrm{Re}\{\overline{A}_k\} & \mathrm{Im}\{\overline{A}_k\} \\ -\mathrm{Im}\{\overline{A}_k\} & \mathrm{Re}\{\overline{A}_k\} \end{bmatrix} \begin{bmatrix} \mathrm{Re}\{\overline{Q}_k\} & \mathrm{Im}\{\overline{Q}_k\} \\ \mathrm{Im}\{\overline{Q^T}_k\} & \mathrm{Re}\{\overline{Q}_k\} \end{bmatrix} +$$

$$\begin{bmatrix} \mathrm{Re}\{\overline{Q}_k\} & \mathrm{Im}\{\overline{Q}_k\} \\ \mathrm{Im}\{\overline{Q^T}_k\} & \mathrm{Re}\{\overline{Q}_k\} \end{bmatrix} \begin{bmatrix} \mathrm{Re}\{\overline{A}_k\} & -\mathrm{Im}\{\overline{A}_k\} \\ \mathrm{Im}\{\overline{A}_k\} & \mathrm{Re}\{\overline{A}_k\} \end{bmatrix}^T + \begin{bmatrix} \mathrm{Re}\{\overline{\Sigma}_k\} & \mathrm{Im}\{\overline{\Sigma}_k\} \\ \mathrm{Im}\{\overline{\Sigma^T}_k\} & \mathrm{Re}\{\overline{\Sigma}_k\} \end{bmatrix} = 0 \tag{3.63}$$

which is now a standard Lyapunov equation of order $2n$.

The benefit of this approach is that it allows standard real programs such as reference [41] to be employed. These typically have been written to provide very accurate solutions and are usually numerically robust. The disadvantage is that the system size has doubled, so instead of $N(n)^3$, the cost is $N(2n)^3$, which negates some of the benefit derived from transforming the equations, but still represents a significant saving over the original cost of $(Nn)^3$

Up to this point, it has been shown how the control problems can be transformed into the spatial frequency domain, decoupled, and reduced in dimension. For the case where no constraints were placed on the gain matrix and all the states are available to be fed back, it was also shown that the resulting equations are decoupled, but when a constraint on the allowable form of the gain matrix is imposed, then two of the equations remain decoupled, but the third turns into a summation over the free gain blocks. The advantage of size reduction is still retained, which makes it feasible to employ a numerical solution procedure to obtain the optimal gains. The purpose of the next section will be to provide a discussion of the techniques that were employed to obtain the solutions of the optimal constrained gain feedback problem.

3.3.4 An Overview of Multivariate Function Minimization

The numerical techniques that can be employed to locate the extremal values of a multivariate function, $M(x)$, have been well documented, for example see reference [58]. Consequently, the aim of this section is only to provide an overview of the techniques that were employed to find the optimal gains for the constrained control that was outlined in the previous sections. If it can be assumed that $M(x)$ (taken to be the augmented cost L as a function of the gain matrix) has continuous second derivatives, then the function may be approximated in the neighborhood of x (*i.e.*, at $x + \Delta x$) as

$$M(x + \Delta x) = M(x) + \Delta x^T g(x) + \frac{1}{2}\Delta x^T H(x)\Delta x + \dots \tag{3.64}$$

Briefly, the necessary conditions for x_1 to be a strong minimum (assuming the cost is to be minimized as the typical problem) of the function can be summarized as

$$g(x_1) = 0 \tag{3.65}$$

$$H(x_1) \geq 0 \tag{3.66}$$

The aim here is to minimize the cost subject to the constraints imposed on the gain matrix which have been included in the necessary conditions. The free parameters are the elements of the gain matrix. Since the function is not in general quadratic, the solution technique will be inherently iterative in nature, with each step of the form

$$x_{k+1} = x_k + \alpha_k p_k \tag{3.67}$$

where x_k is the current estimate of the minimum, x_{k+1} is the updated estimate, α_k is the step size, and p_k is the direction of the step at time k. Most of the notion in this section is in the form of column vectors, but the rectangular gain matrix F can be rearranged so that its columns are the elements of a column vector. The various techniques that can be employed to solve for the minimum of this function are distinguished by the method used to formulate the direction vector p_k, *i.e.*, whether they use the first or second derivatives and whether these are found analytically or by numerical approximation.

A typical iteration involves a line search along the direction p_k from the original estimate x_k until a new minimum has been found. This new value, x_{k+1} is then used to reevaluate the search direction, and a new line search is started. This continues until the error in the solution of the necessary conditions is below a given tolerance or until it is determined that no solution exists (the number of iterations exceeds a maximum) or that an incorrect path and/or a local minimum has been found.

One of the simplest methods of computing p_k is the *method of steepest descent* which involves the calculation of the gradient of the function with respect to the gain F at the current estimate. For the problem at hand, the gradient of the cost with respect to the gain is one of the three necessary conditions and it can be obtained analytically. Since a successful search step requires the function M to decrease along the line, then it is required that $M_{k+1} < M_k$, so using Equation 3.67

$$M_{k+1} = M(x_k + \alpha_k p_k) \approx M_k + \alpha_k g_k^T p_k \tag{3.68}$$

as $\alpha \rightarrow 0^+$, then it is required that

$$g_k^T p_k < 0 \tag{3.69}$$

simply choosing

$$p_k = -g_k \tag{3.70}$$

will give the steepest descent direction for p_k.

So, given that a direction for the line search can be obtained from the first derivative of the function, all that remains is to determine the step size α_k. This is actually done by incrementing the value of α until a *region of uncertainty* can be found. This essentially is a bracket about a local minimum of $M(x)$ in the direction of p_k. The value of α is increased or decreased by multiplicative scale factors depending on the perceived slope of the surface along the direction of the line search and the function is evaluated at $x_k + \alpha p_k$ and $x_k + \frac{\alpha}{2} p_k$ until the middle value is lower than the two extremes. Once this coarse region of uncertainty has been located, the next step is to employ a technique to reduce the width of the bracket. Reference [58] discusses several of these methods. Some of these methods involve function evaluations within the bracket, whereas others employ polynomial interpolation of the function within this small region to find the local minimum. These latter group can be shown to have better rates of convergence, but have the disadvantage of requiring more information per step. In the program written for this work, a quadratic polynomial fit was selected to reduce the bracket size as it gives a high rate of convergence. Although the line search requires repeated function evaluations, it is found that these are a small fraction of the time required to evaluate the second derivative as will be discussed later.

This first order method provides acceptable rates of convergence far from the solution, but a second order method can offer much higher rates of convergence near the minimum. One commonly employed second order technique is known as Newton's method. This approach is based on a Taylor series expansion of the

gradient of the function

$$g_{k+1} = g(x_k + p_k) \approx g_k + H_k p_k \tag{3.71}$$

where H is the second derivative matrix known as the hessian. The motivation for this method is to produce a step such that $g_{k+1} = 0$. Of course, since the function is not in general quadratic, this cannot usually be achieved in one step, so an iteration is required. However, this statement is sufficient to define the current line search direction as

$$0 = g(x_k + p_k) \approx g_k + H_k p_k \tag{3.72}$$

$$p_k = -H_k^{-1} g_k \tag{3.73}$$

provided that the hessian matrix can be inverted which will generally be true near a solution if it is a strong mimimum. This method actually gives both the direction and the step size, but this can be modified by including a line search. For this direction to be one along which a descent occurs, it is necessary that

$$-g_k^T p_k = g_k^T H_k g_k > 0 \tag{3.74}$$

which is true provided $H_k > 0$ and $g_k \neq 0$. These conditions will be met near a strong minimum, but in general they will not be, so this method is only particularly useful when a good initial guess exists. The main benefit of this method is that the rate of convergence is second order, which is the fastest rate available [58].

As will be shown later, the major problem with this approach is that the hessian matrix is very expensive to determine numerically for a large order system, and from Equation 3.73 it can be seen that this matrix must be inverted as well. This poses problems in terms of the computation requirements and in terms of the numerical robustness. These problems demand that the calculations be done to a high precision, a fact which significantly slows down the running speed of the program. Another major problem is that the region for which convergence is guaranteed for the second order technique is fairly limited. This problem can partially

be overcome by employing a first order gradient minimization technique for the first set of line searches until the step sizes become relatively small indicating that this type of method is no longer effective. This in turn can be taken to indicate that a stationary point is being approached, and a switch to the second order Newton technique is made. Unfortunately, the first problem cannot really be avoided as the hessian must be calculated. However, it is possible to just update the result once the estimate is adequately close to the optimal answer using an approximate Quasi-Newton method. Reference [58] outlines several of these Quasi-Newton methods, but the Broyden-Fletcher-Goldfarb-Shanno (BFGS) technique is recommended as the most widely accepted.

For the BFGS method, the update is actually done for the inverse of the hessian as Equation 3.73 shows that it is this matrix which is required to determine the direction vector. So, if

$$\hat{H}_k = H_k^{-1} \tag{3.75}$$

and

$$\Delta x_k = x_{k+1} - x_k \tag{3.76}$$

$$\Delta g_k = g_{k+1} - g_k \tag{3.77}$$

then the update equation for $\hat{H}_{k+1}$ is given by

$$\hat{H}_{k+1} = \left[I - \frac{\Delta x_k \Delta g_k^T}{\Delta x_k^T \Delta g_k}\right] \hat{H}_k \left[I - \frac{\Delta x_k \Delta g_k^T}{\Delta x_k^T \Delta g_k}\right]^T + \frac{\Delta x_k \Delta x_k^T}{\Delta x_k^T \Delta g_k} \tag{3.78}$$

which is a far cheaper operation than the procedure discussed below for computing the hessian directly.

This completes the discussion of the techniques used in the numerical solution of the necessary conditions. The next section outlines the algorithm employed to calculate the hessian and gradient matrices which were shown above to be central to the solution procedure. The next section also shows why the size reduction allows the solution of this problem to become computationally feasible.

3.3.5 Numerical Approximation of the Gradient and Hessian

The analysis in this section makes frequent use of the concept of the derivative of a scalar or a matrix with respect to another matrix. As mentioned in the previous section, to perform this step, the matrices can be written as vectors. In this way, the differentiation is equivalent to the derivative of a vector valued function of a vector variable with respect to the vector. The vector representation of a matrix will be written in lower case, so that

$$f = \text{Vect}[F] \quad F = \text{Mat}[f] \tag{3.79}$$

The following is a brief outline of the steps involved in the calculation of the hessian and gradient of a function. The gradient, $\frac{\partial L}{\partial f}$, is actually one of the necessary conditions and it is derived in Appendix A. It is shown there that the resulting equation for the optimal output feedback problem with no constraints on the form of the gain matrix is

$$L_F = \frac{\partial L}{\partial F} = CQC^T F^T R_{uu} - CQPB \tag{3.80}$$

$$L_f = \text{Vect}[L_F] \tag{3.81}$$

In order to be able to calculate this value, it is necessary to evaluate the current values of $P(F)$ and $Q(F)$ from the appropriate Lyapunov equations which are also given in Appendix A. These three values P, Q, and F can then be substituted into Equation 3.80 to yield the current value of the gradient. This process requires the solution of two Lyapunov equations to obtain the updated values. For this case, the extension to the circulant or toeplitz transformed systems is straightforward, as it only involves a switch to the appropriate set of necessary conditions, which are also given in Appendix A.

However, it is far more complicated and expensive to determine the hessian of the function. Using the definition of the gradient given above, the hessian can be

written as

$$\frac{d}{df}(L_f)\,\Delta f = \frac{\partial L_f}{\partial f}\Delta f + \frac{\partial L_f}{\partial p}\Delta p + \frac{\partial L_f}{\partial q}\Delta q \tag{3.82}$$

If the gradient and gain matrices are written in vector form, then the evaluation of this expression will result in a symmetric matrix. The partial derivatives of the augmented cost with respect to P, Q, and F can be determined analytically from Equation 3.80 in the following way

$$\begin{aligned}\frac{\partial L_F}{\partial P}\Delta P &\approx L_F(P+\Delta P) - L_F(P) \\ &= \left[CQC^TF^TR_{uu} - CQ\left(P+\Delta P\right)B\right] - \left[CQC^TF^TR_{uu} - CQPB\right] \\ &= -CQ\Delta PB \end{aligned} \tag{3.83}$$

Then $\frac{\partial L_f}{\partial p}\Delta p = \text{Vect}[\frac{\partial L_F}{\partial P}\Delta P]$. Similarly, it can be shown that

$$\frac{\partial L_F}{\partial Q}\Delta Q \approx C\Delta Q\left(C^TF^TR_{uu} - PB\right) \tag{3.84}$$

$$\frac{\partial L_F}{\partial F}\Delta F \approx CQC^T\Delta F^TR_{uu} \tag{3.85}$$

which can then also be written in vector form. In Equations 3.83 through 3.85, it still remains to determine the appropriate values of ΔP and ΔQ. It is possible to calculate these values from the other two necessary conditions. Since the solutions of the Lyapunov equations, P and Q, depend on F, then the derivatives of these three variables are not independent, and the changes of the first two must be consistent with the changes in F. This constraint can be imposed through the Lyapunov equations by requiring that

$$\begin{aligned}&(P+\Delta P)\left[A - B\left(F+\Delta F\right)C\right] + \left[A - B\left(F+\Delta F\right)C\right]^T\left(P+\Delta P\right) + R_{xx} \\ &\qquad + C^T\left(F+\Delta F\right)^T R_{uu}\left(F+\Delta F\right)C = 0\end{aligned} \tag{3.86}$$

The zeroeth order (in Δ) expression will then just be the original Lyapunov equation. The first order expression will be a constraint equation for the change in the P given a change in F which can be written as

$$\Delta PA_{cl} + A_{cl}^T\Delta P + \left[C^T\Delta F^TR_{uu}FC + C^TF^TR_{uu}\Delta FC\right] = 0 \tag{3.87}$$

where $A_{cl} = A - BFC$. The same will hold for the other necessary condition, with the resulting constraint equation of the form

$$A_{cl}\Delta Q + \Delta Q A_{cl}^T - \left[B\Delta FCQ + Q(B\Delta FC)^T\right] = 0 \tag{3.88}$$

These two equations represent Lyapunov equations in ΔP and ΔQ driven by the combinations of the change in the gain matrix.

These Equations 3.80 through 3.88 allow the hessian to be evaluated using the following algorithm. The first step is to solve for the updated values of P and Q. The next step is to set the $(i,j)^{th}$ element of the ΔF matrix equal to one and the rest equal to zero. Then the resulting ΔP and ΔQ matrices are evaluated from Equations 3.87 and 3.88. These three values of ΔP, ΔQ, and ΔF are then used in Equations 3.83 through 3.85 to evaluate these separate derivatives, which are combined using Equation 3.82. The result will be the derivative of L_F with respect to the $(i,j)^{th}$ element of the gain matrix, which represents a column of the hessian matrix. Repeating this for each element of the gain matrix, will eventually yield a numerical approximation of the hessian. Notice that it is necessary to solve two Lyapunov equations to determine $P(F)$ and $Q(F)$, and that two more must be solved to determine ΔP and ΔQ, a task which must be repeated for every element of the gain matrix. This explains why the calculation of the hessian can be such a time consuming and expensive process, and why a reduction in the number of free parameters in the gain matrix and the size of the plant (the Lyapunov equation) is so important.

The extension to circulant systems is a little trickier for this case as there are $\overline{P}_i$ and $\overline{Q}_i$ matrices to be calculated for each value of $i \in [0,\ldots,\text{N-1}]$. The derivative of the gradient must be taken with respect to each of these terms. The resulting equation is very similar to Equation 3.82 except that it must be written as a summation over all values of the index variable. The resulting equation for the

special case of a block diagonal gain matrix so that $\overline{F}_k = F_0 \ \forall \ k \ \in [0,\ldots,\text{N-1}]$ is

$$\frac{d}{df_0}(L_f)\,\Delta f_0 = \frac{\partial L_f}{\partial f_0}\Delta f_0 + \sum_{i=0}^{N-1}\frac{\partial L_f}{\partial \overline{p}_i}\Delta\overline{p}_i + \sum_{i=0}^{N-1}\frac{\partial L_f}{\partial \overline{q}_i}\Delta\overline{q}_i \tag{3.89}$$

where the same procedure given above can now be employed, except that it must be done for each value of the index variable, so this will require the solution of many more Lyapunov equations per iteration, but, as mentioned earlier, each of the problems is much smaller in size.

3.3.6 The Solution Algorithm

The previous sections have developed theory necessary to present a method of calculating the gains for the constrained feedback problem for a block circulant system. The purpose of this section is to combine the discussions from these sections and to provide an outline of the algorithm used to calculate the feedback gains.

A circulant model of a beam (to be discussed in detail in Chapter 4) similar to the one shown in Figure 3.3 was used as the plant in Equations 3.9 and 3.10. This step requires the selection of both the number of bays in the model, and the number of nodes per bay. As will also be discussed in Chapter 4, the distance between the nodes was maintained at 1 unit so that the actual "size" of the model changes with the total number of nodes. In this example, the control problem for the local controller was selected to be a displacement weighted shape controller, and every actuator was taken to have an equal contribution to the cost. With these assumptions, each of the plant and control weighting matrices are then of the block circulant form shown in Equation 3.19. It was assumed in this work that every state in the bay can be measured so that $C = I$.

The next step was to use Equation 3.26 to transform the system and control matrices into the spatial frequency domain. Note that this in fact only requires the top row of each of the circulant matrices, which saves a large amount of storage

space. Due to the relative ease of performing matrix multiplications in this enviroment, these two steps were performed using a MATRIX$_X$ program. The next step was to use the optimization program that was developed to minimize the cost of the transformed system subject to the imposed constraints. This program was written in VAX FORTRAN because of the higher processing speeds available and is essentially a direct coding of the algorithms presented in Sections 3.3.4 and 3.3.5. The program is an extension of the work performed by Mercadal [42]. Both the gradient and Newton methods were employed to find the solution. The Quasi-Newton method was investigated, but examples showed that the convergence properties were particularly poor, so this technique was not included in the final set of programs.

One problem with most optimization procedures is that they typically are very sensitive to the initial conditions. A good approach that was implemented to eliminate this problem was to expand the results from one bay size so that they can be used as the initial guess for a larger bay. This helped to reduce the initial error in the solution and decreased the required number of gradient steps before the second order method could be employed.

The final step in the algorithm was to check that these are in fact the optimal gains. Another MATRIX$_X$ program was used to check that the gains solved the necessary conditions. The discussion as to whether the solutions are in fact the global minimum (as opposed to a local one) is delayed until the next section which will provide an overview of the results obtained.

3.3.7 Discussion of the Results

The purpose of this section is to present some of the results obtained using the algorithm outlined in Section 3.3.6. As was discussed there, convergence was found to occur much faster if the results from one bay size were used as the initial conditions for the next size up. However, for the sake of clarity, the results for the smaller bay

sizes have not been included, and only the results for the largest bay investigated, which has 9 nodes per bay, are shown in Figure 3.4 through 3.7. There are two components to the gain, the displacement and velocity parts. A row of these matrices corresponds to the feedback gains of all nine states to the actuator. A column of these matrices corresponds to the feedback gains on the state to all of the actuators. Note that the figures include three dimensional plots of the gains which allow the diagonal dominance to be easily visualized. Two dimensional plots across the rows are also included so that the peaks and gain shapes can be seen.

As was noted in the previous section, the question arises as to whether the optimal solution has in fact been obtained since both local minima and saddle points would solve the first order necessary conditions. An answer to this question can be found by considering the gains for the optimal unconstrained problem which will be developed in the next section, the results of which are shown in Figure 3.13. These graphs indicate that the gain matrices are diagonally dominant, and that the width of the non-zero part is on the order of 5 nodes. Of course, this is completely dependant on both the plant and the control weighting. However, for the example being investigated here, this indicates that it should be possible to develop a model with bays which are sufficiently large enough that the boundary effects are negligible for the middle controllers and the gains for the constrained and unconstrained cases can be compared directly. The results shown in Figures 3.4 through 3.7 show that this is in fact the case. Whereas the gains for the smaller bay sizes (2 or 3 nodes) are dominated by the boundary effects, the results for a much larger bay show that, for instance, the velocity gains for the middle five actuators are virtually identical to the optimal unconstrained solution. Note that the displacement gains are "thicker", so the boundary effects persist further into the gain block.

It can also be seen from this figure that the boundary effects have quite an influence on the gains of the controllers at both ends of the bay. The peak value of the gain for the end controllers is less than one half that for the controllers at the

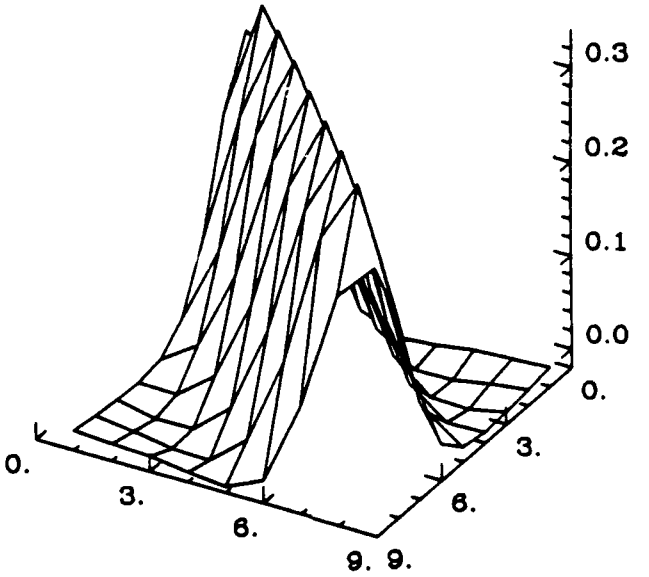

Figure 3.4: The displacement weighted displacement gain matrix for a nine node bay.

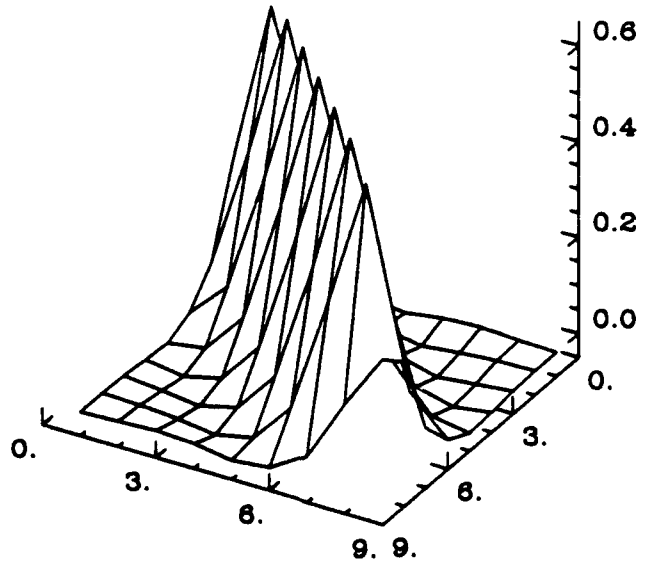

Figure 3.5: The displacement weighted velocity gain matrix for a nine node bay.

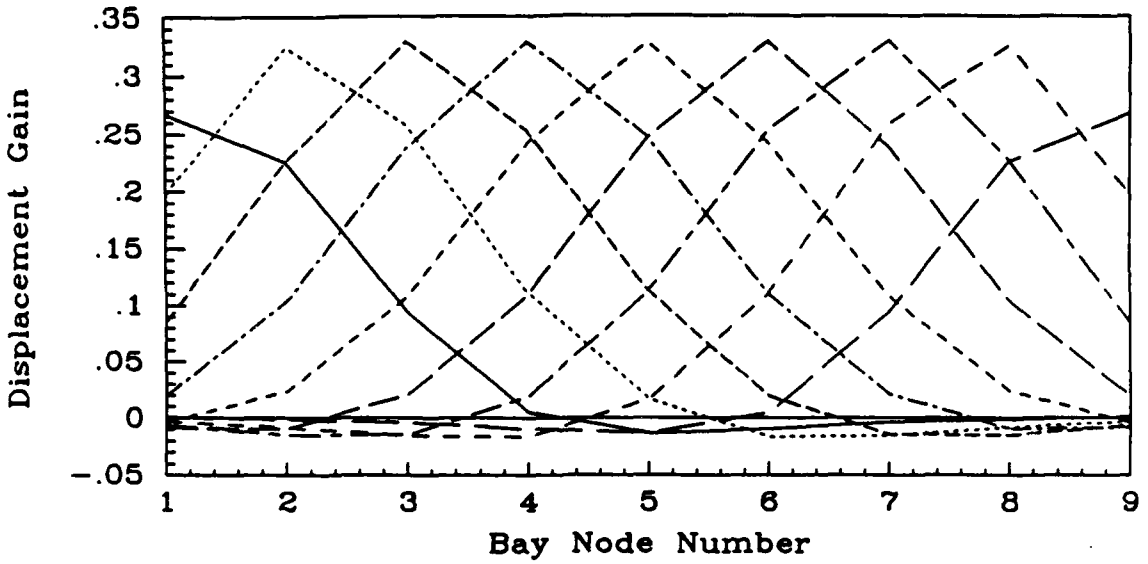

Figure 3.6: The displacement weighted displacement gain matrix for a nine node bay. This plot shows the variation across the rows of the matrix.

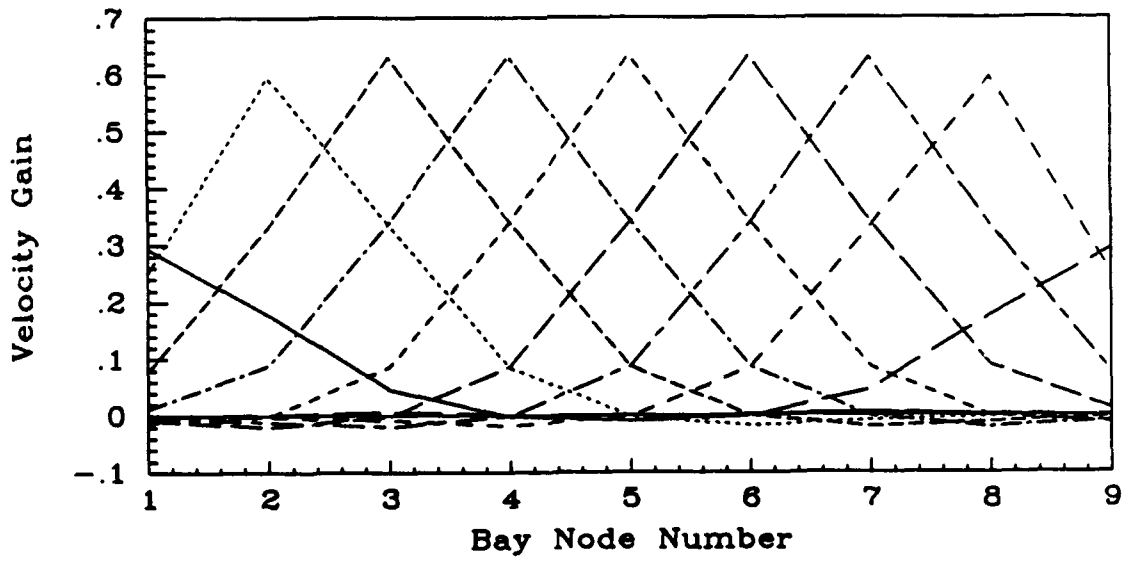

Figure 3.7: The displacement weighted velocity gain matrix for a nine node bay. This plot shows the variation across the rows of the matrix.

internal nodes. However, it also appears that the entire gain for the end controllers has been reduced by a similar scale factor. Since there are no significant non-zero gains at nodes further away from the controller than a central controller would require, it appears that an end controller does not use any additional information from inside the bay. This is an interesting point because it indicates that, although almost half of the information has been truncated for the end controllers (they cannot feedback displacments or velocities outside of the bay), the gain "shape" is very similar to that for the unconstrained case (to within a scale factor).

One other point to be discussed about this technique is that, although the size reduction does make it feasible to obtain the solution, calculating the optimal gains can be a very time consuming process. In particular, the calculation of the hessian is a very expensive operation, and typically would take 24 hours of CPU time on a Vax Station II for a bay size of 9 nodes and 10 bays in the system. Of course, this is nothing compared to the amount of time that would have been required for the full model. Computational times for smaller bay sizes are more reasonable, with problems of 5 or 6 nodes per bay and 20 bays requiring about 1 day to completely finish the algorithm. It is interesting to note that the second order Newton method was found to converge very rapidly to the optimal solution, with step reductions in the error of 4 or 5 orders of magnitude typically occurring on the last step.

3.4 Block Tri-Diagonal Feedback

3.4.1 Introduction

This form of the gain structure is important because it allows for some communication between the local controllers. In contrast to the previous cases that were examined, an exchange of information both internal and external to the finite control element is allowed, but it is restricted to occur only with adjacent elements.

Since each controller has more information available than the previous cases, this should allow the overall performance to improve. It also helps to eliminate the problem mentioned earlier in which a controller is a short distance from a sensor but they are separated by an element boundary so the measurement cannot be used for feedback. However, there are the associated penalties that the local processors must be more sophisticated since they are required to perform more tasks, and the computer architecture will be more complicated to allow information to be exchanged between elements.

As is shown in Figure 3.8, this type of control can be implemented in two ways. The first allows each local controller to measure the sensors in its element and then local communication between the controllers is employed to exchange the information with the adjacent processors. The second approach allows each controller to directly measure the sensors from its own element and its neighbors. Either setup will allow for the block tri-diagonal gain structure that is desired. A comparison of these designs will show the trade-off between having the extra measurement hardware built into the structure and having to do local communication between processors.

The second technique requires a more complicated wiring set up and several processors must obtain the measurements from each sensor, but little local coordination between the controllers is required. The first approach is more compact in that it is conceptually neater, but it has a major disadvantage in that it requires the local controllers to be coordinated and dedicate some portion of their loop cycle to sending and receiving information from its neighboring processors. There are delay issues involved here as well, as some information is transferred rather than directly measured.

There is a subset of the full block tri-diagonal form of the gain matrices which is of particular importance. This is the banded gain matrix where the band width is small enough to be covered by only one extra set of off-diagonal block matrices.

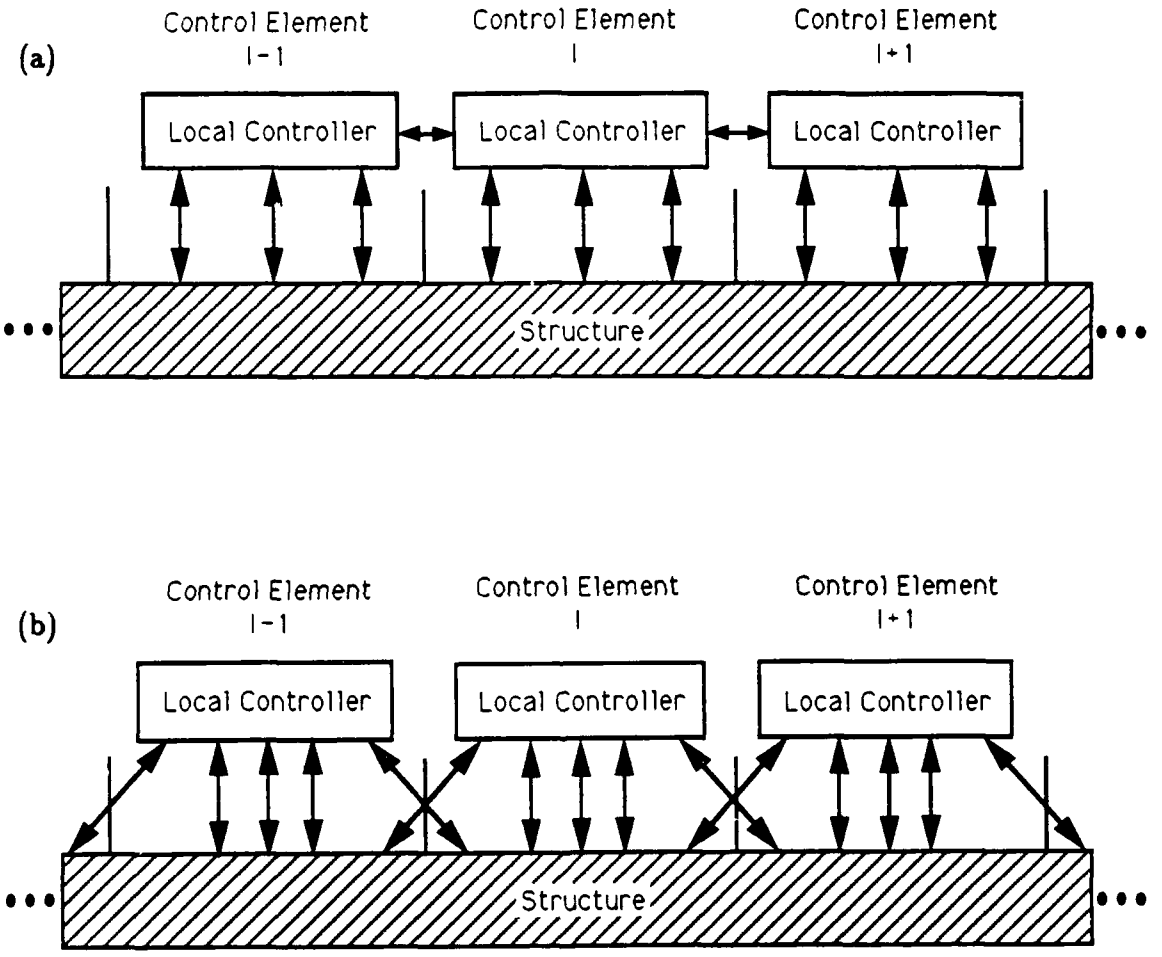

Figure 3.8: The architecture for a local controller based on block tri-diagonal feedback. The top figure (a) corresponds to the case where a local controller measures the sensors within that element and then shares this information with adjacent processors. The lower figure (b) is the case where each local controller measures the required information directly from each finite control element.

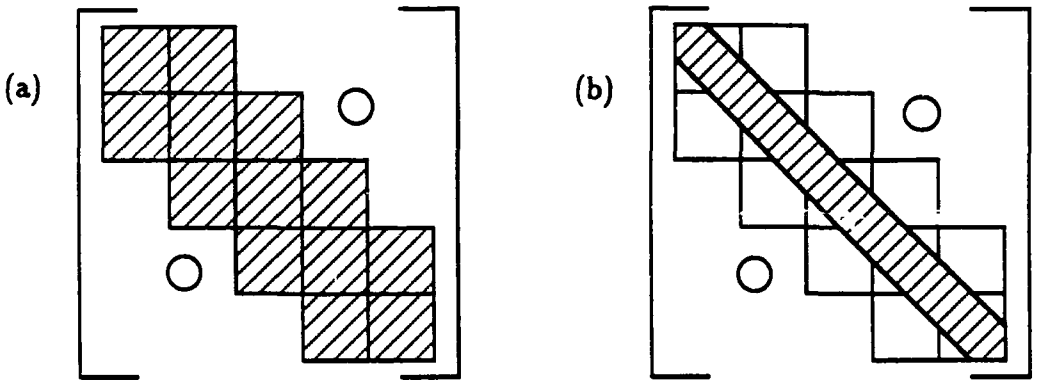

Figure 3.9: Two types of gain matrices for the block tri-diagonal feedback approach. The figure on the left (a) corresponds to the full block tri-diagonal feedback, and the one on the right (b) to the banded feedback.

If the bandwidth is smaller than the element size then it is not necessary for all of the main diagonal block to be full. Consequently, only parts of the three block matrices in a given row need to be non-zero. The advantage of this technique is that it reduces the amount of information that must be passed from processor to processor, or conversely, how far into the adjacent elements the extra measurement wires must be extended. The form of the gain matrices for the two cases are shown in Figure 3.9.

The resulting form of the control equation now is

$$\begin{bmatrix} u_1 \\ u_2 \\ u_3 \\ \vdots \\ u_N \end{bmatrix} = - \begin{bmatrix} F_{1q_1} & F_{1q_2} & 0 & \cdots & 0 \\ F_{2q_1} & F_{2q_2} & F_{2q_3} & & 0 \\ 0 & F_{3q_2} & F_{3q_3} & & 0 \\ \vdots & & & \ddots & \\ 0 & 0 & 0 & F_{Nq_{N-1}} & F_{Nq_N} \end{bmatrix} \begin{bmatrix} q_1 \\ q_2 \\ q_3 \\ \vdots \\ q_N \end{bmatrix}$$

$$- \begin{bmatrix} F_{1\dot{q}_1} & F_{2\dot{q}_1} & 0 & \cdots & 0 \\ F_{2\dot{q}_1} & F_{2\dot{q}_2} & F_{2\dot{q}_3} & & 0 \\ 0 & F_{3\dot{q}_2} & F_{3\dot{q}_3} & & 0 \\ \vdots & & & \ddots & \\ 0 & 0 & 0 & F_{N\dot{q}_{N-1}} & F_{N\dot{q}_N} \end{bmatrix} \begin{bmatrix} \dot{q}_1 \\ \dot{q}_2 \\ \dot{q}_3 \\ \vdots \\ \dot{q}_N \end{bmatrix} \tag{3.90}$$

where q_i and u_i again represent the vectors of the states or control for each element, and F_{kq_i} the gain block matrix for controller k from the state component q_i. For this tri-diagonal restriction, $i = k-1, k, k+1$, *i.e.*, only the closest neighbor gain blocks are allowed to be non-zero. In this case, no restriction is made on the actual structure within the gain blocks, only on the blocks which can be non-zero. In this way, the case of the purely banded gain matrix can also be included. The following section will outline a simple method for calculating the appropriate gain matrices.

3.4.2 Calculation of the Gains

One approach to selecting the gain blocks is to compute the optimal full state feedback (assuming all measurements can be made within the element) gains for the structure and then employ some form of truncation on the allowable extent of the gains so that the desired structure can be obtained. This assumes that the gains will be fairly banded so that the block tri-diagonal structure will include all of the important gain values. In the limit, as the gains become more banded, it may be conceivable to capture the important structure within the width of one element, so the off-diagonal blocks will only be non-zero in the upper right or lower left corners to compensate for information lost near the ends of the element (this is shown by the shaded part of the gain matrix in Figure 3.9). The gains obtained for the examples investigated here do possess a high degree of bandedness. For other cases where this assumption does not hold another approach will be discussed later.

The full state feedback gains are computationally intensive to calculate for the

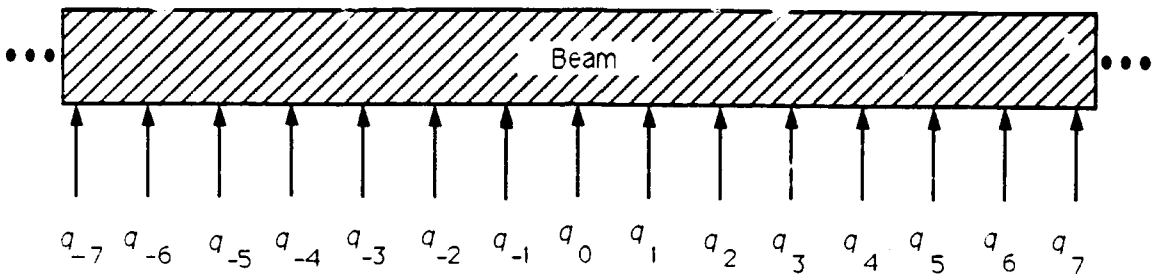

Figure 3.10: A model of an infinite dimensional symmetric beam.

full sized system. Consequently, a procedure for calculating the gains for very large structures that possess a high degree of spatial symmetry will be developed. For this work, it is assumed that the structure, taken to be a uniform beam, is symmetric along its entire length. The previous work with the block diagonal feedback it only assumed that the beam consisted of repeated bays. Of course, a uniform beam is symmetric at this level as well.

The first step in the design procedure is to employ the z-transformation on the symmetric structure to obtain the transformed dynamics $A(z), B(z)$, and $C(z)$. This can be done by recognizing the length of the structure which is being repeated and then performing the analysis given below. First, take a uniform beam as shown in Figure 3.10. By recognizing that the bay $(q_0 - q_1)$ is repeated along the entire length of the beam, it is possible to reduce this infinite system using a z-transform. As with the more familiar example of the discrete time case, it is possiblc to associate a power of z with the relative displacement between the node of interest, q_0, and any other node.

Using q to denote the degrees of freedom at a node, then a finite element model of the beam in Figure 3.10 would give the dynamic equations as

$$M\ddot{q} + Kq = \Psi u \tag{3.91}$$

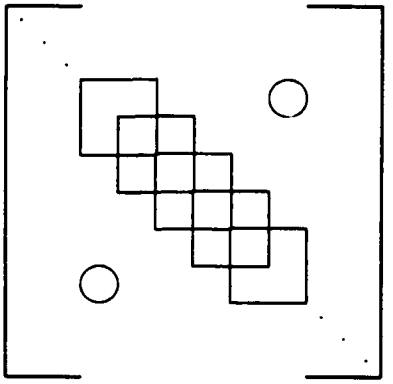

Figure 3.11: The form of the FEM mass and stiffness matrices for the infinite beam example. Each square corresponds to the appropriate element matrix of the FEM.

where M, K, Ψ, q, and u are infinite dimensional, and M and K have the internal form shown in Figure 3.11. Ψ is in fact diagonal as each actuator is associated directly with a node $\Psi = \text{diag}(\psi_i)$. Each block along the diagonal in Figure 3.11 is the element mass or stiffness matrix for the FEM, and these can be partitioned in the following way

$$M_{ele} = \left[\begin{array}{c|c} M_{11} & M_{12} \\ \hline M_{21} & M_{22} \end{array}\right] \quad K_{ele} = \left[\begin{array}{c|c} K_{11} & K_{12} \\ \hline K_{21} & K_{22} \end{array}\right] \tag{3.92}$$

For a beam, M_{ele} is a 4×4 matrix consisting of 4, 2×2 block matrices since there are two degrees of freedom (displacement and rotation) per node, and 2 nodes per element. Then, employing the z-transform on the vector of states and controls as

discussed above, q and u can be re-written in the transformed representation as

$$q(z) = \begin{bmatrix} \vdots \\ z^{-2}q_0 \\ z^{-1}q_0 \\ q_0 \\ z^1 q_0 \\ z^2 q_0 \\ \vdots \end{bmatrix} \quad u(z) = \begin{bmatrix} \vdots \\ z^{-2}u_0 \\ z^{-1}u_0 \\ u_0 \\ z^1 u_0 \\ z^2 u_0 \\ \vdots \end{bmatrix} \tag{3.93}$$

Looking across the row of Equation 3.91 which uses the states q_{-1}, q_0, and q_1 ($z^{-1}q_0$, q_0, and zq_0), this equation can be written as

$$M_{21}z^{-1}\tilde{q}_0 + (M_{11} + M_{22})\tilde{q}_0 + M_{12}z\tilde{q}_0 + K_{21}z^{-1}q_0 + (K_{11} + K_{22})q_0 + K_{12}zq_0 = \psi_0 u_0 \tag{3.94}$$

which, in fact would be the same for all the rows. This follows directly from the definition of $u(z)$ and Equation 3.91. Equation 3.94 can be rewritten in a far more compact manner as

$$\begin{bmatrix} I \\ zI \end{bmatrix}^T \begin{bmatrix} M_{11} & M_{12} \\ M_{21} & M_{22} \end{bmatrix} \begin{bmatrix} I \\ zI \end{bmatrix} \tilde{q}_0 + \begin{bmatrix} I \\ zI \end{bmatrix}^T \begin{bmatrix} K_{11} & K_{12} \\ K_{21} & K_{22} \end{bmatrix} \begin{bmatrix} I \\ zI \end{bmatrix} q_0 = \psi_0 u_0 \tag{3.95}$$

for all values of $z = e^{j\theta}, \theta \in [0, 2\pi]$. Note that, since $\|z\|_2 = 1$, then $z^{-1} = z^*$. This provides for a very easy way to develop the transformed system matrices directly from the element matrices of the FEM. This result can easily be extended to the case where the symmetry is at the bay level by introducing a different transformation matrix T_2. For a repeated bay with n nodes

$$T_2 = \left[\begin{array}{cc} I_2 & 0 \\ 0 & I_{n-2} \\ \hline zI_2 & 0_{2\times n-2} \end{array}\right] \tag{3.96}$$

After this step of transforming the system dynamics, it is possible to perform the mass condensation procedure discussed in Chapter 2 to eliminate the rotational

degrees of freedom from the model. The resulting $M(z)$ and $K(z)$ matrices can then be used to form $A(z)$, $B(z)$, and $C(z)$.

As is shown in Section 3.3.3, this transformation greatly simplifies the unconstrained full state feedback control design as it decouples the necessary conditions and allows for much smaller systems to be used. The penalty is that this design process must be done for every value of z around the unit circle to generate the gains at each spatial frequency. Clearly, this cannot be done analytically for any system of appreciable size, so the solution must be approximated. As with digital control design [25], it is convenient at this point to introduce a new variable w which is related to z via

$$w = \frac{2}{l}\frac{z-1}{z+1} \tag{3.97}$$

where, if $z = e^{j l \theta}$, then $w = j\nu = j\frac{2}{l}\tan\frac{\theta l}{2}$. So, as z goes around the unit circle anti-clockwise from 1 to -1, w moves up the $j\nu$ axis from 0 to ∞. It is then useful to use ν to define θ which in turn defines z. Then log-spacing ν allows for a convenient representation of the gains in the spatial frequency domain. The next step requires that the control problem (*i.e.*, the weighting matrices) be transformed into the frequency domain using techniques very similar to those used in Section 3.3.3.

Given that the system and control weighting matrices can easily be transformed, it is then possible to employ a LQR solver at each frequency to obtain the gains as a function of frequency at a discrete number of points around the unit circle. Typical plots for various state weightings are given in Figures 3.12, 3.14, and 3.16. The weightings investigated were velocity, energy, and displacement. The next step is to perform the inverse z-transform defined by Equation 3.46 to generate the optimal gains as a function of the spatial coordinate. The results for the same set of weightings are given in Figures 3.13, 3.15, and 3.17. For the sake of comparison, the optimal regulator gains for a long beam were computed for the displacement weighting case, and the gains for an actuator located in the middle of the beam are presented in Figure 3.18. As would be expected, the results are virtually identical.

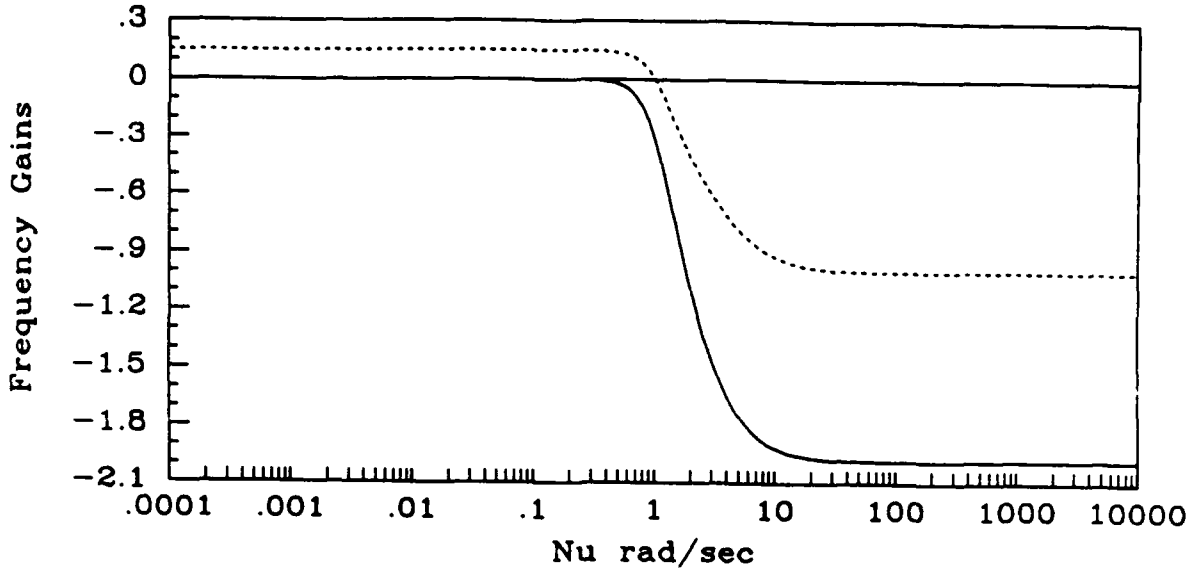

Figure 3.12: The displacement weighted gains in the frequency domain. The dotted line is the feedback on velocity and the solid is the feedback on the displacement.

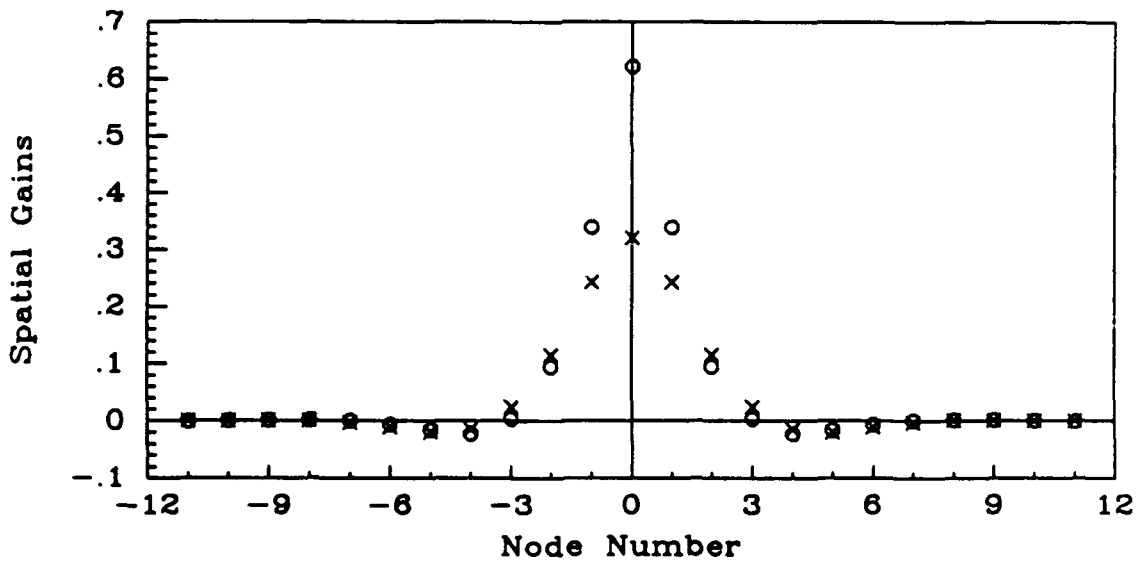

Figure 3.13: The displacement weighted gains in the spatial domain. The circles are the feedback on the velocity at that node for an actuator at the origin, and the crosses are the feedback on the displacement.

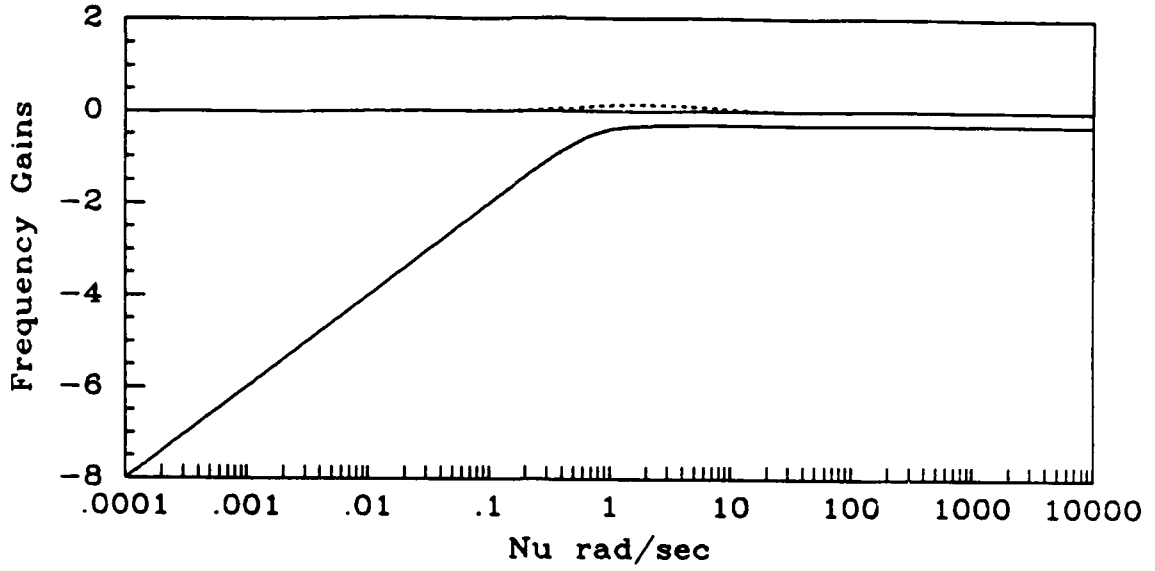

Figure 3.14: The energy weighted gains in the frequency domain. The dotted line is the feedback on velocity and the solid is the feedback on the displacement.

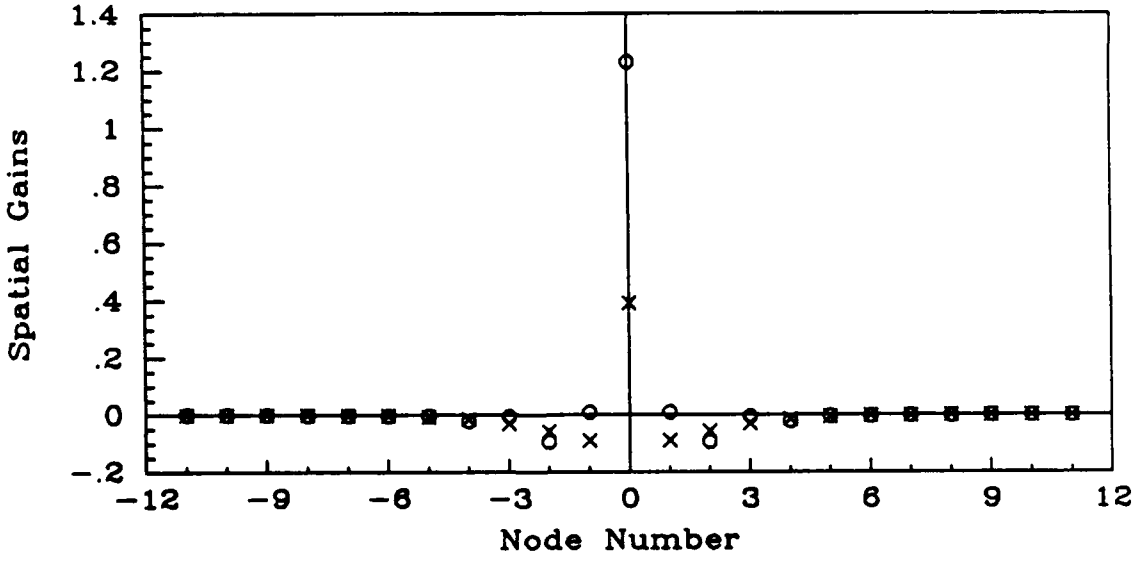

Figure 3.15: The energy weighted gains in the spatial domain. The circles are the feedback on the velocity at that node for an actuator at the origin, and the crosses are the feedback on the displacement.

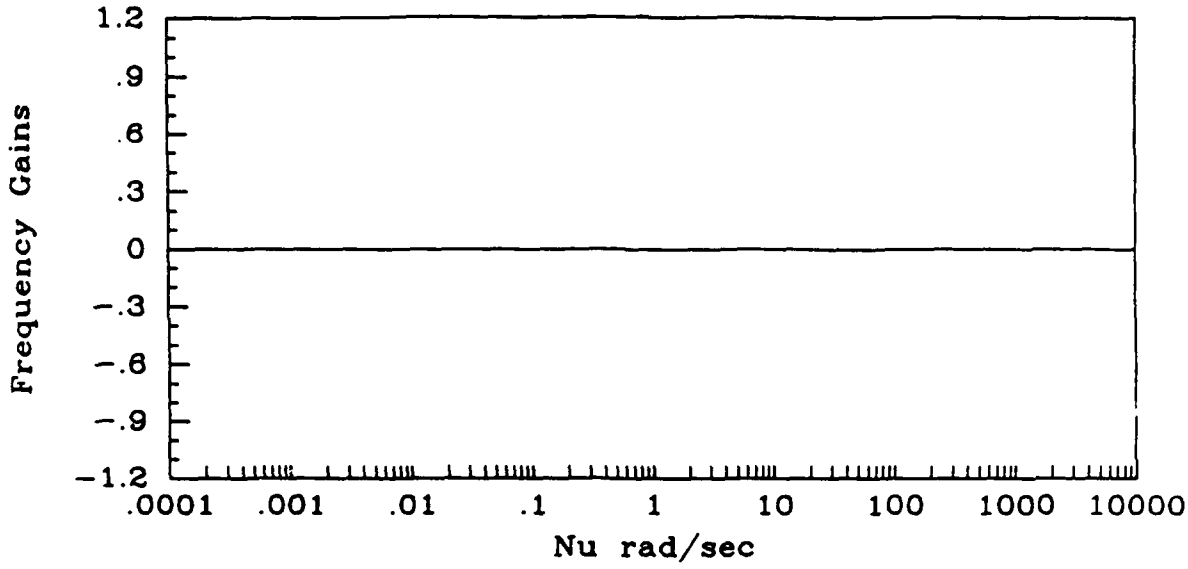

Figure 3.16: The velocity weighted gains in the frequency domain. The dotted line is the feedback on velocity and the solid is the feedback on the displacement.

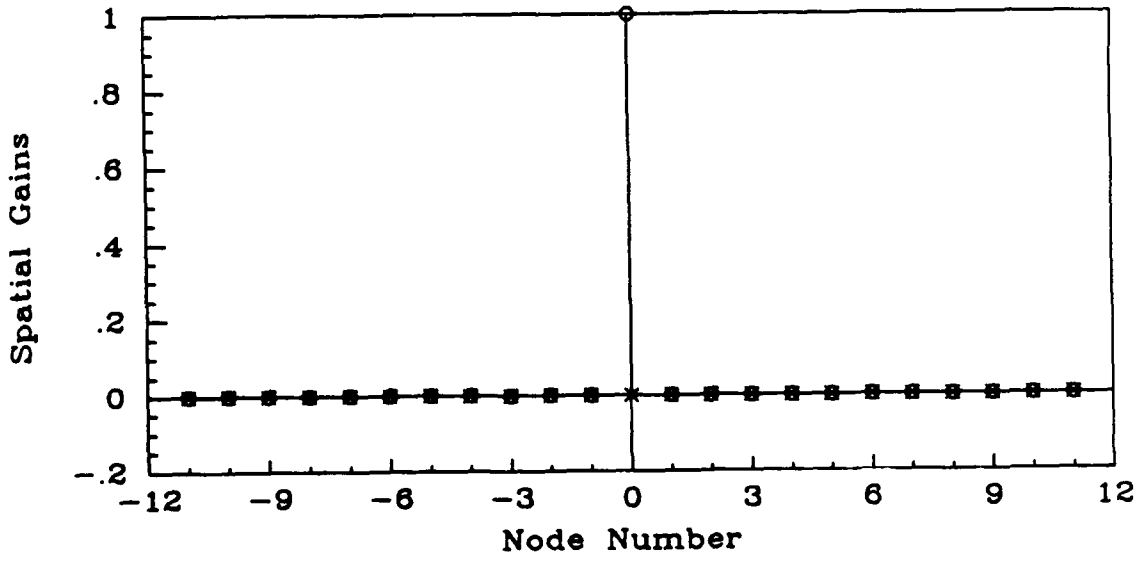

Figure 3.17: The velocity weighted gains in the spatial domain. The circles are the feedback on the velocity at that node for an actuator at the origin, and the crosses are the feedback on the displacement.

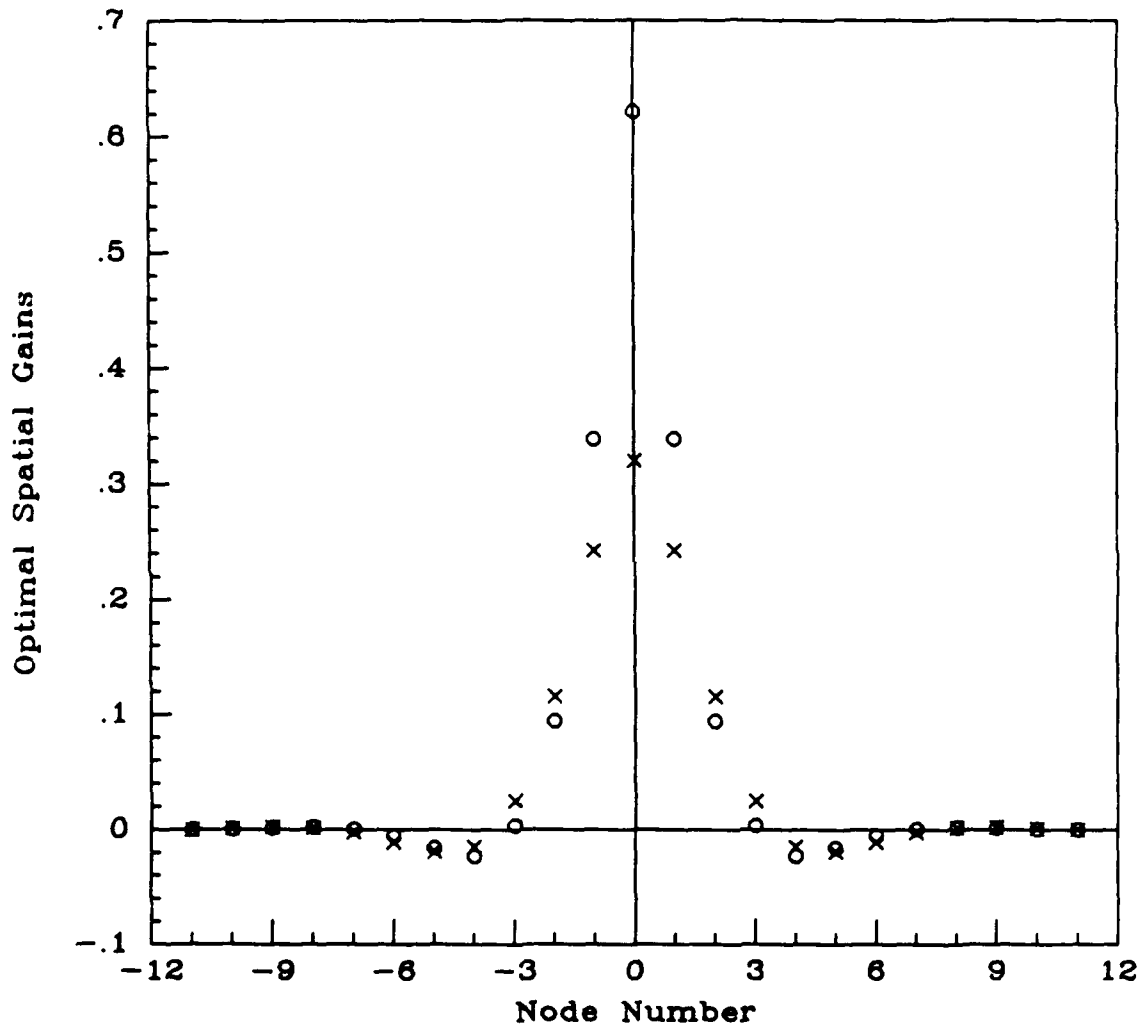

Figure 3.18: The optimal displacement weighted regulator gains for an actuator in the middle of a long beam. The circles are the feedback on the velocity at that node for an actuator at the origin, and the crosses are the feedback on the displacement.

3.4.3 Conclusions

From the results presented, it is clear that this technique represents a relatively easy and convenient method to calculate the optimal feedback gains for a large structure with spatial symmetry. The results for the different weightings show that the gains for this example are quite strongly banded, with the displacement weighting having the largest "width". Provided that the gains are banded sufficiently relative to the finite control element size, then just using the truncated optimal gains will be a sufficiently good approximation for the suboptimal gains. Results in Chapter 4 will show how well the banded and full block tri-diagonal gain structures approximate the optimal solution.

If the analysis shows that too much information is lost by the truncation operation, *i.e.*, the important part of the gain structure is relatively "wide", then it may be necessary to perform an optimization similar to the one done in the previous section, with the modification that the restriction on the form of the gain matrix be relaxed so that F can be block tri-diagonal.

3.5 A Decentralized Implementation of Full State Feedback

3.5.1 Introduction

The purpose of this section is to discuss the final form for the local controller. This architecture uses the gains calculated for the centralized full state feedback but they are implemented in a decentralized manner. This design is based on the concept of the disturbance information "flowing" along the structure as "waves". A control architecture is developed which complements this way of looking at the movement of information in a structure. This is achieved by approximating the

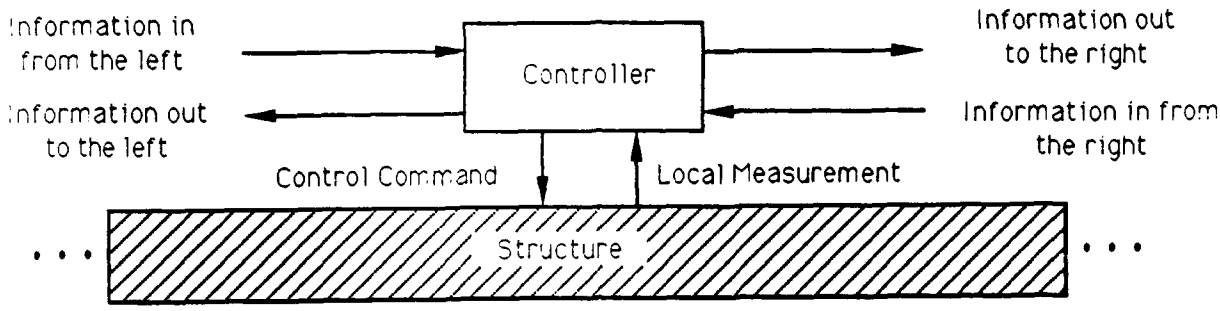

Figure 3.19: A schematic of the decentralized implementation of full state feedback.

gains obtained in the previous section as a function of the spatial frequency and writing them in a state space representation. The controllers use the measurements from either side of their location to calculate the appropriate commands. These measurements are then passed onto the adjacent processors to continue the cycle. The resulting architecture is shown in Figure 3.19. The information is very rapidly transmitted from controller to controller in both directions along the structure, and the actual command calculation at each node will be shown to be relatively simple. In contrast to the other types of controllers considered earlier, the one developed in this section relies almost entirely on the direct communication between local controllers. The purpose of this section is to provide an overview of the architecture and to present a methodology for calculating the state space representation. As was done in Sections 3.3 and 3.4, an example based on the displacement gain of a displacement weighted controller will be examined.

3.5.2 Calculation of the Gains

It will be assumed during this discussion that the procedure outlined in Section 3.4.2 for calculating the gains as a function of spatial frequency has already been employed, so that $F_o(w)$ exists. The next step is to form an approximation for this gain over a specified frequency range. For the displacement weighted gains shown in Figure 3.12, it has been found through experience that matching the gains at low frequencies is far more important in terms of obtaining a good approximation for the gains in the spatial domain than matching at high frequencies. A curvefitting program (see reference [52]) was employed to obtain the poles and zeroes for a transfer function approximation of the original curve. Since the number of poles determines the order of the finite difference approximation, it is desirable to obtain a good match with as few poles as possible. However, due to the complexity of the gains shapes, it was not always possible to match the curves exactly at every frequency with a small set of poles and zeroes.

The gain curve is approximated in the w-plane. The approximation was constrained to have only four poles and zeroes, so it can be expressed as

$$F(w) = K_w \left[\frac{(w-b_1)(w-b_2)(w-b_3)(w-b_4)}{(w-a_1)(w-a_2)(w-a_3)(w-a_4)} \right] \tag{3.98}$$

For this example, the zeroes were found to be in two real pairs which are symmetric about the imaginary axis. The four poles were found to be symmetric about both axes, so, for example, $b_3 = -b_1$ and $a_3 = a_1^*$. It is possible to obtain a representation of the approximate gain in the z-plane using the method of pole-zero mapping and the transformation

$$z = \frac{1 + \frac{wl}{2}}{1 - \frac{wl}{2}} \tag{3.99}$$

which is the inverse transform of Equation 3.97. In direct analogy to the discrete time case, l represents the distance between the nodes in the spatial domain. In this example, $l = 1$. Equation 3.99 is used with w taking on the values of $\pm b_1, \pm b_2, \ldots, a_2^*$

as in Equation 3.98, to generate the corresponding poles in the z-plane. The mapping is completed by imposing the condition that

$$F(w)|_{w=0} = F(z)|_{z=1} \tag{3.100}$$

so, in the z-plane, the gain can be approximated as

$$F(z) = K_s \left[\frac{(z - z_1)\,(z - \frac{1}{z_1})\,(z - z_2)\,(z - \frac{1}{z_2})}{(z - p_1)\,(z - p_1^*)\,(z - p_2)\,(z - p_2^*)} \right] \tag{3.101}$$

In the z-plane, the poles lie on two radial lines and are reciprocals with respect to the unit circle $\|z\|_2 = 1$. This result is a direct consequence of the assumed symmetry of the plant. A pole distribution with this symmetry with respect to the unit circle will have non-causal pulse responses (equivalent to a spatial representation of the gains) which are symmetric about the origin. So, as would be expected, the information obtained from both directions will be treated in the same manner.

Once this step of obtaining a rational fraction z-plane approximation of the gains has been completed, it is possible to inverse z-transform the gains and express them as functions of the spatial coordinate. For this example of the displacement gain for the displacement weighted control design the approximate gain can be shown to be of the form

$$F(x) = K_s \left[\delta(x) + G_1 r^{|x|} \left(c_1 \cos x\theta + c_2 \sin |x|\theta \right) \right] \tag{3.102}$$

where $x \in (-\infty, \infty)$ is an integer which denotes the relative number of nodes that separates the two points of interest. The poles are given by $p_1 = re^{j\theta}$ and $p_2 = \frac{1}{r}e^{j\theta}$. The coefficients K_s, G_1, c_1 and c_2 are coefficients which depend on the pole and zero locations. $\delta(x)$ denotes the Kronecker delta function which is equal to one for $x = 0$ and zero for all other values of x. Plots of this function for typical values of r and θ calculated for this example are given in Figure 3.21 where the analytic result is also compared to the numerical inversion of the optimal gain.

This completes the analysis required to approximate the gain. The next step is to develop a way of expressing the control calculation in terms of a simple multiplication of the measurement information which is travelling to the left and right of a

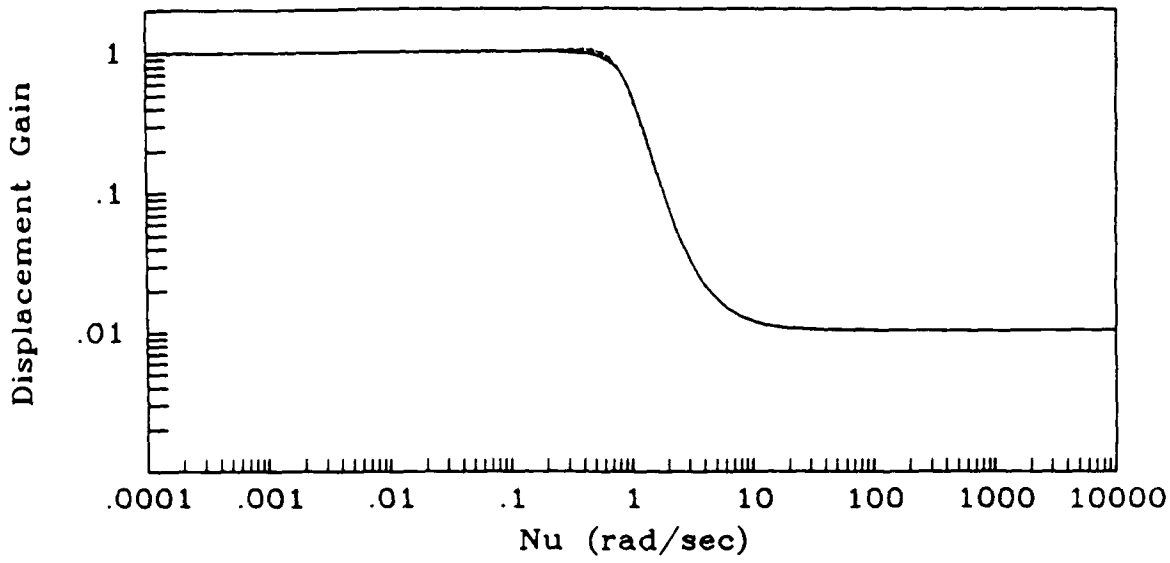

Figure 3.20: Comparison of the optimal (solid) and approximate gains (dotted) in the frequency domain (w).

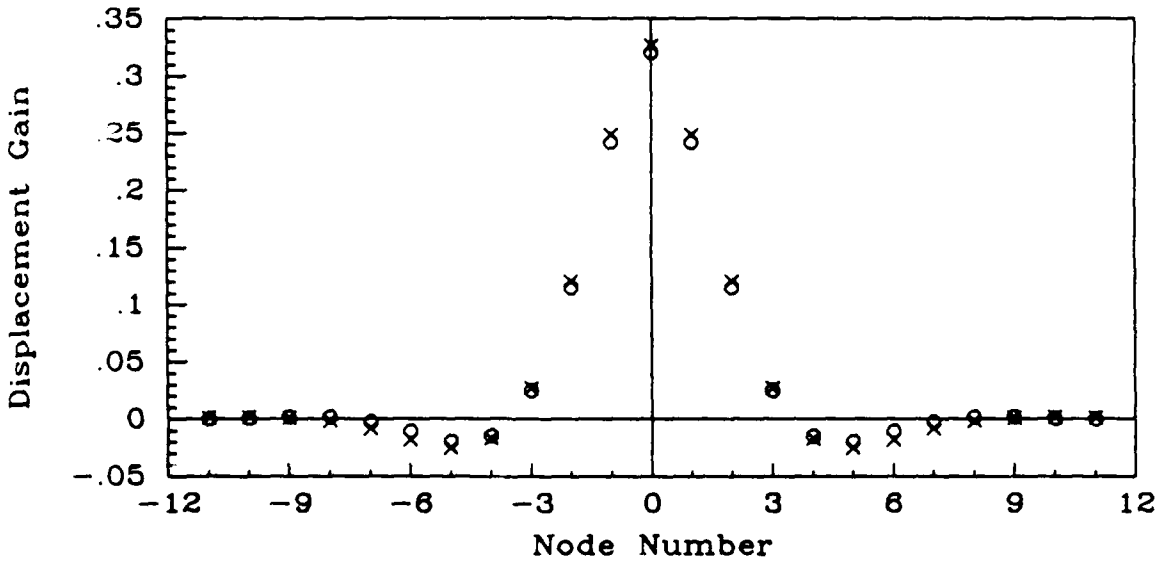

Figure 3.21: Comparison of the optimal (circles) and approximate (x's) gains as a function of the node number.

given location. A more detailed schematic showing this split is given in Figure 3.22. With a transfer function representation of the gain available in z-plane, it is possible to obtain a more useful state-space description. This can easily be done using any conversion algorithm (such as the one in MATRIX$_X$). The result is two sets of finite difference equations which relate the control commands to the information "flowing" past the actuator location from either the left or right. This information is stored in the vectors $q_c(i)$ and $q_{ac}(i)$. For the displacement part of the gain, the finite difference equations can be written as

$$q_c(i+1) = A_c q_c(i) + B_c y_d(i) \tag{3.103}$$

$$u_{c_d}(i) = C_c q_c(i) + D_c y_d(i) \tag{3.104}$$

$$u'_{c_d}(i) = C_c q_c(i) \tag{3.105}$$

$$q_{ac}(i-1) = A_{ac} q_{ac}(i) + B_{ac} y_d(i) \tag{3.106}$$

$$u_{ac_d}(i) = C_{ac} q_{ac}(i) \tag{3.107}$$

where $(\cdot)_c$ represents the causal part, and $(\cdot)_d$ represents the displacement part of the gain. It can easily be shown that the system matrices are equal (*i.e.*, $A_{ac} = A_c$, $B_{ac} = B_c$, and $C_{ac} = C_c$), which is to be expected given the symmetry of the gains.

The state space representation is developed in two parts, with the the distinction between the two being the information that each has available to calculate the control commands. The causal $(\cdot)_c$ representation uses the information which is moving to the right, and the anti-causal $(\cdot)_{ac}$ uses that which is moving to the left. Implementating the models in Equations 3.103 through 3.107 Figure 3.22, and including the correct gains and the delta function at the origin, the complete architecture is of the form shown in Figure 3.23. The complete control at any station i is then

$$u(i) = K_s \left[y(i) + G_1 \left[u_c(i) + u_{ac}(i) \right] \right] \tag{3.108}$$

$$= K_s \left[y(i) \left(1 + G_1 D_c \right) + G_1 \left[u'_c(i) + u_{ac}(i) \right] \right] \tag{3.109}$$

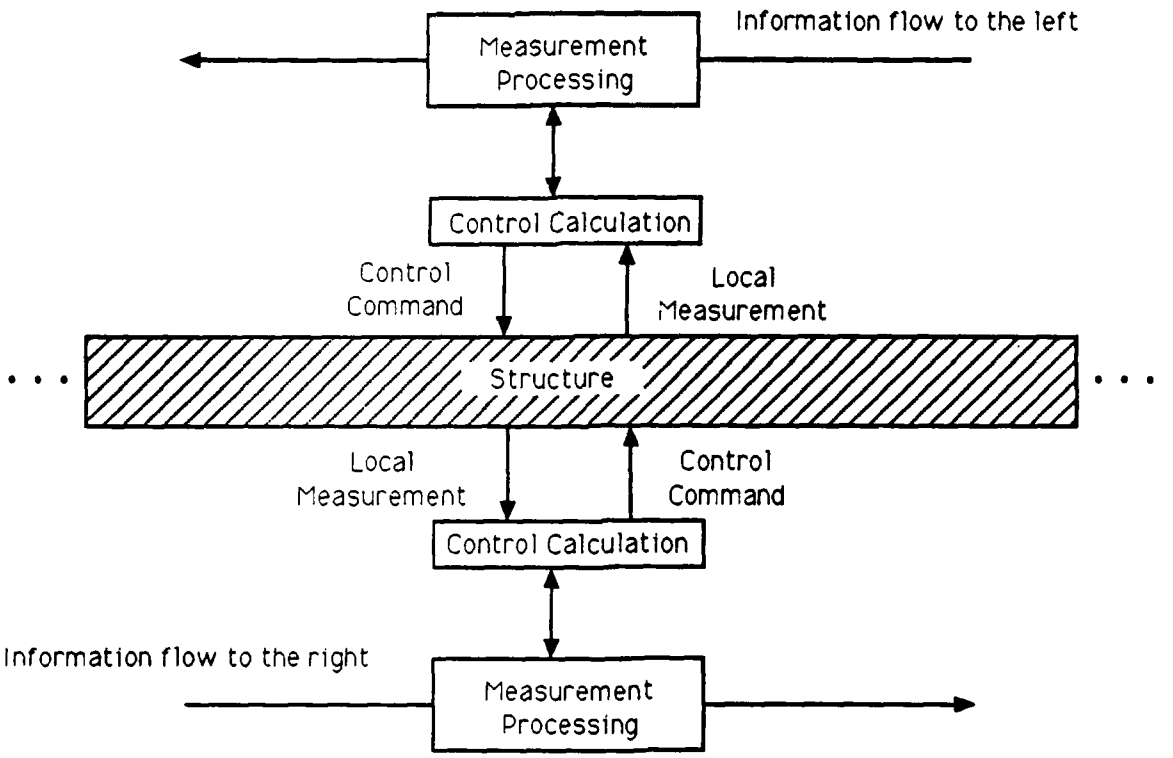

Figure 3.22: A more detailed representation of the control architecture for the decentralized implementation. There are two flows of information. This figure shows that the two tasks of calculating the control commands and processing the information flow can be separated.

which would hold for every node along the structure.

This completes the discussion of the control architecture. The implementation of this controller is somewhat more difficult than the previous designs as it must be discrete in both space and time. Information is not directly measured by every controller. Instead, each sensor is measured by one controller and the information is passed onto the neighboring nodes. The information is then modified to account for the distance travelled (essentially multiplied by the complex pole so that it is reduced in magnitude and phase shifted), added to the current measurement at the new location, and then passed on to continue the cycle. This will require a very rapid flow of information along the length of the structure so that the measurements are still relatively valid. The required "speed" of the information flow will depend on how fast the disturbances propogate in the structure. It will be very easy to pass information from controller to controller within a finite control element if they are all implementated within the same processor. However, this architecture will also require very rapid inter-processor communication. The bandedness of the gains will also play an important role in the implementation since it will determine how far the information must travel before the gains are so small that the influence will be negligible.

3.6 Conclusions

The purpose of this chapter was to present and analyze various types of local control designs for the hierarchic control architecture. Four types of controllers were introduced. Of these, colocated control is the simplest to implement since it only requires the information to be exchanged between the sensor and actuator pairs. Block diagonal feedback represented the next level of sophistication. It does not allow for communication between processors, but the actuator commands are calculated from the measurements at every sensor in the finite control element. Allowances were

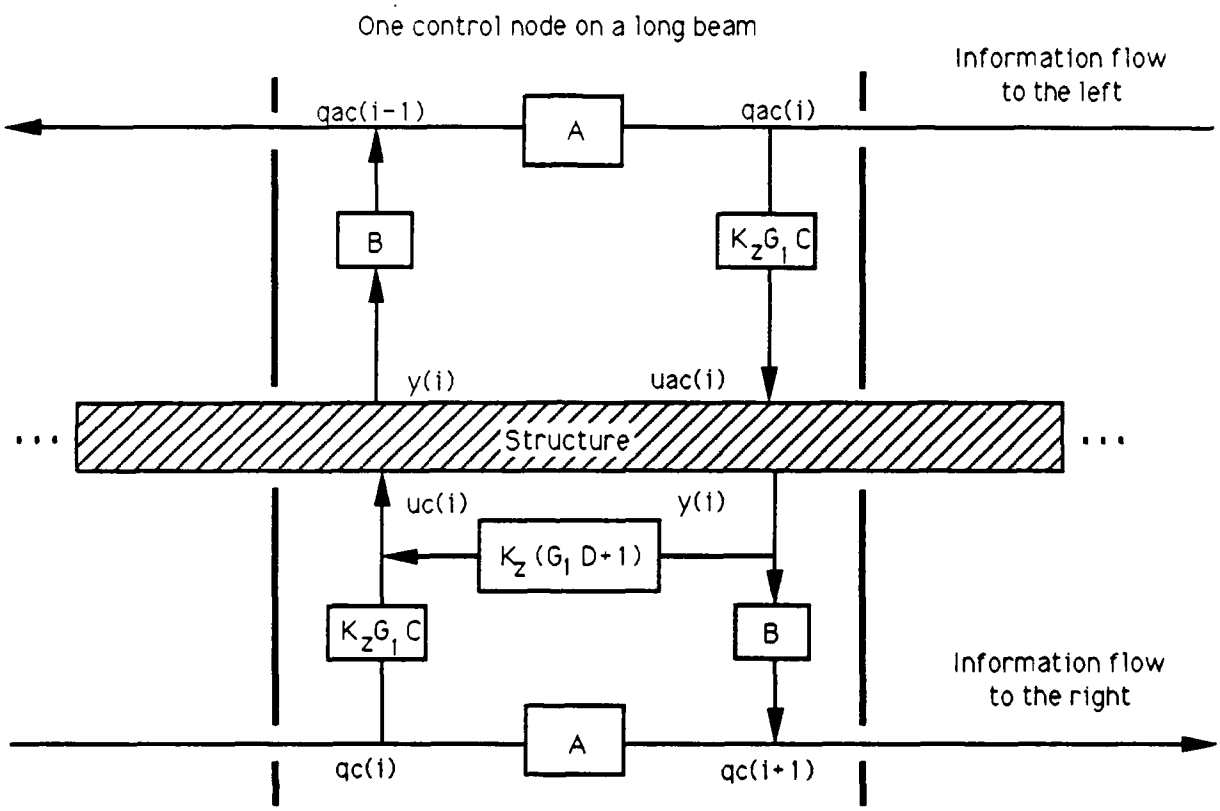

Figure 3.23: A representation of the full local control architecture, showing the split between the causal and anti-causal parts of the control calculation. The complete control command is the sum of u_c and u_{ac}.

also made in this design for splitting the finite control element into smaller "bays" and restricting the information flow within an element. A transformation was introduced which reduced the model dimensions so that a numerical approach to the optimal gain calculation would be feasible. A comparison of the results obtained for a large "bay" with the unconstrained optimal solution showed good agreement, indicating that the global minimum had been found.

The third control architecture makes allowances for communication directly between adjacent processors. The gains used for this case were the truncated unconstrained full state feedback gains which were developed for a long symmetric beam. A transformation based on the beam FEM element mass and stiffness matrices was introduced. This provided an easy method of calculating the gains for various state weighting matrices. Two methods of implementating the controller were discussed. One method only allows each processor to directly obtain the information from the sensors within the corresponding finite control element. This must then be passed to the neighboring processors. In a similar fashion, information is also received from the adjacent processors. The other method allows each processor to directly measure the necessary information from the sensors in all three finite control elements. The resulting gains for both cases could be full block tri-diagonal or banded.

The last controller implements the centralized full state feedback gains in a decentralized manner. Information is passed in "pipelines" in both directions along the structure. The controllers are finite difference representations of the optimal gains which have been approximated in the spatial frequency domain. In this way, each actuator can eventually obtain the information from every sensor. The implementation of this controller will require a very rapid exchange of information between the processors.

These controllers will be compared in the following two chapters. Chapter 4 will investigate their performance as decentralized controllers and as local controllers in the hierarchic control architecture. Chapter 5 will then compare their implementa-

tion requirements.

Chapter 4

Examples

4.1 Introduction

The purpose of this chapter is to show by example the benefits that can be obtained by using an hierarchic control architecture to control the vibratory motion of an "intelligent" structure. The secondary purpose is to expand on the design algorithm presented in Chapter 2 and to develop a hierarchic controller for a one dimensional structure. In the examples that will be discussed here, a long beam with many sensors and actuators distributed along its length will be analyzed. The design and evaluation models for this structure will be discussed in Section 4.2. Some issues concerning the implementation of the control architecture will be discussed in this section as well.

Due to the assumed nature of the structure, *i.e.*, the large number of sensors and actuators, it will be very difficult to develop a suitable test article in the laboratory. There is also a major difficulty associated with the computer architecture that will be required to implement this form of control. This problem was originally investigated by Miller in reference [48] and a solution was developed. However, test results appeared to indicate that this setup was very difficult to operate and program and

was not particularly suitable for expansion to a large scale system. There are numerous studies which have investigated computer architectures for large scale systems, see references [55,36]. There is an accompanying work by David Warkentin which is investigating the problem of designing a more suitable computer architecture, with special emphasis on the single chip micro-computer technology that is now readily available. Further experimentation in the laboratory will have to be delayed until the results of that work are known. Consequently, the evaluation models for the controller will only be computer models. To further clarify the capabilities of the control design, it will be assumed that the sensors and actuators are perfect. Some of the analysis performed on the beam in this chapter was originally done for a rod in reference [29].

Several examples will be studied in this chapter. For clarity, these will be separated into several parts. Section 4.2 discusses the development of the evaluation model of the beam. The mass condensation procedure discussed in Section 2.3 is used to reduce the order of the system and generate the design model. Some approximations required to efficiently implement the technique are also discussed. The section concludes with a discussion of the interpolation matrix, leading to the formation of the global model. Section 4.3 presents the control design for this coarser model of the beam. The influence of just the global controller on the structure is compared with a full order design. This process is then repeated for the alternative case where only the n_l lower modes of the global design model are retained. Section 4.4 studies the various local control designs developed in Chapter 3. The designs investigated include the colocated natural control, two block diagonal controllers, and two block tri-diagonal controllers. These are studied in terms of their performance as both decentralized controllers and as local controllers in the hierarchic architecture. They are compared directly with a full order LQR design. Section 4.5 then combines the local and global controllers from the previous two sections. The pole locations are shown for two cases. A comparison of the perfor-

mance of these combined controllers is done using a graph which examines the state cost and control effort trade-off at several design points.

The aim of this analysis will be to show that near optimal performance can be obtained using the hierarchic architecture if an appropriate local controller is used. A comparison of the local controllers will indicate that the more sophisticated designs can offer a slight performance improvement. The decision of which to use is delayed until the operations count is analyzed in Chapter 5.

4.2 Discussion of the Model

The purpose of this section is to introduce the evaluation and design models for the structure, and to discuss some of the issues involved in the implementation of the control architecture. The evaluation model for the control architecture was taken to be a beam because it provides some degree of complexity and can be used to approximate other structures, but it can still be modelled as a one dimensional structure. A 30 node beam (Figure 4.1) was selected for this example. To simplify some of the analysis of the local control designs in Chapter 3, the distance between the structural nodes of the beam was taken to be 1 unit so that the length of the entire beam is $n-1$ (*i.e.*, 29) units. The characteristic length of the beam was taken to be the distance between the structural nodes since the actual length of the beam is relatively unimportant provided that there are a sufficient number of nodes in the structure that the end effects have a negligible influence for most of the central portion of the beam.

A finite element model of an undamped free-free uniform beam was developed using the standard element matrices given in reference [46] which have been slightly modified so that the states are (q, θ) rather than $(q, h_1\theta)$. The element mass and

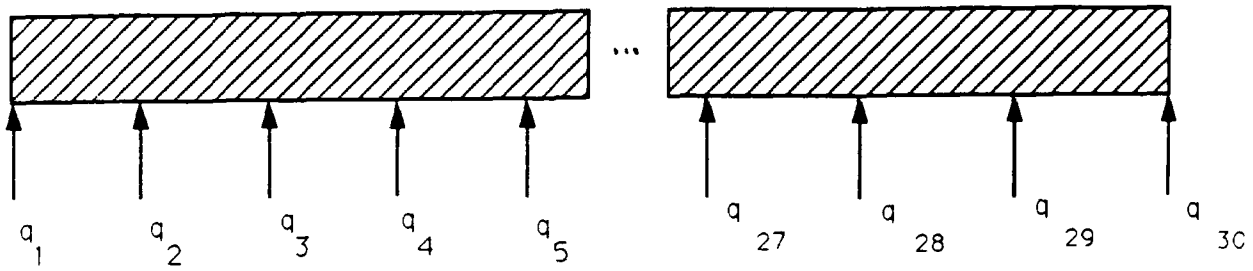

Figure 4.1: A 30 node beam model.

stiffness matrices are

$$M_{ele} = \frac{m_1 h_1}{420} \begin{bmatrix} 156 & 22h_1 & 54 & -13h_1 \\ 22h_1 & 4h_1^2 & 13h_1 & -3h_1^2 \\ 54 & 13h_1 & 156 & -22h_1 \\ -13h_1 & -3h_1^2 & -22h_1 & 4h_1^2 \end{bmatrix} \tag{4.1}$$

$$K_{ele} = \frac{\mathrm{EI}}{h_1^3} \begin{bmatrix} 12 & 6h_1 & -12 & 6h_1 \\ 6h_1 & 4h_1^2 & -6h_1 & 2h_1^2 \\ -12 & -6h_1 & 12 & -6h_1 \\ 6h_1 & 2h_1^2 & -6h_1 & 4h_1^2 \end{bmatrix} \tag{4.2}$$

where m_1 and EI are the corresponding structural properties per unit length, and h_1 is the length of each element. For the work performed here, both EI and m_1 were assumed to be unity. Since the nodes are spaced one unit apart, h_1 is unity as well. By assembling these element matrices and then rearranging the states to correspond to those shown below, the resulting equations of motion can then be

expressed as

$$\begin{bmatrix} M_{qq} & M_{q\theta} \\ M_{\theta q} & M_{\theta\theta} \end{bmatrix} \begin{bmatrix} \ddot{q} \\ \ddot{\theta} \end{bmatrix} + \begin{bmatrix} K_{qq} & K_{q\theta} \\ K_{\theta q} & K_{\theta\theta} \end{bmatrix} \begin{bmatrix} q \\ \theta \end{bmatrix} = \begin{bmatrix} F \\ 0 \end{bmatrix} \tag{4.3}$$

where q and θ are the vectors of the states at the nodes, and only force actuators are assumed to exist. Typical relative magnitudes of these block matrices (in a two-norm sense) are

$$\|M_{qq}^{-1}K_{qq}\|_2 \approx 48 \quad \|M_{\theta\theta}^{-1}K_{\theta\theta}\|_2 \approx 360$$

These ratios, combined with the selection of the force actuators, indicate that the rotational coordinates are suitable to be designated as the slave degrees of freedom in the condensation procedure outlined in Section 2.3.

Following the procedure in that section, it is then possible to develop a condensed model of the beam which only consists of the displacement degrees of freedom with system matrices M_{cond} and K_{cond} defined as

$$K_{cond} = K_{qq} - K_{q\theta}K_{\theta\theta}^{-1}K_{\theta q} \tag{4.4}$$

$$M_{cond} = M_{qq} - K_{q\theta}K_{\theta\theta}^{-1}M_{\theta q} - M_{q\theta}K_{\theta\theta}^{-1}K_{\theta q} + K_{q\theta}K_{\theta\theta}^{-1}M_{\theta\theta}K_{\theta\theta}^{-1}K_{\theta q} \tag{4.5}$$

as given in Chapter 2. It is interesting at this point to compare the modal frequencies of the full order model with those of the condensed model. The results are given in Table 4.1 and plotted in Figure 4.2. As mentioned in Section 2.3, and as will be discussed in more detail later in this section, it is often more convenient to use the condensed stiffness with a lumped mass approximation of the finite element model (*i.e.*, a statically condensed model). The modal frequenices for this case are also included in Table 4.1. These frequencies are compared with the quoted values from reference [12] and the frequencies from the full order beam model. Archer [2] shows that a beam finite element model based only on the translational coordinates can provide a reasonable model of the lower frequency modes of a free-free beam.

Archer compared the percentage difference between experimental results and the modal frequencies obtained from models using both the rotational and translational coordinates and just the translational coordinates. The analysis shows that the errors for both cases are reasonably small for the first five flexible modes, and that the first method has a relative error which is about $\frac{1}{3}$ as large as the second. These results are also compared with the frequencies from models based on lumped mass approximations and the relative errors for these methods were typically found to be an order of magnitude larger. The results presented here confirm that the frequencies for a condensed model are a much better match than those from a model based on a lumped mass approximation. The results for both approximations are close to the reference values for the first 12 flexible modes. The deviation is more readily apparent for the higher frequency modes.

Figure 4.3 contains a three dimensional plot of the condensed mass matrix for this example. The most important thing to notice from this figure is that the matrix is very strongly banded which indicates that the lumped approximation should be fairly good. One other important point is that the influence of the end effects on the central portion of the beam are negligble, leaving a symmetric uniform beam for most of the structure. This is important for some of the local control designs in Chapter 3. Several design methodologies assume that the structure is symmetric (*i.e.*, the block diagonal and block tri-diagonal approaches), so it is important that the design and evaluation models consist of a large central region which is uniform.

As discussed in Section 2.7, the first step in the algorithm is to select the number and the locations of the global nodes. For the examples done here, 6 global nodes (n_{gn}) were employed, which results in 5 finite control elements (n_e), of which the middle 3 are identical, but the end two are different due to the fact that one of the global nodes coincides with a structural node (Figure 5.5). Notice that it is not in general necessary for the global and structural nodes to coincide. In this example with a beam, each global node has 2 degrees of freedom, *i.e.*, $n_{g_{dof}} = 2$, for a design

Table 4.1: A comparison of the flexible mode frequencies (rad/sec) with various approximations of the mass matrix in the FEM.

Flexible Mode Number	Full Mass Matrix FEM	Condensed Mass Matrix FEM	Lumped Mass Matrix FEM	Reference
1	0.0266	0.0266	0.0265	0.0266
2	0.0733	0.0733	0.0729	0.0733
3	0.144	0.144	0.143	0.144
4	0.238	0.238	0.235	0.238
5	0.355	0.355	0.350	0.355
6	0.496	0.496	0.488	0.496
7	0.660	0.660	0.648	0.660
8	0.848	0.849	0.830	0.848
9	1.06	1.06	1.03	1.06
10	1.30	1.30	1.26	1.29
11	1.55	1.56	1.51	1.55
12	1.84	1.84	1.78	1.83
⋮	⋮	⋮	⋮	⋮
21	5.51	5.70	4.95	5.42
22	6.06	6.31	5.33	5.94
23	6.62	6.96	5.70	6.48
24	7.22	7.63	6.03	7.04
25	7.84	8.30	6.33	7.63
26	8.49	8.93	6.58	8.24
27	9.13	9.46	6.77	8.88
28	9.69	9.81	6.89	9.53

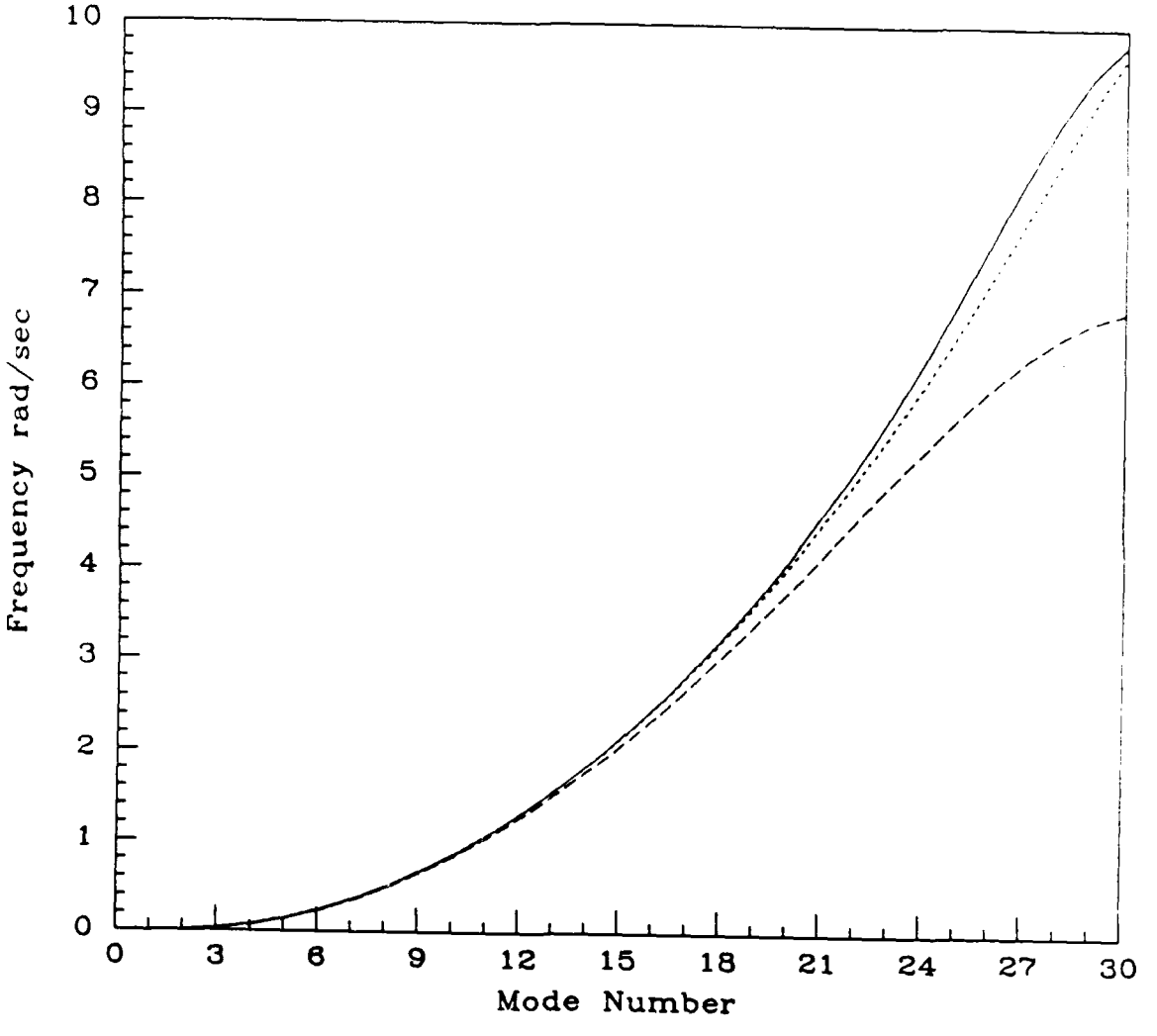

Figure 4.2: A comparison of the modal frequencies (rad/sec) for various approximations of the mass matrix in the FEM. The dotted line corresponds to the full model. The solid line corresponds to the condensed model, and the dashed line is the lumped model. These results show that using the condensed mass matrix provides a much better approximation of the original model than does the lumped mass approach.

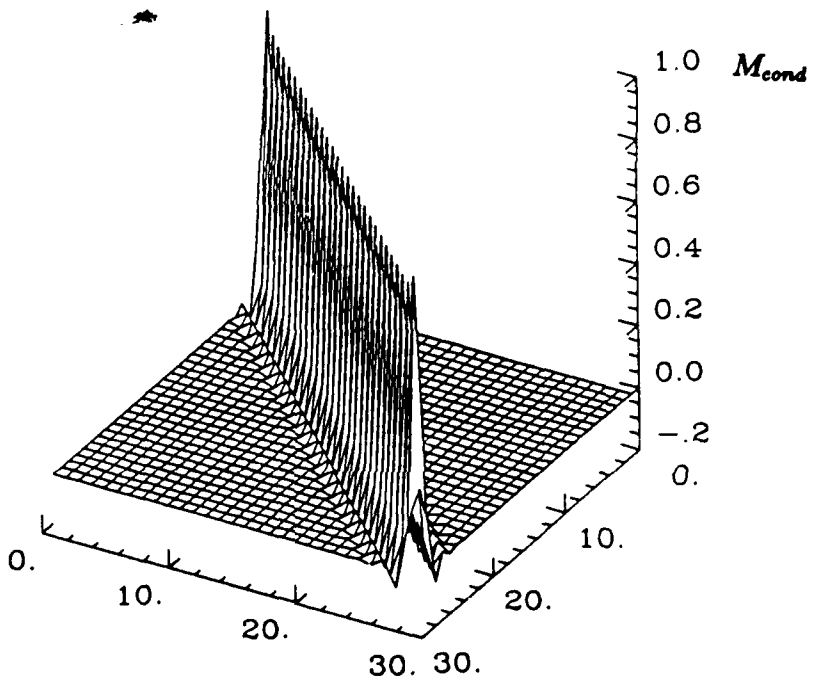

Figure 4.3: A 30 node beam mass matrix for which the rotation coordinates have been condensed out. This is plotted to display both the bandedness and symmetry of the mass matrix. The figure also shows that the central portion of the beam is uniform.

model total of $n_g = 12$. The interpolation functions used in the formation of the T_g matrix were the standard Hermite polynomials, L_i [46] which were used in the formation of the element matrices of the beam FEM. These relate the displacement at each internal node of the finite control element to the displacements and rotations at the end points. The displacement can then be written in terms of four functions which are parameterized by the variable η

$$q(\eta) = L_1(\eta)\, q_{g_l} + L_2(\eta)\, \theta_{g_l} + L_3(\eta)\, q_{g_r} + L_4(\eta)\, \theta_{g_r} \tag{4.6}$$

where

$$\begin{aligned} L_1(\eta) &= 1 - 3\eta^2 + 2\eta^3 \quad & L_2(\eta) &= h_1(\eta - 2\eta^2 + \eta^3) \\ L_3(\eta) &= 3\eta^2 - 2\eta^3 & L_4(\eta) &= h_1(-\eta^2 + \eta^3) \end{aligned} \tag{4.7}$$

and $0 \leq \eta \leq 1$. The subscript $(\cdot)_{gl}$ corresponds to the information at the left global node, $(\eta = 0)$, and $(\cdot)_{gr}$ to the right global node, $(\eta = 1)$. Plots of these four shape function are given in Figure 4.4. The interpolation matrix T_g is then found by evaluating the expression in Equation 4.6 at each of the values of η within the finite control element which correspond to structural nodes and then storing the resulting coefficients in a matrix. The full T_g matrix can then be formed by assembling these blocks for each finite control element, as shown in Figure 4.5.

Note the form of the T_g matrix for a finite control element. It can be split into two parts. One part relates the nodes in the finite control element to the global node on the left, and the other relates the nodes to the global node on the right. For finite control element i, with global nodes i and $i+1$, the corresponding blocks of the T_g matrix are T^i_{gi} and $T^i_{g(i+1)}$, a notation which was introduced in Figure 2.2. As was discussed in Section 2.6, it is also possible to use modes rather than approximate shape functions in the formulation of T_g.

From Equation 2.14 with the weighting matrix $W = M$, Equation 2.31, Figure 2.4, and the discussion in Section 2.5, it can be seen that to form the estimates of the global node values, the measured displacements and velocities must be mul-

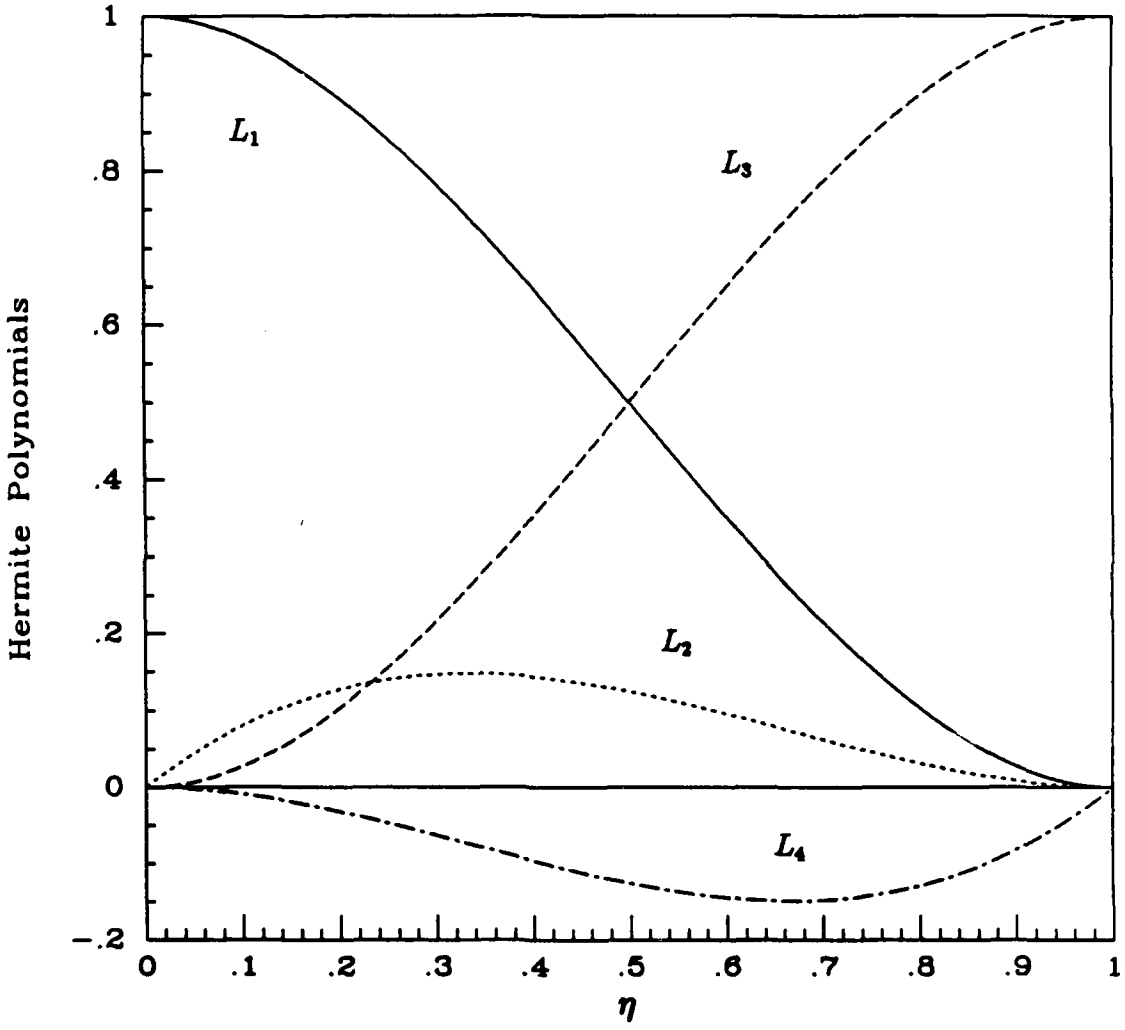

Figure 4.4: The four Hermite polynomials as a function of η.

$$T_g^T = \begin{bmatrix} \ddots & & & & & & & & & & & & \\ & 0.980 & 0.843 & 0.623 & 0.376 & 0.156 & 0.019 & 0.000 & 0.000 & 0.000 & 0.000 & 0.000 & 0.000 \\ & 0.420 & 0.843 & 0.850 & 0.607 & 0.281 & 0.038 & 0.000 & 0.000 & 0.000 & 0.000 & 0.000 & 0.000 \\ & 0.019 & 0.156 & 0.376 & 0.623 & 0.843 & 0.980 & 0.980 & 0.843 & 0.623 & 0.376 & 0.156 & 0.019 \\ & -0.038 & -0.281 & -0.607 & -0.850 & -0.843 & -0.420 & 0.420 & 0.843 & 0.850 & 0.607 & 0.281 & 0.038 \\ & 0.000 & 0.000 & 0.000 & 0.000 & 0.000 & 0.000 & 0.019 & 0.156 & 0.376 & 0.623 & 0.843 & 0.980 \\ & 0.000 & 0.000 & 0.000 & 0.000 & 0.000 & 0.000 & -0.038 & -0.281 & -0.607 & -0.850 & -0.843 & -0.420 \\ & & & & & & & & & & & & \ddots \end{bmatrix}$$

Figure 4.5: The form of the interpolation function matrix T_g^T. The blocks enclose the parts of the matrix which correspond to a specific finite control element.

tiplied by an aggregation matrix, $T_g^T M$. As shown in Figure 4.5, the T_g matrix is in some sense diagonal, but Figure 4.3 shows that, although the condensed mass matrix, M_{cond} is highly banded, it is in general a full matrix. Thus, $T_g^T M_{cond}$ would in general be a full matrix as well. In the ideal case, the matrix $T_g^T M$ would be block diagonal. This would correspond to a situation where the information from each finite control element could be aggregated to the global values without any reference to information from the neighboring elements. However, if this aggregation matrix is full, then the measurements from each element (column dimension of $T_g^T M$) would contribute to every global value (row dimension of $T_g^T M$). This is shown below in an example for a simpler case which assumes that the mass matrix is block tri-diagonal. Based on the bandedness of M_{cond} shown before, this should be a very good approximation for the mass matrix. The mass matrix will be assumed to consist of blocks M_0 along the diagonal and the first minor diagonal consists of blocks M_1. The resulting form of the $T_g^T M$ matrix is shown in Figure 4.6.

The significance of this result is that, if $M_1 \neq 0$, then there are four non-zero matrices in each column of $T_g^T M$. Consequently, each set of measurements within an element must be multiplied by four matrices to obtain the four vectors of information which must be communicated to the central computer. This is in contrast to the multiplication by two matrices and the communication of two vectors of information if $M_1 = 0$, *i.e.*, the mass matrix is block diagonal (or diagonal). The advantage of having more off-diagonal blocks in the mass matrix is that it provides a much better approximation. This gives a better weighted distribution of the control and it allows for a better filter when the control is applied to the evaluation model. However, as can be seen from the analysis above, this involves a substantial increase in the workload of the local controllers, virtually doubling the number of operations required to perform this aggregation step. This fact, plus the strong bandedness of the condensed mass matrix shown in Figure 4.3 led to decision to implement the observation and control filtering using a block diagonal mass approximation

$$
\begin{bmatrix}
\ddots & & & & \\
 & T_{g(i-1)}^{T(i-1)} & 0 & 0 & 0 \\
 & T_{gi}^{T(i-1)} & T_{gi}^{Ti} & 0 & 0 \\
 & 0 & T_{g(i+1)}^{Ti} & T_{g(i+1)}^{T(i+1)} & 0 \\
 & 0 & 0 & T_{g(i+2)}^{T(i+1)} & T_{g(i+2)}^{T(i+2)} \\
 & & & & \ddots
\end{bmatrix}
\begin{bmatrix}
\ddots & & & & \\
 & M_0 & M_1 & 0 & 0 \\
 & M_1 & M_0 & M_1 & 0 \\
 & 0 & M_1 & M_0 & M_1 \\
 & 0 & 0 & M_1 & M_0 \\
 & & & & \ddots
\end{bmatrix} =
$$

$$
\begin{bmatrix}
\ddots & & & \\
 & T_{g(i-1)}^{T(i-2)} M_1 + T_{g(i-1)}^{T(i-1)} M_0 & T_{g(i-1)}^{T(i-1)} M_1 & 0 \\
 & T_{gi}^{T(i-1)} M_0 + T_{gi}^{Ti} M_1 & T_{gi}^{T(i-1)} M_1 + T_{gi}^{Ti} M_0 & T_{gi}^{Ti} M_1 \\
 & T_{g(i+1)}^{Ti} M_1 & T_{g(i+1)}^{Ti} M_0 + T_{g(i+1)}^{T(i+1)} M_1 & T_{g(i+1)}^{Ti} M_1 + T_{g(i+1)}^{T(i+1)} M_0 \\
 & 0 & T_{g(i+2)}^{T(i+1)} M_1 & T_{g(i+2)}^{T(i+1)} M_0 + T_{g(i+2)}^{T(i+3)} M_1 \\
 & & & \ddots
\end{bmatrix}
$$

Figure 4.6: The aggregation matrix with a block tri-diagonal approximation of the condensed mass matrix. This figure shows that the matrix $T_g^T M$ contains four non-zero rows per column if $M_1 \neq 0$, which increases the workload of each local controller.

Table 4.2: The flexible mode frequencies (rad/sec) from the global model.

Flexible Mode Number	Global Model Frequency
1	0.0266
2	0.0735
3	0.145
4	0.239
5	0.384
6	0.550
7	0.762
8	1.03
9	1.59
10	1.66

as the weighting matrix W. In fact, since a block diagonal approximation has discontinuities at the finite control boundaries, a lumped mass approximation was used, which results in a diagonal W matrix.

Having discussed some of the implementation issues, it is now possible to derive the global, or coarser, model of the structural dynamics which can be represented by the equation

$$M_{gg}\ddot{q}_g + K_{gg}q_g = (\Psi S_g)\, Q_g \tag{4.8}$$

where the condensed mass and stiffness matrices have been used in the formation of the global values to provide the best model possible. The open loop frequencies of this reduced order model are given in Table 4.2. These values can be seen to agree well with the lower frequency modes for the full and condensed models given in Table 4.1. As would be expected from any finite element approximation, this agreement degrades for the higher frequency modes. This is a result of the fact that the coupling influence of the residual system is much higher for these modes. As was discussed in Chapter 2, this suggests that it would beneficial (in terms of reducing the amount of coupling between the global and residual systems), to use

a high number of global nodes but only retain a subset of the global modes. This should improve the performance of the combined systems since it will reduce the dynamic coupling, but as mentioned in Section 2.6, care must be taken to ensure that the desired closed loop performance can still be obtained with the reduced set of modes, *i.e.*, the global control authority must be kept high enough.

To implement this alternative which uses only the lower set of modes, the following steps should be performed. First, the global system of Equation 4.8 should be formed as before. The eigenvalues and eigenvectors of this system should then be calculated, sorted, and normalized. Only the eigenvectors of the n_l lower frequency modes should be retained to form ϕ_g^l. The new interpolation matrix, $T_{gl} = T_g \phi_g^l$, can then be formed, and a new model and closed loop system based on this shape function can be derived exactly as before in Chapter 2.

The influence of the reduced coupling on the closed loop performance will be explored in more detail in the next section once the global controller has been derived. The implementation differences between retaining all or only a subset of the global modes was addressed in Section 2.6, and the differences in terms of the computational requirements will be investigated in Chapter 5.

4.3 The Global Control Design

The next step in the design procedure is to formulate the control problem. A regulator based on a LQR design is used as the global controller. As with any design of this type, the question of what to optimize, or how to pick the penalty matrices remains. The aim here is to use a realistic cost function which includes a penalty on the overall motion of the structure. A suitable performance objective is to minimize the line-of-sight (LOS) displacement between the two ends of the beam. An additional penalty on the displacement at each node was also included, with the goal of performing shape control on the entire structure. Finally, a third term

penalizing the total energy of the system was added to maintain a sufficient level of damping in the higher frequency modes of the system. To be consistent with the assumption that the beam is uniform along its length, each actuator was penalized by the same amount. Then, the cost function is taken to be of the standard form

$$J = \int_0^\infty \left(x^T R_{xx} x + u^T R_{uu} u \right) \, dt \tag{4.9}$$

with the state $x = [q^T \; \dot{q}^T]^T$ and the penalty matrices R_{xx} and R_{uu} defined as

$$\begin{aligned} R_{xx} &= \frac{1}{2} C_{los}^T C_{los} + \alpha_1 \begin{bmatrix} I_n & 0 \\ 0 & 0 \end{bmatrix} + \alpha_2 \begin{bmatrix} K & 0 \\ 0 & M \end{bmatrix} \qquad (4.10) \\ C_{los} &= \begin{bmatrix} \overset{1}{1} & \overset{2}{0} & \dots & \overset{n-1}{0} & \overset{n}{-1} & \overset{n+1}{0} & \overset{n+2}{0} & \dots & \overset{2n-1}{0} & \overset{2n}{0} \end{bmatrix} \end{aligned}$$

$$R_{uu} = \rho I_n \tag{4.11}$$

where, $\alpha_1 = \frac{20}{n}$ and $\alpha_2 = \frac{3}{4n}$. Then, using Equations 2.13 and 2.22, the appropriate consistently transformed cost for the global model of Equation 4.8 is given by

$$J^g = \int_0^\infty \left(x_g^T R_{xx}^g x_g + Q_g^T R_{uu}^g Q_g \right) \, dt \tag{4.12}$$

$$R_{xx}^g = \begin{bmatrix} T_g^T & 0 \\ 0 & T_g^T \end{bmatrix}^T R_{xx} \begin{bmatrix} T_g^T & 0 \\ 0 & T_g^T \end{bmatrix} \tag{4.13}$$

$$R_{uu}^g = S_g^T R_{uu} S_g \tag{4.14}$$

In this analysis, the filtering matrices are based on a weighting matrix $W = M_{lumped}$. The influence of the global controller on the structure can be compared directly with the full state feedback regulator. The closed loop poles are compared in Figure 4.7. Note that there are the *global design model closed loop poles*, the *closed loop poles* and the *full order regulator closed loop poles*. The first set corresponds to the poles obtained when the global controller is applied to the global design model. The second set are the poles obtained when the global controller is applied to the

condensed design model. The difference between these first two is that the design model ignores the coupling between the global and residual subsystems. The last set corresponds to those obtained when the LQR gains are applied to the condensed model. The effects of the coupling can be seen in the figure through the influence of the global controller on the higher frequency modes and the difference between the *global design model closed loop poles* and the *closed loop poles*. The results in Figure 4.7 indicate that the lower frequency *closed loop poles* are similar to those obtained from the optimal regulator. It is also evident that this agreement degrades for the higher frequency modes of the global model.

There is a negligible difference between using the condensed or lumped mass approximation in the design of the global model as each provides a fairly good representation of the lower frequency modes. Where this choice does become important though is in the weighting matrix used in the filtering. Figure 4.9 shows the same controller designed above using the condensed mass approximation in the design model but implemented using both the condensed mass and the lumped mass approximations as the weighting matrix. Since the condensed mass is a far better approximation to the mass matrix of the full model, it provides a much better filter for the global control on the residual system. This graph indicates that the choice of a good approximation for the mass matrix can significantly improve the filtering out of the control spillover. However, previous analysis has already shown that this requires a substantial increase in the implementation costs at the lower level. In the example presented here the poles of the residual system tend to be stabilized by the interaction, and those of the global model are made slightly less stable. However, this appears to be a result of the internal dynamics of the plant and cannot be generalized to other cases.

When only the $n_l = 9$ lower modes of the global system are retained, the resulting closed loop pole locations are as shown in Figure 4.8. They indicate that the decoupling between the two subsystems is improved. However, a slight performance

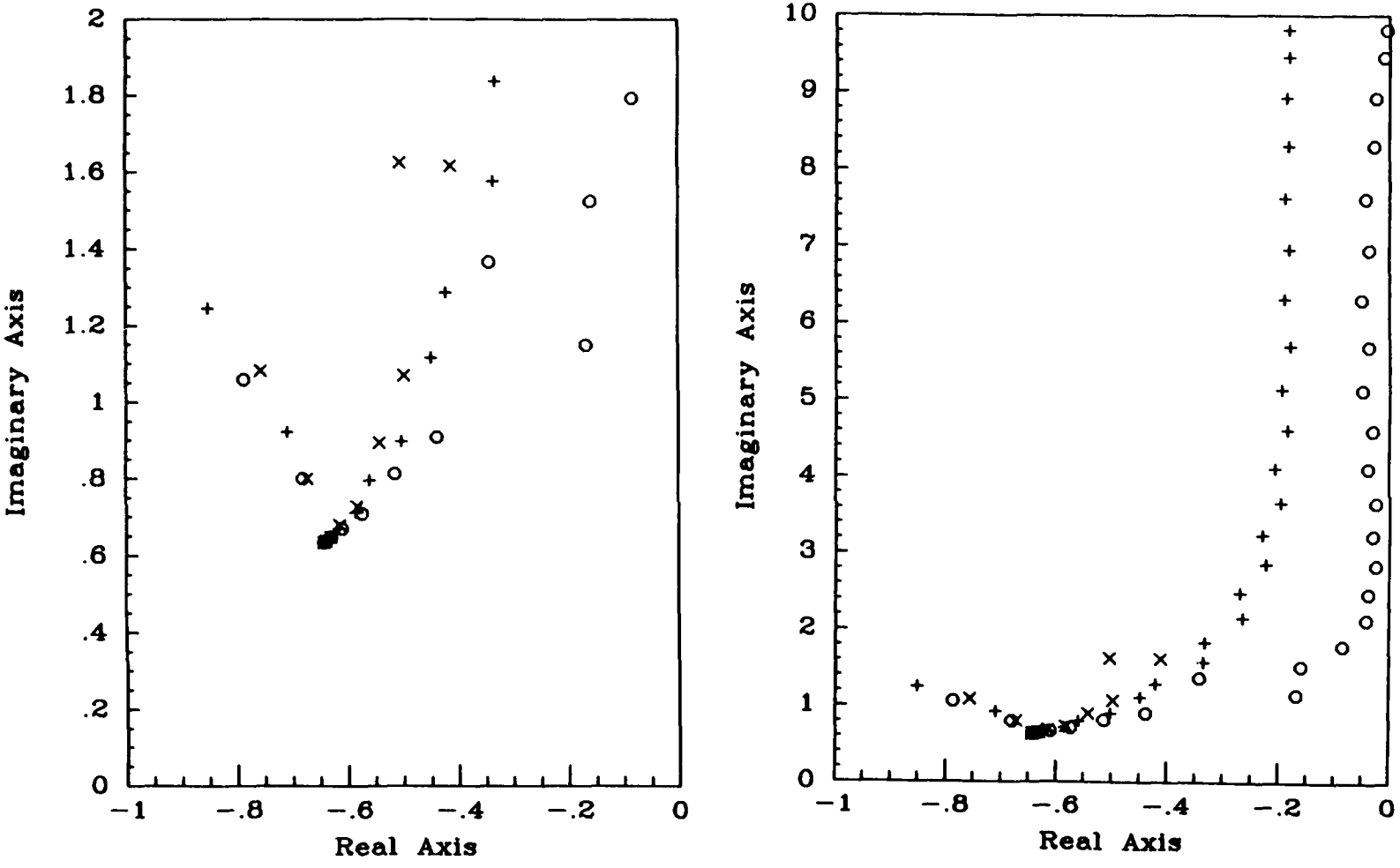

Figure 4.7: The closed loop poles locations from the global control design. The x's are the global design model closed loop poles (defined in the text). The circles are the closed loop poles, and the crosses are the full order regulator closed loop poles.

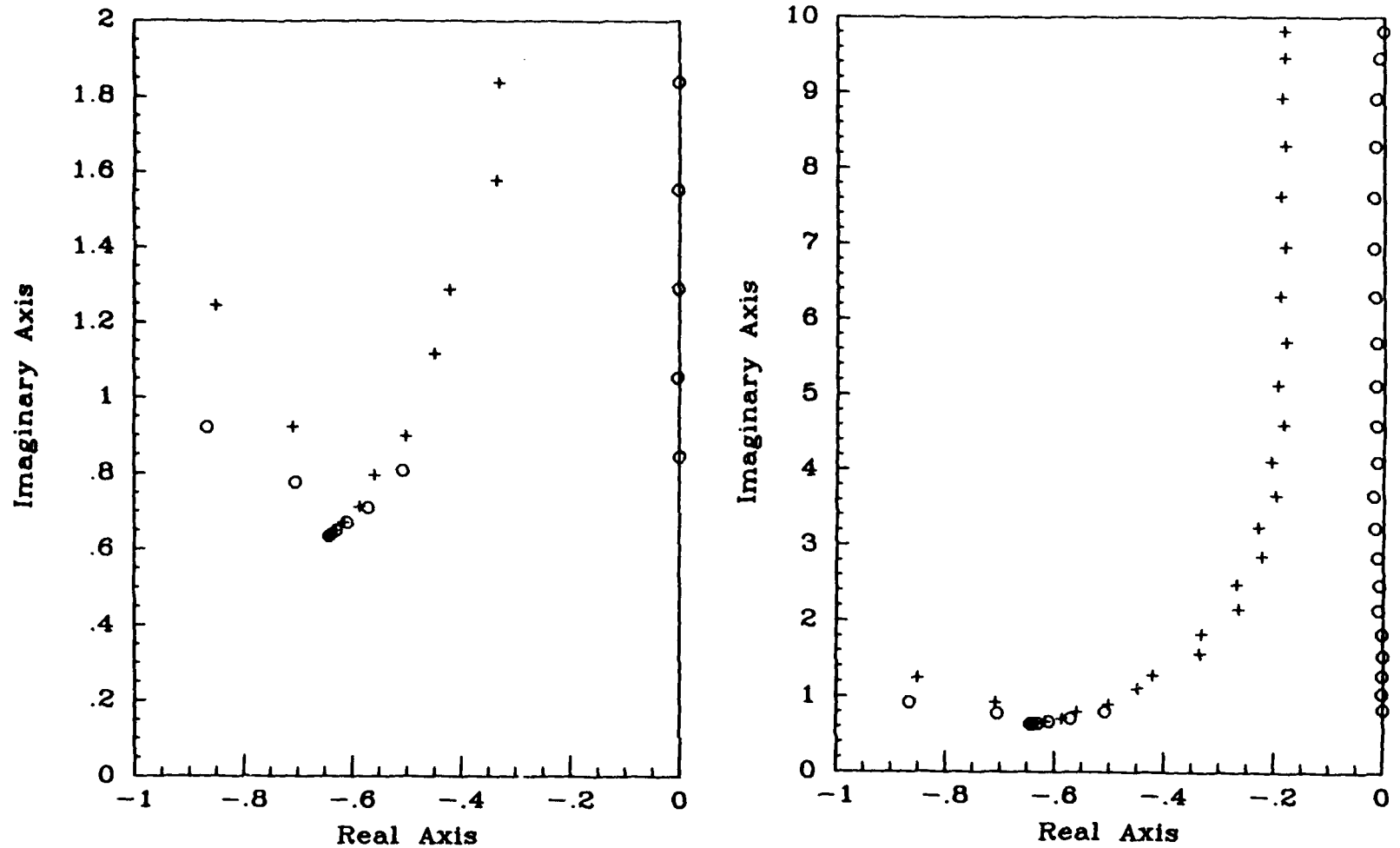

Figure 4.8: The closed loop poles locations from the global control design based on the lower set of the global modes. The circles are the closed loop poles (defined in the text), and the crosses are the full order regulator closed loop poles.

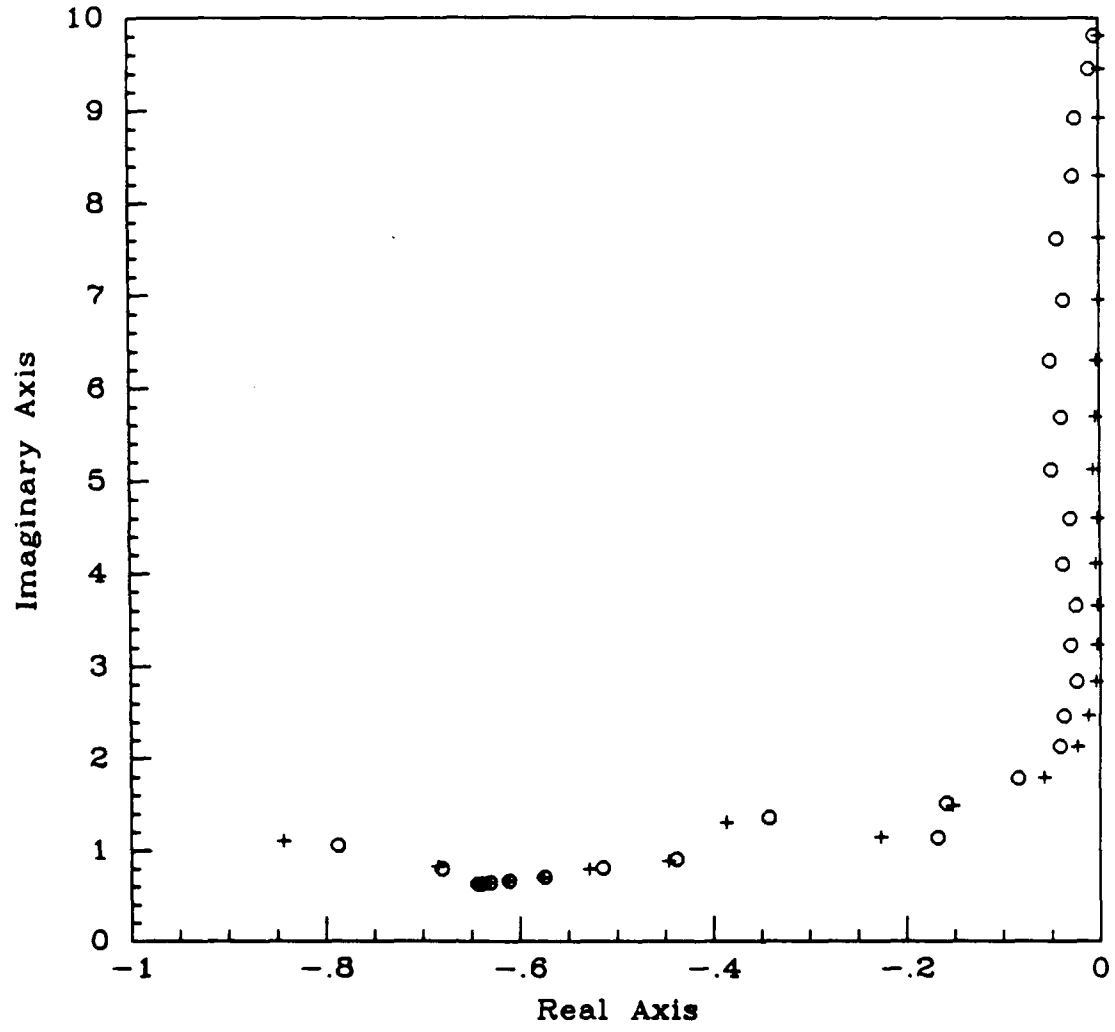

Figure 4.9: A comparison of two approximations of the mass matrix used in the control and observation filtering. Both controllers use the same global control design. The circles represent the closed loop poles obtained when the lumped approximation is used as W. The crosses are the closed loop poles obtained when M_{cond} is used as W.

decrease can be expected due to the fact that the closed loop poles do not agree as well (due to the double aggregation step) with the optimal ones as do the poles obtained when all of the global modes are employed. In this development, some modes are now no longer considered to be part of the global model, so they will be influenced by the residual feedback. If the global model is made too small, then the ability of the central controller to govern the gross motions of the structure will be significantly impaired, and the local controllers will have to control modes which are very important to the performance objective.

4.4 A Comparison of the Local Control Designs

4.4.1 Introduction

The purpose of this section is to investigate the performance of the various local controllers developed in Chapter 3. This will include colocated natural feedback, two types of block diagonal feedback and two forms of the block tri-diagonal feedback. The controllers will be discussed in terms of their applicability as both decentralized controllers and as local controllers in the hierarchic architecture. There are two main points to consider here. The modelling technique using shape functions is not perfect so there will be some dynamic coupling between the global and residual models. Also, the observation and control filtering is not perfect due to some of the decisions made (such as using the lumped mass approximation as the filter weighting matrix) based on implementation issues. Of course there will be errors in the model as well. As a result, the controller from one model can then be expected have an influence on the closed loop poles of the other model. For this reason, it is desirable to develop a local controller that does not have a very high control authority for the lower frequency modes since these typically are the ones which are modelled by the global design model. This will have the effect of reducing the influence of the local

control on the global design model poles. For a given level of spillover or coupling, the higher the control authority, the larger the influence on the closed loop poles. This is in contrast to the aim for the design of a decentralized controller, which is obtain as much control authority as possible (or necessary, depending on the control design) at each frequency. As will be seen, this spillover is most prevalent for the modes which are at the boundary of the global and residual models. The filtering employed in the hierarchic architecture is capable of removing nearly all of the influence of the residual controllers on the lower frequency global design model poles, even with the lumped mass approximation as the weighting matrix (see the discussion in Section 4.2).

The global cost function of Equation 4.9 penalizes three measurements of the structural motion, namely the LOS displacement of the end points, the sum of the squared displacements at each node, and the total energy. Using a modal cost analysis [63], it is possible to show that the higher frequency modes have little contribution to the LOS cost, but they do contribute significantly to the other two. Consequently, the "optimal" local controller is based on a cost function which penalizes only the displacements and the total energy.

The local controllers will be investigated by comparing the location of the closed loop poles relative to the optimal locations for the weighting given above. Two cases are actually presented. The first (lefthand graph) plot compares the poles of the decentralized controller to the optimal pole locations. The second (righthand graph) plot shows the influence of the filtered local controller exactly as it would implemented in the hierarchic architecture. Referring to Equation 2.38, if the local feedback gains are F_e and $F_{\dot{e}}$, then implementating the decentralized control results in closed loop dynamics given by

$$M\ddot{q} + Kq = -F_e q - F_{\dot{e}}\dot{q} \tag{4.15}$$

For the filtered local control case, the resulting dynamics are given by

$$\begin{aligned} M\tilde{q} + Kq = & - \left\{ \left(I - T_g T_g^{-L} \right)^T F_e \left(I - T_g T_g^{-L} \right) \right\} q \\ & - \left\{ \left(I - T_g T_g^{-L} \right)^T F_{\dot{e}} \left(I - T_g T_g^{-L} \right) \right\} \dot{q} \end{aligned} \tag{4.16}$$

4.4.2 Colocated Feedback

Although two colocated control methods were discussed in Chapter 3, only the second, natural control, was implemented in this analysis. A value of $\beta = 0.10$ was selected for this example since it represented an average location of the higher frequency closed poles for the optimal regulator. Later work will look at several different values, so the actual value of β is not critically important.

The closed loop pole locations for the two cases are shown in Figure 4.10. Note the trend that the higher frequency poles have more negative real parts. This is an influence of using the lumped mass, M_{lumped}, to weight the control commands in Equation 3.2 rather than the mass matrix of the model, M_{cond}. Rather than being the identity matrix, $M_{cond}^{-1} M_{lumped}$ is a full matrix with the major difference being at both ends where boundary effects dominate. If M_{cond} had been used instead, then the poles would lie on the vertical line, Re(s) $= -0.10$. Numerical results have shown that the highest frequency pole has a real part which is approximately twice that of the lowest frequency pole. This result was also found to hold for much larger values of β. A comparison with the optimal pole locations shows that matching the two sets of poles at lower frequencies would result in higher frequency poles which are significantly overdamped. Based on these results, this is not expected to be a particularly efficient decentralized controller.

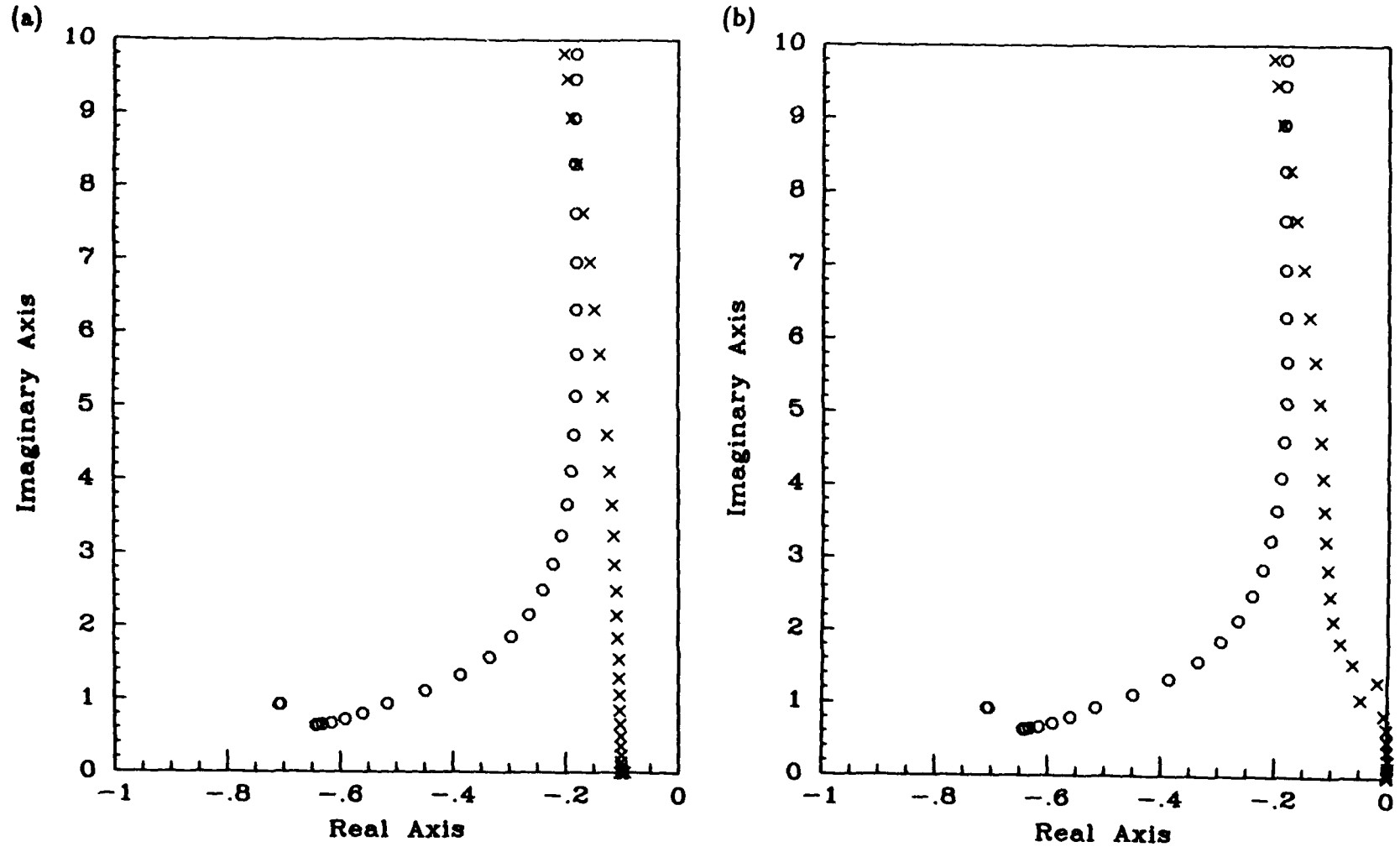

Figure 4.10: The closed loop poles from the colocated controller. The circles are the optimal pole locations, and the x's are the pole locations with the colocated feedback. Figure (a) compares the decentralized controller with the optimal centralized soution. Figure (b) compares the filtered local controller with the optimal solution.

4.4.3 Block Diagonal Feedback

Two block diagonal controllers were developed in this example. One was based on the full finite control element of six nodes, while the other splits this into two bays of three nodes. The actuator commands in a bay are then constrained to be computed only from the sensors within that bay.

The algorithm for calculating the gains was outlined in Section 3.3.6. The model used in the analysis is as shown in Figure 3.3. A finite element model of a beam based on the element matrices of Equations 4.1 and 4.2 was used. To form the circulant model, the assembly steps for the end blocks had to be modified so that, for instance, the structual node to the left of the one at the left end of the beam was in fact the node at the right end. So, the "doughnut" shape was formed by looping the beam elements around upon themselves. This structure was then split into the required number of bays (20 were used in this work on the doughnut), and the transformation developed in Section 3.3.3 was used to reduce the plant size. The controllers when then optimized using the algorithm presented in Section 3.3.6. A displacement and total energy penalty was put on the states and an equal penalty of unity was attributed to each controller.

The results for these two cases are shown in Figures 4.11 and 4.12. The good agreement of the poles in the lefthand graphs of each figure indicates that both types of feedback should provide reasonable performance as decentralized controllers. Since the full sized gain blocks allow information to be fed back over larger distances, the full block diagonal feedback should provide better long wavelength performance than the one which is split up into two bays. This can be seen by the better low frequency agreement of the two sets of closed loop poles in Figure 4.11. The agreement at higher frequencies is fairly good for both cases as well, indicating that these modes are not being significantly overdamped. The important area of agreement of the poles for decentralized controllers is the lower frequency modes.

However, in the hierarchic set-up, this region is governed by the global controller. So, for local controllers, it is important that the poles match well for the lower frequency modes of the residual model. For these filtered controllers, the agreement in this frequency region appears to be good in both cases.

As was discusssed before, the problem with designing a local controller with better control authority over the lower frequency modes is the increase in the coupling that can be expected between the local control and the higher frequency poles of the global design model. This is apparent when the righthand graphs (filtered local control) in Figures 4.11 and 4.12 are compared. The higher authority of the full sized gain block manifests itself through a slightly larger post-filtering influence on the poles of the global design model. However, this filtered feedback still gives a slightly better agreement for the lower frequency residual model modes.

4.4.4 Block Tri-Diagonal Feedback

Due to the diagonal dominance of the displacement and energy weighted optimal gains developed in Chapter 3, the truncation method developed in the Section 3.4 could be used to create both the block tri-diagonal and banded feedback matrices. For the latter case, a width of 5 nodes was found to be necessary to obtain all of the important information in the gain structure. Since these gains are essentially the optimal gains minus the very small feedback terms on distant nodes, it would be expected that the closed loop pole locations will agree quite well with the optimal regulator poles. The results in Figures 4.13 and 4.14 indicate that this is in fact the case. In both cases, the low frequency agreement is excellent, but it would appear that this does not hold quite as well for the higher frequency poles, though the results for the full gain block case appear to agree slightly better. As was discussed before, the higher control authority for the lower frequency poles presents a spillover problem in the filtered case, but the magnitude of the problem would be

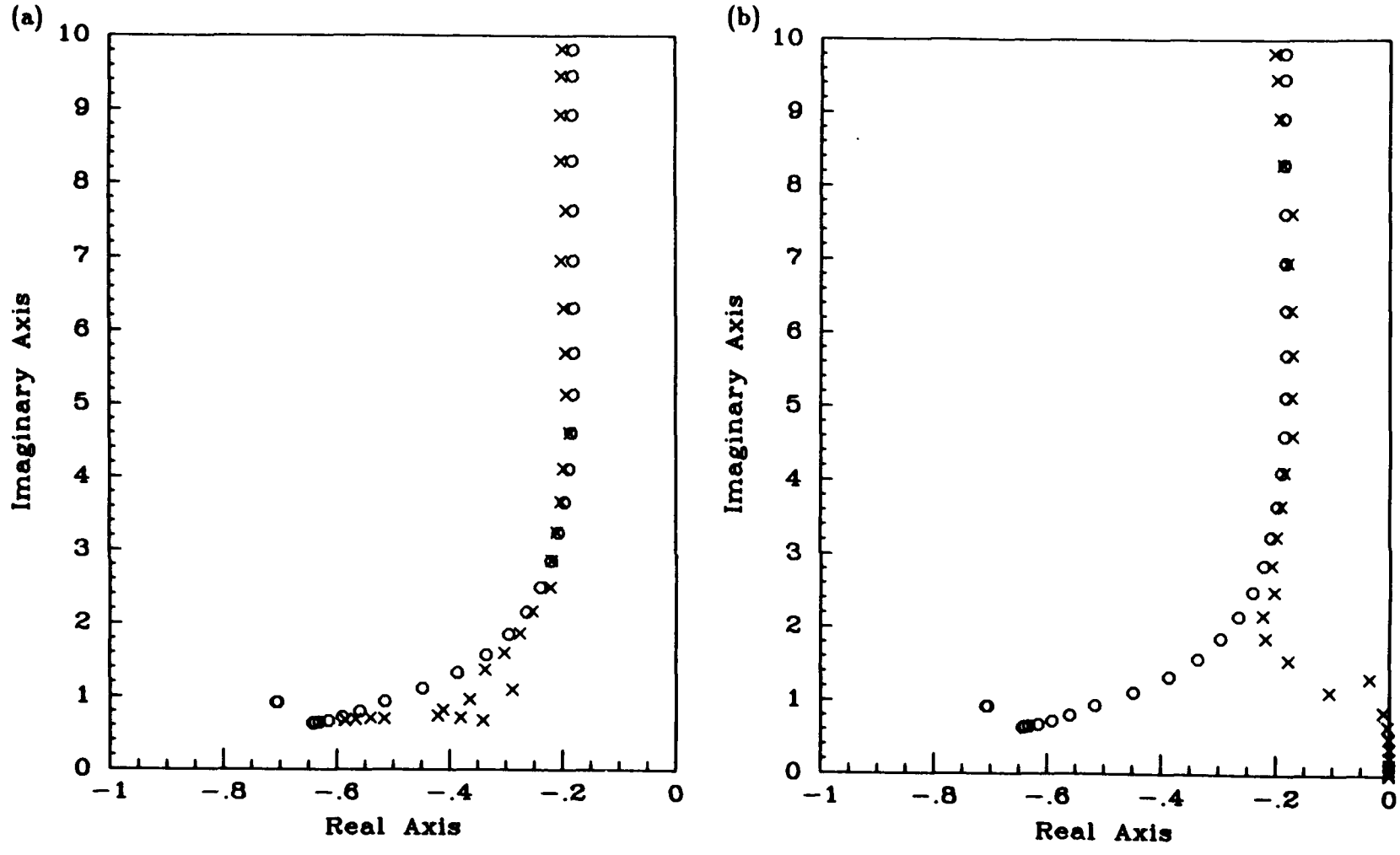

Figure 4.11: The closed loop poles from the full block diagonal local controller. The circles are the optimal pole locations, and the x's are the pole locations with the full block diagonal feedback. Figure (a) compares the decentralized controller with the optimal centralized soution. Figure (b) compares the filtered local controller with the optimal solution.

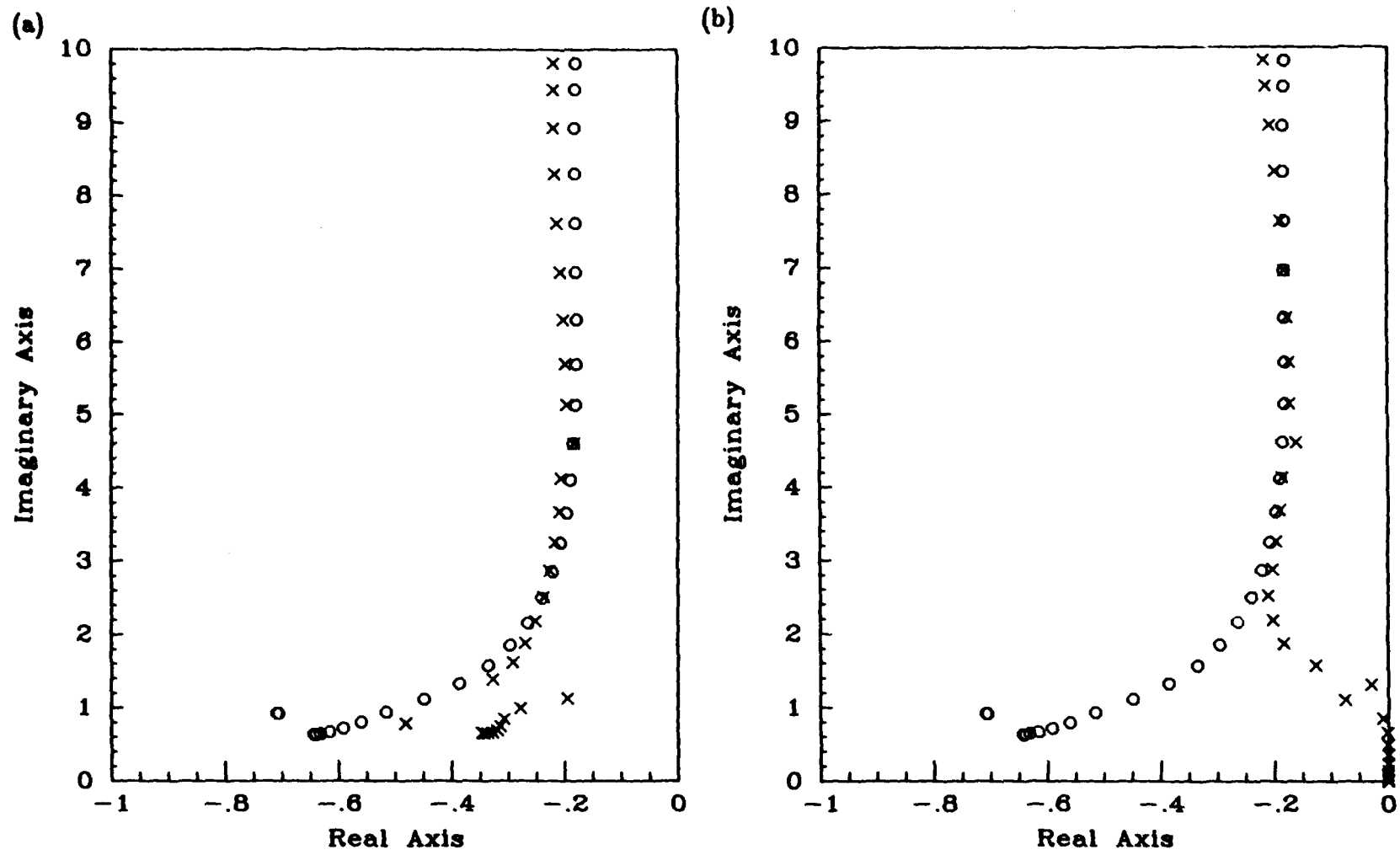

Figure 4.12: The closed loop poles from the two bay block diagonal local controller. The circles are the optimal pole locations, and the x's are the pole locations with the two bay block diagonal feedback. Figure (a) compares the decentralized controller with the optimal centralized soution. Figure (b) compares the filtered local controller with the optimal solution.

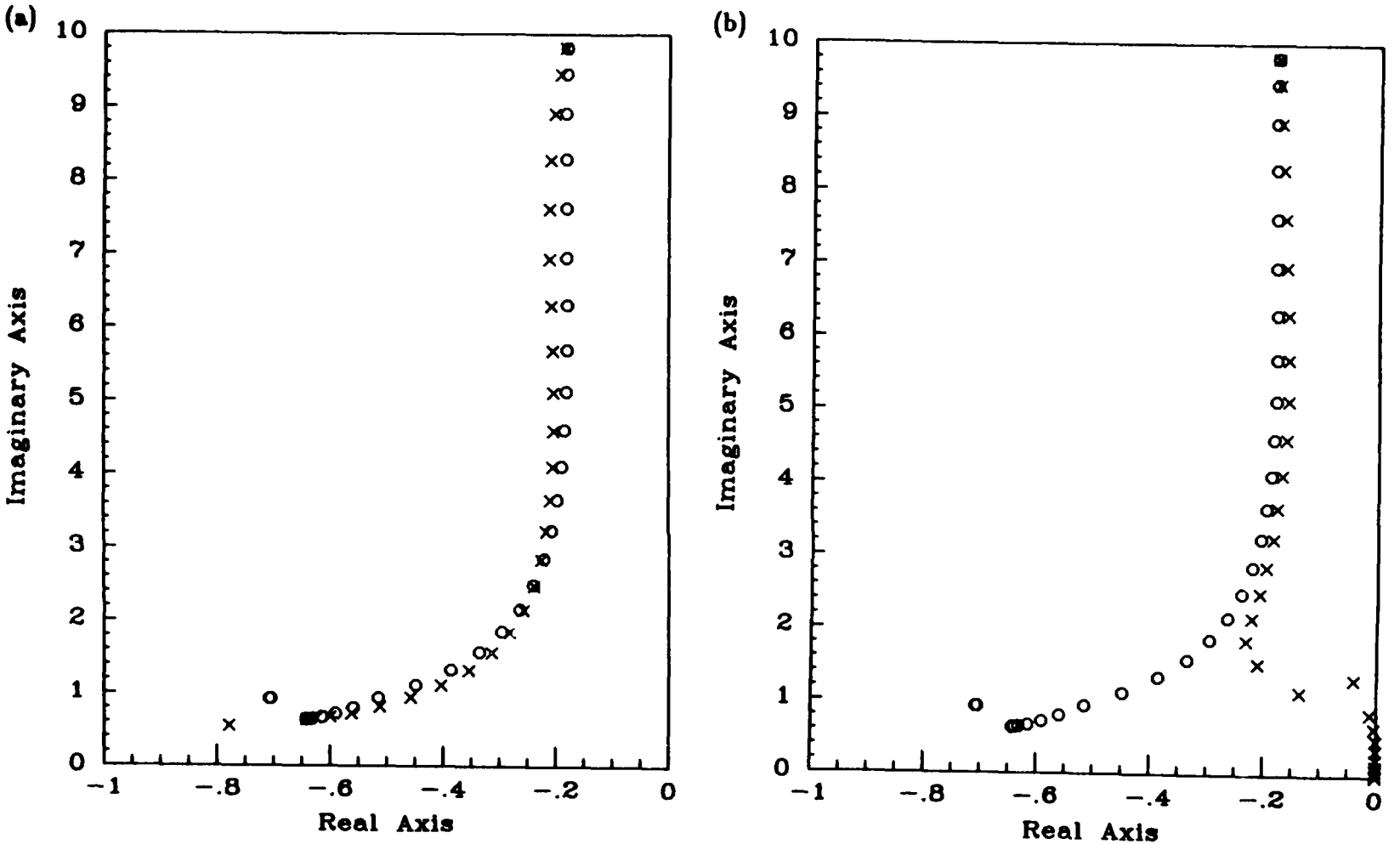

Figure 4.13: The closed loop poles from the full block tri-diagonal local controller. The circles are the optimal pole locations, and the x's are the pole locations with the full block tri-diagonal feedback. Figure (a) compares the decentralized controller with the optimal centralized soution. Figure (b) compares the filtered local controller with the optimal solution.

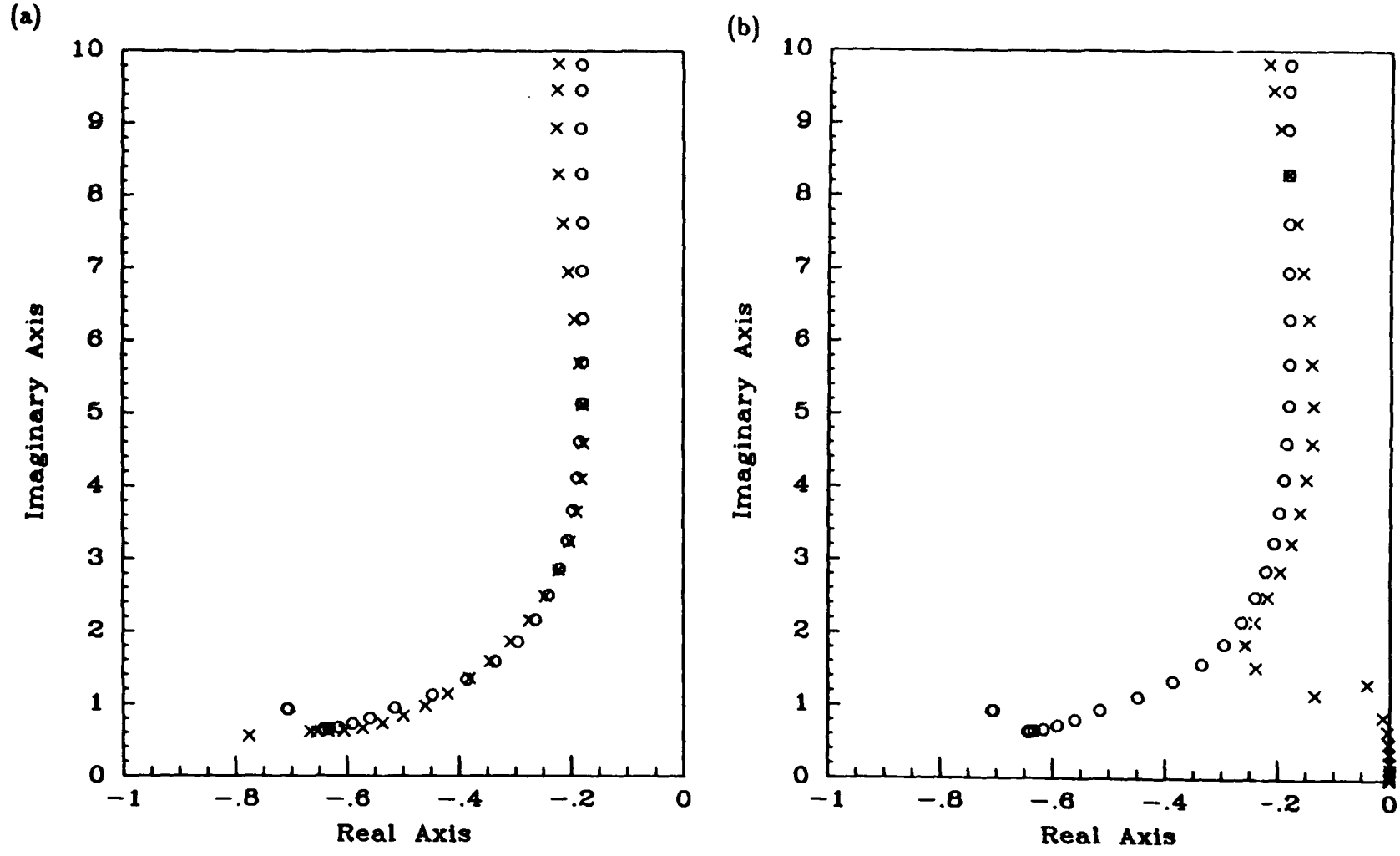

Figure 4.14: The closed loop poles from the banded block tri-diagonal local controller. The circles are the optimal pole locations, and the x's are the pole locations with the banded block tri-diagonal feedback. Figure (a) compares the decentralized controller with the optimal centralized soution. Figure (b) compares the filtered local controller with the optimal solution.

fairly comparable for both of these types of feedback, and worse than that for the block diagonal examples.

The filtered results show that the agreement for the lower frequency residual model poles is very good in both cases. The higher frequency agreement for the full gain block is much better than that for the banded feedback.

4.4.5 Conclusions

As would be expected, the results clearly indicate that the block tri-diagonal designs are the best decentralized controllers. However, they also indicate that the decentralized block diagonal designs can give reasonable closed loop performance. However, comparing the designs in terms of their primary job function as filtered local controllers it is clear that the block diagonal and block tri-diagonal controllers are virtually identical. The colocated uniform damping controller is clearly a poor choice as a decentralized controller.

4.5 An Analysis of the Full Hierarchic Control Designs

As stated earler, the aim of this chapter is to demonstrate that it is possible to obtain closed loop performance which is comparable to the optimal solution using a hierarchic control architecture. The question of the computational savings over other full order centralized controllers will be left until Chapter 5. With this aim of comparing the performance in mind, the various local controllers analyzed in the previous section have been combined with the global controller of Section 4.3. The closed loop poles locations are shown in Figures 4.15 and 4.16. The two cases combine the global controller with local controllers based on natural colocated feedback and a block diagonal feedback. Only two examples are provided since, apart

from the extra coupling due to the addition of the other controller, these plots are virtually identical to those in Figures 4.7, 4.10, and 4.12.

To investigate the closed loop performance even further, the response to a unit velocity impulse applied at about $\frac{1}{3}$ the length of the beam was obtained for each of the global and local control combinations. The measurement matrix, C, was taken to be $R_{xx}^{\frac{1}{2}}$ so that $y^T y$ provides the contribution to the cost function of Equation 4.9 at each time interval. The states were also measured directly so that the squared control effort could be found using the feedback matrices. The totals of these state and control terms were then summed over the entire impulse response. This was repeated for several control weightings, and the results are compared in Figure 4.17. The control axis is actually the average squared control effort as the total sum is divided by n.

The results in Figure 4.17 show the trade-off between the achievable performance and the control effort required. There are several important points to address. By definition, the optimal LQR controller represents the "lowest" achievable line on this graph. Any other design will give a state/control cost pair which lies above this boundary. Another curve has been drawn on the graph to show the expected performance if one of the simplest forms of decentralized feedback, namely natural control, is employed. The difference between the optimal and the uniform damping solution is readily apparent for this fairly realistic cost function. The third set of points corresponds to the hierarchic controller designed using the global controller of Section 4.3 with a local control based on uniform damping. This figure graphically shows the performance improvements that can be obtained by including the second level of control in the hierarchic control architecture (see Figure 2.4).

The optimal curve consists of the results from several control designs (*i.e.*, several ρ values). The marked point corresponds to the design point ($\rho = 1$) for the global controller. This global design was then combined with the various local controllers which were also designed with various parameter settings. As was discussed

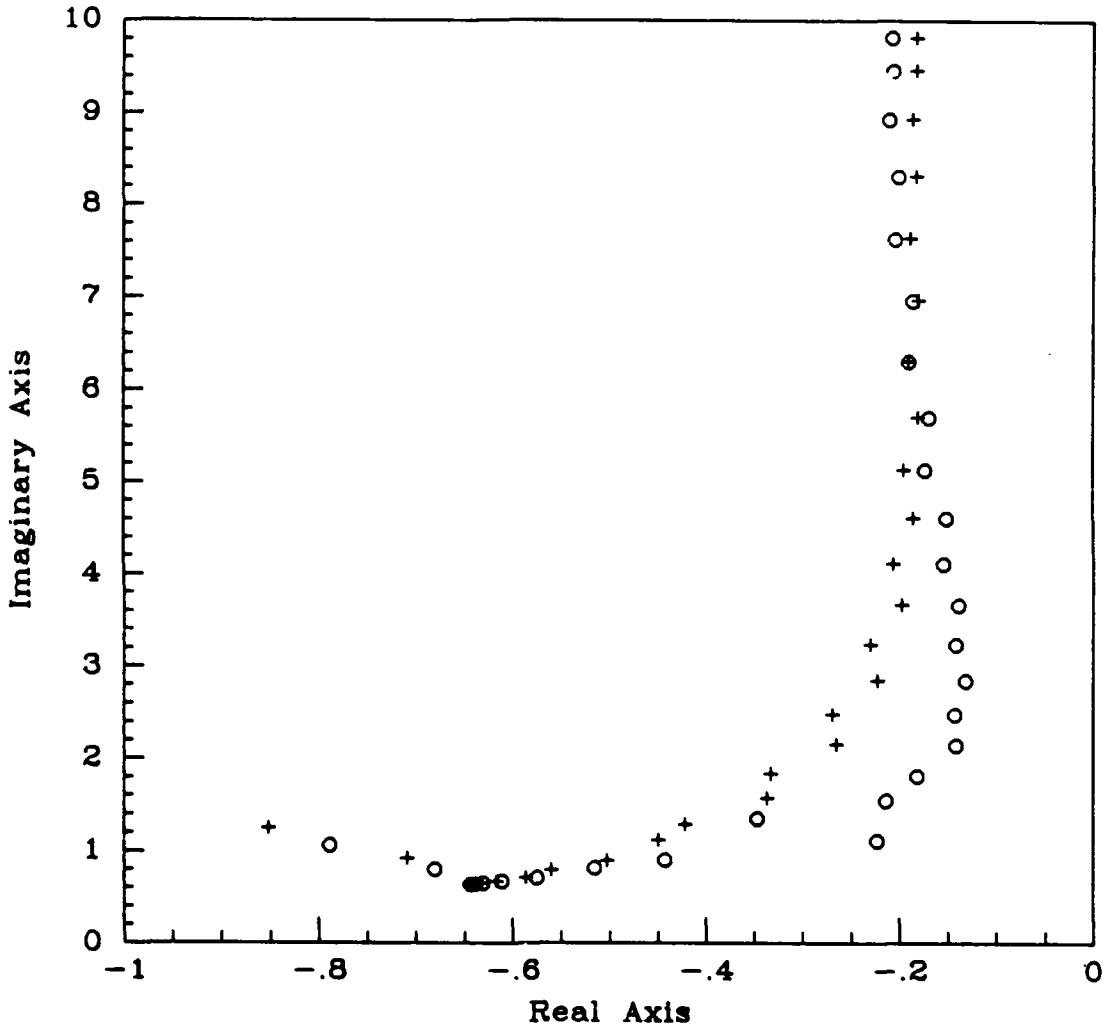

Figure 4.15: The closed loop poles for a full hierarchic controller with a local control based on colocated natural feedback (circles) compared with the full order regulator poles (crosses).

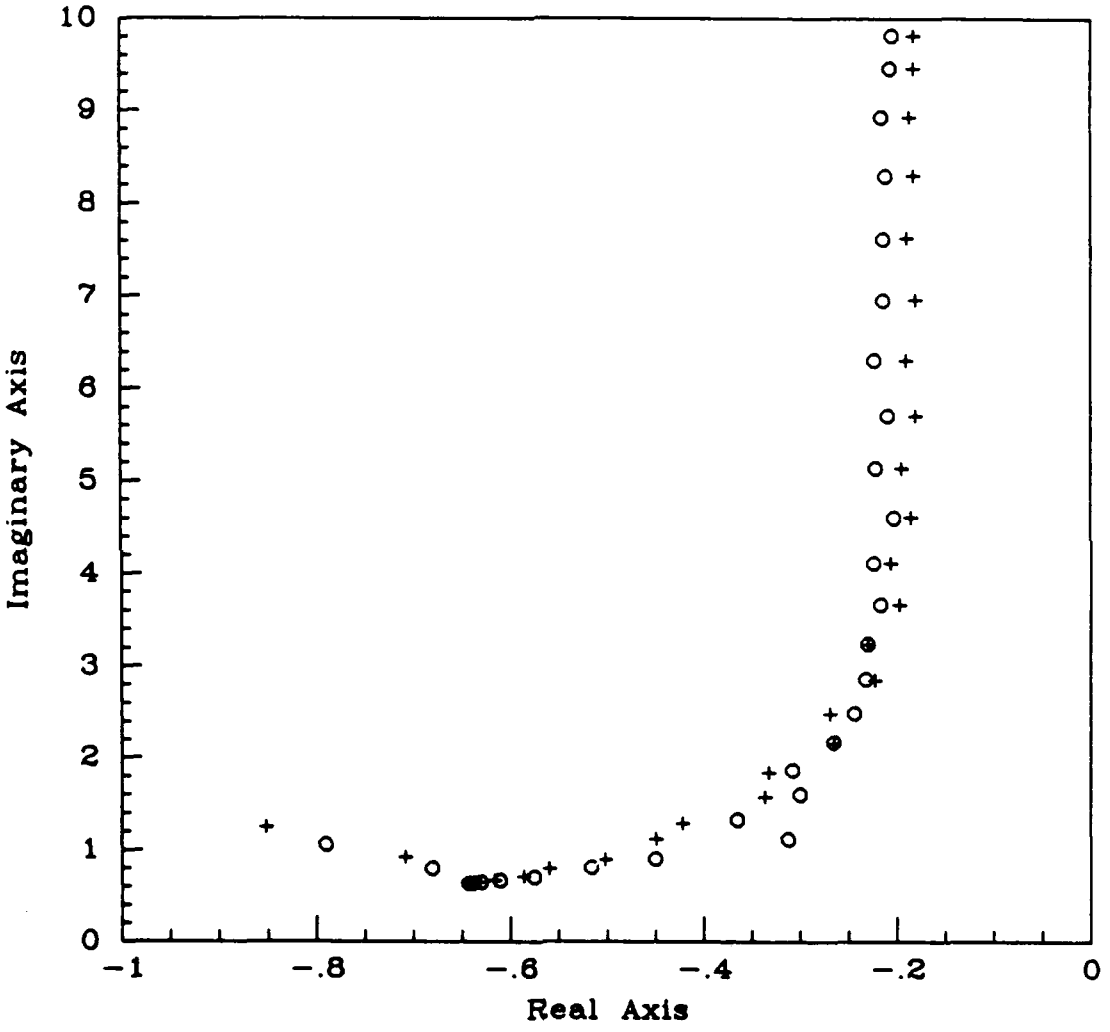

Figure 4.16: The closed loop poles for a full hierarchic controller with a local control based on block diagonal feedback (circles) compared with the full order regulator poles (crosses).

before, each important control parameter (β for uniform damping or ρ for the optimal solutions) was increased and decreased by a factor of about 2 to generate three local control designs. For the hierarchic designs, there are two control parameters. Fixing the global control parameter (ρ) results in a locus of state/control cost points for various values of the local control parameter. For each value of the global parameter, there will be a point on the locus which minimizes the separation from the LQR boundary. This is the "optimal" point for this global design. Repeating this procedure and connecting the set of points then generates the appropriate cost curve for this combination of hierarchic and local designs. For simplicity, only one global control design point is shown, but the results indicate that some very interesting conclusions can be made. The results for the five local control designs are shown in Figure 4.18.

Comparing the performance of the local controllers in terms of the separation of the "optimal" point from the LQR boundary, it is clear that the two block tridiagonal designs are the best. The full block diagonal approach is slightly worse, but better than the two bay approach. All four of these designs are better than the results obtained using the uniform damping as the local controller, so these results agree with the observations made from investigating the pole locations. What is also apparent from this figure is that most of the performance improvement relative to the decentralized controller has been obtained by including the global controller, and that the extra performance improvements obtained by using the more sophisticated local control designs are apparent but relatively small.

One important point is that the performance of the local controller would be more critical for the global design based on fewer global modes. In this case, the local control will influence more lower frequency modes which will have a large influence on the cost, so it is important that the controller be designed appropriately. Just damping these modes at the same level as the higher frequency ones will either result in very poor closed loop performance or many overdamped modes.

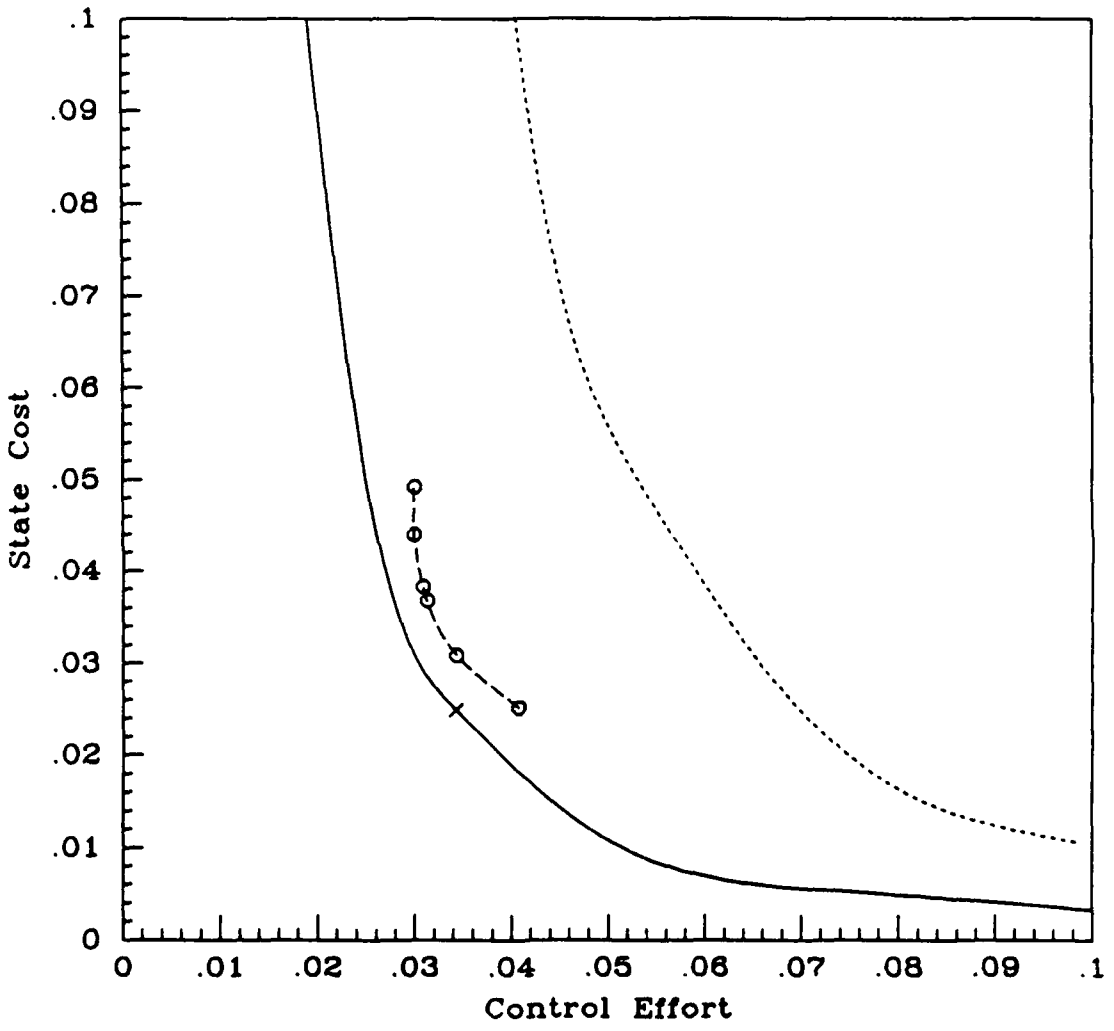

Figure 4.17: This graph compares the performance of a hierarchic controller based on a uniform damping local control (circles) with the optimal LQR controller (solid) and a decentralized uniform damping controller (dotted).

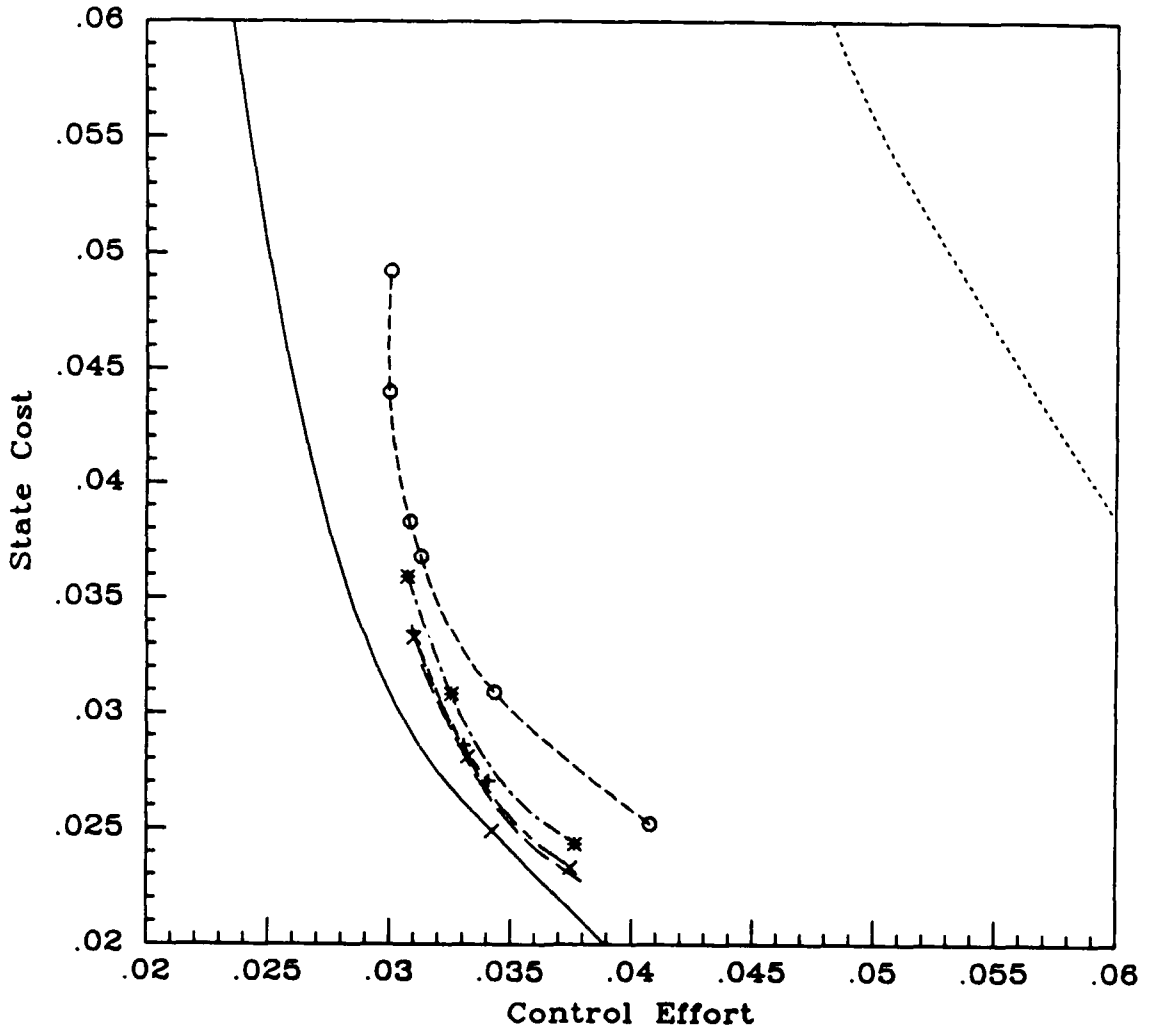

Figure 4.18: The performance of five local control designs are shown. The optimal performance (solid) and decentralized controller (dotted) lines are included for reference. The circles are the uniform damping local control. The stars are the two bay block diagonal design. The crosses are the full block diagonal design. The x's are the banded block tri-diagonal approach, and the line with no symbols is the full block tri-diagonal design. The labels are given in increasing order of performance.

One other way to analyze the results of the hierarchic controller is to apply it to the evaluation model. In this case, this is taken to be the beam finite element model before the condensation procedure is applied. In this way, the evaluation model is twice as large as the design model. The closed loop pole locations for the same same global controller and the uniform damping and block diagonal local controllers are shown in Figure 4.19. These results indicate that the level of spillover to the unmodelled modes is very similar for both designs.

4.6 Conclusions

In conclusion, it is clear that the hierarchic controller can offer much better closed loop performance than the decentralized natural control, and the selection of a good local controller should allow the performance (state cost and control effort required) to approach that of the LQR optimal controller. Both of the block diagonal and block tri-diagonal feedback approaches provide very comparable performance. It would be difficult to recommend one technique over the others based purely on these performance results. Chapter 5 will investigate the implementation costs of these designs to determine the cost of these performance improvements.

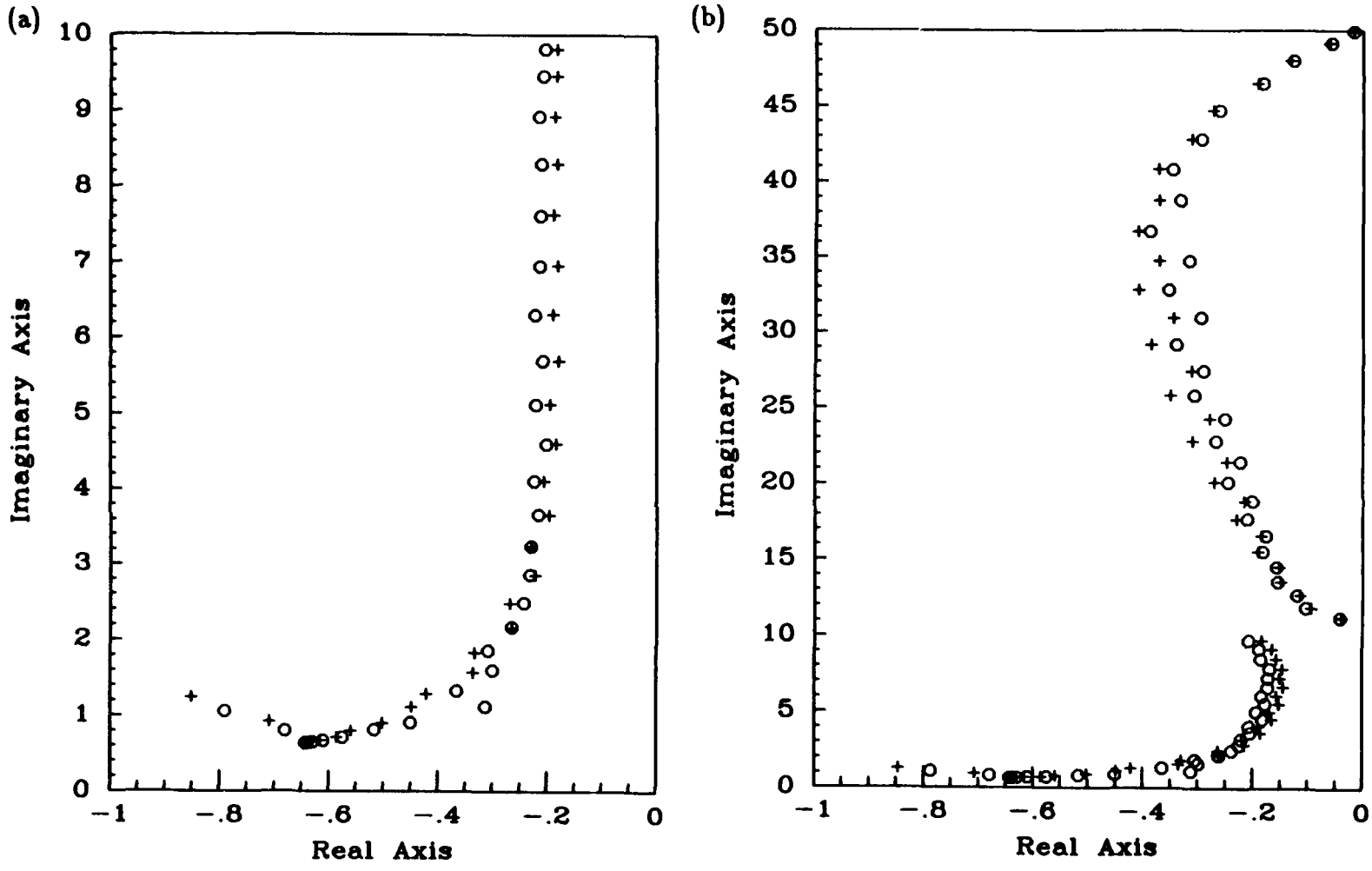

Figure 4.19: The hierarchic control (block diagonal local control) (circles) compared with the full order regulator (crosses) when both are applied to the condensed model (a) and to the evaluation model (b).

Chapter 5

Implementation Issues

5.1 Introduction

The main purposes of this chapter are to present the operations count for the hierarchic control architecture and to show the implementation benefits that can be obtained by employing this design. In particular, the local control designs discussed in Chapters 3 and 4 will be investigated, and some conclusions about the relative implementation costs will be made. These results will then be combined with the performance analysis in Section 4.5 to make a final decision concerning the most efficient local controller. Section 5.3 then discusses the closed loop stability of the hierarchic architecture. Section 5.4 addresses the issue of the robustness of the architecture to sensor and actuator failure, and Section 5.5 investigates the question of how to locate the processors.

5.2 Operations Count

5.2.1 Introduction

The primary purpose of this section of the chapter is to develop the operations count for the local and global controllers for the special case of the hierarchic control architecture being applied to a one dimensional structure. The computational requirements will be expressed in terms of the number of multiplications and additions required in total and for each type of processor in particular. Figure 5.1 shows the assumed form of the structure. With the following definitions

n = the number of structural nodes

n_g = the total number of global degrees of freedom

n_{gn} = the number of global nodes

$n_{g_{dof}}$ = the number of degrees of freedom per global node

h_g = the number of structural nodes per finite control element

n_e = the number of finite control elements

n_l = the number of retained global modes

These values are related through the following set of relations

$$n_e = n_{gn} - 1 \tag{5.1}$$

$$n = n_e(h_g) \tag{5.2}$$

$$n_g = n_{gn} n_{g_{dof}} \tag{5.3}$$

Note that it is not assumed that the global nodes coincide with the structural nodes in general, but it is assumed that the internal finite control elements are all identical, with h_g nodes between the global nodes. The finite control elements at either end have $h_g - 1$ internal nodes and one node that coincides with a global node.

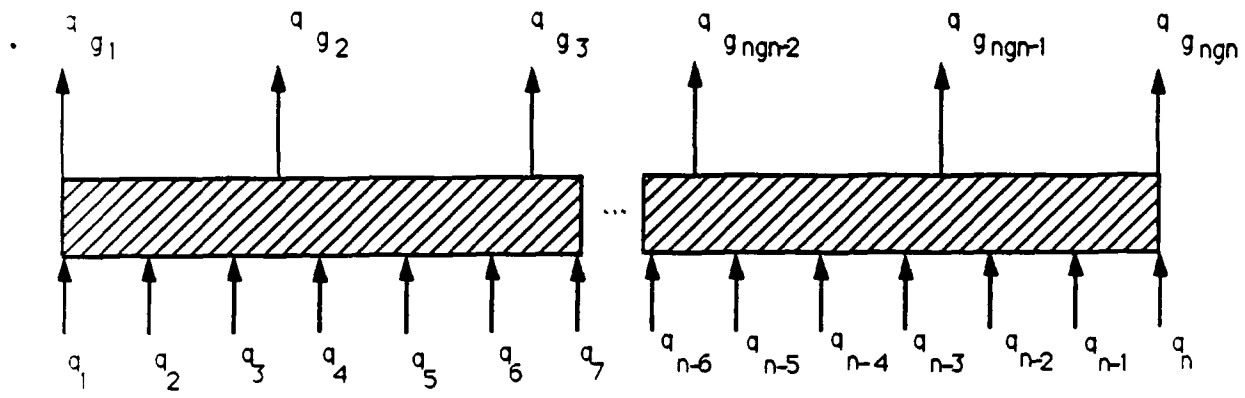

Figure 5.1: The assumed layout of the global and structural nodes for the operations count.

5.2.2 Task Analysis for the Controllers

As can be seen from Figure 2.4, there are several tasks that the controllers at each level must perform. Going around the control loops as the operations would be done, the jobs are:

I. Each local processor must read the information from the sensors and form the contributions to the global node values [local].

II. These values must be communicated to the global processor [combined], added together [global] and then normalized [global].

III. These global values, q_g, are then returned to the local processors [combined], interpolated [local], and subtracted from the original measurements [local].

IV. The local control commands Q_e can then be calculated from residuals e [local].

V. The global control commands Q_g can be caculated from q_g [global].

VI. The local processors must calculate the global component of the local control Q_e^g [local].

VII. These values are then communicated to global processor [combined], added together [global], and subtracted from the global commands [global], to form $Q_g - Q_e^g$.

VIII. These commands are then normalized [global] and communicated down to the local processors [combined].

IX. These control commands are then interpolated, added to the original set Q_e to form u, and then applied to the actuators [local].

The following is a detailed calculation of the operations count for a one dimensional structure where it is assumed that there are two global nodes per finite control element and that each structural node has one degree of freedom. The mass matrix is assumed to be diagonal so that, in terms of the operation count, $T_g M \sim T_g \sim [n \times n_g]$. The communication required at the i^{th} step is denoted by comm_i.

I. Form the contributions to the global node values.

$$\left(T_g^T M q\right)_{ele} \sim \left[2n_{g_{dof}} \times h_g\right] \cdot [h_g \times 1]$$

$$C_1 = 2n_{g_{dof}} \begin{cases} h_g & \text{M} \\ h_g - 1 & \text{A} \end{cases} \tag{5.4}$$

per element. This amount should be doubled to account for $\dot{q}$ as well.

II. Communication of the states up and normalization.

i. Communicate $2n_{g_{dof}}\,(n_{gn} - 1)$ pieces of information from the local processors to the global processor.

ii. Aggregrate the information to form the full set of global values.

$$C_{2_2} = n_{g_{dof}} (n_{gn} - 2)\,\mathrm{A} \tag{5.5}$$

iii. Normalization.

$$M_{gg}^{-1} \hat{q}_g \sim [n_g \times n_g] \cdot [n_g \times 1]$$

$$C_{2_3} = \begin{cases} (n_g)^2 & \mathrm{M} \\ n_g (n_g - 1) & \mathrm{A} \end{cases} \tag{5.6}$$

so that

$$C_2 = \begin{cases} (n_g)^2 & \mathrm{M} \\ (n_g)^2 - 2n_{g_{dof}} & \mathrm{A} \end{cases} + \mathrm{comm}_1 \tag{5.7}$$

where these results must be doubled to account for $\dot{q}$.

III. Communication of the global states down and interpolation.

i. Communicate $2n_{g_{dof}} (n_{gn} - 1)$ pieces of information from the global processor to the local processors.

ii. Interpolation.

$$(T_g q_g)_{ele} \sim \left[h_g \times 2n_{g_{dof}}\right] \cdot \left[2n_{g_{dof}} \times 1\right]$$

$$C_{3_2} = h_g \begin{cases} 2n_{g_{dof}} & \mathrm{M} \\ 2n_{g_{dof}} - 1 & \mathrm{A} \end{cases} \tag{5.8}$$

per element.

iii. For the subtraction, there will be h_g sign changes and additions per element.

so that

$$C_3 = 2h_g \begin{cases} n_{g_{dof}} & \mathrm{M} \\ n_{g_{dof}} & \mathrm{A} \end{cases} + \mathrm{comm}_2 \tag{5.9}$$

per element and these results must be doubled to account for $\dot{q}$.

IV. C_4 for the local control calculation will be added later.

V. Global control.

$$F_g q_g \sim [n_g \times n_g] \cdot [n_g \times 1]$$

$$C_{5_1} = \begin{cases} (n_g)^2 & \text{M} \\ n_g (n_g - 1) & \text{A} \end{cases} \tag{5.10}$$

which must be doubled to account for $\dot{q}_g$ and then (n_g) A must be done to combine the two components of the control, so that

$$C_5 = \begin{cases} 2 (n_g)^2 & \text{M} \\ n_g (2n_g - 1) & \text{A} \end{cases} \tag{5.11}$$

VI. Global component of the local control.

$$Q_e^g = T_g^T Q_e$$

$$C_6 = 2n_{g_{dof}} \begin{cases} h_g & \text{M} \\ h_g - 1 & \text{A} \end{cases} \tag{5.12}$$

per element.

VII. Communication of the control up and subtraction.

i. Communicate $2n_{g_{dof}} (n_{gn} - 1)$ pieces of information from the local processors to the global processor.

ii. Aggregate the information to form the complete set of global values.

$$C_{7_1} = n_{g_{dof}} (n_{gn} - 2) \text{ A} \tag{5.13}$$

iii. For the subtraction, there will be n_g sign changes and additions.

so that

$$C_7 = 2n_{g_{dof}} (n_{gn} - 1) \text{ A} + \text{comm}_3 \tag{5.14}$$

VIII. Normalization and communication of the modified control down.

i. Normalization.

$$C_{8_1} = \begin{cases} (n_g)^2 & \text{M} \\ n_g(n_g - 1) & \text{A} \end{cases} \tag{5.15}$$

ii. Communicate $2n_{g_{dof}}(n_{gn} - 1)$ pieces of information from the global processor to the local processors.

so that

$$C_8 = \begin{cases} (n_g)^2 & \text{M} \\ n_g(n_g - 1) & \text{A} \end{cases} + \text{comm}_4 \tag{5.16}$$

IX. Interpolation and addition.

i. Interpolation of the commands.

$$C_{9_1} = h_g \begin{cases} 2n_{g_{dof}} & \text{M} \\ 2n_{g_{dof}} - 1 & \text{A} \end{cases} \tag{5.17}$$

per element.

ii. For the subtraction, there will h_g sign changes and additions per element.

so that

$$C_9 = 2h_g \begin{cases} n_{g_{dof}} & \text{M} \\ n_{g_{dof}} & \text{A} \end{cases} \tag{5.18}$$

per element.

This completes the analysis of the tasks to be performed by each of the controllers. There are several totals which are of importance. These include the total computational requirements, and the totals for each processor. For the total of the global processor, the following summation must be made

$$C_{global} = 2C_2 + C_5 + C_7 + C_8 \tag{5.19}$$

where the communication terms are ignored for now. For the local processors, the corresponding sum is

$$C_{local} = 2C_1 + 2C_3 + C_4 + C_6 + C_9 \tag{5.20}$$

so that, using Equations 5.7, 5.11, 5.14, and 5.16

$$\begin{aligned} C_{global} &= 2\begin{bmatrix} (n_g)^2 & \mathrm{M} \\ (n_g)^2 - 2n_{g_{dof}} & \mathrm{A} \end{bmatrix} + \begin{bmatrix} 2(n_g)^2 & \mathrm{M} \\ n_g(2n_g - 1) & \mathrm{A} \end{bmatrix} \\ &+ \begin{bmatrix} 0 & \mathrm{M} \\ 2n_{g_{dof}}(n_{gn} - 1) & \mathrm{A} \end{bmatrix} + \begin{bmatrix} (n_g)^2 & \mathrm{M} \\ n_g(n_g - 1) & \mathrm{A} \end{bmatrix} \\ &= \begin{bmatrix} 5(n_g)^2 & \mathrm{M} \\ 5(n_g)^2 - 6n_{g_{dof}} & \mathrm{A} \end{bmatrix} \end{aligned} \tag{5.21}$$

and, from Equations 5.4, 5.9, 5.12, and 5.18

$$\begin{aligned} C_{local} &= 4n_{g_{dof}}\begin{bmatrix} h_g & \mathrm{M} \\ h_g - 1 & \mathrm{A} \end{bmatrix} + 4h_g\begin{bmatrix} n_{g_{dof}} & \mathrm{M} \\ n_{g_{dof}} & \mathrm{A} \end{bmatrix} + C_4 \\ &+ 2n_{g_{dof}}\begin{bmatrix} h_g & \mathrm{M} \\ h_g - 1 & \mathrm{A} \end{bmatrix} + 2h_g\begin{bmatrix} n_{g_{dof}} & \mathrm{M} \\ n_{g_{dof}} & \mathrm{A} \end{bmatrix} \\ &= \begin{bmatrix} 12n_{g_{dof}}h_g & \mathrm{M} \\ 6n_{g_{dof}}(2h_g - 1) & \mathrm{A} \end{bmatrix} + C_4 \end{aligned} \tag{5.22}$$

These represent the total computational requirements for each processor. It is these values which are most important in sizing the individual processors. The total for all processors can be obtained from

$$C_{total} = C_{global} + n_e C_{local} \tag{5.23}$$

so that, employing the relations in Equations 5.1 through 5.3

$$\begin{aligned} C_{total} &= \begin{bmatrix} 5(n_g)^2 & \mathrm{M} \\ 5(n_g)^2 - 6n_{g_{dof}} & \mathrm{A} \end{bmatrix} + n_e\begin{bmatrix} 12n_{g_{dof}}h_g & \mathrm{M} \\ 6n_{g_{dof}}(2h_g - 1) & \mathrm{A} \end{bmatrix} + n_e C_4 \\ &= \begin{bmatrix} 5(n_g)^2 + 12nn_{g_{dof}} & \mathrm{M} \\ 5(n_g)^2 + 12nn_{g_{dof}} - 6n_g & \mathrm{A} \end{bmatrix} + n_e C_4 \end{aligned} \tag{5.24}$$

which represents the total computational requirements per update, assuming that the two loops operate at the same rate, an assumption which will be relaxed in the following section.

5.2.3 Incorporating Different Controller Frequencies

Typically it will be undesirable to operate each of the control levels at the same update rate. The aim of this section is to introduce a technique which allows the local controllers to operate at a much higher rate than the global controller since they are governing different modes of the structure. As was mentioned earlier in Section 2.5, the problem with this approach is that it would require the two filtering loops in Figure 2.4 to operate at the much higher rate, thus involving the central processor. However, it is possible to avoid this using a technique of computing the global components of the states and local control, and then using them for an entire global update cycle. The assumption being that, on average, these values will not change much during this time period. Some measure of the deviation during an interval could be evaluated at the local level and a correction then could be applied during the next interval. A decrease in performance relative to the case in which the filtering is done at the faster rate should be expected since the filtering out of the global components of the motion and control is no longer complete. This results in some extra spillover between the two models. However, employing this technique would allow for very fast and simple control to be performed at the local level. This is another trade-off in the performance and/or cost analysis that must be done.

Without the filtering steps, each local processors needs only to perform three operations per loop. These are

I. A subtraction to form the residuals e, h_gA per element

II. Calculate the local control commands, C_4

III. Add the global command (a constant for the time interval) and the filtered local control commands, h_gA per element.

Using the variable ρ to denote the number of local updates per global update, the total computational requirements for each update then is given by

$$\begin{aligned} C_{total}(\rho) &= C_{total}(\rho=1) - \begin{bmatrix} 0 & \mathrm{M} \\ 2n_e h_g & \mathrm{A} \end{bmatrix} + \rho n_e \left\{ C_4 + \begin{bmatrix} 0 & \mathrm{M} \\ 2h_g & \mathrm{A} \end{bmatrix} \right\} \\ &= \begin{bmatrix} 5(n_g)^2 + 12nn_{g_{dof}} & \mathrm{M} \\ 5(n_g)^2 + 12nn_{g_{dof}} - 6n_g - 2n & \mathrm{A} \end{bmatrix} \\ &+ \rho \left\{ n_e C_4 + \begin{bmatrix} 0 & \mathrm{M} \\ 2n & \mathrm{A} \end{bmatrix} \right\} \end{aligned} \tag{5.25}$$

Typically, the command update rate should be faster than the fastest mode being controlled. Thus, ρ can be considered to be a measure of the relative frequencies of the modes to be controlled by the two levels. For a rod, the modal frequency tends to go as n, but for a beam it goes as n^2, so that, since the local model is of order n, and the global is of order n_g, then

$$\text{For a rod : } \rho = \frac{n}{n_g} \tag{5.26}$$

$$\text{For a beam : } \rho = \left(\frac{n}{n_g}\right)^2 \tag{5.27}$$

5.2.4 Operations Count with only the Lower Modes Retained

The advantages of using only the lower half of the global modes available in terms of reducing the dynamic spillover were shown in Section 4.3. The purpose of this section is to produce the operations count when this modification is implemented as shown in Section 2.6 so that a fair comparison with the case where all the global modes are retained can be made. Figure 2.6. shows the appropriate modifications

that must be made to the control architecture. It can be seen that the tasks performed by the local processors are unchanged, but the steps for the global processor are now

I. Aggregate and normalize the data from the local processors, as before, to form q_l.

II. Compute $\phi_g^l q_l$ to be sent down to the local processors.

III. Compute the global control based on the lower modes.

IV. Aggregate the local control and use $\phi_g^{l^T}$ to reduce the information.

V. Normalize the commands.

The number operations required for these steps can be enumerated following the results in Section 5.2.2. It is assumed that only n_l modes are retained so that the ϕ_g^l matrix is $n_g \times n_l$.

I. Aggregation and normalization.

i. Aggregation.

$$L_{1_1} = n_{g_{dof}} \left(n_{gn} - 2\right) \mathrm{A} \tag{5.28}$$

ii. Normalization.

$$\left(\left(\phi_g^l\right)^T M_{gg} \left(\phi_g^l\right)\right)^{-1} \left(\phi_g^l\right)^T \hat{q}_g \sim [n_l \times n_g] \cdot [n_g \times 1]$$

$$L_{1_2} = \begin{cases} n_l \left(n_g\right) & \mathrm{M} \\ n_l \left(n_g - 1\right) & \mathrm{A} \end{cases} \tag{5.29}$$

so that

$$L_1 = \begin{cases} n_l \left(n_g\right) & \mathrm{M} \\ n_l \left(n_g - 1\right) + n_{g_{dof}} \left(n_{gn} - 2\right) & \mathrm{A} \end{cases} \tag{5.30}$$

II. Compute $\phi_g^l q_l$.

$$\begin{aligned} \phi_g^l q_l &\sim [n_g \times n_l] \cdot [n_l \times 1] \\ L_2 &= \begin{cases} (n_g)\, n_l & \mathrm{M} \\ n_g\,(n_l - 1) & \mathrm{A} \end{cases} \end{aligned} \tag{5.31}$$

III. The calculation of the global control is the same as before.

$$L_3 = \begin{cases} 2\,(n_l)^2 & \mathrm{M} \\ n_l\,(2n_l - 1) & \mathrm{A} \end{cases} \tag{5.32}$$

IV. Aggregation and reduction of the control.

i. Add the commands sent from the local controller.

$$L_{4_1} = C_{7_1} = n_{g_{dof}}\,(n_{gn} - 2)\,\mathrm{A} \tag{5.33}$$

ii. Reduce the commands.

$$\begin{aligned} Q_e^l &= \left(\phi_g^l\right)^T Q_e^g \sim [n_l \times n_g] \cdot [n_g \times 1] \\ L_{4_2} &= \begin{cases} n_l\,(n_g) & \mathrm{M} \\ n_l\,(n_g - 1) & \mathrm{A} \end{cases} \end{aligned} \tag{5.34}$$

iii. For the subtraction, there will be n_l sign changes and additions.

so that

$$L_4 = \begin{cases} n_l\,(n_g) & \mathrm{M} \\ n_l n_g + n_g - 2n_{g_{dof}} & \mathrm{A} \end{cases} \tag{5.35}$$

V. Normalization.

$$L_5 = \begin{cases} (n_g)\, n_l & \mathrm{M} \\ n_g\,(n_l - 1) & \mathrm{A} \end{cases} \tag{5.36}$$

The total computational requirements for the central processor can then be obtained from

$$C_{lower} = 2L_1 + 2L_2 + L_3 + L_4 + L_5 \tag{5.37}$$

$$\begin{aligned} C_{lower} &= 2\begin{bmatrix} n_l(n_g) & \mathrm{M} \\ n_l(n_g-1)+n_{g_{dof}}(n_{gn}-2) & \mathrm{A} \end{bmatrix} \\ &+ 2\begin{bmatrix} (n_g)\,n_l & \mathrm{M} \\ n_g(n_l-1) & \mathrm{A} \end{bmatrix} + \begin{bmatrix} 2(n_l)^2 & \mathrm{M} \\ n_l(2n_l-1) & \mathrm{A} \end{bmatrix} \\ &+ \begin{bmatrix} n_l(n_g) & \mathrm{M} \\ n_l n_g + n_g - 2n_{g_{dof}} & \mathrm{A} \end{bmatrix} + \begin{bmatrix} (n_g)\,n_l & \mathrm{M} \\ n_g(n_l-1) & \mathrm{A} \end{bmatrix} \\ &= \begin{bmatrix} 2(n_l)^2 + 6n_l n_g & \mathrm{M} \\ 2(n_l)^2 + 6n_l n_g - 3n_l - 6n_{g_{dof}} & \mathrm{A} \end{bmatrix} \end{aligned} \tag{5.38}$$

where typically $n_l \approx \frac{1}{2}n_g$, so that the total for the central computer now goes as $\frac{7}{2}(n_g)^2$ rather than $5(n_g)^2$ as before. So, it would appear that this modification not only improves the decoupling performance of the controllers, but also requires fewer computations to implement than the case where all the global modes are retained.

5.2.5 Operation Counts for the Local Controllers

Several local controllers were studied in Chapter 3. The purpose of this section is to outline the computational requirements of these various techniques. Three types will be studied. These include colocated rate and displacement feedback, block diagonal feedback, and block tri-diagonal.

I. Colocated Uniform Feedback. The feedback is done directly from a set of measurements to the actuator at the same location as explained in Section 3.2.

$$u_i = -\beta^2 M q_i - 2\beta M \dot{q}_i$$

A calculation which must be performed at each of the n structural nodes, so that the total computational requirements are then

$$n_e C_{4_{COL}} = \begin{cases} 2n & \text{M} \\ n & \text{A} \end{cases} \tag{5.39}$$

II. Block Diagonal Feedback.

The feedback is from all sensors in an element to all actuators in an element. Then, for a finite control element with h_g nodes

$$F_{q_e} q_e \sim [h_g \times h_g] \cdot [h_g \times 1]$$

which requires,

$$C_{4_{BD}} = h_g \begin{cases} h_g & \text{M} \\ h_g - 1 & \text{A} \end{cases} \tag{5.40}$$

operations per element. There are also h_gA to add the displacement and velocity components together The total requirements are then given as

$$\begin{aligned} n_e C_{4_{BD}} &= n_e h_g \begin{cases} 2h_g & \text{M} \\ 2h_g - 1 & \text{A} \end{cases} \\ &= \frac{n}{n_{gn} - 1} \begin{cases} 2n & \text{M} \\ 2n - n_{gn} + 1 & \text{A} \end{cases} \end{aligned} \tag{5.41}$$

The analysis in Chapter 4 also investigates a second case for which the gain matrix is composed of block diagonal matrices which have been developed for "bays" which are smaller than the finite control element. In particular, the case for which the element is split into two independent bays was considered. In this case, the control commands within a bay are only calculated from the the sensor measurements within that bay. For this half block diagonal example, the computational requirements become

$$n_e C_{4_{HBD}} = \frac{n_e h_g}{2} \begin{cases} 2h_g & \text{M} \\ 2h_g - 2 & \text{A} \end{cases}$$

$$= \frac{n}{n_{gn}-1}\begin{cases} n & \mathrm{M} \\ n-n_{gn}+1 & \mathrm{A} \end{cases} \tag{5.42}$$

III. Block Tri-Diagonal Feedback.

There are two cases to be looked at here. The first one is the "worst" case for which the gain is taken to be three full gain blocks. The other interesting case considered in Section 3.4 is the one for which the gains are banded.

i. Full Gain Blocks.

$$\begin{bmatrix} F_{i-1} & F_i & F_{i+1} \end{bmatrix} \begin{bmatrix} q_{i-1} \\ q_i \\ q_{i+1} \end{bmatrix} \sim [h_g \times 3h_g] \cdot [3h_g \times 1]$$

which requires

$$C_{4_{BTD_1}} = h_g \begin{cases} 3h_g & \mathrm{M} \\ 3h_g - 1 & \mathrm{A} \end{cases} \tag{5.43}$$

per element. There are also h_gA to add the displacement and velocity components together The total requirement then, taking the end effects into account, is

$$\begin{aligned} n_e C_{4_{BTD_1}} &= (n_e - 2)\begin{bmatrix} 6h_g^2 & \mathrm{M} \\ h_g(6h_g-1) & \mathrm{A} \end{bmatrix} + 2\begin{bmatrix} 4h_g^2 & \mathrm{M} \\ h_g(4h_g-1) & \mathrm{A} \end{bmatrix} \\ &= n_e h_g \begin{bmatrix} 6h_g & \mathrm{M} \\ (6h_g-1) & \mathrm{A} \end{bmatrix} + \begin{bmatrix} -4(h_g)^2 & \mathrm{M} \\ -4(h_g)^2 & \mathrm{A} \end{bmatrix} \\ &= \begin{bmatrix} \left(\frac{n}{n_{gn}-1}\right)^2 (6n_{gn}-10) & \mathrm{M} \\ \left(\frac{n}{n_{gn}-1}\right)^2 (6n_{gn}-10) - n & \mathrm{A} \end{bmatrix} \end{aligned} \tag{5.44}$$

ii. Purely Banded Feedback.

Assume that the control at each point is calculated from m locations on either side of the point. Then $m = 0$ corresponds to colocated feedback, and $m = 1$ corresponds to feedback from adjacent nodes. Then, each control calculation will require $2m + 1$ M and $2m$ A. These results must be doubled, and then n additions are required to add the displacement and velocity components. The total, taking into account the end effects would then be

$$n_e C_{4_{BTD_2}} = \begin{cases} n(4m+2) - 2m(m+1) & \text{M} \\ n(4m+1) - 2m(m+1) & \text{A} \end{cases} \tag{5.45}$$

5.2.6 Communication Requirements

In the analysis of the tasks to be performed that was detailed in Section 5.2.2, four communication operations were enumerated. Two of these were from the local processor to the global processor, and the remaining two were in the opposite direction. The total number of pieces of information that must be communicated between the levels for these two cases are listd below.

I. Local to global direction.

   i. $\text{comm}_1 \sim 4n_{g_{dof}}(n_{gn} - 1)$

   ii. $\text{comm}_3 \sim 2n_{g_{dof}}(n_{gn} - 1)$

II. Global to local direction.

   i. $\text{comm}_2 \sim 4n_{g_{dof}}(n_{gn} - 1)$

   ii. $\text{comm}_4 \sim 2n_{g_{dof}}(n_{gn} - 1)$

There is also the requirement of local communication between closest neighbors for some of the lower level control designs. These results are difficult to analyze in

the same manner as the operation counts since they depend entirely on the parameters of the system. Parameters which are of particular importance are the types of processor, the operating speed, the bus network, the method of communication (serial or parallel), the work load of the computers (the priority of the communication), and the protocol of the communication. The influence of these parameters are will be analyzed by the upcoming work by David Warkentin.

5.2.7 Typical Examples

For a single chip micro-computer similar to the INTEL 80C196KB it is given in the data books that, using short integers and indirect addressing, a MULT(3) command $(A \times B \rightarrow C)$ requires approximately 19 clock cycles. In comparison, an ADD(3) command requires only 7. So, for the purposes of comparison, it would be a good approximation to use $A \sim \frac{1}{3}M$. Using this result, Equation 5.25 then becomes

$$C_{total} = \frac{4}{3}\left(5\left(n_g\right)^2 + 12nn_{g_{dof}}\right) - 2n_g + \frac{2}{3}n\left(\rho - 1\right) + \rho n_e C_4 \tag{5.46}$$

where

$$\text{For a rod : } n_{g_{dof}} = 1 \ (q) \tag{5.47}$$

$$\text{For a beam : } n_{g_{dof}} = 2 \ (q, \theta) \tag{5.48}$$

and the appropriate values of ρ were given in Equations 5.26 and 5.27. Then, for each global update, the global processor must perform

$$\begin{aligned} C_{global} &= \tfrac{4}{3}\left(5n_{gn}^2 + 12n\right) - 2n_{gn} - \tfrac{2}{3}n \quad \text{Rod} \\ C_{global} &= \tfrac{4}{3}\left(20n_{gn}^2 + 24n\right) - 4n_{gn} - \tfrac{2}{3}n \quad \text{Beam} \end{aligned} \tag{5.49}$$

equivalent operations, while each local processor must perform

$$C_{local} = \tfrac{2}{3}h_g + C_4 \quad \text{Rod or Beam} \tag{5.50}$$

at a rate which is ρ times the global update rate. In comparison, full state feedback requires $2n^2$ M and $n\left(2n-1\right)$ A, or $\frac{1}{3}n\left(8n-1\right)$ equivalent operations, at an update rate that goes as n^2.

These requirements are compared in Figures 5.2, 5.3 and 5.4. It is recognized that the full state feedback approach is inappropriate for this example, but it is included for the sake of comparison. From the figures, it is apparent that the hierarchic architecture offers a significant advantage over the full state feedback in terms of the total operations count. What is more important however, is that the workload of any individual processor is significantly reduced. This fact is particularly true for the local computers, with the workload being reduced to the point where fairly simple inexpensive components could be used, or alternatively, it would be possible to operate at a much higher bandwidth.

For sake of comparison, two points have been taken from the graphs and are listed in Table 5.1. The first column corresponds to the example studied in Chapter 4. The second column corresponds to a system with twice as many global nodes, but four times as many structural nodes.

Table 5.1: A comparison of the operations count for two system sizes.

Controller Type	30 Structural Nodes $n_{gn} = 6$	120 Structural Nodes $n_{gn} = 12$
Full state feedback	2390	38360
Global controller	1876	7552
Average requirements per local controller	5 controllers	11 controllers
Colocated natural control	14	28
Block diagonal: full	82	302
Block diagonal: two bays	46	171
Block tri-diagonal: full	248	980
Block tri-diagonal: banded with width $m = 2$	75	154

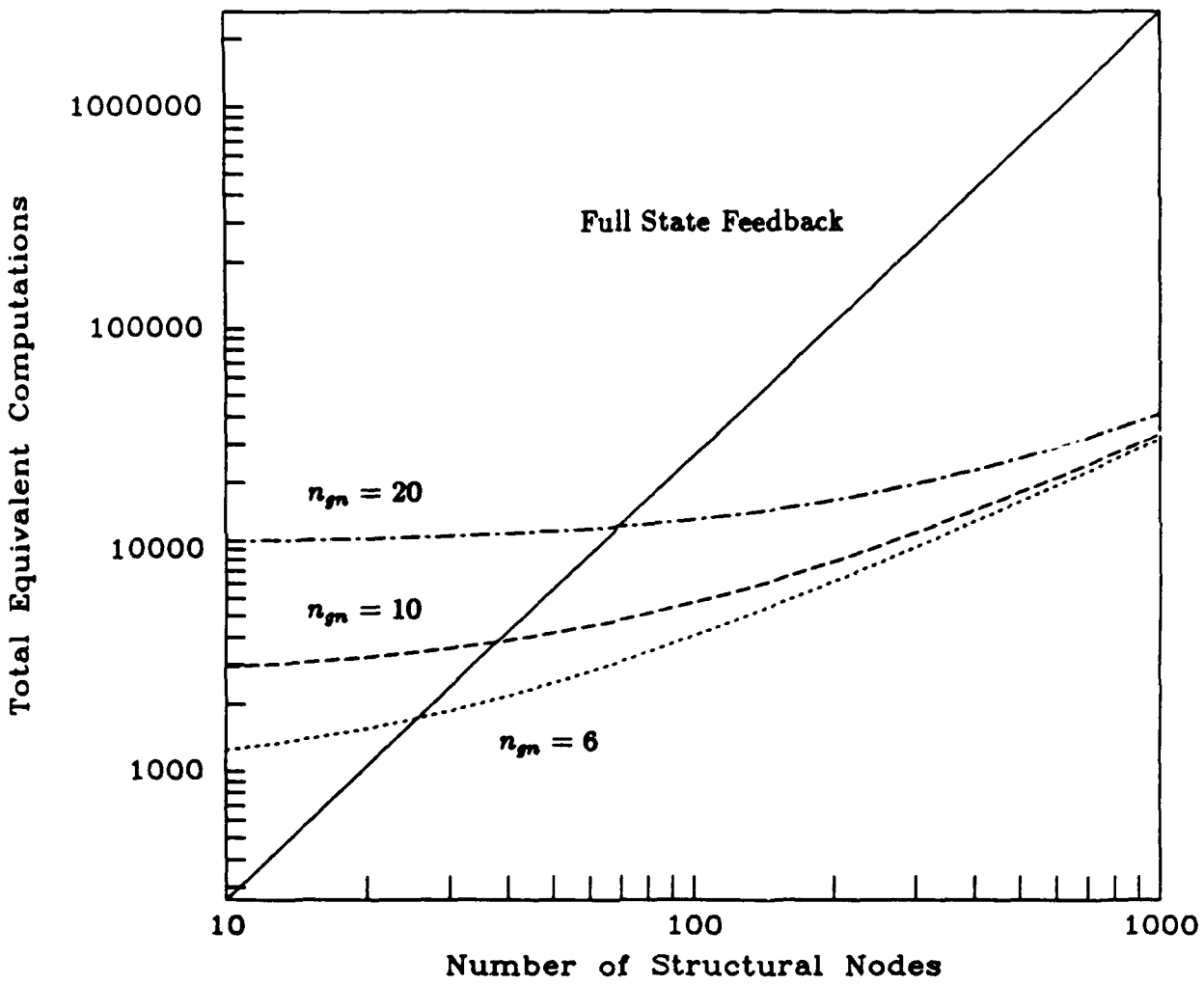

Figure 5.2: The computational requirements for various global controllers.

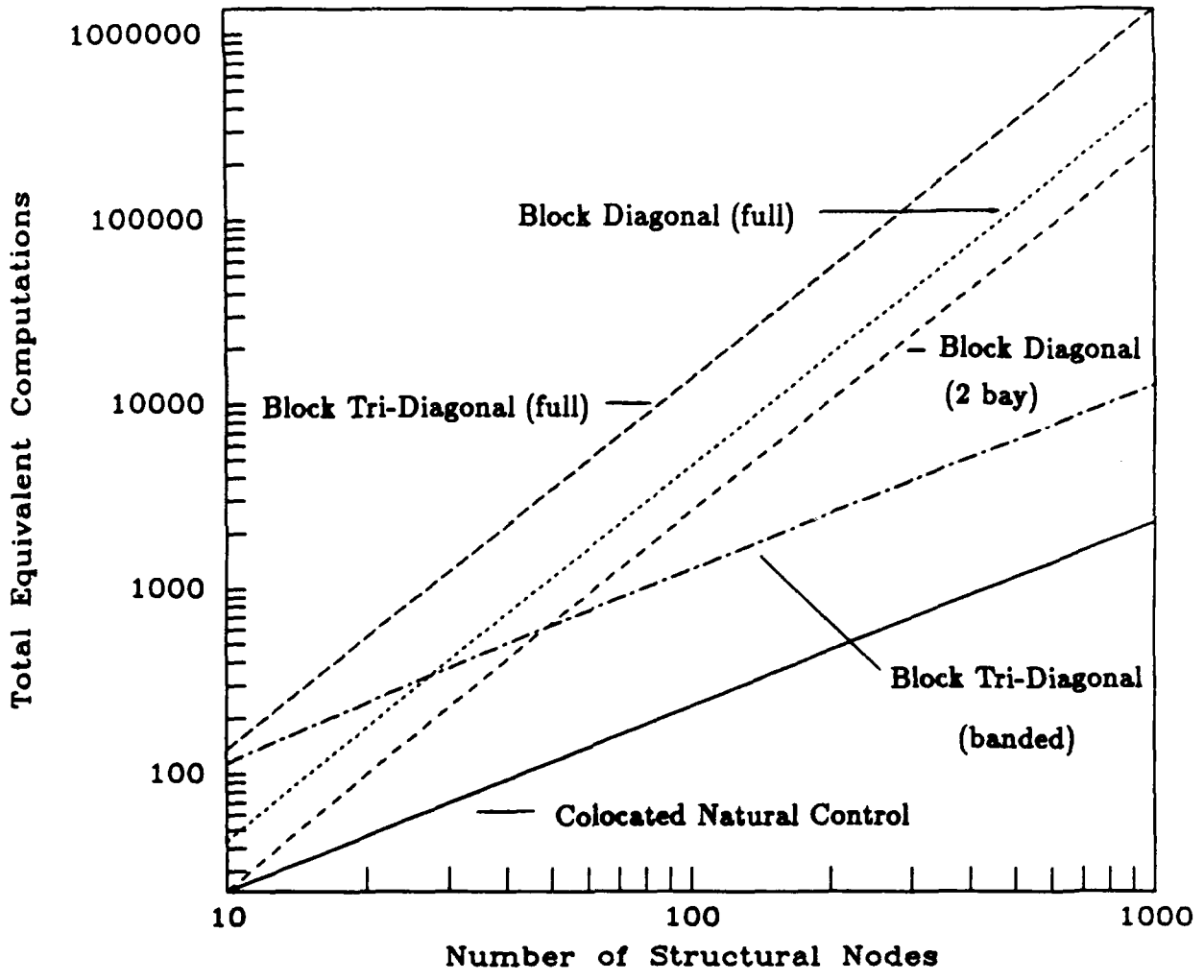

Figure 5.3: A comparison of the computational requirements for various local controllers: $n_{gn} = 6$.

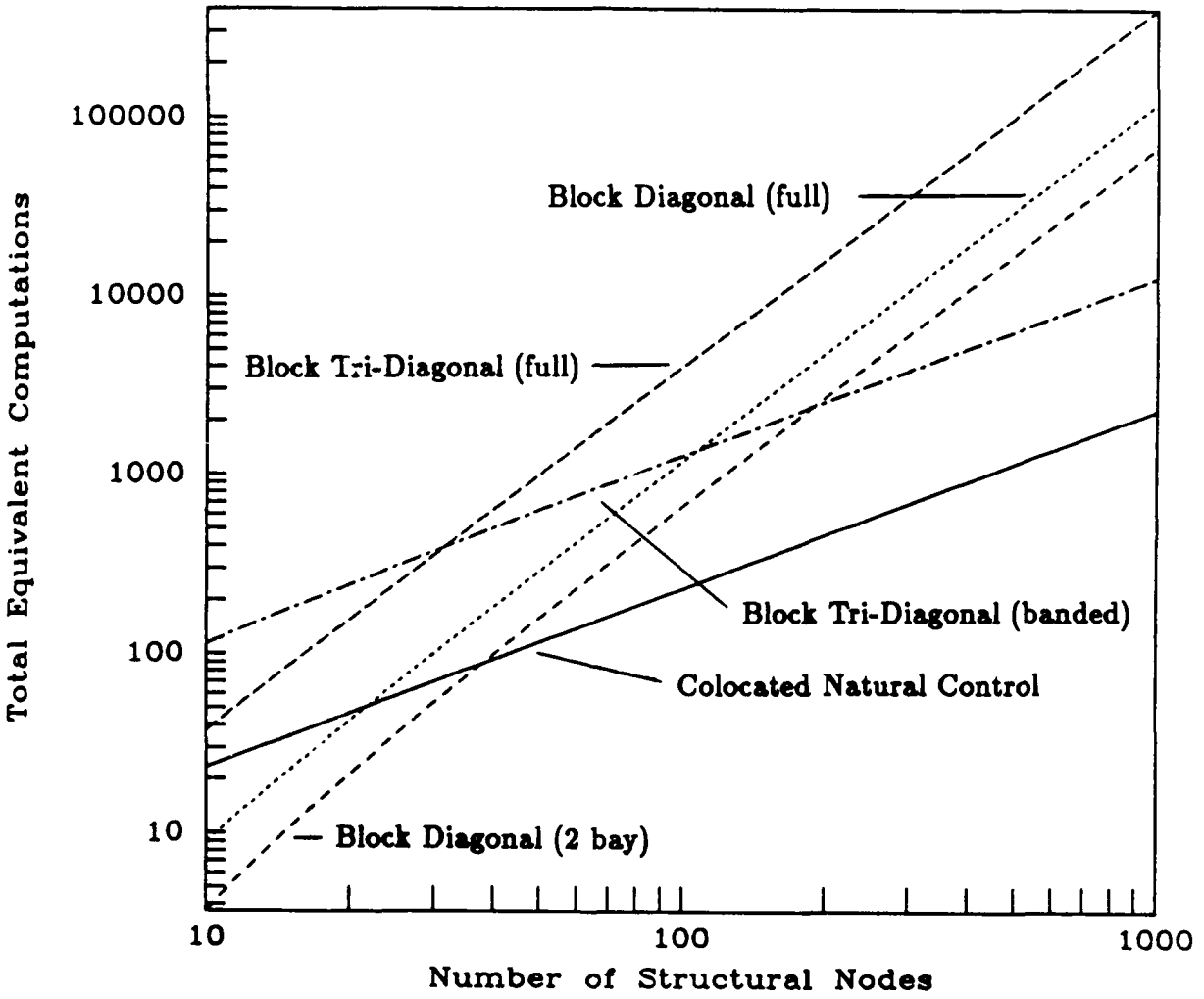

Figure 5.4: A comparison of the computational requirements for various local controllers: $n_{gn} = 20$.

These results compare only the total requirements at each level. They do not include the frequency at which the operations would be performed. A comparison of the global requirements and those for full state feedback clearly indicate that there is a structural model size above which a given global model offers a substantial reduction in the total computations required. For the local controllers, one result that stands out is that using the full block tri-diagonal feedback approach at the local level is very expensive. As would be expected, the simplest local control using colocated natural feedback requires the fewest number of computations in both examples. The full block diagonal feedback approach is more expensive than the colocated and block tri-diagonal banded methods, but it is far cheaper than the full block tri-diagonal technique. Splitting the finite control element into 2 "bays" cuts the requirements approximately in half. So, in summary, it would appear that the colocated approach is the cheapest, the 2 bay block diagonal and block tri-diagonal banded approaches are comparable, the full block diagonal method is slightly more expensive than these two, and the full block tri-diagonal approach is by far the most costly of all. The curves in Figures 5.3 and 5.4 indicate that these trends hold for a wide range of structural and global nodes.

These results, coupled with the small performance improvements associated with the more sophisticated local architectures, indicate that the most efficient hierarchic combination is a good global design with a simple and easy to implement local design which can then operate at much higher frequencies.

5.3 Closed Loop Stability

5.3.1 Introduction

One question that remains to be discussed is that of the overall stability of the closed loop system. As was shown in Chapter 2, for the purpose of the control design, the

system can be written as two coupled dynamic systems. Through the choice of appropriate matrices for the observational and control filtering shown in Figure 2.4, it is discussed in Section 2.5 how it is possible, in the ideal case, to eliminate both the control and observation spillover completely. The resulting systems are then only coupled dynamically through the stiffness matrix if the weighting matrix is selected to be the mass matrix M. However, as was discussed in Chapter 4 and Section 5.2, some of the performance and/or cost trade-offs (such as using the lumped mass matrix as the weighting matrix) allow "leakage" in this filtering, so that in reality it will not be complete.

It was shown in Section 2.6 that it is possible to reduce this dynamic spillover by selecting the appropriate modes as the shape functions, or just using the lower set of the global modes. This is another performance and/or cost trade-off. Theoretically it is possible to reduce the coupling to an arbitrarily small level by choosing the open loop modes as the shape functions. In practice however, this would offer no computational advantage over the full state feedback method. In fact it would require more computations to implement due to the overhead, but this would be done in a partially decentralized manner. With approximate mode shapes or finite element approximations, this dynamic coupling will be present, and it presents a difficult obstacle for the stability analysis since it introduces spillover.

It will be assumed in this work that the separate controllers have been designed so that the two closed loop systems are stable. The purpose of this section is to present some arguments about the stability of the overall system when the two subsystems are dynamically coupled together. As will be shown, it has only been possible to develop necessary conditions if a constraint is imposed on the gain matrices. Sufficient conditions will be derived as well, but they are very conservative and overspecify the required gains by several orders of magnitude. Although it has been hard to develop a more general proof of stability, it should be note that no case of instability has been observed for the examples that have been investigated.

For the modelling approach developed in Chapter 2, the frequency spectrum can be split into three regions called the global modes, the residual modes, and the truncated modes. The influence of the two controllers on each of these three regions must be considered. By design, the influence of the global controller on the global modes, and of the local controllers on the residual modes will be stabilizing and should provide satisfactory performance. For the influence of the global controller on the truncated modes, an argument based on the frequency separation and the controller roll-off can be employed to show that the effect would be negligible. Since the local controllers can be designed to be positive real, then it is guaranteed that, although spillover will occur between the residual and truncated modes, the effect will be to stabilize this latter set. The two remaining controller/system influences to consider are the effect of the local control on the global modes and that of the global control on the residual modes. These depend on how well the modes are approximated and the ability of the filters which are implemented to decouple the subsystems. The basic argument is to claim that the filtering steps eliminate the direct control spillover from one system to another and that the dynamic spillover is a secondary effect so the influence is "small". The results in Chapter 4 showed that the global component of the local controllers was filtered out very well for both of the weighting matrices used, so this claim holds for this case. However, it was also found that the influence of the global controller on the residual model depends to a large extent on the weighting matrix used in the filters, see Figure 4.9. If the condensed mass matrix is used, then the direct control spillover is very small. This issue complicates the analysis even further. The work done here assumes that the observation and control filtering is perfect, and only the influence of the dynamic coupling need be examined.

5.3.2 Lyapunov Test

If an assumption about the structure of the gain matrices (*i.e.*, their positive definiteness) for the global and local controllers is acceptable, then it is possible to prove that the two coupled systems will be stable using a standard Lyapunov function test. The closed loop dynamics are given by

$$\begin{aligned} M\ddot{q} + Kq = & - \left\{ T_g^{-LT} F_g T_g^{-L} + \left(I - T_g^{-LT} T_g^T \right) F_e \left(I - T_g T_g^{-L} \right) \right\} q \\ & - \left\{ T_g^{-LT} F_{\dot{g}} T_g^{-L} + \left(I - T_g^{-LT} T_g^T \right) F_{\dot{e}} \left(I - T_g T_g^{-L} \right) \right\} \dot{q} \\ & = -F_1 q - F_2 \dot{q} \end{aligned} \tag{5.51}$$

or, equivalently, that

$$M\ddot{q} + F_2 \dot{q} + (K + F_1)\, q = 0 \tag{5.52}$$

It is assumed that the mass matrix, M, is both symmetric and positive definite. The stiffness matrix K is symmetric, but is only positive semidefinite since rigid body modes may be included in the model. If a matrix is positive definite, *i.e.*, $A > 0$, and another matrix B is not rank deficient, then it can be shown that $B^T A B > 0$. So the gain matrices F_1 and F_2 defined above will be positive definite provided that the matrices F_g, F_e, $F_{\dot{g}}$, and $F_{\dot{e}}$ are positive definite since the filtering matrices are of full rank. Finally, since the closed loop stiffness matrix $K + F_1$ is the sum of positive semidefinite and positive definite matrices, then it is positive definite as well.

So, if the global and local controllers are positive real, then each of the matrices in Equation 5.51 are positive definite. Stability of the closed loop system can then be proved using a standard Lyapunov function based on the total energy for the closed loop system

$$V(q, \dot{q}) = \frac{1}{2} \dot{q}^T M \dot{q} + \frac{1}{2} q^T (K + F_1)\, q \tag{5.53}$$

Since the closed loop mass and stiffness matrices are positive definite this quadratic function is positive semidefinite. The derivative with respect to time of this function

is

$$\frac{\partial V}{\partial t} = \dot{q}^T M \tilde{q} + \dot{q}^T (K + F_1) q \quad (5.54)$$

$$= -\dot{q}^T F_2 \dot{q} \quad (5.55)$$

The theorem for Lyapunov stability states that the system is stable if a function $V(q, \dot{q})$ can be found such that it is positive semidefinite for all q and only zero at $q = 0$, and that its time derivative is negative semidefinite. The degree of stability (asymptotic or neutral) depends on the range over which the derivative is zero. Asymptotic stability occurs if the derivative is zero only at the origin. Since it is assumed that $M > 0$ and $K + F_1 > 0$, then the system will be asymptotically stable if $F_2 > 0$, and only Lyapunov (neutrally) stable if $F_2 \geq 0$. This argument is basically that coupling two "passive" systems will not destabilize the overall system. This restriction on the gain structure is relatively easy to impose for some of the local controllers, especially for the colocated design. This will be a little more difficult for the global controller as it is designed more with performance in mind. However, several design methods for positive definite controllers are available, for example [40,8].

5.3.3 Connective Stability

The purpose of this section is to investigate the question of the influence of the dynamic coupling on the overall stability of the system. With this aim in mind, a technique developed in reference [60] to analyze the overall stability of complex dynamic systems which can be broken into coupled subsystems is introduced. A similar analysis is developed by Yam [69]. This analysis regards the dynamic coupling between the stable systems as perturbations to the design models, and provides conditions such that the coupled design models will remain stable. From Equation 2.27, the closed loop dynamics matrix of the coupled global and residual design models

is of the form

$$A_{cl} = \begin{bmatrix} A_{gg} & A_{gr} \\ A_{rg} & A_{rr} \end{bmatrix} \tag{5.56}$$

where

$$A_{gg} = \begin{bmatrix} 0 & I_{n_g} \\ -M_{gg}^{-1}\left(K_{gg} + F_g\right) & -M_{gg}^{-1}F_{\dot{g}} \end{bmatrix} \tag{5.57}$$

$$A_{gr} = \begin{bmatrix} 0 & 0 \\ -M_{gg}^{-1}K_{gr} & 0 \end{bmatrix} \quad A_{rg} = \begin{bmatrix} 0 & 0 \\ -M_{rr}^{-1}K_{rg} & 0 \end{bmatrix} \tag{5.58}$$

$$A_{rr} = \begin{bmatrix} 0 & I_{n_r} \\ -M_{rr}^{-1}\left(K_{rr} + T_r^T F_e T_r\right) & -M_{rr}^{-1}T_r^T F_{\dot{e}} T_r \end{bmatrix} \tag{5.59}$$

and the state vector x is of the form

$$x = \begin{bmatrix} x_g \\ x_r \end{bmatrix} \quad x_g = \begin{bmatrix} q_g \\ \dot{q}_g \end{bmatrix} \quad x_r = \begin{bmatrix} q_r \\ \dot{q}_r \end{bmatrix} \tag{5.60}$$

Since it is assumed that the control and observation spillover have been eliminated by the filtering, the full system corresponds to two stable systems coupled by matrices which are independent of the control gains. The coupling is purely a function of how well the interpolation functions model the lower modes of the open loop system. In the perfectly modelled case, they would both be zero.

For this analysis, the Lyapunov function is taken to be a sum of the functions for the individual subsystems

$$V\left(x_g, x_r\right) = \left(x_g^T H_g x_g\right)^{\frac{1}{2}} + \left(x_r^T H_r x_r\right)^{\frac{1}{2}} \tag{5.61}$$

where H_i solves

$$A_{ii}^T H_i + H_i A_{ii} + I_i = 0 \quad i \in \{g, r\} \tag{5.62}$$

The procedure for proving stability requires the introduction of a 2×2 test matrix W

$$W = \begin{bmatrix} \frac{-1}{2\lambda_M(H_g)} & \xi_{gr} \\ \xi_{rg} & \frac{-1}{2\lambda_M(H_r)} \end{bmatrix} = \begin{bmatrix} w_{gg} & w_{gr} \\ w_{rg} & w_{rr} \end{bmatrix} \tag{5.63}$$

where $\lambda_M(\cdot)$ is the maximum eigenvalue of $(\cdot)$ and $\xi_{ij} = \lambda_M^{\frac{1}{2}}\left(A_{ij}^T A_{ij}\right)$ $i,j \in \{g,r\}$. A theorem proved in reference [60] states that the full system is connectively asymptotically stable in the large if the leading principal minors of the test matrix W are such that

$$w_{gg} < 0 \tag{5.64}$$

$$w_{gg}w_{rr} - w_{gr}w_{rg} > 0 \tag{5.65}$$

Note that, from Equation 5.56, only w_{gg} and w_{rr} depend on the feedback gains. Also note that Equation 5.64 is guaranteed by the assumption that the isolated systems are asymptotically stable. Then, Equation 5.65 provides an equation for directly comparing the feedback requirements of the isolated systems (w_{gg}, w_{rr}) and a measure of the dynamic coupling in the model (w_{rg}, w_{gr}). Typical values taken from examples in Chapter 4 would give a test matrix of

$$W = \begin{bmatrix} -0.124 & 11.379 \\ 4.065 & -0.0042 \end{bmatrix} \tag{5.66}$$

so that

$$w_{gg} = -0.124 < 0 \tag{5.67}$$

$$w_{gg}w_{rr} - w_{gr}w_{rg} = -46.254 < 0 \tag{5.68}$$

From these results, the problem with this approach is immediately apparent. The test is very conservative since it is based on the worst case singular values of the off-diagonal coupling matrices. With the levels of coupling seen in the examples of Chapter 4, the closed loop design model poles would have to be orders of magnitude more stable than they are in the current designs to meet this condition. However, the results in Chapter 4 indicate that these large safety margins are unnecessary, as much smaller values for the feedback gains stabilize the overall system.

So, in conclusion, it is clear that arguments based on connective stability will not work in this case as they are far too conservative. However, if the correct mass

matrix is used in the observation and control filtering and the feedback matrices are positive definite, then the overall system can be proven to be stable using a Lyapunov test.

5.4 Controller Robustness

Since a sensor or actuator failure is inevitable in any real structure, it is important to analyze the performance degradation that can be expected in the closed loop response. This discussion will not be concerned with how a failure is detected, as it is assumed that a FDI system exists which can isolate the faults. The aim here will be to provide a method for handling a small number of failures so that the controller is robust enough to provide good performance until the parts can be replaced. The approach used in this work will be to reconfigure the control design based on another condensation technique. The most straightforward way of reconfiguring the design after a failure is to repeat the mass condensation developed in Section 2.3 to obtain a model based on the original degrees of freedom minus those lost due to the failures. However, this process will generally have very little effect on the global model, so it is not necessary to perform all of this reconfiguration. It is only really necessary to redesign the local control.

Since the local mass of the structure plays such an important part in determining the decay rates, the reconfiguration of the local controllers is based on a mass weighted distribution of the gains. This is particularly simple for the uniform damping local controller since the gains are directly mass weighted in the equations. The reconfiguration process simply requires the elimination of the lost node, and the local mass is then shared between the adjacent controllers. The shape function matrix T_g must also be modified as well to remove the lost node. This is a simple step if the lumped mass approximation is being used since just setting the appropriate element of the mass matrix diagonal equal to zero has the effect of eliminating

the node from the analysis.

5.5 Selecting the Appropriate Processor Location

The question of where and how to locate the processors of the local controllers is an issue that remains from the earlier work done in by Ward [67]. From the figures presented in Chapter 2, it would appear that there are two obvious ways that the micro-computers can be distributed. One method is to associate them with the global nodes, and the other is to associate them with the finite control elements. As will be shown in this section, there is one key point which distinguishes these two methods, favouring the second one.

As was discussed in Chapter 2, in particular Section 2.5, the local controller relies on the formation of the residual, e, to calculate the control commands. In order to determine this value, it is necessary to know the measurements at every point, the global values at the end points, and the interpolation functions. It is the formation of the residual vector, e, which distinguishes one method from another. Why this is the case is probably best explained by looking at the operations required in each case. Consider, as an example, the one dimensional cases shown in Figure 5.5. The first case associates the processors with the global nodes, the second associates them with the finite control elements.

First, note that case 2 requires one less processor, a fact which is magnified for the two dimensional case ($4^2 = 16$ versus $3^2 = 9$). However, it is not clear that this is necessarily a benefit because, although it would mean that there are fewer processors to embed, the work load of each processor may be large enough to require a very sophisticated system at the local level.

To discuss the formation of the residual, e, look first at case 1. It can be seen that both processors P_2 and P_3 are required to obtain the same set of measurements

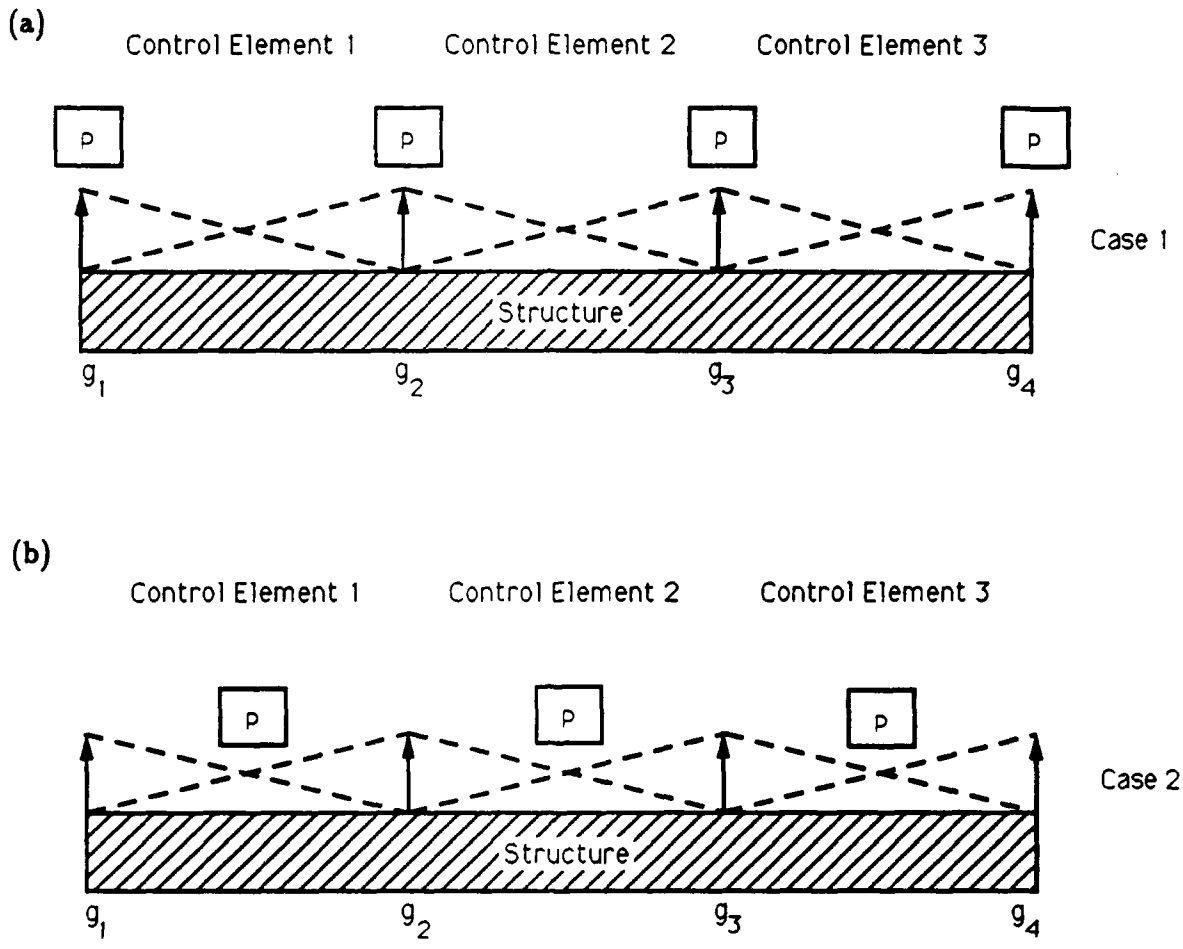

Figure 5.5: Two ways of associating the processors. Case 1 (a) associates the processors with the global nodes. case 2 (b) associates the processors with the finite control elements.

within finite control element 2. So, there is either a duplication of the measurements, or some local communication is required. Once each processor has obtained the necessary measurements, it can form the contributions to the global node value q_{gi} by multiplying this information by the shape function $\left[T_{gi}^{T(i-1)}\ T_{gi}^{Ti}\right]$. These n_{gn} pieces of information are then communicated to the central processor, normalized and communicated back down. This procedure is described in far more detail in Section 5.2.

After the global values have been returned to each local processor, the question remains as to how the residual, e, can be computed. The way to determine it is simply to multiply the shape function by q_{gi}, and then subtract these values from the measurements. However, within an element, it is necessary to obtain both endpoints and use both of the relevant shape functions to determine the interpolated values. So, either each processor can store both shape functions (one for each of the elements to which it is attached), receive both global estimates, and perform the residual calculation independently, or the neighboring processors can pool information and compute the residual vector together. The first method will mean that there must be duplication of effort by neighboring controllers, and the second method will require local communication for each controller to obtain the residual vector. Notice that this will become far more complicated for the two dimensional case.

In contrast to the complexity of case 1, case 2 provides a fairly intuitive set-up. Each controller is associated with one finite control element, and directly measures all of the information required to compute the contributions for the global values. Note that it will be necessary to communicate nearly twice as much information to the central computer since these contributions cannot be added locally. This will also require the global controller to add the estimates together. The same increase in information communicated back down is required since adjacent processors will both require the value at the node which separates them. Again though, in contrast to the first case, each controller has both shape functions (only the same ones used

in the aggregation are required), the measurements, and the global node values all available to internally calculate the residual, e.

Thus, the approach represented in case 2 appears to have a slight disadvantage of requiring more information to be communicated between the central and local computers, but due the apparent advantages mentioned above, the method of associating the processors with the finite control elements was selected for use over the other method presented in case 1.

Chapter 6

Conclusions and Recommendations

6.1 Summary

This thesis has extended the hierarchic control architecture for the control of large flexible intelligent structures which was originally developed in references [29] and [67]. By combining two levels of controllers, the architecture has the advantage of the good global control authority of a central processor and the benefit of reduced implementation costs associated with the parallel design of the local controllers. Several decentralized control designs were developed to act as the lower level controllers. These are distinguished by the constraint on the amount of information available to each actuator to calculate the command. These designs were compared as both decentralized controllers and as local controllers in the hierarchic architecture. This comparison was done using an example of a long uniform beam by investigating the closed loop pole locations and by graphing the state and control costs of the impulse responses of the different closed loop systems. The implementation costs of the various combinations of controllers was also investigated.

6.2 Conclusions and Contributions

1. The performance results in Section 4.5 clearly support the claim that the hierarchic control architecture can yield near optimal performance with a realistic control objective (a combination of LOS, sum of the squared displacements, and total energy) and a fairly complex plant model. The elimination of the observation and control spillover through the filtering loops means that the two control levels can easily be designed separately. This helps to simplify the control synthesis. The architecture is specially designed for intelligent structures which have a large number of actuators and sensors, the implementation cost analysis shows that significant computatonal savings over other full order centralized schemes can be achieved for modest sized systems.

2. For the local control level, several types of decentralized controllers were designed for this beam model. These include a colocated natural control design, two block diagonal approaches, and two block tri-diagonal designs. These latter four were designed as displacement and energy weighted controllers to complement the global design. When compared as decentralized controllers, the two block tri-diagonal clearly designs offered the best performance, but these would require communication between the local processors, so the block diagonal approach probably is the most efficient decentralized design. The results in Section 4.5 indicate that a slight increase in the performance of the closed loop system can be obtained by using a more sophisticated (than colocated natural control) local controller, but the improvement is small compared to the improvement made over just using natural control by adding the higher, global level of control.

3. The implementation costs for the various global and local designs were also compared. The colocated local controller design was shown to be significantly cheaper than the other approaches. The block diagonal designs become par-

ticularly expensive when the finite control elements get large since they are essentially a local full state feedback, and the feedback calculation is quadratic with the element size. The block tri-diagonal designs require local communication of the processors, so these designs are hard to compare directly. The results show that the most efficient hierarchic design is one which has a well designed global controller and a simple, easy to implement local design which performs the required stability of the higher modes. This conclusion is for made for this combination of structure and control objective, and it may change for other examples such as surface control of a segmented mirror which will require more performance at local level. The more sophisticated designs could be used, but the increased calculation cost means that the operation speed would have to be decreased.

4. As mentioned, a block diagonal decentralized control design was developed. This design was based on a circulant model approximation of a long beam. This method takes advantage of the spatial symmetry of the beam to employ the analysis originally developed by Wall [66]. Chapter 3 outlined the procedure for transforming the necessary conditions of the optimal control problem from a sized $Nn \times Nn$ problem to N, $n \times n$ problems, which makes the solution numerically feasible. A series of software programs based on numerical search algorithms were developed to solve for the optimal block diagonal gains. Several sized problems were tried, and comparing the results with the optimal full state feedback gains indicated that the global minimium had been found. For this problem with strongly banded feedback gains, the combination of gradient and Newton search algorithms was found to be particularly effective, but the Quasi-Newton, BFGS method was found to have convergence difficulties.

5. A decentralized control approach based on a finite dimensional approximation of the full state feedback was also developed. This implementation requires that information must be transferred very rapidly from processor to processor,

but it eliminates the need for a central computer. This design is based on a view of the disturbances "flowing" along a structure as "waves", and the implementation is done in such a way as to complement this model. This is a promising technique, but it will require more work before it can be extended to two dimensional problems.

6. An analysis of some of the performance/implementation cost trade-offs yielded some interesting results. It was shown in Section 5.5 that associating the processors with the finite control elements is superior to associating them with the global nodes. This conclusion should hold for both one and two dimensional structures. Also, an analysis of the implementation costs suggest that the filter weighting matrix, W, should be, at worst, block diagonal so that the aggregation step can be done performed more efficiently by the local controllers. Two cases were considered, $W = M_{lumped}$ and $W = M_{cond}$. It was found that the direct residual control spillover onto the global design model was virtually independent of W, with the filtering being performed effectively in either case. However, the direct global control spillover was shown to be strongly influenced by the choice of W, with M_{cond} resulting in almost no direct spillover at all. However, due to the associated implementation penalty, this value was not used, and all of the results in Chapter 4 use $W = M_{lumped}$.

7. The stability of the closed loop system for a positive semi-definite ($M > 0$, $K \geq 0$) plant can be guaranteed using a hierarchic control architecture if the gain matrices are constrained to be positive definite. Other stability arguments, such as connective stability, are far too conservative for this approach.

8. The first alternative implemetation procedure of Section 2.6 was shown in Chapter 4 to significantly decrease the dynamic coupling of the global and residual models. This is especially important for eliminating the global control spillover onto the residual modes. It was also noted that care must be made

to ensure that the global model has sufficient authority over the important modes for the control objective. This design would probably require a more sophisticated local control design since fewer of the lower frequncy modes are under the direct influence of the global controller.

6.3 Recommendations

1. The work in this thesis has been based on a computer model of a long uniform beam. To really test the architecture, it is necessary that a "real" model of a large flexible structure be controlled. This could either be in the form of a more complex computer model or an actual laboratory experiment. Due to the overhead associated with the architecture, this latter task is recognized as being a particularly difficult one. However, this would allow the architecture to be compared with other designs, and would highlight the benefits that it offers.

2. Other work is being done on this project by David Warkentin to investigate the most efficient microprocessor architecture and the feasibility allowing local processor communication when the electronics are embedded. When this work has been completed, the two investigations can be combined to yield a complete analysis of the local control design.

3. In Chapter 2 the mass condensation approach was introduced to allow for examples in which not every degree of freedom has an actuator and sensor. This needs to be extended to more complicated models which have regions of both high and low sensor and actuator density.

4. Other global control design approaches should be used to meet other performance objectives such as robustness to plant uncertainty.

References

[1] Arbel, A. and Gupta, N., "Robust Colocated Control for Large Flexible Space Structures," *AIAA Journal of Guidance, Control, and Dynamics*, Vol. 4, No. 5, pp. 480-486, Sept.-Oct. 1981

[2] Archer, J., "Consistent Mass Matrix for Distributed Mass Systems," *Journal of the Structural Division, Proceedings of the American Society of Civil Engineering*, pp. 161-178, August 1963

[3] Aubrun, J., "Theory of the Control of Structures by Low-Authority Controllers," *AIAA Journal of Guidance and Control*, Vol. 3, No. 5., 78-1689R, pp. 444-451, Sept.-Oct. 1980

[4] Aubrun, J., Lorell, K., Mast, S., and Nelson, J., "Dynamic Analysis of the Actively Controlled Segmented Mirror of the W. M. Keck Ten-Meter Telescope," *IEEE Control Systems Magazine*, pp. 3-10, December 1987

[5] Balas, M., "Trends in Large Space Structure Control theory: Fondest Hopes, Wildest Dreams," *IEEE Transactions On Automatic Control*, Vol. AC-27, No. 3, June 1982

[6] Balas, M., "Feedback Control of Flexible Systems," *IEEE Transactions On Automatic Control*, Vol. AC-23, No. 4, pp. 673-679, August 1978

[7] Baz, A., Poh, S., and Studer, P.,"Modified Independent Modal Space Control Method For Active Control Of Flexible Systems," *Presented at the VPI/AIAA Symposium on the Dynamics and Control of Large Flexible Spacecraft* 1987

[8] Benhabib, R., Iwens, R., and Jackson, R., "Stability of Large Space Structure Control Systems using Positivity Concepts," *AIAA Journal of Guidance and Control*, Vol. 4, No. 5, AIAA 79-1780R, Sept.-Oct. 1981

[9] Bennet, W. and Lindberg, R., "Decentralized Control Design for Large Flexible Spacecraft," *Dynamics and Control of Large Space Structures Proceedings of the 4^{th} VPI and SU/AIAA Symposium*, Blacksburg Virginia, June 1983

[10] Bernstein, D. and Hyland, D., "Optimal Projection of Uncertain Systems: A Unified Theory of Reduced-Order, Robust Control Design," in *Large Space Structures: Dynamics and Control,* Atluri and Amos (ed.), Springer-Verlag, 1988

[11] Bernstein, D., Davis, L., and Hyland, D., "The Optimal Projection Equations for Reduced-Order, Discrete-Time Modelling, Estimation, and Control," *AIAA Journal of Guidance and Control*, Vol. 9, No. 3, pp. 288-293, May-June 1986

[12] Blevin, D., *Formulas for Natural Frequency and Mode Shapes*, Robert E. Krieger Publishing Company, Malabar, Florida, 1987

[13] Canavin, J.,"Control Techniques for Large Flexible Space Structures," *AIAA Conference on Large Space Platforms: Future Needs and Capabilities*, Los Angeles, Sept. 1978, 78-1691

[14] Choi, S. and Sirisena, H., "Computation of Optimal Output Feedback Gains for Linear Multivariable Systems," *IEEE Transactions on Automatic Control*, pp. 257-258, June 1974

[15] Chong, C. and Athans, M., "On the Coordination of Linear Stochastic Systems," *Automatica*, Vol. 12, pp. 321-335, 1976

[16] Chu, K.-C., "Optimal Decentralized Regulator for a String of Coupled Systems," *IEEE Transactions On Automatic Control*, Vol. AC-19, No. 3, pp. 243-246, June 1974

[17] Coradetti, T.,"Orthogonal Subspace Reduction of Optimal Regulator Order," AIAA 79-1742

[18] Craig, R. and Hale, A., "Block Krylov Component Synthesis for Structural Model Reduction," *AIAA Journal of Guidance, Control, and Dynamics*, Vol. 11, No. 6, pp. 562-570, Nov.-Dec. 1988

[19] Craig, R., *Structural Dynamics: an Introduction to Computational Methods*, John Wiley and Sons, New York, 1981

[20] Crawley, E., *16.93 Course Notes,* Spring 1989

[21] Crawley, E. and de Luis, J., "Use of Piezo-Ceramics as Distributed Actuators in Large Space Structures," Proceedings of AIAA/ASME/ASCE/AHS 26^{th} Structures, Structural Dynamics and Materials Conference, Orlando, Florida, pp. 126-133, April 1985

[22] Crawley, E. and Anderson, E., "Detailed Models of Piezoelectric Actuation of Beams," *Proceedings of the AIAA* 30^{th} *Structures, Structural Dynamics and Materials Conference*, Mobile, Alabama, 89-1388, April 1989

[23] Das, B. and Balas, M., "Stabilizing Hierarchical Compensator for Locally Controlled Large Flexible Structures," *Proceedings of the 1989 American Control Conference*, Pittsburgh, pp. 687-691, June 1989

[24] de Luis, J., *Design and Implementation of Optimal Controllers for Intelligent Structures using Infinite Order Structural Models,* PhD Thesis, MIT Department of Aeronautics and Astronautics, (Space Systems Laboratory Report #3-89), January 1989

[25] Franklin, G. and Powell, J., *Digital Control of Dynamic Systems,* Addison-Wesley, Reading Massachusetts, 1980

[26] Gregory Jr., C., "Reduction of Large Flexible Spacecraft Models using Internal Balancing Theory," *AIAA Journal of Guidance, Control, and Dynamics*, Vol. 7, No. 6, pp. 725-732, Nov.-Dec. 1984

[27] Gupta, N., Lyons, M., Aubrun, J., and Marguiles, G., "Modelling, Control and Identification Methods for Flexible Structures," *Spacecraft Pointing and Position Control*, AGARD0graph No.260, pp. 12-1 - 12-41

[28] Guyan, R., "Reduction of the Stiffness and Mass Matrices," *AIAA Journal*, Vol. 3, No. 2, p. 380, Feb. 1965

[29] Hall, S., Crawley, E., How, J., and Ward, B., "A Hierarchic Control Architecture for Intelligent Structures," Submitted to the *AIAA Journal Guidance, Control, and Dynamics*, (Space Systems Laboratory Report #19-88), November 1988

[30] Hyland, D., and Bernstein, D.,"The Optimal Projection Equations for Model Reduction and the relationships among the methods of Wilson, Skelton, and Moore," *IEEE Transactions On Automatic Control*, Vol. AC-30, No. 12, pp. 1201-1211, December 1985

[31] Irons B., "Structural Eigenvalue problems: elimination of the unwanted variables," *AIAA Journal*, Vol. 3, No. 5, pp. 961-962, May 1965

[32] Jazwinski, A., *Stochastic Process and Filtering Theory*, Academic Press, New York, 1970

[33] Joshi, S.,"Robustness Properties of Collocated Controllers for Flexible Spacecraft," *AIAA Journal of Guidance, Control, and Dynamics*, Vol. 9, No. 1, pp. 85-91, Jan.-Feb. 1986

[34] Kosut, R., "Suboptimal Control of Linear Time-Invariant Systems subject to Control Structural Constraints," *IEEE Transactions On Automatic Control*, Vol. AC-15, No. 5, pp. 557-563, Oct. 1970

[35] Kwakernak, H. and Sivan, R., *Linear Optimal Control Systems*, Wiley Inter-Science, New York, 1972

[36] Lala, J. and Adams, S., "Intercomputer Computer Architecture for a Mixed Redunancy Distributed System," *AIAA Journal of Guidance, Control, and Dynamics*, Vol. 12, No. 4, pp. 539-545, July-Aug. 1989

[37] Kronsjö, L., *Algorithms: Their Complexity and Efficiency*, Wiley-Interscience Publications, 1987

[38] Levine, W. and Athans, M., "On the Determination of the Optimal Constant Output Feedack Gains for Linear Multivariable Systems," *IEEE Transactions On Automatic Control*, Vol. AC-15, No. 1, pp. 44-48, Feb. 1970

[39] Linder, D. and Reichard, K., "A Survey of Decentralized Control techniques for Large Space Structures," *Dynamics and Control of Large Space Structures Proceedings of the* 6^{th} *VPI and SU/AIAA Symposium*, Blacksburg Virginia, pp. 87-101, July 1987

[40] MacMartin, D., *An* $\mathcal{H}_\infty$ *Power Flow Approach to the Control of Uncertain Structures*, SM Thesis, MIT Department of Aeronautics and Astronautics, October 1989

[41] Madiwale, A. and Greeley, S., Program based on "The Solution of the Matrix Equation $AX + XB = C$," By Bartels and Stewart, ACM Communications, Vol. 15, pp. 820-826, 1972

[42] Mercadal, M., *Joint Nonlinearity in the Design of a Flexible Truss Structure Control System,* SM Thesis, MIT Department of Aeronautics and Astronautics, December 1986

[43] Mesarovic, M., Macko, D., and Takahara, Y., "Two Coordination Principles and their Application in Large Scale System Control," *Automatica,* Vol. 6, pp. 261-270

[44] Mierovitch, L., *Computational Methods in Structural Dynamics,* Sijthoff and Noordhoff, Rockville, Maryland 1980

[45] Mierovitch, L., "Control Of distributed Structures," in *Large Space Structures: Dynamics and Control,* Atluri and Amos (ed.), Springer-Verlag, 1988

[46] Mierovitch, L., *Elements of Vibration Analysis,* McGraw-Hill Book Company, New York, 1986

[47] Miller, D., *Modelling and Active Modification of Wave Scattering in Structural Networks,* ScD Thesis, MIT Department of Aeronautics and Astronautics, (Space Systems Laboratory Report #12-88), May 1988

[48] Miller, D., *Development of Finite Active Control Elements for Large Flexible Space Structures,* SM Thesis, MIT Department of Aeronautics and Astronautics, (Space Systems Laboratory Report #6-85), February 1985

[49] Miller, D. and Crawley, E., "Theoretical and Experimental Investigation of Space-Realizable Inertial Actuation for Passive and Active Structural Control," *AIAA Journal of Guidance and Control,* Vol. 11, No. 5, Sept.-Oct. 1988

[50] Noble, D. and Daniel, J., *Applied Linear Algebra,* (Second Edition) Prentice-Hall, Inc., New Jersey, 1977

[51] Oppenheim, A. and Schafer, R., *Digital Signal Processing,* Prentice Hall Inc., New Jersey, 1975

[52] Padilla, C.. "An Outline to the Curvefit Program"

[53] Petkovski, DJ. and Rakic, M., "On the Calculation of Optimum Feedback Gains for Output Constrained Regulators," *IEEE Transactions on Automatic Control*, Vol. AC-23, No. 4, p. 760, August 1978

[54] Pitman, F. and Ahmdian, M. "Decentralized Control of Large Scale Systems," *Dynamics and Control of Large Space Structures Proceedings of the* 6^{th} *VPI and SU/AIAA Symposium*, Blacksburg Virginia, pp. 103-115, July 1987

[55] Rosenberg, F. and Ruhman, S., "Hierarchical Partitions in Cyclic Closed Systems: A Hardware Orientation Approach," *AIAA Journal of Guidance, Control, and Dynamics*, Vol. 12, No. 4, p. 530-538, July-Aug. 1989

[56] Ryaciotaki-Boussalis, H. and Wang, S., "A Decentralized Approach to Vibration Suppression in Segmented Reference Telescopes," *Proceedings of the 1989 American Control Conference*, Pittsburgh, pp. 2548-2553 June 1989

[57] Sandell, N., Varaiya, P., Athans, M., and Safonov, M., "Survey of Decentralized Control Methods for Large Scale Systems," *IEEE Transactions on Automatic Control*, Vol. AC-23, No. 2, pp. 108-128, April 1978

[58] Scales, L., *Introduction to Nonlinear Optimization,* Springer-Verlag New York Inc., London, 1987

[59] Sesak, J., "Control of Large Space Structures via Singular Perturbation Optimal Control," *Presented at the AIAA conference on Large Space Platforms*, AIAA 78-1690, September 1978

[60] Siljak, D., "Complex Dynamic Systems: Stability, Control, and Reliability," *Lecture Notes For the* 4^{th} *Summer Session on Control Systems Theory and Applications, Arab School On Science and Technology*, August 1981

[61] Silverberg, L., "Uniform Damping Control of Spacecraft," *AIAA Journal of Guidance, Control, and Dynamics*, Vol. 9, No. 2, pp. 221-227, May-April 1986

[62] Singh, M., Drew, S., and Coales, J., "Comparison of Practical Hierarchical Control methods for Interconnected Dynamical Systems," *Automatica*, Vol. 11, pp. 331-350

[63] Skelton, R., Hughes, P., and Hablani, H., "Order Reduction for Models of Space Structures Using Modal Cost Analysis," *AIAA Journal of Guidance and Control*, Vol. 5, No. 4, pp. 351-357, July-Aug. 1982

[64] Su, T. and Craig, R., "Model Reduction and Control of Flexible structures using Krylov Subspaces," *Proceedings of the AIAA* 30^{th} *Structures, Structural Dynamics and Materials Conference*, Mobile, Alabama, pp.691-700, April 1989

[65] Wang, S., and Davison, E., "On the Stability of Decentralized Control Systems," *IEEE Transactions on Automatic Control*, Vol. AC-18, No. 5, pp. 473-478, Oct. 1973

[66] Wall, J., "Control and Estimation for Large-Scale Systems having Spatial Symmetry," PhD Thesis, MIT Department of Electrical Engineering and Computer Science, August 1978

[67] Ward, B., *A Hierarchical Control Architecture for Large Flexible Structures,* SM Thesis, MIT Department of Aeronautics and Astronautics, (Space Systems Laboratory Report #18-85), May 1985

[68] West-Vukovich, G., Davison, E., and Hughes, P., "The Decentralized Control of Large Flexible Structures," *IEEE Transactions on Automatic Control*, Vol. AC-29, No. 10, Oct. 1984

[69] Yam, Y., Johnson, J., and Lang, J., "Flexible System Model Reduction and Control System design based on Actuator and Sensor Influence Functions," *IEEE Transactions on Automatic Control*, Vol. AC-32, No. 7, pp. 573-582, July 1987

[70] Young, K., "An Application of Decomposition Techniques to Control of Large Structures," *Dynamics and Control of Large Space Structures Proceedings of the* 4^{th} *VPI and SU/AIAA Symposium*, Blacksburg Virginia, June 1983

[71] Young, K., "A Distributed Finite Element Modelling and Control Approach for Large Flexible Structures," *Proceedings of the 1988 American Control Conference*, pp. 253-263, June 1988

[72] Yousuff, A. and Skelton, R., "Controller Reduction by Component Cost Analysis," *IEEE Transactions on Automatic Control*, Vol. AC-29, No. 6, pp. 520-530, June 1984

Appendix A

The Necessary Conditions for a Constrained Optimal Regulator

The aim of this appendix is to develop the necessary conditions for various control problems. This will include cases where the gain matrix is both unconstrained and where several blocks of the matrix are specified *à priori* to be equal to zero. The necessary conditions will also be derived for the normal case and the transformed cases as discussed in Chapter 3.

The first example to be considered is the output feedback problem, resulting in the necessary conditions developed by Levine and Athans [38]. Taking the system dynamics to be of the standard form

$$\dot{x} = Ax + Bu \tag{A.1}$$

$$y = Cx \tag{A.2}$$

and the cost to be

$$J = \frac{1}{2}\int_0^\infty \left(x^T R_{xx} x + u^T R_{uu} u\right) dt \tag{A.3}$$

where $R_{xx} = R_{xx}^T \geq 0$, $R_{uu} = R_{uu}^T > 0$, and the triple $\left(A, B, R_{xx}^{\frac{1}{2}}\right)$ is both stabilizable and detectable. An additional constraint that the control be determined from the

outputs y is then imposed

$$u = -Fy = -FCx \tag{A.4}$$

so that the cost can be rewritten as

$$J = \frac{1}{2}\int_0^\infty x^T \left(R_{zz} + C^T F^T R_{uu} FC\right) x\, dt \tag{A.5}$$

In general the minimization of the cost J will be a function of the initial condition of the states $x(0)$. To eliminate this dependence, it is assumed that the initial states are zero mean random variables with covariance Σ which is typically taken to be the identity matrix. The problem then becomes the minimization of the expected value of the cost, $E[J]$, which can be written as

$$\hat{J} = E[J] = \frac{1}{2}\text{trace}\left\{R_{zz}Q + C^T F^T R_{uu} FCQ\right\} \tag{A.6}$$

with the condition that the symmetric positive definite matrix Q solves

$$(A - BFC)\,Q + Q\,(A - BFC)^T + \Sigma = 0 \tag{A.7}$$

This constraint can be appended to the cost with a Lagrange multiplier matrix P to give the definition of the augmented cost

$$\begin{aligned} L &= \frac{1}{2}\text{trace}\left\{R_{zz}Q + C^T F^T R_{uu} FCQ\right. \\ &+ \left. P\left((A - BFC)\,Q + Q\,(A - BFC)^T + \Sigma\right)\right\} \end{aligned} \tag{A.8}$$

The necessary conditions for optimality can then be determined by evaluating the equations

$$\frac{\partial L}{\partial Q} = 0 \tag{A.9}$$

$$\frac{\partial L}{\partial P} = 0 \tag{A.10}$$

$$\frac{\partial L}{\partial F} = 0 \tag{A.11}$$

Clearly, Equation A.10 will return Equation A.7. Equation A.9 will yield the expression for P

$$P(A - BFC) + (A - BFC)^T P + R_{zz} + C^T F^T R_{uu} FC = 0 \tag{A.12}$$

and Equation A.11 yields

$$CQC^T F^T R_{uu} - CQPB = 0 \tag{A.13}$$

These three equations constitute the necessary conditions for the output feedback problem provided that no *à priori* constraints are placed on the gain matrix.

The case for which only certain blocks of the gain matrix F are allowed to be non-zero will be examined for the special case that the system is block circulant. This type of matrix is defined and discussed in Chapter 3. For a N^{th} order block circulant system, F is a $Nn \times Nn$ matrix that can be written in terms of N, $n \times n$ matrices

$$F = \sum_{k=0}^{N-1} \sum_{j=0}^{N-1} \Pi_{i+1} F_k \Pi_{j+1}^T \quad i=(j+k) \bmod N \tag{A.14}$$

where Π_i is a $Nn \times n$ column vector of $n \times n$ block matrices of which the i^{th} block is the $n \times n$ identity matrix and the remaining $N-1$ blocks are zero. Substituting this expression into Equation A.8 and rearranging, it can be shown that the resulting form of the necessary condition of Equation A.11 is

$$\frac{\partial L}{\partial F_k} = \sum_{j=0}^{N-1} \Pi_{i+1}^T \left(B^T PQC^T - R_{uu} FCQC^T \right) \Pi_{j+1} = 0 \quad i=(j+k) \bmod N \tag{A.15}$$

If it is assumed that the system matrices (A, B, C, Σ) are block circulant, then as was shown by Wall [66], the resulting P, Q, and F matrices will also be block circulant and the expression for the augmented cost can be transformed using the techniques developed in Section 3.3.3 to obtain

$$\begin{aligned} L &= \frac{1}{2} \text{trace} \left\{ \overline{R}_{zz}\, \overline{Q} + \overline{C}^H \overline{F}^H \overline{R}_{uu}\, \overline{F}\, \overline{C}\, \overline{Q} \right. \\ &+ \left. \overline{P} \left(\left(\overline{A} - \overline{B}\, \overline{F}\, \overline{C} \right) \overline{Q} + \overline{Q} \left(\overline{A} - \overline{B}\, \overline{F}\, \overline{C} \right)^H + \overline{\Sigma} \right) \right\} \end{aligned} \tag{A.16}$$

where, by the results discussed in that section, each of these transformed matrices is block diagonal, *i.e.*, $P = BD(\overline{P_k})$. Since the aim of this work is to look at the example in which parts of the gain matrix are constrained to be zero, the expression of particular interest is the derivative of the augmented cost with respect to the transformed gain blocks. This expression can be determined from Equation A.16, and it will be seen that there are two terms which are associated with the $\overline{P}$ expression, and a third which comes from the quadratic expression in $\overline{F}$. Using the identity

$$\text{trace}\left(A^T B^T\right) = \text{trace}\left(AB\right) \tag{A.17}$$

it can be shown that

$$\frac{\partial L}{\partial \overline{F_i}} = \left(\overline{C}_i \overline{Q}_i \overline{C}_i^H \overline{F}_i^H \overline{R}_{uu_i} - \overline{C}_i \overline{Q}_i \overline{P}_i \overline{B}_i\right) \qquad \forall\, i \in [0, 1, \ldots, \text{N-1}] \tag{A.18}$$

The other two Equations A.7 and A.12 transform directly as discussed in Section 3.3.3 and are given by

$$\left(\overline{A} - \overline{B}\,\overline{F}\,\overline{C}\right)\overline{Q} + \overline{Q}\left(\overline{A} - \overline{B}\,\overline{F}\,\overline{C}\right)^H + \overline{\Sigma} = 0 \tag{A.19}$$

$$\overline{P}\left(\overline{A} - \overline{B}\,\overline{F}\,\overline{C}\right) + \left(\overline{A} - \overline{B}\,\overline{F}\,\overline{C}\right)^H \overline{P} + \overline{R}_{zz} + \overline{C}^H \overline{F}^H \overline{R}_{uu}\,\overline{F}\,\overline{C} = 0 \tag{A.20}$$

The component of the total derivative of the augmented cost with respect to the gain matrix F can then be expressed as

$$\Delta L = \frac{1}{2}\text{trace}\left\{\sum_{i=0}^{N-1}\left(\frac{\partial L}{\partial \overline{F_i}}\right)^T \Delta \overline{F_i}\right\} \tag{A.21}$$

Since, by Equation 3.26

$$\overline{F_i} = \sum_{k=0}^{N-1} F_k \omega_N^{-ki} \qquad \forall\, i \in [0, 1, \ldots, \text{N-1}] \tag{A.22}$$

so that

$$\Delta \overline{F_i} = \sum_{k=0}^{N-1} \Delta F_k \omega_N^{-ki} \qquad \forall\, i \in [0, 1, \ldots, \text{N-1}] \tag{A.23}$$

and

$$\Delta L = \frac{1}{2}\text{trace}\left\{\sum_{i=0}^{N-1}\left(\frac{\partial L}{\partial \overline{F}_i}\right)^T \sum_{k=0}^{N-1}\Delta F_k \omega_N^{-ki}\right\} \tag{A.24}$$

$$= \frac{1}{2}\text{trace}\left\{\sum_{k=0}^{N-1}\left(\sum_{i=0}^{N-1}\left(\frac{\partial L}{\partial \overline{F}_i}\right)^T \omega_N^{-ki}\right)\Delta F_k\right\} \tag{A.25}$$

So the necessary condition (from $\Delta L = 0$) can be written from Equation A.21 as

$$\frac{\partial L}{\partial \overline{F}_i} = 0 \quad \forall\, i \in [0,1,\ldots,\text{N-1}] \tag{A.26}$$

or, equivalently from Equation A.25, as

$$\frac{\partial L}{\partial F_k} = \sum_{i=0}^{N-1}\left(\left(\frac{\partial L}{\partial \overline{F}_i}\right)^T \omega_N^{-ki}\right) = 0 \quad \forall\, k \in [0,1,\ldots,\text{N-1}] \tag{A.27}$$

This is exactly the same as Equation A.13 since this corresponds to the unconstrained gain case. What is important to note here is that these necessary conditions are uncoupled in the sense that each of the transformed subsystems are completely independent of the dynamics, measurements, or control of all of the other subsystems. This allows the designer to obtain the solution for each of the N transformed systems without reference to any of the others. It is this decoupling and size reduction which makes this approach particularly appealing.

However, for the case where only a subset of the gain blocks are free, the $\Delta\overline{F}_i$ are not independent since only a subset of the untransformed gain blocks ΔF_k can be varied arbitrarily. If the set of the indices of the free gain blocks is denoted as α, where $\alpha \in [0,1,\ldots,\text{N-1}]$ then Equation A.23 must be replaced with

$$\Delta\overline{F}_i = \sum_{k\in\alpha}\Delta F_k \omega_N^{-ki} \quad \forall\, i \in [0,1,\ldots,\text{N-1}] \tag{A.28}$$

and the necessary condition of Equation A.27 becomes,

$$\sum_{i=0}^{N-1}\left(\left(\frac{\partial L}{\partial \overline{F}_i}\right)^T \omega_N^{-ki}\right) = 0 \qquad \forall\, k \in \alpha \tag{A.29}$$

By substituting the expression for the partial derivative from Equation A.18, and noting that the transpose of the complex matrices becomes the hermitian, then the necessary conditions can be rewritten as

$$\sum_{i=0}^{N-1} \left(\overline{C}_i \overline{Q}_i \overline{C}_i^H \overline{F}_i^H \overline{R}_{uu_i} - \overline{C}_i \overline{Q}_i \overline{P}_i \overline{B}_i \right) \omega_N^{-ik} = 0 \qquad \forall k \in \alpha \qquad \text{(A.30)}$$

an equation which was originally developed by Wall [66]. For this case, the other two necessary conditions of Equations A.19 and A.20 remain unchanged. Notice that constraining some of the gain blocks to be zero recouples the necessary conditions in the transformed domain. However, the size reduction is still preserved as the plant dimensions have been reduced from $Nn \times Nn$ to N, $n \times n$ systems. The special case for which all the states can be measured can be easily obtained by setting $C = \overline{C} = I$.

As discussed in Chapter 3, for toeplitz systems the transformation is very similar, so the equations will not be developed here completely. The notation for this sections follows that adopted by Chu [16]. Then, assuming that the conditions discussed in Chapter 3 about the existance on the transformation are met, and that

$$< A(z) >_0 = \frac{1}{2\pi j} \oint A(z) z^{-1} dz \qquad \text{(A.31)}$$

which is the zeroeth element of the inverse z-transformation introduced in section 3.3, then the transformed necessary conditions are

$$< C(z)Q(z)C(z)^H F(z)^H R_{uu}(z) >_0 - < C(z)Q(z)P(z)B(z) >_0 = 0 \qquad \text{(A.32)}$$

where $P(z)$ and $Q(z)$ solve

$$P(z)\left[A(z) - B(z)F(z)C(z)\right] + \left[A(z) - B(z)F(z)C(z)\right]^H P(z) +$$

$$+ R_{xx}(z) + C(z)^H F(z)^H R_{uu}(z) F(z) C(z) = 0 \qquad \text{(A.33)}$$

$$\left[A(z) - B(z)F(z)C(z)\right] Q(z) + Q(z)\left[A(z) - B(z)F(z)C(z)\right]^H + \Sigma(z) = 0 \qquad \text{(A.34)}$$

where it is recognized that, since z will be evaluated on the unit circle, $z^{-1} = z^*$ and then $A\left(z^{-1}\right)^T = A^H$.

EDWARD F. CRAWLEY

DOB: September 7, 1954
Phone: 617-253-7510

EDUCATION

Massachusetts Institute of Technology,.ScD, Aeronautics and Astronautics, 1980
Massachusetts Institute of Technology, SM, Aeronautics and Astronautics, 1978
Massachusetts Institute of Technology, SB, Aeronautics and Astronautics, 1976
Semester spent at Leningrad State University, 1975

PROFESSIONAL SUMMARY

Current major area of teaching and research is in the design and development of space systems, including structural designs, dynamics and control, erection and deployment, materials and on-board fluid management, and the development of intelligent components. A second major interest is the structures and dynamics of aeroelastic components in aircraft, jet engines and turbopropellors.

EXPERIENCE

Massachusetts Institute of Technology
July 1988 - Co-Director, Space Engineering Research Center
July 1984 - Associate Professor of Aeronautics and Astronautics
Sept. 1980 - June 1984 - Boeing Assistant Professor of Aeronautics and Astronautics

Stanford University
Spring 1988 - Visiting Scholar in the Department of Aeronautics and Astronautics

NASA Johnson Space Center
Summer 1981- Conducted an assessment of the dynamics and control of the Shuttle Remote Manipulator System, and the simulation requirements for crew training.

AWARDS/HONORS

Associate Fellow AIAA, 1989
NSF Presidential Young Investigator, 1985-.
Faculty advisor to student team which received the Kremer World Speed Prize for Human Powered Flight of the Royal Aeronautical Society, 1984.
Visiting Lecturer, Beijing Institute of Aeronautics and Astronautics, Beijing, China, January 1984.
Finalist - NASA Mission Specialist Astronaut Selection, 1980
Graduate Fellowship of the Hertz Foundation, 1976-1980

PROFESSIONAL ACTIVITIES

Director of Engineering Education, International Space University
Associate Editor, AIAA Handbook of Astronautics
Member, NASA Advisory Committee on Space Station
Advisor, National Research Council Committee on Space Station (1987)
Chairman, Structures & Dynamics Comm., ASME Gas Turbine Inst. (1986-1988).
Chairman, Structures & Materials Committee, Soaring Society of America.
Member Sigma Xi, Tau Beta Pi, AIAA, ASME, SSA.

Edward F. Crawley
February 1990

Journal Articles

Wada, B.K., Fanson, J.L., Crawley, E.F., "Adaptive Structures," to be presented at the ASME Winter Annual Meeting, San Francisco, CA, December 1989, to appear in the *Journal of Intelligent Material Systems and Structures.*

Crawley, E.F., Lazarus, K.B., "Induced Strain Actuation of Isotropic and Anisotropic Plates," AIAA paper No. 89-1326, presented at the 30th AIAA/ASME/ASCE/AHS Structures, Structural Dynamics, and Materials Conference, Mobile, Alabama, April 1989, to appear in the *AIAA Journal.*

Crawley, E.F., Anderson, E.H., "Detailed Modeling of Piezoelectric Actuation of Beams," *Journal of Intelligent Material Systems and Structures,* Vol. 1, No. 1, Jan. 1990, pp 4-25.

Crawley, E.F., Hagood, N.W., "A Frequency Domain Analysis for Damped Space Structures," AIAA paper No. 89-1387, presented at the 30th AIAA/ASME/ASCE/AHS Structures, Structural Dynamics, and Materials Conference, Mobile, Alabama, April 1989, to appear in *AIAA Journal.*

Crawley, E.F., Ducharme, E.H., "Parametric Trends in the Flutter of Advanced Turboprops," ASME paper GT 89-280, presented at the 1989 ASME Gas Turbine Conference, Toronto, Canada, June 1989, to appear in the *Transactions ASME, Journal for Gas Turbines and Power.*

Crawley, E.F., Sigler, J.L., van Schoor, M.C., Gronet, M.J., "Hybrid Scaled Structural Models and Their Use in Damping Prediction," to appear in the *AIAA Journal of Guidance, Control and Dynamics.*

Hall, S.R., Crawley, E.F., How, J., Ward, B.A., "A Hierarchic Control Architecture for Intelligent Structures," to appear in to the *AIAA Journal of Guidance, Control and Dynamics.*

Peterson, L.D., Crawley, E.F., Hansman, R.J., "The Nonlinear Dynamics of a Spacecraft Coupled to the Vibration of a Contained Fluid," *AIAA Journal,* Vol. 27, No. 9, Sept. 1989, pp 1230-1240.

Hall, K.C., Crawley, E.F., "Calculation of Unsteady Flows in Turbomachinery Using Linearized Euler Equations," *AIAA Journal,* Vol. 27, No. 6, June 1989, pp 777-787.

Kampf, K.P., Crawley, E.F., Hansman, R.J., "Experimental Investigation of the Crashworthiness of Composite Sailplane Fuselages," *Journal of Aircraft,* Vol. 26, No. 7, July 1989, pp 675-681.

Miller, D.W., Crawley, E.F., "Theoretical and Experimental Investigation of Space-Realizable Inertial Actuation for Passive and Active Structural Control, *AIAA Journal of Guidance, Control and Dynamics,* Vol. 11, No. 5, Sept.-Oct. 1988, pp 449-458.

Peterson, L.D., Crawley, E.F., "Improved Exponential Time Series Approximation of Unsteady Aerodynamic Operators," *AIAA Journal of Aircraft,,* Vol 25, No. 2, Feb. 1988, pp 121-127.

Crawley, E.F., O'Donnell, K.J., "A Procedure for Calculating the Damping in Multi-Element Space Structures," *Acta Astronautica,* Vol. 15, No. 12, pp 987-996, 1987.

Crawley, E.F., de Luis, J., "Use of Piezoelectric Actuators as Elements of Intelligent Structures," *AIAA Journal,* Vol. 25, No. 10, October, 1987, pp 1373-1385.

Crawley, E.F., O'Donnell, K.J., "Force-State Mapping Identification of Nonlinear Joints," *AIAA Journal,* Vol. 25, No. 7, July 1987, pp 1003-1010.

Crawley, E.F., van Schoor, M.C., "Material Damping in Aluminum and Metal Matrix Composites," *Journal of Composite Materials,* Vol. 21, June 1987, pp 553-568.

Crawley, E.F., Ducharme, E.H., Mokadam, D., "Analytical and Experimental Investigations of the Coupled Bladed Disk/Shaft Whirl of a Cantilevered Turbofan," *Transactions ASME, Journal of Engineering for Gas Turbines and Power,* Vol. 108, No. 4, Oct. 1986, pp 567-576.

Crawley, E.F., Aubert, A., "Identification of Nonlinear Structural Elements by Force-State Mapping," *AIAA Journal,* Vol. 24, No. 1, January 1986, pp 155-162.

Hertz, T.J., Crawley, E.F., "Displacement Dependent Friction in Space Structure Joints," *AIAA Journal,* Vol. 23, No. 12, December 1985, pp 1998-2000.

Crawley, E.F., Hall, K.C., "Optimization and Mechanisms of Mistuning in Cascades," *Transactions ASME, Journal of Engineering for Gas Turbines and Power,* Vol. 107, No. 2, April 1985, pp 418-426.

Crawley, E.F., Mohr, D.G., "Experimental Measurement of Material Damping in Free Fall with Tunable Excitation," *AIAA Journal,* Vol. 23, No. 1, January 1985, pp 125-131.

Crawley, E.F., Jenson, D.W., "Comparison of Frequency Determination Techniques for Cantilever Plates with Bending Torsion Coupling," *AIAA Journal*, Vol. 22, No. 3, March 1984, pp 415-420.

Crawley, E.F., Mokadam, D., "Stagger Angle Dependence of Inertial and Elastic Coupling in Bladed Disks," in Advances in Structural Dynamics of Bladed Disk Assemblies, ASME, 1983, and *Transactions ASME, Journal of Vibration, Acoustics, Stress and Reliability in Design*, Vol. 106, No. 2, April 1984, pp 181-189.

Crawley, E.F., Sarver, G.L., Mohr, D.G., "Experimental Measurements of Passive Material and Structural Damping for Flexible Space Structures," *Acta Astronautica*, Vol. 10, May-June 1983, pp 381-393.

Crawley, E.F., "Aerodynamic Measurements in a Transonic Compressor," *Transactions ASME, Journal of Engineering for Power*, Vol 105, No. 3, pp 575-584, July 1983.

Crawley, E.F., "In-Plane Inertial Coupling in Tuned and Severely Mistuned Bladed Disks," *Transactions ASME, Journal of Engineering for Power*, Vol. 105, No. 3, July 1983, pp 585-590.

Jensen, D.W., Crawley, E.F., Dugundji, J., "Vibration of Cantilevered Graphite/Epoxy Plates with Bending-Torsion Coupling," *Journal of Reinforced Plastics and Composites*, Vol. 1, No. 3, July 1982, pp 254-269.

Crawley, E.F., Dugundji, J., "Frequency Determination and Nondimensionalization of Composite Cantilever Plates," *Journal of Sound and Vibration*, Vol. 72, No. 1, 8 September 1980, pp 1-10.

Crawley, E.F., "The Natural Modes of Graphite/Epoxy Cantilever Plates and Shells," *Journal of Composite Materials*, Vol. 13, July 1979, pp 195-205.

Edward F. Crawley
February 1990

Conference Publications

van Schoor, M.D., Peterson, L.D., Crawley, E.F., "The Coupled Nonlinear Dynamic Characteristics of Contained Fluids in Zero Gravity," Proceedings of the 31st AIAA/ASME/ASCE/AHS Structures, Structural Dynamics and Materials Conference, Long Beach, CA, April 1990.

de Luis, J., Crawley, E.F., "Experimental Results of Active Control on a Prototype Intelligent Structure," presented at the 31st AIAA/ASME/ASCE/AHS Structures, Structural Dynamics, and Materials Conference, Long Beach, CA, April 1990, submitted to the *Journal of Intelligent Material Systems and Structures.*

Hagood, N.W., Crawley, E.F., "Experimental Investigation into Passive Damping Enhancement for Space Structures," AIAA paper No. 89-3436, presented at the AIAA Guidance, Navigation and Control Conference, Boston, MA, August 1989, submitted to the *AIAA Journal of Guidance, Control and Dynamics.*

Crawley, E.F., "A Program for Towplane Noise Reduction; Flight Test Results," presented at the 1989 OSTIV Meeting, Vienna, Austria, May 1989.

Gronet, M.J., Crawley, E.F., Kienholz, D., "Design, Analysis, and Testing of a Hybrid-Scale Structural Dynamic Model of the Space Station," AIAA paper No. 89-1340, presented at the 30th AIAA/ASME/ASCE/AHS Structures, Structural Dynamics, and Materials Conference, Mobile, Alabama, April 1989.

Kienholz, D.A., Crawley, E.F., Harvey, T.J., "Very Low Frequency Suspension Systems for Dynamic Testing," AIAA paper No. 89-1194, presented at the 30th AIAA/ASME/ASCE/AHS Structures, Structural Dynamics, and Materials Conference, Mobile, Alabama, April 1989.

Hagood, N.W., Crawley, E.F., de Luis, J. Anderson. E.H. "Development of Integrated Components for Control of Intelligent Structures," presented at ARO Workshop on Smart Materials, Structures and Mathematical Issues, Virginia Polytechnic Institute, Blacksburg, VA, September 15, 1988.

Crawley, E.F., de Luis, J., Hagood, N.W., Anderson, E.H., "Development of Piezoelectric Technology for Applications in Control of Intelligent Structures," 1988 American Control Conference, Atlanta, GA, June 1988.

Crawley, E.F., Ducharme, E.H., "Velocity Scaled Aeroelastic Testing of Advanced Turboprops," ASME Paper No. 87-GT-209, presented at the 1987 ASME Gas Turbine Conference, Anaheim, CA, June 1987.

O'Donnell, K.J., Crawley, E.F., Ward, B.A., Hall, S.R., "A Hierarchic Control Architecture for Intelligent Structures," AAS Guidance and Control Conference, Keystone, CO, Jan. 31-Feb. 4, 1987.

Peterson, L.D., Crawley, E.F., Hansman, R.J., "Experimental Measurements of the Nonlinear Coupled Dynamics of Fluids and Spacecraft in Low Gravity," IAF paper 86-275, presented at the XXXVIIth I.A.F. Congress, Innsbruck, Austria, 4-11 October 1986.

Crawley, E.F., Zhang, J., "Method for Calculating the Frequency of a Rotating Turboprop Blade," presented at First World Congress on Computational Mechanics, IACM, Austin, Texas, September 22-26, 1986.

Crawley, E.F., O'Donnell, K.J., "Analysis and Incorporation of the Effects of Localized Nonlinearities on the Dynamics of Multi-Element Space Structures," Tenth National Congress of Applied Mechanics, Austin, Texas, June 16-20, 1986.

Crawley, E.F., de Luis, J., "Use of Piezo-Ceramics as Distributed Actuators in Large Space Structures," AIAA paper 85-0626-CP, presented at the 26th AIAA/ASME/ASCE/AHS Structures, Structural Dynamics and Materials Conference, Orlando, Florida, April 1985.

Miller, D.W., Crawley, E.F., Ward, B.A., "Inertial Actuator Design for Maximum Passive and Active Energy Dissipation in Flexible Space Structures," AIAA paper 85-0777-CP, presented at the 26th AIAA/ASME/ASCE/AHS Structures, Structural Dynamics and Materials Conference, Orlando, Florida, April 1985.

Peterson, L.D., Crawley, E.F., "Simulation of the Nonlinear Motion of a Flexible Body with Variable Geometry," AIAA paper 85-0729-CP, presented at the 26th AIAA/ASME/ASCE/AHS Structures, Structural Dynamics and Materials Conference, Orlando, Florida, April 1985.

Crawley, E.F., "Aeroelastic Formulations for Turbomachines and Propellors," presented at the Symposium on the Unsteady Aerodynamics of Turbomachines and Propellors," Cambridge University, September 1984.

Crawley, E.F., Sheen, R.L., "Experimental Measurement of Material Damping in Simulated Zero-G," presented at the Air Force Vibration Damping Workshop I, Long Beach, California, February 1984.

Crawley, E.F., Kerrebrock, J.L., Dugundji, J., "Preliminary Measurements of Aerodynamic Damping of a Transonic Compressor Rotor," in Measurement Methods in Rotating Components of Turbomachinery, ASME, March 1980.

Crawley, E.F., "Designing the Space Colony," Technology Review, Vol. 79, No. 8, July/August 1977.

Covert, E.E., Mar, J.W., Crawley, E.F., "Some Considerations in the Choice of Man Powered Aircraft Configurations," Symposium on Man Powered Flight, Royal Aeronautical Society, London, England, January 1977.

Crawley, E.F., Wendell, J.H., "Advanced Composites in BURD II," Third Conference on Fibrous Composites in Flight Vehicle Design, 1975, NASA TM-X-3377.

STEVEN R. HALL

Department of Aeronautics and Astronautics
Massachusetts Institute of Technology
Cambridge, Massachusetts 02139
Room 33-103
Phone: (617) 253-0869

Education

MASSACHUSETTS INSTITUTE OF TECHNOLOGY Cambridge, Mass.

Sc.D. in Aeronautics and Astronautics, June 1985.
Thesis: "A Failure Detection Algorithm for Linear Dynamic Systems." Major included classical and modern control theory, stochastic processes, estimation, optimization algorithms, and fault-tolerance.

S.M. in Aeronautics and Astronautics, February 1982.
Thesis: "Parity Vector Compensation for FDI."

S.B. in Aeronautics and Astronautics, June 1980.

Honors and Professional Activities

Fannie & John Hertz Foundation Fellow, 1983-1985.
Hertz Foundation Doctoral Thesis Prize, 1985.
Member Tau Beta Pi, AIAA, IEEE.

Experience

MIT DEPARTMENT OF AERONAUTICS AND ASTRONAUTICS - Cambridge, Mass.
1985-present
Boeing Assistant Professor of Aeronautics and Astronautics.
Research includes development of actuator technology for helicopter rotor control; development of strategies for precision control of flexible structures; and development of control laws for the distributed control of structures.
Teaching includes digital control, fault-tolerance control, and control of aircraft.

CHARLES STARK DRAPER LABORATORY, Cambridge, Mass.
1980 - 1985
Research Staff.
Research Assistant.
Worked on the design and evaluation of failure detection and isolation (FDI) algorithms for the restructurable control problem, using C130 aircraft simulation.(1983-85)
Developed redundancy management algorithms and redundant hardware concepts for the A-10 Digital Command Augmentation System (1982).

Publications for Steven R. Hall

Papers

D.G. MacMartin and S.R. Hall, "An H_∞ Power Flow Approach to Control of Uncertain Structures," *AIAA Journal of Guidance, Control, and Dynamics* (to appear).

D.W. Miller and S.R. Hall, "Experimental Results using Active Control of Travelling Wave Power Flow," *AIAA Journal of Guidance, Control, and Dynamics* (to appear).

S.R. Hall, E.F. Crawley, J. How, and B. Ward, "A Hierarchic Control Architecture for Intelligent Structures," *AIAA Journal of Guidance, Control, and Dynamics* (to appear).

S.R. Hall and B.K. Walker, "The Orthogonal Series Generalized Likelihood Ratio Test for Failure Detection and Isolation," *AIAA Journal of Guidance, Control, and Dynamics* (to appear).

D.W. Miller, S.R. Hall, and A.H. von Flotow, "Optimal Control of Power Flow at Structural Junctions," *Journal of Sound and Vibration* (to appear).

D.G. MacMartin and S.R. Hall, "Structural Control Experiments using an H_∞ Power Flow Approach," submitted to *Journal of Sound and Vibration.*

D.G. MacMartin and S.R. Hall, "Investigation of a Cost Functional for H_∞/H_2 Minimization of Structural Energy," submitted to the 29th IEEE Conference on Decision and Control, Honolulu, HI, December 5-7, 1990.

N.M. Wereley and S.R. Hall, "Frequency Response of Linear Time Periodic Systems," submitted to the 29th Conference on Decision and Control, Honolulu, HI, December 5-7, 1990.

D.G. MacMartin and S.R. Hall, "Structural Control Experiments using an H_∞ Power Flow Approach," 1990 AIAA Guidance, Navigation, and Control Conference, Portland, OR, August 20-22, 1990.

S.R. Hall, E.F. Crawley, J. How, and B. Ward, "A Hierarchic Control Architecture for Intelligent Structures," 1990 AIAA Guidance, Navigation, and Control Conference, Portland, OR, August 20-22, 1990.

D.G. MacMartin and S.R. Hall, "An H_∞ Power Flow Approach to Control of Uncertain Structures," 1990 American Control Conference, San Diego, CA, May 23-25, 1990.

S.R. Hall and N.M. Wereley, "Generalized Nyquist Stability Criterion for Linear Time Periodic Systems," 1990 American Control Conference, San Diego, CA, May 23-25, 1990

R.L. Spangler and S.R. Hall, "Piezoelectric Actuators for Helicopter Rotor Control," 31st Structures, Structural Dynamics and Materials Conference, Long Beach, CA, April 2-4, 1990.

D.W. Miller, S.R. Hall, and A.H. von Flotow, "Optimal Control of Power Flow at Structural Junctions," 1989 American Control Conference, Pittsburgh, PA, June 21-23, 1989.

S.R. Hall and N.M. Wereley, "Linear Control Issues in the Higher Harmonic Control of Helicopter Vibrations," 45th Annual Forum of the American Helicopter Society, Boston, MA, May 22-24, 1989.

S.R. Hall and B.K. Walker, "Fault Diagnosis in Dynamic Systems by the Orthogonal Series GLR Method," in P. Borne et al. (ed.), *Computing and Computers for Control Systems*, Scientific Publishing Co., 1989, pp. 291-294. (Presented at the 12th IMACS World Congress on Scientific Computation, Paris, France, July 18-22, 1988.)

D.W. Miller, A. von Flotow, and S.R. Hall, "Active Modification of Wave Reflection and Transmission in Flexible Structures," 1987 American Control Conference, Minneapolis, MN, June 10-12, 1987.

K.J. O'Donnell, E.F. Crawley, B.A. Ward, and S.R. Hall, "A Hierarchic Control Architecture for Intelligent Structures," AAS 87-006, 10th Annual Rocky Mountain Guidance and Control Conference, Keystone, CO, Jan 31-Feb 4, 1987.

W.F. Bonnice, P. Motyka, E. Wagner, and S.R. Hall, "Aircraft Control Surface Failure Detection and Isolation using the OSGLR Test," 1986 AIAA Guidance and Control Conference, Williamsburg, VA, August 18-20, 1986.

P. Motyka, W. Bonnice, S.R. Hall, and E. Wagner, "A Comparison of Aircraft Control Surface Failure Detection and Isolation Algorithms," 1986 American Control Conference, Seattle, WA, June 18-20, 1986.

W.F. Bonnice, E. Wagner, P. Motyka, and S.R. Hall, "The Application of the Detection Filter to Aircraft Control Surface and Actuator Failure Detection and Isolation," 1985 Guidance and Control Conference, Snowmass, CO, August 19-21, 1985.

S.R. Hall and B.K. Walker, "The Orthogonal Series Generalized Likelihood Ratio Test," 1985 American Control Conference, Boston, MA, June 19-21, 1985.

S.R. Hall, P. Motyka, E. Gai, and J.J. Deyst, Jr., "In-Flight Parity Vector Compensation for FDI," *IEEE Transactions on Aerospace and Electronic Systems*, Vol. AES-19, No. 5, September 1983, pp. 668-676.

S.R. Hall, P. Motyka, E. Gai, and J.J. Deyst, Jr., "Inflight Parity Vector Compensation for FDI," IEEE 1982 National Aerospace and Electronics Conference (NAECON 1982), Dayton, OH, May 18-20, 1982.

Reports

J. deLuis, E.F. Crawley, and S.R. Hall, *Design and Implementation of Optimal Controllers for Intelligent Structures Using Infinite Order Structural Models*, SSL #3-89, MIT Space Systems Laboratory, January 1989.

W. Goldenthal,, L. Valavani, P. Motyka, S. Hall, and B. Eberman, *Design, Development, and Evaluation of a Model Based Compensator Concept for Higher Harmonic Control*, CSDL-R-1939, The Charles Stark Draper Laboratory, Inc., March 1987.

W. Bonnice, E. Wagner, S. Hall, and P. Motyka, *The Evaluation of the OSGLR Algorithm for Restructurable Control*, NASA Contractor Report 178083, May 1986.

P. Motyka, W. Bonnice, S. Hall, and E. Wagner, *The Evaluation of Failure Detection and Isolation Algorithms for Restructurable Control*, NASA Contractor Report 177983, November 1985.

P. Motyka, S. Hall, J. Lala, and R. Luppold, *Fault-Tolerant System Concepts for a C130 STOL Aircraft, Volume 1*, CSDL-R-1593, The Charles Stark Draper Laboratory, Inc., November 1982.

P. Rosner, R.R. Bairnsfather, S.R. Hall, and P.R. Motyka, *A-10 Digital Command Augmentation System, Volume III: Redundancy Management System and Mission Reliability Model*, CSDL-C-5676, The Charles Stark Draper Laboratory, Inc.,October 1982.

W. Guinon, S. Hall, J. Harper, A. Lynch, P. Motyka, and P. Van Broekhoven, *Reference Systems Technology Development, Volume III*, AFAL-TR-79-1189, January 1982.

Presentations and Symposia

S.R. Hall, E.F. Crawley, and J. How, "A Hierarchic Control Architecture for Intelligent Structures," First Annual Symposium of the MIT Space Engineering Research Center, Jet Propulsion Laboratory, Pasadena, CA, August 31, 1989.

S.R. Hall and N.M. Wereley, "Linear Control Issues in the Higher Harmonic Control of Helicopter Vibrations," First Annual Symposium of the MIT Space Engineering Research Center, Jet Propulsion Laboratory, Pasadena, CA, August 31, 1989.

S.R. Hall, "Intelligent Actuators for Intelligent Control," MIT Industrial Liaison Program Symposium: Intelligent Components in Aerospace, Cambridge, MA, November 15, 1988.

S.R. Hall, "Thoughts on Stability Analysis and Control Design for Linear Periodic Systems," MIT/Draper Seminar Series, Cambridge, MA, October 24, 1988.

S.R. Hall, E. Crawley, and J. How, "A Hierarchic Control Architecture for Intelligent Structures," Sixth Annual Air Force Forum on Space Structures, Atlanta, GA, April 7-8, 1988.

Patents

S.R. Hall and R.L. Spangler, Jr., "Piezoelectric Helicopter Blade Flap Actuator," patent applied for.

Revised March 28, 1990.

STEPHEN D. SENTURIA

Biographical Information

Stephen D. Senturia is presently a Professor of Electrical Engineering at the Massachusetts Institute of Technology, having joined the department immediately after completing his education (Harvard, B. A. in Physics, 1961, and MIT, Ph.D. in Physics, 1966). His research interests have included nuclear magnetic resonance and other physical studies in semiconductors, including lead-salt semiconductors and amorphous chalcogenide semiconductors. A parallel thread in his research has been the application of tne methods of physical measurement to practical problems. These have included high-precision thermometry, oil-well logging, NMR instrumentation methods, the automated reclamation of resources from urban solid waste, and integrated-circuit sensing devices. The charge-flow transistor for use with thin-film sensor materials and the microdielectrometer for chemical reaction monitoring in resins, adhesives, and plastics are among his recent developments. He is author or co-author of more than 80 scientific papers, is co-author of Electronic Circuits and Applications, an introductory electronics text, and is the solid-state-sensors Associate Editor of the IEEE Transactions on Electron Devices. He is co-winner of an IR-100 Award for his work on Automated Reclamation of Urban Solid Waste. Honor and professional societies include Phi Beta Kappa, Sigma Xi, IEEE, the Americal Physical Society, the American Chemical Society, the Adhesion Society, and SAMPE. In 1982, he founded Micromet Instruments, Inc., and currently serves on its Board of Directors.